
University of Trento

Paolo Grossi

EXPERIMENTAL INVESTIGATIONS ON SEISMIC
BEHAVIOUR OF LIGHT TIMBER FRAMED BUILDINGS
AND LOG-HOUSE TRADITIONAL CONSTRUCTIVE
SYSTEM

Prof. Maurizio Piazza

Prof. Roberto Tomasi

April, 2015

UNIVERSITY OF TRENTO

Engineering of Civil and Mechanical Structural Systems - XXVII Cycle

Final Examination 22/ 04 / 2015

Board of Examiners

prof. Jiří Mäca , Czech Technical University in Prague

prof. Maria Rosaria Pecce, Università' degli Studi del Sannio

prof. Daniele Zonta, Università' degli Studi di Trento

Dott. Paolo Clemente, UTPRA - ENEA CRE Casaccia

Dott. Loris Vincenzi, Università' di Modena e Reggio Emilia

ACKNOWLEDGEMENTS

Al termine del percorso di studi desidero ringraziare coloro che a vario titolo ed in diversi momenti hanno contribuito al compimento di questa proficua esperienza professionale ed umana. In particolare desidero esprimere la mia riconoscenza al professor Maurizio Piazza e Roberto Tomasi per la fiducia e il continuo incoraggiamento ed a tutti i membri del gruppo di ricerca sulle strutture in legno dell'Università degli Studi di Trento. Sono riconoscente inoltre agli amici che hanno condiviso questi anni di vita universitaria.

Esprimo sincera gratitudine all'azienda Rubner ed allo staff tecnico del reparto ricerca e sviluppo che nel corso degli anni ha dimostrato estrema sensibilità nel promuovere e assistere alle campagne sperimentali condotte.

Infine un caloroso ringraziamento è dedicato allo staff tecnico del laboratorio prove materiali per il supporto e la preziosa collaborazione nelle fasi sperimentali del lavoro di tesi.

SUMMARY

This document presents a part of the wide research carried out on modern timber buildings by the timber research group of the University of Trento. In the last five years several experimental and numerical analysis have been performed on crucial structural topics about multi-storey timber construction.

The efforts have been focused on the traditional light timber framed system (LTF) and on the log-house system (LH).

Concerning the LTF, different aspects of the structural behaviour to the lateral load bearing structure such as walls and connection devices were investigated through experimental tests from the single component up to the full-scale building tested on shake table. The goals of these capstone tests, carried out on three-storey buildings, were the investigation of peculiar aspects which especially for the European constructive tradition were not sufficiently discussed.

The same layout was follow for the traditional log-house system. In a first step of the research campaign the behaviour of single components (joints, reinforce elements) was tested and analysed in order to form the basis of the second part that was dedicated to the full scale shear walls tests and analysis.

The thesis is organized in two main parts. In the opening chapters, after a brief introduction to the constructive system, the seismic

behaviour of light timber framed constructions is analysed. The validation of the predictive models and the mechanical characterization of the gypsum fibreboard sheathing material are presented. Different steps of the S.E.R.I.E.S. project are summarized (tests on connection and real scale walls - shake table tests). The aim of the discussion is the deeper understanding of the boundary condition and the reliability of the tests on the single component on the real scale model.

In the second part, the mechanical characterization of modern timber log-house building through experimental tests is presented. The strong cooperation among Rubner Haus Company and the timber research group of the University of Trento made possible a detailed experimental campaign organized on two steps. The first is focused on the evaluation of the corner joints proprieties by means of analysis of small portion of walls. The second part deals with the behaviour of full-scale walls with vertical loads in different geometries (corner joints types, length and presence of openings). The two innovative test setup were designed to reproduce the boundary condition of the structural elements of the building, and to minimize the effects of the test apparatus on the results.

The outcomes of the tests show a complex interaction between contributions provided by different mechanisms. In the last chapters, a simplified model suitable to predict the overall load displacement curves of the wall is introduced.

Contents

1 INTRODUCTION	1
1.1 Background	1
1.2 Seismic design of timber buildings	6
1.3 Dissertation overview	8
 I Timber framed building	 9
2 Introduction	11
3 Preliminary tests on the single components	17
3.0.1 Steel to timber connection	17
3.0.2 Hold-down tension connection	24
3.0.3 Angle bracket shear connection	33
3.0.4 Shear wall	39
3.1 Theoretical considerations	56
3.1.1 Hold-down	56
3.1.2 Angle brackets	70
3.1.3 Shear walls	76
3.2 Component method	97
3.2.1 Bi-linearisation of the experimental curves	98

3.2.2	Hold-down equivalent spring - H	102
3.2.3	Angle brackets equivalent spring - A	104
3.2.4	Sheathing to frame connection - SH	106
3.2.5	Complete model - H-A-SH interaction	108
3.2.6	Comment	116
3.3	Conclusions	116
4	Full scale shake table tests	119
4.1	Introduction	119
4.1.1	State of the art	120
4.1.2	SERIES project	126
4.2	Shake table tests on full-scale TFS buildings	129
4.2.1	Scope of the tests	130
4.2.2	Geometry	131
4.2.3	Design of the buildings	132
4.2.4	Test set-up	145
4.2.5	Instrument layout	147
4.2.6	Test procedure	152
4.2.7	Results	156
4.2.8	Conclusions	177
II	LOG-HOUSE	183
5	LOG-HOUSE	185
5.1	Introduction	185
5.1.1	Design principle	188
5.1.2	State of the art	191
5.2	Experimental investigation	194

5.2.1	Tests on corner joints	194
5.2.2	Tests on shear walls	202
5.3	Analysis of the results	225
5.3.1	Theoretical considerations	225
5.3.2	Corner joints: discussion	236
5.3.3	Shear walls: discussion	241
5.3.4	Friction and mounting tolerance	251
5.4	Analytical simplified models	259
5.5	Discussion	273
5.6	Conclusions	274
A	Common definition	277
A.0.1	Test-protocol	279
B	Corner joint Tests	283
B.1	Timber Density/moisture	284
B.2	Photo documentation	286
B.3	Corner joint <i>Standard</i>	286
B.4	Corner joint <i>Tiroler Schloss</i>	289
B.5	Dovetail reinforcement system	290
C	Shear Walls	291
C.0.1	Monotonic test: M_ST_90	292
C.0.2	Monotonic test: M_ST_OP	294
C.0.3	Monotonic test: M_TR_90	296
C.0.4	Monotonic test: M_ST_130	298
C.0.5	Monotonic test: M_ST_SH	300
C.0.6	Cyclic test: C_ST_90	302
C.0.7	Cyclic test: C_ST_OP	304

C.0.8	Cyclic test: C_TR_90	306
C.0.9	Cyclic test: C_ST_130	308
C.0.10	Cyclic test: C_ST_SH	310
C.0.11	Log-house shear-walls: Cyclic tests results	312
C.1	Photo documentation	317
C.2	Tests on 90 mm and 130 mm wall thickness	317
C.3	Tests on wall with openings	319
C.4	Tests on Tirollerschloss corner joint style walls	322
C.5	Tests on shorter walls	324
C.5.1	Monotonic test	324
C.5.2	Cyclic test	326
Bibliography		329

Chapter 1

INTRODUCTION

1.1 Background

Timber buildings have a long tradition in many countries across the globe, such as U.S., Canada, Germany-Sweden-Norway, Japan and New Zealand. In these areas despite of different climatic and topographic condition, cultures and historical heritage timber is commonly used with similar systems to build residential houses.

The advantages of using timber as building material are nowadays widely recognized. It's not easy to summarize all the technical and economical features which in different zone had promoted the large diffusion of this material. The good mechanical proprieties (weight to strength ratio) and the environmental sustainability related to aspect such as energy consumption in production and transport and renewability have a great importance. Moreover, a timber house can be built in almost half the time of other construction methods based on different materials such as reinforce concrete or masonry. It is largely for this reason that timber construction is becoming the preferred method for many building companies.

In Italy, two main issue has promoted a rapid increase in the number of wooden buildings: the first was the introduction of severe limits in the energy consumption for heating and cooling and the second was the protection against the seismic hazard.

Concerning this issues this material provide relevant advantages. A common characteristic, related to the physical proprieties of wood is the low mass. Compared to other material such as concrete or steel, timber exhibit a lower mass of the

structural members which ensure a lower mass excited by the ground motion during earthquakes. Moreover despite of a brittle behaviour of the members (tension and bending) the joints ensure a good energy dissipation and good ductility. These characteristic is strongly related to the constructive system and on the design rules.

The most common construction systems can be summarized into four main categories: "log-house" (LH), "post and beams" (PB), "cross laminated panel" (CLT) and "light-frame" (LTF) platform systems (Figure 1.1).



Figure 1.1: (a) Post and beam multi-storey residential building TrÅd8 Sweden (<http://www.moelven.com/>) - (b) Log-house building (<http://www.haus.rubner.com>) - (c) CLT platform construction (from Web) - (d) Timber framed walls platform construction (from web).

The log-house building (also knows as "block-haus") is a traditional construction system used in the northern region, where large amounts of straight and tall trees were easily available. The constructive principle of the walls is the superposition of linear elements connected to the orthogonal walls by corner joints (Figure 1.2). The vertical forces are transmitted from the roof and floors to the foundation by tension perpendicular to the grain. This is one of the limit of the system to the vertical load bearing capacity (number of storey), furthermore the orientation of the element gives rise to another important issue: the dimensional variation of the wall due to the moisture content changing. The swelling and the shrinkage of the single element and the differential displacement are the main limit of this system. The lateral load bearing

capacity is guaranteed by two main contribution: the static/dynamic friction and the corner joints stiffness.

The seismic behaviour of the system is very complex because these two mechanisms are exploitable at different displacement level. If no other fasteners are used, the mounting tolerance contribution are fundamental.

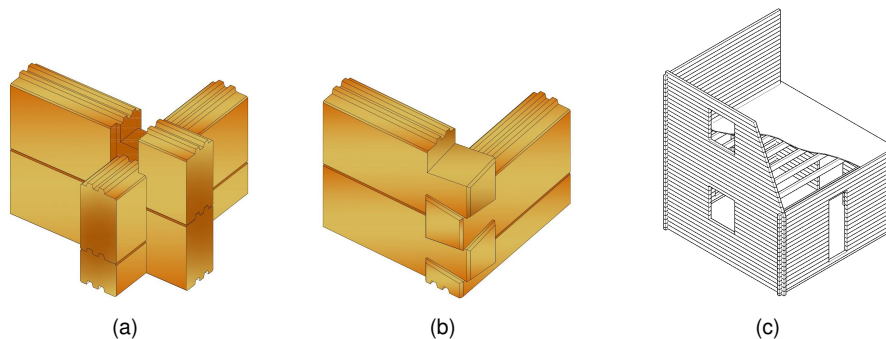


Figure 1.2: (a) Half lapped joint - (b) Tirollershloss joint - (c) Log-house building.

Another well-known traditional system is the "post and beam". Since the medieval age, this type of construction was built following different techniques. The ancient structures were composed by heavy timber members connected by "mortise and tenon" joints or other carpentry joints (Figure 1.3(a)). The horizontal load carrying capacity was ensured by diagonal bracing or filling the frame with masonry. In the modern buildings, steel fasteners (dowels, bolt, screws etc) are used instead of the traditional carpentry joints. In terms of strength and ductility, the advantages are substantial because the brittle failure of the timber joints are replaced by ductile mechanisms of the steel fasteners (Figure 1.3(c)). Diagonal bracing is used to provides lateral stability of the structure. Also shear walls or, less common, moment resisting connection can be used for the same purpose.

The seismic performance of the modern system is strongly related to the behaviour of the connection between the structural elements. Good results can be obtained if the fasteners ensure itself a good energy dissipation and a high ductility and all the brittle failure (of the timber members and in the connection) are avoided.

The last two systems namely CLT and LTF are probably the most used all over the world. The vertical and horizontal load are transferred from the floors to the foundations by the load bearing walls. For this reason, both are classified as "load bearing walls system". Two structural layouts can be used, namely the platform frame (PF) or

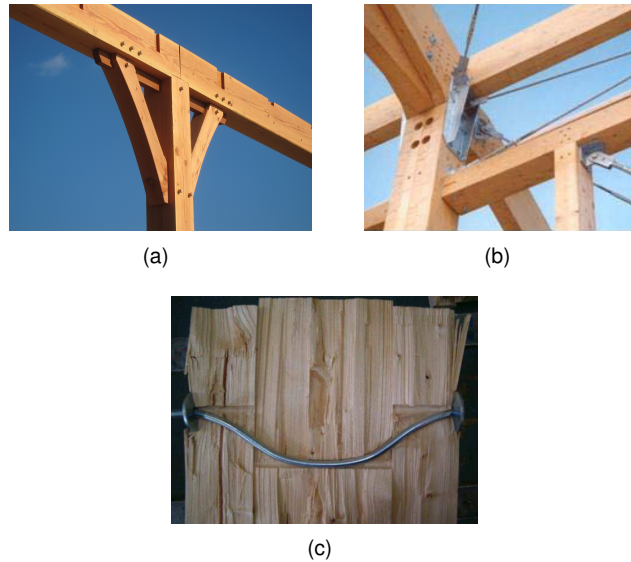


Figure 1.3: (a) *Traditional carpentry joint* - (b) *Column- beam connection* - (c) *Test on timber to timber connection* (M. Piazza UniTn).

balloon frame (BF). In the PF each storey is built on the previous one and the walls are interrupted at each floor. In the BF option, the intermediate floor structures are connected to the vertical structure that are continuous from the foundation to the roof. Nowadays the most common constructions are built according to the platform frame option because of their fire resistance and significant advantages during the erection phases.

The older, but still most widely used, system is the light timber frame. In this system the floors and walls are created by assembling timber studs (for walls) or timber joists (for floors) in a framed element which is sheathed with different materials, in order to act as structural diaphragm to allow the transfer of lateral loads (e.g. seismic or wind load) to the foundation. Under cyclic loads, the high number of steel fasteners (nails or staples) used in the frame to panels connection ensure a good energy dissipation and a large ductility. In addition, other important contributions are related to the connection between elements (anchor to the foundation and between walls at different levels). These two features, associated to the low weight, confer an excellent behaviour during earthquake.

Especially in the European area, the modern productions are focused on a prefabricated high performance system (Figure 1.4(a)), while in other countries, such as U.S. Canada and New Zealand, a more traditional layout is still preferred (Figure 1.4(b)). To fulfil these requirements all the timber members (wall frame and floors) are composed by larger cross section and the finishing layers are more sophisticated. Moreover, an advanced prefabrication process is applied to achieve high quality standards with a quality control typical of industrial products. In so doing, all the mounting tolerance of the in situ process are minimized. On the other hand, the North American system is often based on a traditional in situ construction. The carpenters built the frame using two by four inch standard element and then proceed then with the fixing of the sheathing panels. The serviceability limit states (i.e. admissible vibration and the acoustic performance) are completely different from the European case.



Figure 1.4: *European prefabricated system (SERIES project)*

The CLT platform system is based on large bi-dimensional element of massive cross-laminated timber (Figure 1.5). The same material is used for vertical and horizontal elements. The main advantages of the cross laminating process is the compensation of the anisotropy (dimensional stability) and the reduction of the negative impact of knots and other defects in each component board.

The load path is similar to the timber-framed houses. Therefore, the connections used in the "light frame" were adopted also for CLT when, in the mid-nineties, this technologies was developed. But in this case, the wall panels act mainly like rigid blocks, thanks to the high stiffness and strength of the CLT. The seismic behaviour of CLT is different from the TF because the main contribution to the energy dissipation is given by the deformation of the connections (the panels behave as elastic-brittle elements).



Figure 1.5: (a) CLT building in Spain - (b) CLT building in Spain (www.ecoqualityhouse.com))

1.2 Seismic design of timber buildings

In the last fifteen years, especially in Italy and in the southern part of Europe, timber began to be used as building material. The application of this material was limited to heavy glulam timber structures (warehouses, sport arenas, pedestrian bridges). Thus only few buildings were erected by specialized factory and specialized engineering staff.

The lack of confidence was demonstrated by the approach of technical institutions; until 2009 in the Italian building code no information was provided for timber construction. Before that date all the timber structures were designed according to the German building code (DIN1052). Despite the studies carried out in different countries have shown that the modern timber buildings exhibit an excellent seismic behaviour, confirmed also by the building codes of the most seismic prone areas such as US and Japan, that in a certain way represent a measure of the confidence in these systems.

In 2009 the final version of the actual Italian national standard was approved. This document was created from processing the previous edition and two documents introduced after seismic events (OPCM 3274 - OPCM 3431). Anyway, the result of this procedure did not satisfy all the issues about the design of the structure. Only few pages, in the current version, are dedicated to the static design procedure and only five pages for the specific rules for seismic design. Thus, the only way for a complete design of a structure is to refer to the specific regulations admitted by the standard (Eurocodes and technical documents by the national research council).

However, also in the European codes, there is still a lack of adequate design provisions. For instance, no specific design rules for CLT and LH construction systems exist in Eurocode 5 (timber design Standard) and Eurocode 8 (earthquake design Standard). In the case of structural materials like cross-laminated timber panels, the lack of a specific technical product Standard means that each producer must obtain specific technical approvals by supplying proprietary technical information applicable to the design of the structure. This makes difficult to create generic CLT structural projects, as in the case of steel or RC structures.

Except for CLT and LH cases the static design and the design criteria of the structural component are explained in the EN 1995. The main weaknesses of the current codes regard the seismic behaviour and the design prescription of the timber buildings. The modern theory of the structural analysis of building are based on the concept of load bearing capacity, energy dissipation and displacement capacity. These proprieties of the system are strongly related to the structural design through the Capacity Based Design approach which is a key feature to achieving a ductile failure.

Compared with the provisions for the other materials, the rules for the capacity design are still missing or only few prescriptions are reported. In the chapter dedicated to RC buildings (48 pages) are illustrated the criteria and the prescription to fulfil the limit states design for the different structural system (wall - frame - frame - equivalent dual system - wall-equivalent dual system - torsionally flexible system - inverted pendulum system).

The procedures, with an increasing level of complexity, are described for the design in low (L) - medium (M) - high (H) ductility classes (DC). The purpose is to ensure that the demand in term of available displacement and rotation are verified. If the requirement, for a fixed design DC, are fulfilled the inelastic capacity of the structure is coherent with the initial assumption. Following this procedure the overall response of the structure in terms of stiffness-strength-ductility is controlled (the failure mode is coherent). The same layout was also adopted for the steel and composed steel-concrete buildings chapter (42 pages).

On the other hand, for timber buildings only five pages are dedicated for all the structural system. The rules listed in this part are organized as an integration of the static design code UNI EN 1995. After a brief introduction to the design concepts (dissipative structural behaviour; low-dissipative structural behaviour), the issues related to the materials and properties of dissipative zones are explained. The key points are focused on the requirement in terms of ductility, energy dissipation and appropriate

low cycle fatigue behaviour to cyclic loads, evaluated by the results of laboratory tests according to common test procedures (EN 12512). This procedure, for the design practice, is expensive and time consuming therefore at the same point is clarified that if geometric configuration of the joint (diameters of the fasteners and thickness of the timber elements) are met the provisions may be regarded as satisfied.

Another crucial issue of the design of inelastic structure is introduced: the over-strength of the member and connection out of the dissipative zones. This rule according to the capacity design ensure the development of cyclic yielding in the dissipative zones. However, only few words are spent on these requirements.

The next sections address some of these issues through the analysis of the experimental results of the single components of the buildings.

1.3 Dissertation overview

The first part of the thesis deal with the seismic behaviour of the light timber framed walls system. In the second chapter are reported the main outcomes of a experimental campaign on the connection systems (hold-down, angle brackets) and the full scale tests on shear walls. Theoretical analysis of the results are summarized to understand the mechanical behaviour under monotonic and cyclic tests.

The third chapter present the shake table tests carried out in the framework of the series project on two building characterized by the same geometry but with different sheathing material. Moreover after a first test protocol, common to the two buildings, the two test series were dedicated to specific aspects.

The second part of the thesis report the main outcomes of an experimental test campaign carried out on the log-house walls. The lateral load bearing capacity of this traditional constructive system was investigated through experimental tests on corner joints that represent in the most ancient form the connection between the superimposed logs and by tests on full scale walls tests. Moreover simplified models to reproduce the mechanical behaviour under lateral and vertical forces is presented. In the last subsections the effect of a reinforce system based on self-tapping screws is analysed.

Part I

Timber framed building

Chapter 2

Introduction

Light timber-framed system is based on load-bearing walls and floors made with standardized dimensional timber and structural-wood based panel products. The internal frame is connected to the external structural sheathing by means of nails or other steel fasteners (staples, screws). These composed structures are designed to bear both to vertical (self-weight, live loads) and horizontal loads (wind, earthquake). The horizontal structures (floors, roof) are, in the most conventional form, made with timber beams or I-joists sheathed on the upper side by structural boards connected by means of nails or staples. In the latest evolution modular box elements are used; nevertheless the structural principle is similar to the previous mentioned solution (Figure 2.1).

The worldwide large diffusion of these buildings have been promoted by the reliability and from simplicity of the design often based on simplified standard based on empirical-based design rules. Indeed, one of the main key point is the structural robustness ensured by a high number of small diameter fasteners and from energy dissipation related to ductile failure modes. Despite these peculiarities the simplified approaches have demonstrated, some problems about the resistance and the damage levels after severe earthquake. These catastrophic events promoted a revision and improvement of the codes and the development of new approaches to the design in order to prevent local failure damages on the structural and non-structural components of the buildings.

Regarding the vertical loads, the structural design should satisfy different verifications about the maximum compressive stress and instability (studs), bending (beams, lintels) and compression orthogonal to the grain (sill beams) as reported

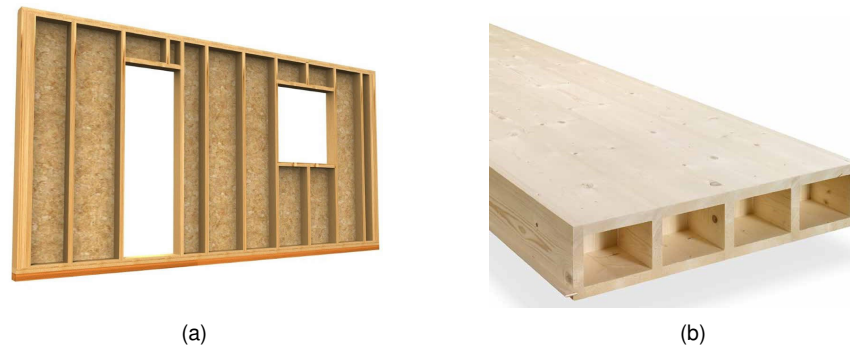


Figure 2.1: *Timber framed wall and modular box element (ref. lignature).*

by EN 1995:2009. Usually the design is carried out according to a simple pinned scheme in both direction, where the instability of the studs can occur only in out of plane direction. The buckling of the studs in the plane of the wall is prevented by the connection to the sheathing boards.

In case of regular opening layout the compression along the grain and the stability verifications are not restrictive, because the loading path ensure a good distribution of the forces along the bearing elements.

For the common practice the main limits of the conventional platform frame relies with the high values of compression orthogonal to the grain (mid-rise and tall buildings) and the continuity of the loading path from the upper levels to the foundation (regularity of the opening layouts).

For the horizontal load carrying capacity, according to the principal codes, the design rule is based on the lower bound theorem of the limit analysis assuming the conventional hypothesis of rigid-plastic behaviour of the steel fasteners and the rigid behaviour of the sheathing panels (the failure mode is related only to the connection).

Detailed provisions on the mechanical and geometrical proprieties of the sheathing panels (thickness and density) ensure the coherence of this assumption. Moreover, geometrical rules about the minimum nail spacing and the ratio between the spacing between the studs and the board thickness are reported to prevent the instability of the sheathing boards. The performance in terms of resistance depends only from the mechanical proprieties and number of fasteners (spacing). The stiffness of the bracing is not reported in the current version of the eurocodes ([1], [2]) whereas other national standards (DIN, NZS, IBC, CBC) adopt different approaches which will be summarized in the next sections.

The rigid-body equilibrium of each single wall segment, usually assumed as a cantilever beam, is ensured by anchor systems. Tension ties and angle brackets are commonly adopted to prevent the wall uplift and the slippage from the foundation or intermediate floors, as illustrate from the schematic failure mechanisms in Figure 2.2.

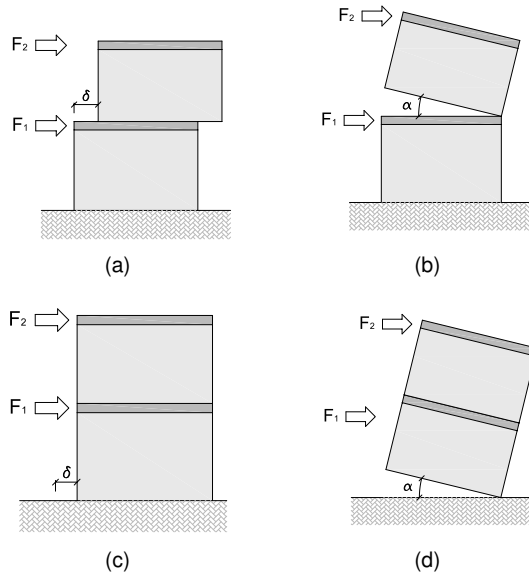


Figure 2.2: Failure modes due to rigid body mechanisms: a,b) upper storey slippage and rocking - c,d) global mechanism.

In the north American areas, this system have been organized with a high level of standardization of materials, cross sections, studs and nail spacing since its origins around the mid nineteenth century. Nowadays in the US the most common structural layout is organized using "two by four" inches cross section and plywood or OSB sheathing connected on one or both sides of the wall by means of nails (smooth or ribbed). Gypsum wallboards are often used as sheathing panels as well or combined with plywood or OSB. When single stud is not enough to transfer a high vertical load, for instance near wide opening or under heavy loaded beam, two or three section are connected together (studs pack). The most common basic modular inter-spaces for the studs (walls), joist (floor) and rafter (roof) are 16 and 24 inches respectively corresponding to 40 and 60 cm [3]. This spacing are based on the fundamental module of 4-foot (1.2 m) according to the commercial sizes of the common plywood and oriented strands boards. The structure, according to a well-established tradition, is assembled directly on the construction site Figure 2.4(b). According to this practice,

the anchor systems described in the previous paragraphs are inserted inside the frame with some interesting advantages such as a compact size and a lower force eccentricity on the anchors (Figure 2.3).



Figure 2.3: *Anchor system against uplift and slippage.*

The European woodframe system, widely adopted in the northern areas such as Scandinavia, Germany, despite of the common background - construction principle and materials shows important differences. The performance in terms of structural response (strength, stiffness) and comfort (sound and thermal insulation, vibrations) are widely different. Stringent requirements on energy consumption and on the home comfort have promoted a high-performance system, based on an advanced level of prefabrication. The advantages of this solution are emphasized for timber building, thanks to the lightweight of the components: large panels such as walls and floor completed with finishing and installation can be easily transported from the factory to the construction site Figure 2.4(a). Walls and floor panels take advantages on the production method, typical of the industrial process, ensuring a constant quality and a high precision.

The load bearing structure for the European woodframe thicker studs and beams are used (commonly $60 \times 160 \text{ mm}$, $80 \times 160 \text{ mm}$, $100 \times 160 \text{ mm}$), whereas similar thickness and materials are adopted as sheathing (OSB, plywood - 15 mm). The fasteners spacing range between 50 mm up to 150 mm on the external chords whereas on the internal studs the spacing is twice to ensure an adequate support for the sheathing.

The good performance of the timber buildings both for vertical and horizontal loads have promoted since from the origin a standardized building procedure based on the experience and on construction practice. For instance, according to the local regulations, in the US regular dwellings up to three stories in height may be built using prescriptive conventional rules. These buildings "deemed to comply" with earthquake



Figure 2.4: (a) *European prefabricated system (courtesy of legnocese.srl)* - (b) *American timber frame construction (from web)*

provisions without formal design ([4]).

The modern design procedures as for other materials were developed around the mid-1940s when standard racking tests were developed to assess the real performance of the system. A large number of experimental and analytical studies have been carried out to investigate the mechanical behaviour of woodframe buildings in the North American country (Canada, United States).

Concerning the response of light timber frame buildings under seismic loads the Loma Prieta (1989), Northridge (1994) and Kobe (1995) earthquakes have shown some critical aspects of the design provisions and on the construction practice. After these events many structural collapses were caused by soft-storey failure due to wide opening (garages) and local collapses. Moreover heavy damage were detected both to structural and non-structural materials which cause a high cost to repair and re-built the structures.

Hence, these events have promoted a revision of the technical regulation and the developing of new design approaches aimed to obtain a more engineered process.

The main result of this "new approach" was the developing of a new strategies which is the base of the current researches not only in US but all-over the globe. In fact, despite of the differences, US and EU systems are considered as good seismic behaviour systems thanks to the post elastic resources and energy dissipation due to the sheathing to frame connection.

The modern structural design is based on two approaches. According to the first, the capability of parts of the structure (dissipative zones) to resist earthquake actions out of their elastic range is taken into account ([2]).

As pointed out in the previous section, in order to achieve high-seismic perfor-

mance, the brittle failures (members, non-ductile joints) have to be prevented. Following to the capacity design procedure, the non-dissipative zones of the building should ensure a resistance higher than the dissipative zone resistance. Hence, the global failure mode is related to this failure mode, which lead to a ductile global mechanism.

In the second, the action effects are calculated on the basis of an elastic global analysis without taking into account non-linear material behaviour. The resistance of the members and connections should be calculated in accordance with EN 1995-1:2004 without any additional requirements ([2]).

Both strategies, despite of theoretical and economical differences, are focused on the relationship between connection system and members: strength for LDC and strength, ductility and energy dissipation for M/HDC.

Therefore, it is necessary, especially for the high ductility a mechanical characterization of the connection systems. In the next chapters some solution will be discussed in the details.

Chapter 3

Preliminary tests on the single components

The first step of the research campaign described in this document was the analysis of the behaviour of the single components of the structural load bearing walls through experimental tests and analytical models. As mentioned in the introductory paragraphs the overall seismic response of the structure is strongly related to the mechanical proprieties of the connections between the elements (walls/foundation - wall/wall) and from the proprieties of the sheathing to frame connection (panels-fasteners). This chapter is focused on the anchor system and on the performance of shear walls sheathed by gypsum fibre boards. Other materials and anchor systems have been studied in previous work, [5], [6] and [7]. In these reference papers are summarized the results of the tests carried out for the "chi quadrato" research project in the laboratory of the University of Trento. Geometry and materials used in the preliminary tests, presented in the next subsection, are the same of those adopted in the three-storey building tested on shake table in the framework of the SERIES project, that have never been studied.

3.0.1 Steel to timber connection

In order to investigate the performance of the anchor devices the attention was focused firstly on the mechanical characterization of the fasteners used for the steel to timber connection (hold-down or tie down/stud - angle brackets/bottom beam). Monotonic tests were performed in different configuration to obtain the load bearing capac-

ity, stiffness and ductility of the fasteners. Three test layouts were adopted using the same test machine. The first was a symmetric configuration with two steel flanges (Figure 3.1(a)) nailed on a timber element. The second was an unsymmetrical configuration where the timber element was fixed to the frame of the test machine (Figure 3.1(b)). The third was a symmetrical condition but with a higher number of nails 24 instead of 8 (Figure 3.1(c)). Table 3.1 and Table 3.2 summarize the geometrical proprieties and the tested material.

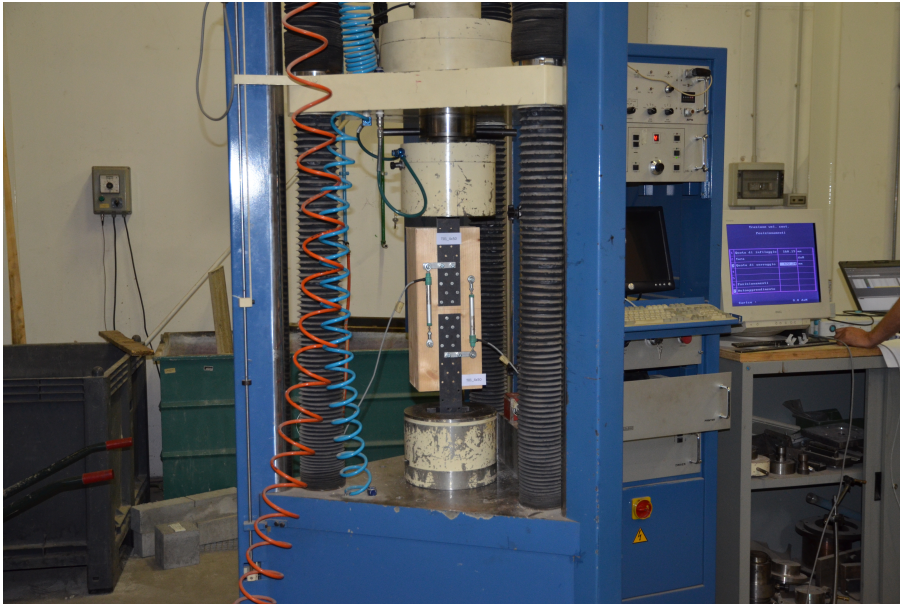
Type:	Ringed shank nail for structural timber (Anker nail)
Description:	Improved adherence wood nails, the nails are to be in possession of a 40° tip, truncated conical grooves with 1.3 mm pitch, with minimum diameter 3.6 mm and maximum diameter 4.4 mm, large head $\phi = 8$ mm, with conical under-head $\phi_{min} = 4$ mm and $\phi_{max} = 5.4$ mm.
Material:	Non-alloy steel rod according to EN 10016-2. Characteristic tensile strength $f_{u,k,min} = 600$ N/mm ²
Nominal diameter	4 mm
Length	50 mm
Characteristic yield moment:	6260 N · mm
Characteristic withdrawal parameter:	5.51 N/mm ²
Characteristic tensile capacity:	7.69 kN

Table 3.1: Data sheet (CE marking according to EN 14592:2008)

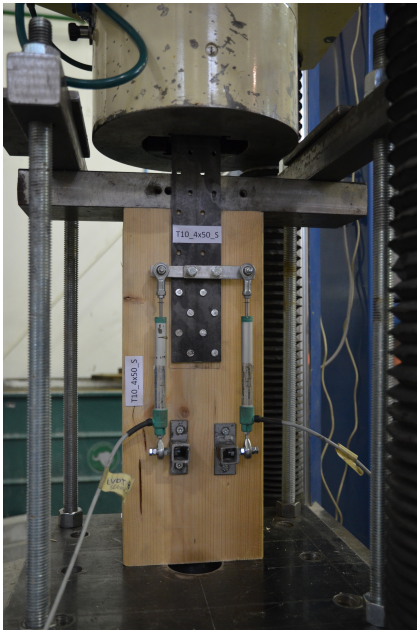
Type:	Steel plate
Description:	Perforated steel plate (56 x 4 mm) steel S235 according to EN 10025 - holes $\phi = 5$ mm. - row spacing 22.5 mm - line spacing 26.5 mm
Material:	Characteristic tensile strength $f_{u,k} = 360$ N/mm ² Characteristic yielding strength $f_{y,k} = 235$ N/mm ²
Nominal thickness:	4 mm

Table 3.2: Steel flange characteristics

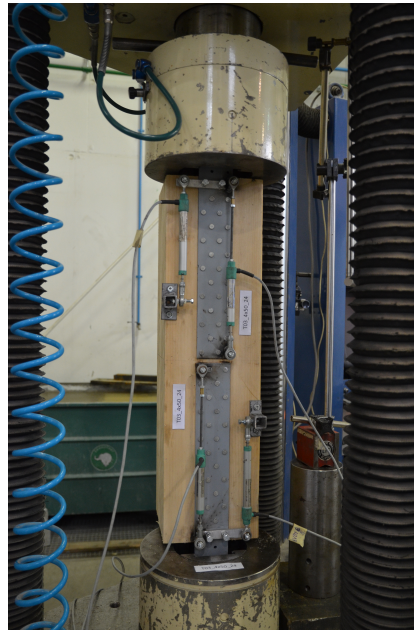
The tests were conducted following a monotonic quasi-static test procedure applying a fixed time/displacement ratio of 6 mm/min. During the tests the absolute displacement imposed by the test machine and the relative timber/steel displacement were measured by displacement transducers. However the absolute displacement was affected by the slippage between the steel flange of the sample and the grip devices. Therefore as other instruments installed in the test was used only to verify the test parameters. Hence only the sensors connected between timber and steel flanges were used to obtain the load displacement curves of the fasteners. Thanks to the transducers layout, in the symmetric configuration, two independent curves



(a)



(b)



(c)

Figure 3.1: Test setup - a) layout 1 (symmetrical - 8 nails) - b) layout 2(un-symmetrical - 8 nails) - c) layout 3 (symmetrical - 24 nails).

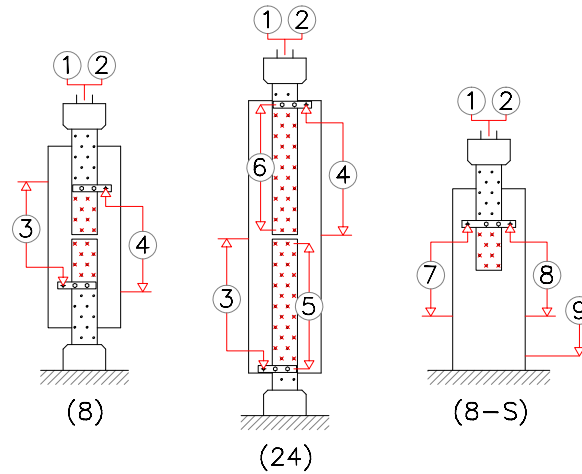


Figure 3.2: Arrangement of measuring instruments - a) layout 1 (symmetrical - 8 nails) - b) layout 2 (unsymmetrical - 8 nails) - c) layout 3 (symmetrical - 24 nails).

were obtained in each single test. According to the "in series springs configuration" only the data regard the weaker springs can be obtain by the tests, however some information about the elastic stiffness of the stronger spring can be useful. Table 3.3 and Figure 3.3 shows the results of the tests on the nailed connection of the first test layout (symmetrical - 8 nails). The value of the elastic stiffness K_{ser} , is defined as the slope of the secant line between the point on the load slip curve corresponding $0.1 \cdot F_{max}$ and the point on the load slip curve corresponding $0.4 \cdot F_{max}$. In order to obtain a mean values on a sufficient number of tests this value is calculated as arithmetic mean of both the nailed connections. This assumption take into account the influence of the boundary conditions when two flanges are connected to the test machine (one was fixed to the frame of the test machine while the other moves at the imposed displacement ratio).

Table 3.4 and Figure 3.4 shows the results of the tests on the nailed connection of the second layout (unsymmetrical 8 nails). It is worth noting that tests T10 and T11 shows higher performances because the density of the timber element was higher (466 instead of 370 kg/m^3).

Table 3.5 and Figure 3.5 shows the results of the tests on the nailed connection of the third layout (symmetrical - 24 nails).

The data summarized in the previous tables shows a good agreement with the load bearing capacity calculated according to the Johansen theory reported in the Eurocode 5. However the formulae used for the stiffness do not shows the same

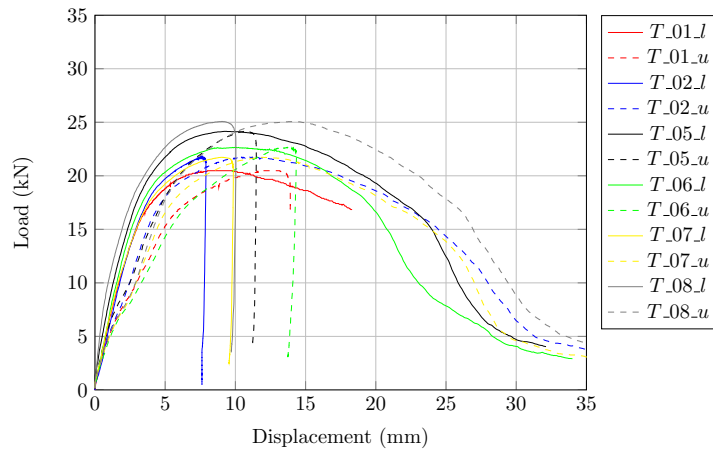


Figure 3.3: Load vs. displacement curves for ringed shank nails - first layout.

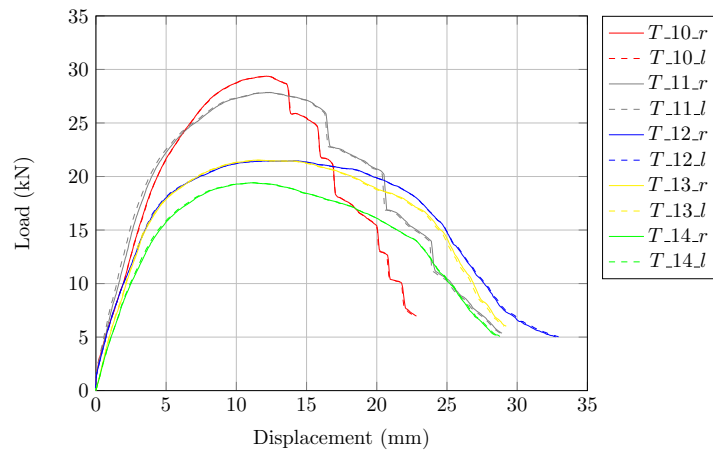


Figure 3.4: Load vs. displacement curves for ringed shank nails - second layout.

		T01	T02	T05	T06	T07	T08	Mean
ρ	$[kg/m^3]$	374.1	374.1	374.1	374.1	374.1	374.1	374.1
F_{max}	$[KN]$	20.5	21.8	24.2	22.7	21.7	25.1	22.6
v_{max}	$[mm]$	8.9	11.0	9.2	9.8	11.9	14.2	10.8
F_u	$[KN]$	16.38	17.4	19.3	18.1	17.4	20.1	18.1
v_u	$[mm]$	18.26	21.6	20.0	18.9	20.9	23.0	20.4
F_y	$[KN]$	16.5	19.0	19.3	18.0	19.4	22.8	19.2
v_y	$[mm]$	2.7	4.9	2.7	2.8	6.1	7.2	4.4
K_{ser}	$[N/mm]$	4670.8	4714.1	5128.6	4529.4	4390.2	5929.5	4893.8
K_{ser}/n_{Tot}	$[N/mm]$	583.8	589.3	641.1	566.2	548.8	741.2	611.7
K_{ser}/n_{eff}	$[N/mm]$	626.1	632.9	688.52	608.1	589.4	796.4	657.0

Table 3.3: Test results (symmetrical 8 nails)

		T10	T11	T12	T13	T14	Mean
ρ	$[kg/m^3]$	466.5	466.5	372.6	374.1	374.1	410.8
F_{max}	$[KN]$	29.4	27.9	21.5	21.5	19.4	23.9
v_{max}	$[mm]$	12.2	12.3	12.3	11.5	11.1	11.9
F_u	$[KN]$	23.5	22.3	23.5	17.2	15.5	20.4
v_u	$[mm]$	15.8	17.7	23.5	22.6	20.7	20.0
F_y	$[KN]$	25.9	21.9	17.2	17.4	15.7	19.6
v_y	$[mm]$	5.7	3.5	3.5	3.7	3.7	4.0
K_{ser}	$[N/mm]$	4208.9	5759.0	4525.0	4634.2	4194.4	4664.3
K_{ser}/n_{Tot}	$[N/mm]$	526.1	719.9	565.6	579.3	524.3	583.0
K_{ser}/n_{eff}	$[N/mm]$	565.1	773.1	607.5	622.1	563.1	626.2

Table 3.4: Test results second layout (unsymmetrical 8 nails)

agreement with the experimental results. The relationships proposed in the Eurocode 5 for the slip modulus of steel to timber connection are based on the timber to timber case. These formulation were obtained from the analysis of test results of different experimental campaign developed by several authors. According to the proposed equations the stiffness depends only from the diameter of the fasteners and from the mean density and, to take into account the different layout, for the steel to timber connection a simplified corrective coefficient is proposed. This value is fixed equal to two both for steel to timber connection and concrete to timber connection. The physical interpretation of this assumption is illustrated in Figure 3.2. The contribution of the rigid parts (steel or timber) is negligible compared to the timber contribution thus, the total slip for the same level of load is a half of the timber to timber case slip. Nevertheless the influence of other important variables related to the steel flange deformation such as clearance between the fasteners and the holes, the rotation of the fasteners in the steel plate are neglected [8]. Therefore, the actual stiffness of the connection is overestimated.

Moreover, when more than one fasteners is loaded on a row (wood fibre), in order to define the capacity of the connection usually an effective number of fasteners is

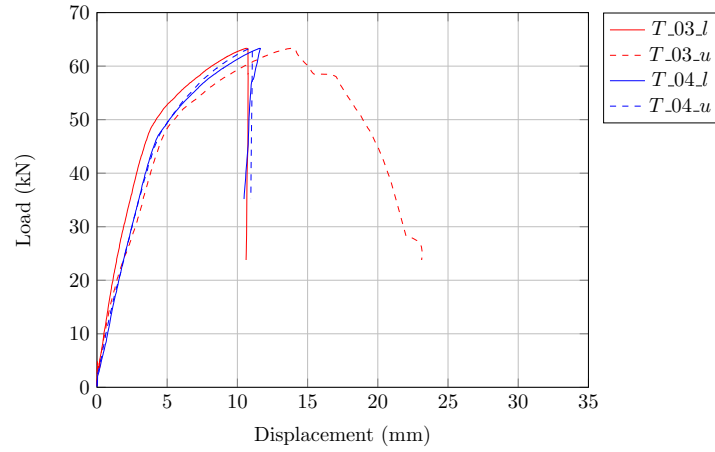


Figure 3.5: Load vs. displacement curves for ringed shank nails - second layout.

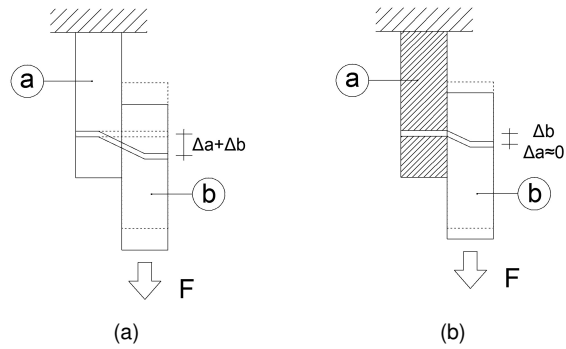


Figure 3.6: Instantaneous slip in a connection.

		T03	T04	Mean
ρ	$[kg/m^3]$	369.5	369.5	369.5
F_{max}	$[KN]$	63.3	63.3	63.3
v_{max}	$[mm]$	13.9	11.6	12.8
F_u	$[KN]$	50.7	50.7	50.7
v_u	$[mm]$	18.8	11.6	15.2
F_y	$[KN]$	49.9	49.3	49.6
v_y	$[mm]$	4.5	4.0	4.2
K_{ser}	$[N/mm]$	10465.8	12017.6	11241.7
K_{ser}/n_{Tot}	$[N/mm]$	436.1	500.7	468.4
K_{ser}/n_{eff}	$[N/mm]$	524.5	602.2	563.3

Table 3.5: Test results second layout (symmetrical 24 nails)

considered. This value take into account the force distribution between the fasteners. The effect of the interaction lead to a total capacity of the connection lower than the single element capacity multiplied by the actual number of fasteners. The correlation between the spacing and the effective number of fasteners is reported in the codes but only regard the load bearing capacity. The effect of the force distribution on the stiffness of the connection is not reported explicitly. The comparisons between the experimental values and the mean values calculated according to the European and national standard is summarized in Table 3.6.

Standard		Formulae	Timber to timber $[N/mm]$	Steel to timber $[N/mm]$	Experimental $[N/mm]$
UNI EN 1995:2009		$k_{ser} = \rho_m^{1.5} \cdot \frac{d^{0.8}}{30}$	870	1740	
CNR DT 206:2007		$k_{ser} = \rho_m^{1.5} \cdot \frac{d^{0.8}}{25}$	794	1587	
DIN 1052:2004		$k_{ser} = \rho_m^{1.5} \cdot \frac{d^{0.8}}{25}$	794	1587	550
SIA 265:2003		$60 \cdot d^{1.7}$ for $\alpha = 0$	633	1266	
		$30 \cdot d^{1.7}$ for $\alpha = 90$	317	633	

Table 3.6: Comparison between the analytical value of k_{ser} and the experimental results.

3.0.2 Hold-down tension connection

The second step of the tests on the single connection was focused on the analysis of the behaviour of the hold down connection through monotonic and semi-cyclic tests. The geometry of the connection is showed in Figure 3.7. On the contrary of the most widespread commercial system this hold - down is composed of two separate pieces connected by means of a bolt. The first element is the perforated steel plate nailed on the studs of the frame. The second is the stiffened angle bracket

Standard	Formulae	Value [kN]	Mean [kN]	Experimental [kN]
UNI EN 1995:2009 CNR DT 206:2007				2.8 (Ref. to n_{tot})
DIN 1052:2004	$\min \left\{ \begin{array}{l} f_{h,t} t_1 d \\ f_{h,t} t_1 d \left[\sqrt{2 + \frac{4 M_{y,Rk}}{f_{h,k} d t_1^2}} - 1 \right] + \frac{F_{ax,Rk}}{4} \\ 2, 3 \sqrt{M_{y,Rk} f_{h,k} d} + \frac{F_{ax,Rk}}{4} \end{array} \right.$	1.92	2.9	3.2 (Ref. to n_{eff})
SIA 265:2003	$R_d = 132 \cdot d^{1.7}$ for $\alpha = 0$ $R_d = 109 \cdot d^{1.7}$ for $\alpha = 90$	2.1 1.7	3.1 2.6	

Table 3.7: Comparison between the analytical value of the load bearing capacity and the experimental results.

that connect the device to the concrete foundation through threaded bars. The main advantage of this solution is that the nailed flange is pre-assembled in the factory. Thanks to this layout both the mechanical behaviour (the sheathing panel is not interposed) and the in-situ assembly are more efficient. The main characteristics of the tension tie are summarized in Table 3.8 and Figure 3.7.

Type:	Tension tie
Description:	Hold down element composed by a perforated plate and a reinforced base connected by means of a single bolt.
Material:	Steel S235 according to EN 10025 Characteristic tensile strength $f_{u,k} = 360 \text{ N/mm}^2$ Characteristic yielding strength $f_{y,k} = 235 \text{ N/mm}^2$
Connection:	Bolt graded 8.8 according to UNI EN ISO 898-1:2001 Characteristic tensile strength $f_{u,k} = 800 \text{ N/mm}^2$ Characteristic yielding strength $f_{y,k} = 360 \text{ N/mm}^2$

Table 3.8: Materials

The test setup and the geometry of the sample are showed in Figure 3.8. The hold-down was nailed on a timber element connected to the hydraulic jack by means of four threaded steel bars. The timber element, graded Gl 24 according to UNI EN 14080:2013, was reinforced by means of three $\phi = 7 \text{ mm}$ fully threaded screws to prevent the failure due to tension perpendicular to the grain (caused by the force on the restrain system).

Two geometries were tested. The first was characterized by 24 nails (test label HD_WS). In the second two additional nails were added to prevent the withdrawal effect on the lower part of hold down due to the eccentricity between the nailed steel

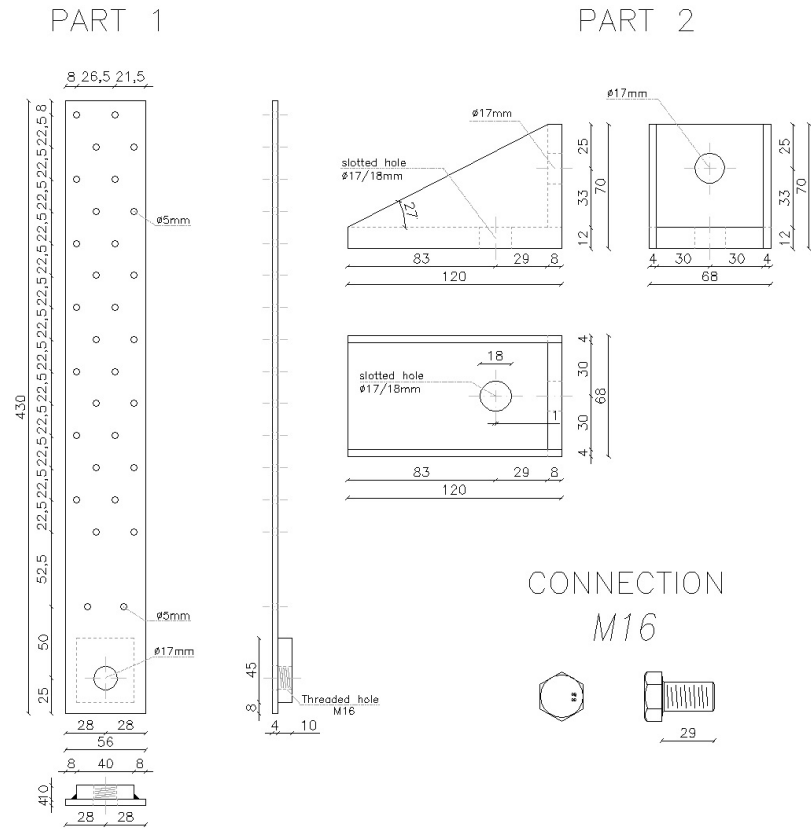


Figure 3.7: Geometry.

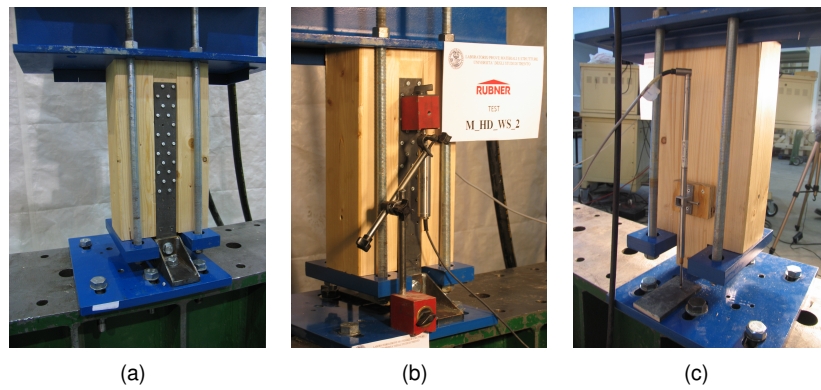


Figure 3.8: Hold-down test setup and transducers position.

flange and the anchor bolt (test label HD_S). The monotonic test sequence was carried out applying a constant quasi-static displacement (ratio 0.05 mm/s). The semi-cyclic test procedure was carried out applying the principle of the UNI EN 12512 but the reference displacement v_y was modified to perform a sufficient number steps the complete procedure is summarized in Table 3.9.

Cycle	Amplitude [mm]	nr. Cycle	Velocity [mm/s]
$0.25 \cdot V_y$	0.75	1	0.05
$0.5 \cdot V_y$	1.5	1	0.05
$0.75 \cdot V_y$	2.25	3	0.05
$1 \cdot V_y$	3	3	0.1
$2 \cdot V_y$	6	3	0.2
$4 \cdot V_y$	12	3	0.2
$6 \cdot V_y$	18	3	0.2
$8 \cdot V_y$	24	3	0.2

Table 3.9: Quasi-static cyclic test protocol.

The arrangement of measuring instruments was planned to get the load displacement curve (MTS), the deformation of the steel parts (AEP) and the deformation of the nailed connection (LVDT-AEP).

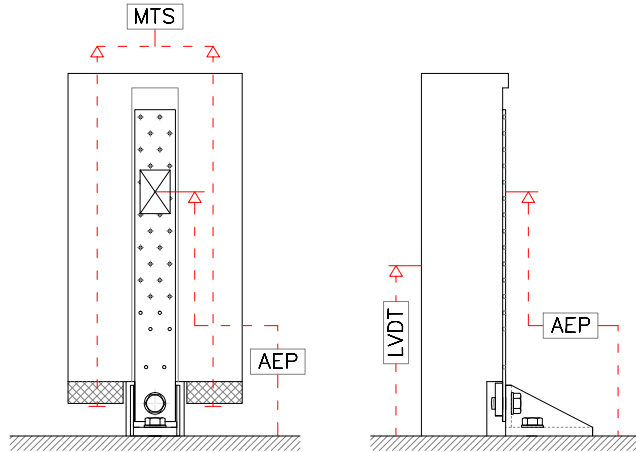


Figure 3.9: Hold-down test setup and transducers position.

In Figure 3.11, 3.12 and 3.13 are shown the test results of the monotonic and cyclic tests. As general remarks from the analysis of the load vs displacement curves a good agreement can be found between the envelope curves of the cyclic tests and the monotonic curve. This behaviour, typical of the steel-to-timber connections, is an index that the cyclic tests were not influenced by the rough errors (ie. gaps). The

consideration is easily clarified by observing the scheme of Figure 3.10. During a the second and the third loops, at a fixed displacement level, the fastener moves in the cavity that was created during the first cycle. Thus the timber deformation contribution is not active and the load at the same displacement of the first cycle is lower. When the level of displacement of the first cycle is exceeded the timber embedding contribution is activated and the total force on the fastener increase.

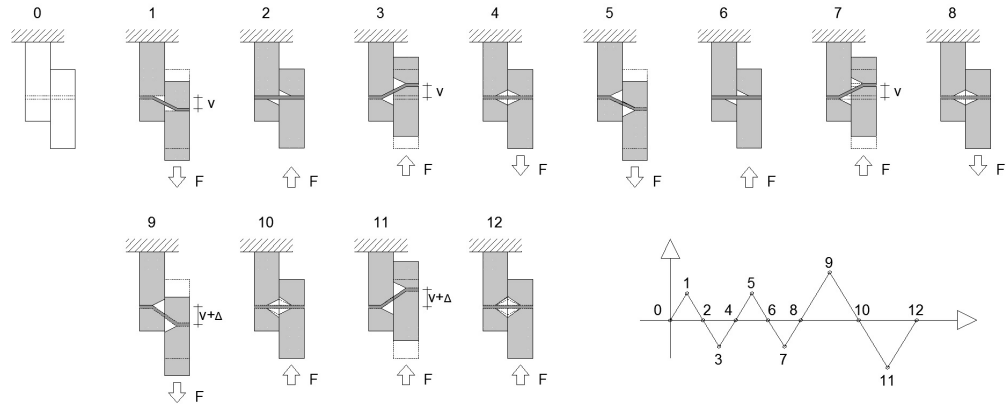


Figure 3.10: Cyclic behaviour of metal dowel-type fasteners connection - "pinching effect".

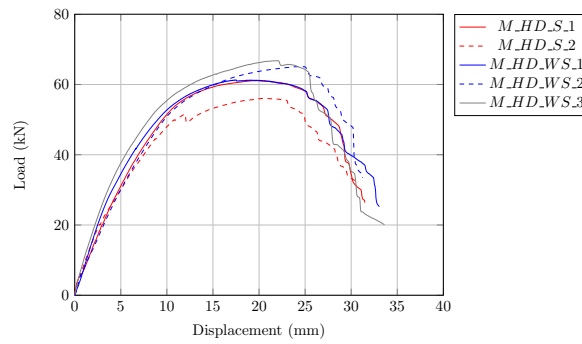


Figure 3.11: Load vs displacement curves of the hold-down - monotonic tests.

Test	M_HD_S_1	M_HD_S_2	M_HD_WS_1	M_HD_WS_2	M_HD_WS_3
F_{max} [KN]	61.1	56.1	61.3	65.1	66.8
v_{max} [mm]	19.8	20.7	17.5	24.2	22.1
F_u [KN]	48.9	44.9	49.0	52.1	53.4
v_u [mm]	28.4	26.4	27.7	28.9	26.4
$F_{0,1}$ [KN]	6.1	5.6	6.1	6.5	6.7
$v_{0,1}$ [mm]	0.8	0.6	0.8	0.7	0.6
$F_{0,4}$ [KN]	24.4	22.4	24.5	26.1	26.7
$v_{0,4}$ [mm]	3.7	3.2	3.1	4.2	3.1
F_y [KN]	52.5	46.2	48.9	54.6	51.5
v_y [mm]	8.2	6.9	6.2	9.3	6.2
K_s [N/mm]	6215.9	6466.7	7949.0	5629.0	8012.9

Table 3.10: *Test results-monotonic protocol.*

		C_HD_1											
		0.75 Vy			1 Vy			2 Vy			4 Vy		
		I	II	III	I	II	III	I	II	III	I	II	III
$F_{max}+$	[kN]	7.0	6.8	6.7	12.9	12.5	12.5	32.0	30.8	30.5	53.1	50.5	49.5
$vF_{max}+$	[mm]	2.2	2.2	2.2	3.0	3.0	3.0	5.9	5.9	5.9	11.9	11.9	11.9
E_d	[J]	1.7	1.2	1.2	4.1	2.7	2.6	45.7	17.6	15.7	246.3	69.7	62.7
E_p	[J]	7.8	7.6	7.5	19.1	18.6	18.6	95.2	91.6	90.7	317.0	301.4	295.7
v	[%]	3.5	2.5	2.5	3.4	2.3	2.2	7.6	3.1	2.8	12.4	3.7	3.4

		C_HD_2											
		0.75 Vy			1 Vy			2 Vy			4 Vy		
		I	II	III	I	II	III	I	II	III	I	II	III
$F_{max}+$	[kN]	19.4	19.0	18.8	24.9	24.3	24.2	42.2	40.9	40.5	60.2	58.4	57.3
$vF_{max}+$	[mm]	2.2	2.2	2.2	3.0	3.0	3.0	5.9	5.9	5.9	11.9	11.9	11.9
E_d	[J]	8.4	5.2	4.8	13.4	8.5	7.9	83.5	33.2	30.5	332.5	122.1	113.1
E_p	[J]	21.6	21.1	20.9	36.8	36.0	35.7	124.8	121.1	119.9	358.8	348.0	341.6
v	[%]	6.2	3.9	3.6	5.8	3.7	3.5	10.7	4.4	4.1	14.8	5.6	5.3

		C_HD_1											
		0.75 Vy			1 Vy			2 Vy			4 Vy		
		I	II	III	I	II	III	I	II	III	I	II	III
$F_{max}+$	[kN]	7.0	6.8	6.7	12.9	12.5	12.5	32.0	30.8	30.5	53.1	50.5	49.5
$vF_{max}+$	[mm]	2.2	2.2	2.2	3.0	3.0	3.0	5.9	5.9	5.9	11.9	11.9	11.9
E_d	[J]	1.7	1.2	1.2	4.1	2.7	2.6	45.7	17.6	15.7	246.3	69.7	62.7
E_p	[J]	7.8	7.6	7.5	19.1	18.6	18.6	95.2	91.6	90.7	317.0	301.4	295.7
v	[%]	3.5	2.5	2.5	3.4	2.3	2.2	7.6	3.1	2.8	12.4	3.7	3.4

		C_HD_2											
		0.75 Vy			1 Vy			2 Vy			4 Vy		
		I	II	III	I	II	III	I	II	III	I	II	III
$F_{max}+$	[kN]	19.4	19.0	18.8	24.9	24.3	24.2	42.2	40.9	40.5	60.2	58.4	57.3
$vF_{max}+$	[mm]	2.2	2.2	2.2	3.0	3.0	3.0	5.9	5.9	5.9	11.9	11.9	11.9
E_d	[J]	8.4	5.2	4.8	13.4	8.5	7.9	83.5	33.2	30.5	332.5	122.1	113.1
E_p	[J]	21.6	21.1	20.9	36.8	36.0	35.7	124.8	121.1	119.9	358.8	348.0	341.6
v	[%]	6.2	3.9	3.6	5.8	3.7	3.5	10.7	4.4	4.1	14.8	5.6	5.3

Table 3.11: Test results-cyclic protocol.

		C_HD_1											
		0.75 Vy			1 Vy			2 Vy			4 Vy		
		I	II	III	I	II	III	I	II	III	I	II	III
$F_{max}+$	[kN]	7.0	6.8	6.7	12.9	12.5	12.5	32.0	30.8	30.5	53.1	50.5	49.5
$vF_{max}+$	[mm]	2.2	2.2	2.2	3.0	3.0	3.0	5.9	5.9	5.9	11.9	11.9	11.9
E_d	[J]	1.7	1.2	1.2	4.1	2.7	2.6	45.7	17.6	15.7	246.3	69.7	62.7
E_p	[J]	7.8	7.6	7.5	19.1	18.6	18.6	95.2	91.6	90.7	317.0	301.4	295.7
v	[%]	3.5	2.5	2.5	3.4	2.3	2.2	7.6	3.1	2.8	12.4	3.7	3.4

		C_HD_2											
		0.75 Vy			1 Vy			2 Vy			4 Vy		
		I	II	III	I	II	III	I	II	III	I	II	III
$F_{max}+$	[kN]	19.4	19.0	18.8	24.9	24.3	24.2	42.2	40.9	40.5	60.2	58.4	57.3
$vF_{max}+$	[mm]	2.2	2.2	2.2	3.0	3.0	3.0	5.9	5.9	5.9	11.9	11.9	11.9
E_d	[J]	8.4	5.2	4.8	13.4	8.5	7.9	83.5	33.2	30.5	332.5	122.1	113.1
E_p	[J]	21.6	21.1	20.9	36.8	36.0	35.7	124.8	121.1	119.9	358.8	348.0	341.6
v	[%]	6.2	3.9	3.6	5.8	3.7	3.5	10.7	4.4	4.1	14.8	5.6	5.3

Table 3.12: Test results-cyclic protocol, impairment of strength.

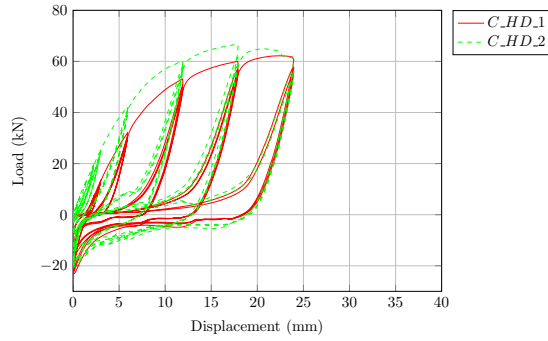


Figure 3.12: Load vs displacement curves of the hold-down - cyclic tests.

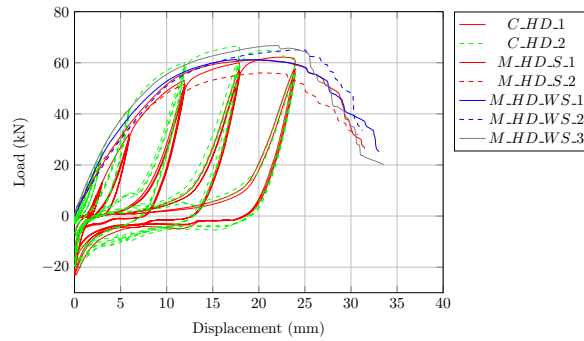


Figure 3.13: Load vs displacement curves of the hold-down - comparison between cyclic and monotonic tests.

The most relevant outcomes of the tests are the load versus displacement curves. However some other useful information can be obtained by the analysis of other recorded data. The elongation of the steel element (pre-drilled flange - connection - hold-down) can be obtained by the "AEP" measure. Furthermore the difference between the displacement recorded through the instruments "AEP" and "LVDT" represent the contribution of the timber deformation (embedding). Figure 3.14 shows the plots of the curves on the same diagram.

As shown by the previous diagrams and tables the influence of the two additional nails at the bottom of the flange is negligible. The withdrawal effect on the nails, introduced by the eccentricity between the steel flange and the anchor bolt, is clearly visible in Figure 3.15. Probably using other type of connectors with higher axial capacity (i.e. self-tapping screws) the overall behaviour of the connection would have improved.

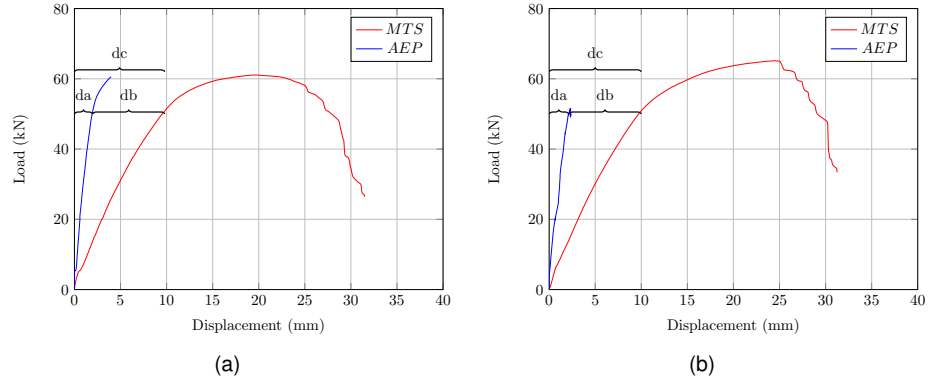


Figure 3.14: Different deformation contributions "da" is the seformation of the steel element, "db" is the contribution of the nails and "dc" is the total displacement for a) $M_{HD_S_1}$ b) $M_{HD_WS_2}$.

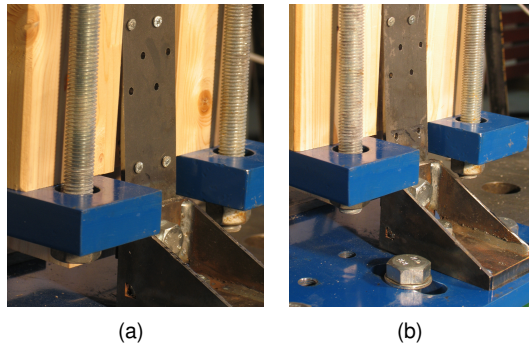


Figure 3.15: Effect of the load eccentricity on the bottom part of the steel flange - with additional nails a) - without additional nails b).

Other general remark concerning the connection are summarized in the bullet list above:

- the mean slip modulus value of the connection is 6855 kN/m and the main contribution is given by the nailed connection;
- the mean value of the maximum strength for the monotonic tests is 62 kN .
- the ultimate condition correspond to an impairment of strength of $0.2 \cdot F_{max}$, the mean value of strength is 50 kN whereas the mean displacement is 27.56 mm ;
- The mean value of the maximum strength for the cyclic tests is 64 kN . The impairment of strength between the first and third loop in the step where the maximum condition was reach is below 10%. No brittle failure occurs both in the load condition;

The analysis of the mechanical parameters was carried out through the definition of the UNI EN 12512 and UNI EN 26891. This standard reports the rules according to the definition and the prescription of the European standard (Eurocode 5 and Eurocode 8). However different codes and document reports other limits and procedure. However the requirement for the structural components of the constructive system, i.e. ductility requirement for the dissipative connections, must be coherent with the experimental outcomes.

3.0.3 Angle bracket shear connection

The third step of the tests on the single connection was the analysis of the behaviour of the connection against the horizontal sliding through monotonic and cyclic tests. The geometry of the connection is showed in Figure 3.16.

Angle brackets as well as the tension ties presented in this section are composed by two separate parts (pre-drilled flange and base). In this case the steel flange is connected in a groove on the bottom beam of the framed wall. In fact, on the contrary of other most common constructive practice, the sill beam and the bottom beam of the wall are not two separate elements. The "one element solution" allows a more efficient connection against the wall slippage. As can be seen in Figure 3.17 the most effective solution is achieved when the eccentricities between the centroid of the fasteners and the foundation in the vertical and horizontal plane are minimized. In this case also the effect of the two torsional moments on the stiffness and load

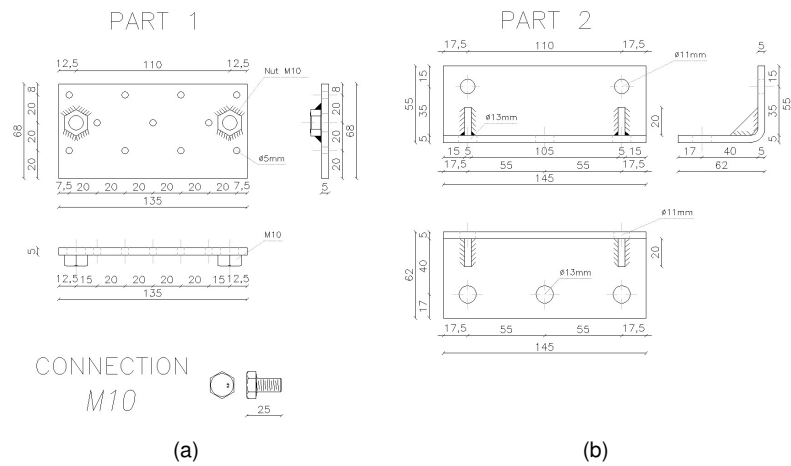


Figure 3.16: *Geometry.*

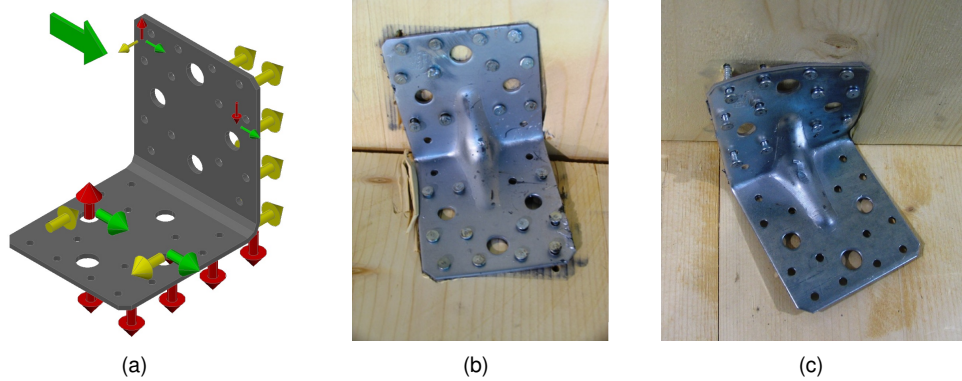


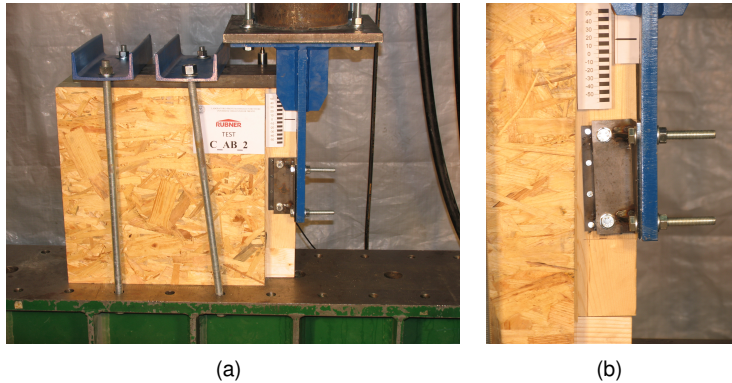
Figure 3.17: Effect of the load eccentricity between the nail centroid and the anchor bolts - schematic view a) - connection between timber floor and wall (CLT panels, [9]) - connection between concrete foundation slab and wall (CLT panels, [9]) b).

Type:	Foundation Wall Angles
Description:	angle bracket element composed by a perforated plate and a reinforced base connected by means of two bolts.
Material:	Steel S235 according to EN 10025 Characteristic tensile strength $f_{u,k} = 360 \text{ N/mm}^2$ Characteristic yielding strength $f_{y,k} = 235 \text{ N/mm}^2$
Connection:	Bolt graded 8.8 according to UNI EN ISO 898-1:2001 Characteristic tensile strength $f_{u,k} = 800 \text{ N/mm}^2$ Characteristic yielding strength $f_{y,k} = 360 \text{ N/mm}^2$

Table 3.13: *Materials*

bearing capacity are minimized. The main characteristics of the angle bracket are summarized in Table 3.13 and Figure 3.16.

The test setup and the geometry of the sample are showed in Figure 3.18(a) and Figure 3.18(b). As shown by the picture the angle bracket is connected to a timber box fixed to the test rig through four threaded bars. The foundation is mirrored by a vertical steel plate connected to the hydraulic jack. The setup was the same already used on commercial device tests. As mentioned in these case often the angle brackets are nailed directly on the sheathing panels (OSB). In order to reproduce the geometry of the wall the sample is composed by the same material used in the walls. To achieve a higher reliability, where only the influence of the interposed sheathing panels is taken into account, the OSB is glued onto the external frame of the box (rigid connection) except for the nailed zone. Thanks to the glued connection and the stiffness of the OSB the overall box deformation is negligible. In the presented tests the flange is nailed on the timber frame of the box and the geometry of the restrain element should not affect the results, however the same geometries is maintained.

**Figure 3.18:** *Tests on angle brackets - setup.*

Two monotonic and one cyclic tests were performed. In the first monotonic test (test label M_{AB_1}) $2.8 \times 70 \text{ mm}$ smooth nails were used instead of $4 \times 50 \text{ mm}$ ringed shank nails.

The monotonic test sequence was carried out applying a constant quasi-static displacement (ratio 0.05 mm/s). The cyclic test procedure was carried out applying the principle of the UNI EN 12512 whereas the reference displacement v_y was modified to perform a sufficient number steps the complete procedure is summarized in Table 3.14.

Cycle	Amplitude [mm]	nr. Cycle	Velocity [mm/s]
$0.25 \cdot V_y$	0.875	1	0.05
$0.5 \cdot V_y$	1.75	1	0.05
$0.75 \cdot V_y$	2.625	3	0.05
$1 \cdot V_y$	3.5	3	0.1
$2 \cdot V_y$	7	3	0.2
$4 \cdot V_y$	14	3	0.2
$6 \cdot V_y$	21	3	0.2
$8 \cdot V_y$	24.5	3	0.2

Table 3.14: *Quasi-static cyclic test protocol.*

The arrangement of measuring instruments was planned to get the load displacement curve (MTS). Moreover the relative displacement between the box lower frame element and the vertical steel plate was measured (AEP).

Figure 3.19 and 3.20 shown the test results of the monotonic and cyclic tests. As general remarks from the analysis of the load vs displacement curves a good agreement can be found between the envelope curves of the cyclic tests and the monotonic curve until 14 mm cycles. After this value the cyclic tests exhibit an impairment of strength of the third loop greater than the 20% of the maximum value recorded at the first loop. The monotonic curve reach the ultimate value, corresponding in this case also to the maximum condition, 22 mm .

Another interesting consideration is the difference between the behaviour of the connection when smooth nails are adopted. The performance of the system is lower because of the smaller diameter (2.8 instead of 4 mm), the improved adherence is missing and the clearance allowance is higher (2.2 instead of 1 mm).

Test		M_AB_1	M_AB_2
F_{max}	[KN]	22.3	40.4
v_{max}	[mm]	17.2	22.4
F_u	[KN]	19.1	30.0
v_u	[mm]	30.0	23.6
$F_{0,1}$	[KN]	2.2	4.0
$v_{0,1}$	[mm]	0.4	0.6
$F_{0,4}$	[KN]	8.9	16.2
$v_{0,4}$	[mm]	2.8	3.8
F_y	[KN]	18.6	32.3
v_y	[mm]	6.4	8.0
K_s	[N/mm]	2721.0	3813.3

Table 3.15: *Results of the monotonic tests.*

	C_AB_1											
	0,75 Vy			1 Vy			2 Vy			4 Vy		
	I	II	III	I	II	III	I	II	III	I	II	III
F_{max+} [kN]	13.5	13.1	12.9	15.7	15.4	15.1	23.8	22.1	21.4	30.1	23.7	22.2
$v F_{max+}$ [mm]	2.6	2.6	2.6	3.5	3.5	3.5	7.0	7.0	7.0	14.0	14.0	14.0
F_{max-} [kN]	-13.1	-12.7	-12.5	-16.6	-16.0	-15.6	-25.1	-23.7	-22.9	-30.8	-25.6	-22.9
$v F_{max-}$ [mm]	-2.6	-2.6	-2.6	-3.5	-3.5	-3.5	-7.0	-7.0	-7.0	-14.0	-14.0	-14.0
E_d [J]	25.9	18.1	16.4	39.4	31.6	29.3	167.6	124.8	113.0	501.1	306.1	240.5
E_p [J]	34.8	33.8	33.2	56.4	54.8	53.4	170.6	160.0	154.8	425.1	344.6	315.0
v [%]	11.9	8.5	7.9	11.1	9.2	8.7	15.6	12.4	11.6	18.8	14.1	12.2

Table 3.16: Test results-cyclic protocol.

	0,75 Vy			1 Vy			2 Vy			4 Vy		
	I - II	I - III	I - III	I - II	I - III	I - III	I - II	I - III	I - III	I - II	I - III	I - III
Δ [kN]	0.4	0.6	0.6	0.4	0.6	0.6	0.4	0.6	1.7	2.4	6.4	7.9
Δ [kN]	0.4	0.6	0.6	2.7	2.6	2.6	3.1	3.3	1.4	2.2	4.8	5.0
											5.1	6.2
											0.2 * F_m	6.0

Table 3.17: Test results-cyclic protocol-impairment of strength.

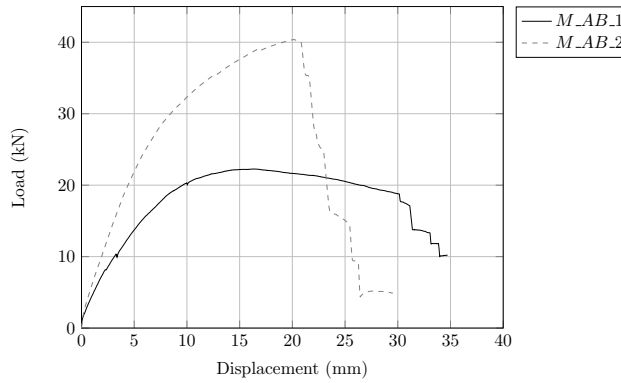


Figure 3.19: Load vs displacement curves of the angle bracket - monotonic tests.

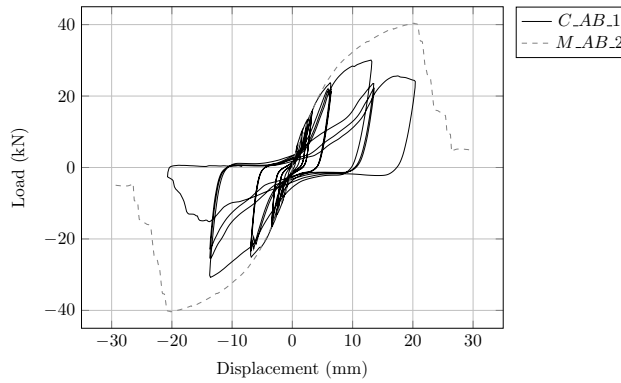


Figure 3.20: Load vs displacement curves of the angle bracket - comparison between cyclic and monotonic tests.

The mean stiffness value of the connection is 3813 kN/m . The elastic behaviour is not significantly affected by the cyclic loads. The first part of the load-versus displacement curves in the cyclic and monotonic test are almost the same. On the contrary the maximum strength for the monotonic tests (40.4 kN) is higher than the cyclic test (30.1 kN). The impairment of strength between the first and third loop in the 4th step of the cyclic load protocol is about the 25%. So the ultimate condition in the monotonic test is considerably greater both in terms of strength and displacement.

3.0.4 Shear wall

The fourth and final step of the preliminary tests on the single connection was the analysis of the behaviour of the shear walls. The geometry of the tested walls is

summarized in Table 3.18 and in Figure 3.21. Both vertical and horizontal loads were applied on the walls in order to take into account the stabilizing effect of the vertical load. The tests were carried out on full-scale samples connected to the reaction floor through the same devices described in the previous sections. Therefore all the contribution of to the total displacement of the walls are introduced. However thanks to the transducers installed on the sample all the single components could be analysed separately. This choice, as other technical solution in the testing phases, presents advantages and disadvantages. The main disadvantage is that when the first component of the system reach its yielding point the load cannot increase (isostatic system). On the other hand the real behaviour of the wall is analysed under the real boundary condition and with all the contribute of the connections. In order to obtain information about the behaviour of the single components of the wall a "capacity design" should be performed. In order to achieve the parameters about the load bearing capacity, stiffness and ductility of the sheathing to frame connection all the other components must be over-designed both for stiffness and resistance (fully anchored wall). However in this case the different contributions have to be analysed in different tests. Concerning the test methods for timber frame wall testing the European standard [10] specifies some key points about the calculation of lateral load resisting parameters but only a few general guidelines are introduced about the test apparatus (i.e. measure points - measures accuracy). The main prescription is that the test apparatus shall be able to apply separately the vertical load and the horizontal load without providing significant resistance to the sample tested. However, there is no practical indication within this document regarding the constraints and the load system. Different research center in Europe and in other countries develop test devices suitable to perform tests on the racking loads and stiffness of timber shear walls. The restrain system and the load application devices reproduce different "boundary condition". These boundary condition strongly influence the overall behaviour of the system and make comparisons between the acquired data difficult. The relative stiffness's between the element (connection+walls) is also an important parameter to select the correct test-setup.

The bearing mechanisms of the buildings relies on the proprieties of the lateral bracing system (walls panels, connections) and the response of the other components of the structure such as floor-slabs and links between transversal walls. Therefore the boundary condition of the laboratory tests may be different from the actual constraints since the interaction of these elements could change. An interesting studies about the influence of this issue is described in [11]. About this issue, the facilities

developed from the timber research group of the University of Trento, was designed to prevent the influence of the load application on the results. In the following paragraphs the main features of the apparatus will be introduced.

The horizontal displacement of the wall is provided by an hydraulic jack. A special device is connected to the actuator rod in order to release the rotation and the vertical sliding of the wall. The vertical joint, shown in the drawing, is a constraint only against horizontal displacement. Thus, for the "non-fully" anchored the wall uplift cannot introduce an additional stiffness against the rocking effect. To apply cyclic loading procedures the hydraulic jack is connected to a reacting plate to the opposite side of the wall with four steel bars.

The application of vertical loads was obtained by counterweights suspended on horizontal lever hinged on a fixed frame. Use of spherical hinges allowed the three-dimensional independent free displacement of the beams. Thanks to these rotational degrees of freedom the vertical loads magnitude is not influenced by the vertical uplift and at the same time the horizontal displacement is not influenced by the deformation of the wall. This part in the author opinion is one of key point that ensure several advantages compared to other system (i.e. vertical hydraulic actuators) which require a sophisticated control system in order to modify the jack pressure during the test in different point depending from the wall uplift. Moreover the position of the forces and the magnitude can be easily modified. The reaction forces on the top of the walls are related to the suspension points positions which can be easily moved along each lever. The position along the wall can be changed moving the spherical hinges through a steel guides along the support (beam of the reaction frame).

The steel basement is realized by two "c-shape" profiles spaced by a central cast of concrete which reproduce the frictional resistance between the wall and the foundation of the building. The angle brackets and the hold-downs of the walls are connected on the upper flanges of the channel (pre-drilled holes). Below these anchor holes a reinforcement system made by gusset plates was arranged. On the flanges of the metal profiles there are anchoring holes for angle brackets and hold down. The lateral overturning of the samples is avoided by two vertical metal braces connected to the frame. Between these structures and the surface of the sample panels in plastic material with low friction are positioned.

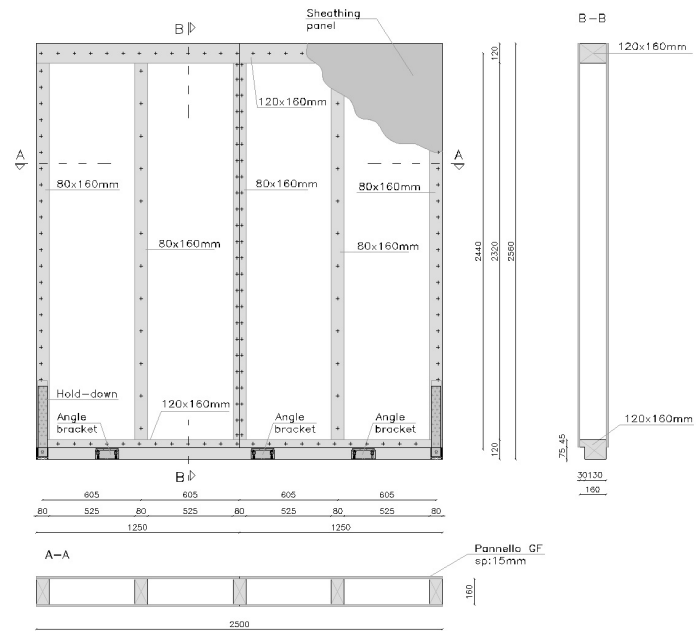


Figure 3.21: Geometry.

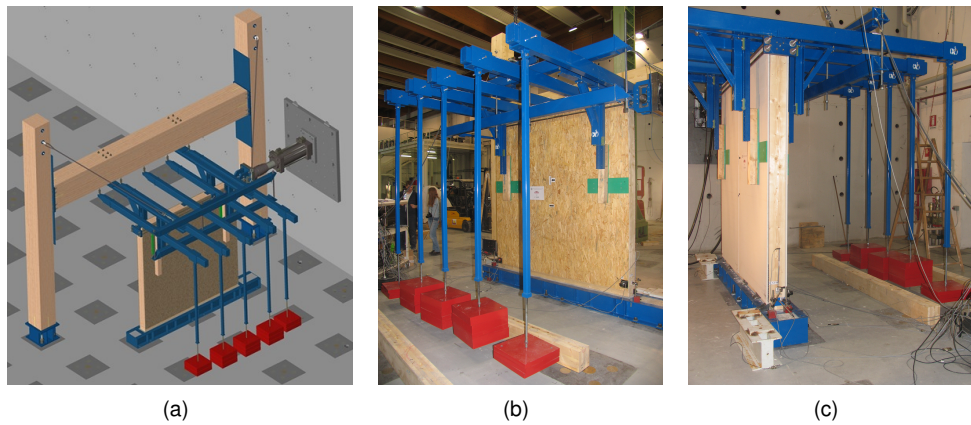


Figure 3.22: Test on shear walls.

Type:	Timber framed wall	
Description:	Timber framed walls braced by different sheathing panels connected to the timber frame through mechanical fasteners (staples). The walls were connected to the test setup by hold-down and angle brackets.	
Material:	Layout 1	Layout 2
Sheathing:	Oriented stands panels (OSB/3 1250x2500 x 15 mm) . Approval provided by EN 300 "Oriented Strand Boards (OSB) - Definitions, classification and specifications" and EN 13501-1 "Wood-based panels - Characteristic values for structural design Part 1: OSB, particleboards and fibreboards"	Gypsum fibre panels (1250 x 2500 x 12.5 mm on one side of the wall and 1250 x 2500 x 12.5 mm on the other). Approval provided by European organization for technical approvals ETA-03/0050 (14/11/2006)
Frame:	Double and triple laminated elements (graded C24 according to EN338). Top beam 120 x 160 mm, bottom beam 120 x 160 mm, studs 80 x 160 mm.	
Fasteners	Staples 1.35 x 1.59 x 45 mm according to the German technical approval Z-9-1-37 (26/03/2007)	
Spacing	The spacing between the fastener was 125 mm on the edge of the panels while on the internal studs was 250 mm	
Connections:	Three angle brackets (3.16) and hold down (3.7)	

Table 3.18: Materials

The displacement and force transducers arrangement is shown in Figure ref:fig:P20. The force and displacement transducer (1) and (2), mounted inside the hydraulic jack, have been used as reference instruments for the load vs displacement curve. Another sensor (7) was installed on the opposite side of the wall to measure the horizontal absolute displacement of the top of the wall (redundant measure). The linear potentiometers (3) and (4) are installed along the main diagonals of the walls to measure the shear deformation of the wall. The rocking effect (uplift of the wall) and the wall slippage are measured through the ldt (8) (9) and (10). This measure is strongly correlated to the tension in the hold-down forces measured by the dynamometric washers (11) and (6). The last instrument is connected to the steel base of the setup to detect if relative slip occurs.

In Figure 3.24, 3.25 and 3.26 are shown the load versus displacement curves of the monotonic and cyclic tests. The weaker component in both GFB and OSB sheathing layout was the connection between the boards and the timber frame whereas the anchor devices did not showed relevant damages. Two monotonic envelope curve were obtained from the cyclic tests according to the theory highlighted in 3.10. The reliability of this hypothesis is confirmed by the Figure 3.27 where the two curves are plotted on a chart. The envelope curve of the cyclic test (C_{GFB}) is closer to the monotonic load vs displacement curve M_{GFB} . Nevertheless in the monotonic tests on the failure load and the ultimate displacement were higher than the ones achieved during the cyclic test. The impairment of strength between the first and the

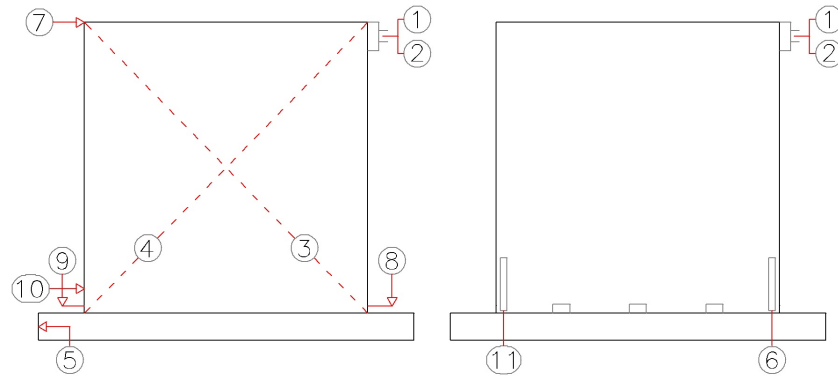


Figure 3.23: *Instrument arrangement*

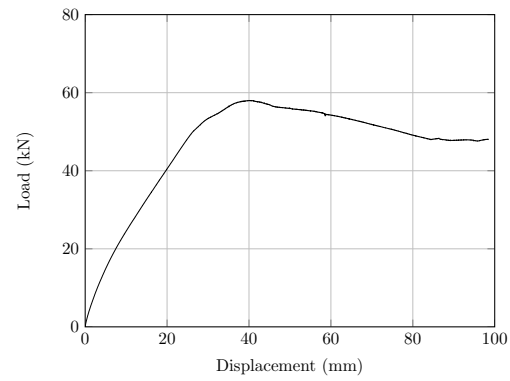


Figure 3.24: *Monotonic test (M_{GFB})*

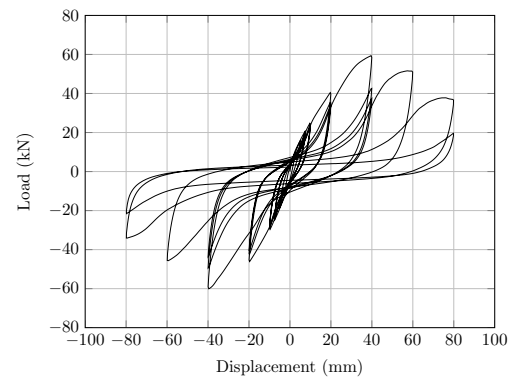


Figure 3.25: *Cyclic test (C_{GFB})*

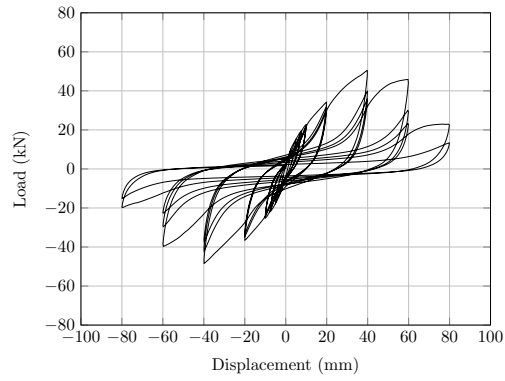


Figure 3.26: *Cyclic test (C_OSB)*

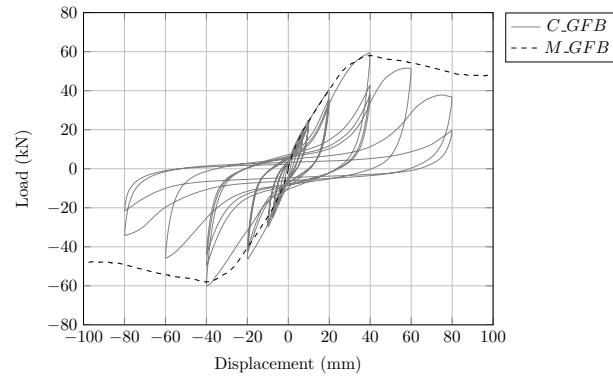


Figure 3.27: *Comparison between monotonic (M_GFB) and cyclic test (C_GFB)*

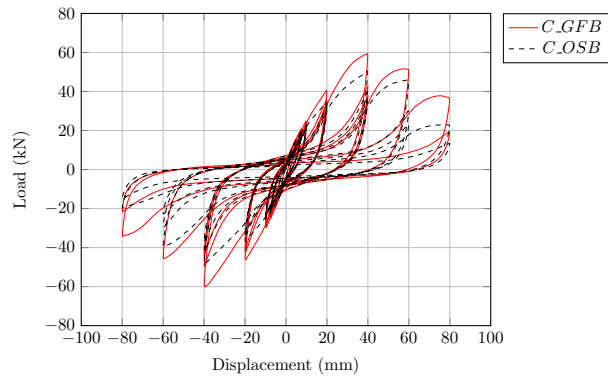


Figure 3.28: *Comparison between cyclic (M_OSB) and cyclic test (C_GFB)*

third cycle after the imposed displacement equal to 20mm is higher than the value proposed by the "conventional" failure criterion. The impairment of strength is due both to the yielding of the fasteners and to the withdrawal effect on the smooth shank of the staples. This failure mode was observed from different authors during tests campaign on the same connections (timber/gypsum fibre board) ([12] and [13]). The small shank diameters of the staples prevent cracking phenomena along the border of the panels when the wall is assembled but the level of ductility is lower compared to the ring nails adopted in the wood based panels. The oligo-cyclic fatigue failure and the withdrawal effect is showed in Figure 3.30.

On the contrary of the literature information and previous experimental campaigns [6], no significant pull-through and tear-off effects were observed on the panels and no out of plane failure were occur during the rests.

A further interesting consideration about the test results is the comparison of the results collected during a tests carried out with the same test setup but with different geometry (angle brackets and hold-down). In this previous test, carried out in the framework of the "chi-quadrato" research program, the connection were nailed above the gypsum fibre sheathing panels and the staple spacing was 100 mm along the edge of the panels and 200 mm [14]. figurename 3.29 show the load displacement curves for the two tests in the fully anchored condition.

The "fully anchored" displacement is obtained from the total displacement at the top of the wall (transducer *nr.7*) to which the contribution of the horizontal slippage (transducer *nr.10*) and rocking effect (transducer $nr.10 \cdot h/b$ and $nr.9 \cdot h/b$) have been removed. The last contribution take into account the uplift on the tension tie and the compression orthogonal to the grain of the sill beam and lower beam of the frame. The differences in terms of fasteners spacing (100 instead of 125 mm) is taken into account, approximately, multiplying the data acquired from the transducer *nr.2* (load-cell) by the ratio between the spacing in Figure 3.29(b). The rupture of the wall tested in the previous campaign [14] was caused by the out of plane failure of the panels.

This mode probably was emphasized by the constraint given by the hold-down and angle brackets which were directly nailed above the panels, however the direct comparison between the results, highlight a similar behaviour in terms of stiffness and load carrying capacity.

Test		M_GFB	MC_GFB	MC_OSB
F_{max}	[KN]	58.0	59.4	50.4
v_{max}	[mm]	40.2	39.6	39.8
F_u	[KN]	48.0	-	-
v_u	[mm]	100	-	-
$F_{0,1}$	[KN]	5.8	5.9	5.0
$v_{0,1}$	[mm]	1.5	1.2	0.9
$F_{0,4}$	[KN]	23.2	23.8	20.2
$v_{0,4}$	[mm]	9.2	9.2	8.2
F_y	[KN]	51.7	53.1	43.5
v_y	[mm]	21.9	22.4	19.4
K_s	[N/mm]	2253	2221	2079

Table 3.19: *Results of the monotonic tests and envelope curves.*

	C_GFB										C_OSb									
	0.75 Vy		1 Vy		2 Vy		4 Vy		6 Vy		8 Vy		0.75 Vy		1 Vy		2 Vy		4 Vy	
	I	II	I	III	I	III	I	II	I	III	I	II	I	II	I	III	I	II	I	II
$F_{max}+$ [kN]	20.7	19.8	24.9	24.0	23.5	23.5	40.6	35.7	34.0	37.4	51.6	-	19.3	18.8	22.7	21.9	21.5	34.1	39.7	35.6
$v F_{max}+$ [mm]	7.5	7.5	10.0	10.0	10.0	10.0	20.0	20.0	20.0	40.0	59.9	-	7.4	7.5	9.9	9.9	9.9	19.9	39.9	35.6
$F_{max}-$ [kN]	-24.7	-24.1	-23.6	-29.9	-28.3	-28.3	-46.2	-42.7	-40.7	-43.5	-45.8	-	-24.7	-24.1	-25.2	-24.3	-23.8	-34.4	-37.4	-37.4
$v F_{max}-$ [mm]	-7.5	-7.5	-10.0	-10.0	-10.0	-10.0	-20.0	-20.0	-20.0	-39.9	-59.9	-	-7.5	-7.5	-10.0	-10.0	-10.0	-20.0	-40.0	-40.0
E_d [J]	142.5	119.4	212.5	189.0	179.2	825.2	589.3	520.0	2304.3	1320.3	2568.3	-	119.4	97.4	176.3	155.0	147.5	690.2	1200.8	1040.1
E_p [J]	169.7	165.5	272.6	263.5	258.2	866.8	783.3	745.4	2386.2	1847.5	2918.6	-	164.0	148.5	238.0	229.7	225.6	704.6	1630.5	1456.2
v [%]	13.4	11.5	12.4	11.4	11.1	15.2	12.0	11.1	15.4	11.0	14.0	-	12.4	10.4	11.8	10.7	10.4	13.6	11.7	11.4

Table 3.20: Test results-cyclic protocol.

	C_GFB										C_OSb									
	0.75 Vy		1 Vy		2 Vy		4 Vy		6 Vy		8 Vy		0.75 Vy		1 Vy		2 Vy		4 Vy	
	I-II	I-III	I-II	I-III	I-II	I-III	I-II	I-III	I-II	I-III	I-II	I-III	I-II	I-III	I-II	I-III	I-II	I-III	I-II	I-III
$\Delta F_{max}+$ [kN]	0.5	0.9	0.9	1.4	5.0	5.0	4.9	6.6	8.1	16.5	10.3	-	0.5	0.9	0.8	1.1	4.5	2.4	3.7	6.8
$\Delta F_{max}-$ [kN]	0.6	1.1	1.0	1.5	6.0	3.5	3.5	5.5	9.2	10.4	16.5	-	0.6	1.1	0.9	1.4	5.0	2.1	3.3	7.3

	C_GFB										C_OSb									
	0.75 Vy		1 Vy		2 Vy		4 Vy		6 Vy		8 Vy		0.75 Vy		1 Vy		2 Vy		4 Vy	
	I-II	I-III	I-II	I-III	I-II	I-III	I-II	I-III	I-II	I-III	I-II	I-III	I-II	I-III	I-II	I-III	I-II	I-III	I-II	I-III
$\Delta F_{max}+$ [kN]	0.5	0.9	0.8	1.1	4.5	2.4	3.7	6.8	10.7	14.9	10.1	-	0.5	0.9	0.8	1.1	4.5	2.4	3.7	6.8
$\Delta F_{max}-$ [kN]	0.7	1.2	0.9	1.4	5.0	2.1	3.3	7.3	6.4	11.0	9.7	-	0.7	1.2	0.9	1.4	5.0	2.1	3.3	7.3

Table 3.21: Test results-cyclic protocol, impairment of strength.

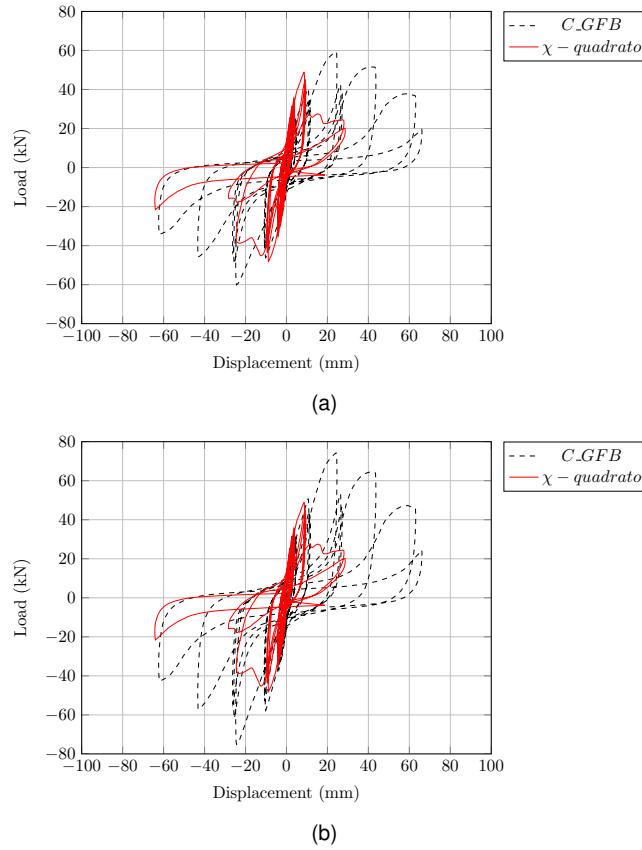


Figure 3.29: Comparison between load vs displacement curves for different configurations (fully anchored). a) actual recorded load - b) modified load (multiplied by the ratio between the two different nails spacing)

Figure 3.31, 3.32, 3.33, 3.34 and 3.35 shown the load-displacement curves obtained from analysis of the data acquired by the sensor 6 - 8 and 9 - 11. The plot of the load-displacement curves correspond to the actual until the failure of the weaker element of the wall. After the yielding of this component the system cannot increase the load and the full capacity of the other elements are not exploited. The same operation cannot be performed on the angle bracket devices, in this case the accuracy is lower because different effects influence the force distribution and the friction force is cannot be quantified.

The contribution of the friction force (pre-sliding) according to the Coulomb approximate model is governed by the equation $F_f = \mu \cdot V$. Thus for a vertical load of $20kN/m$ and an additional contribution caused by the overturning moment due to the

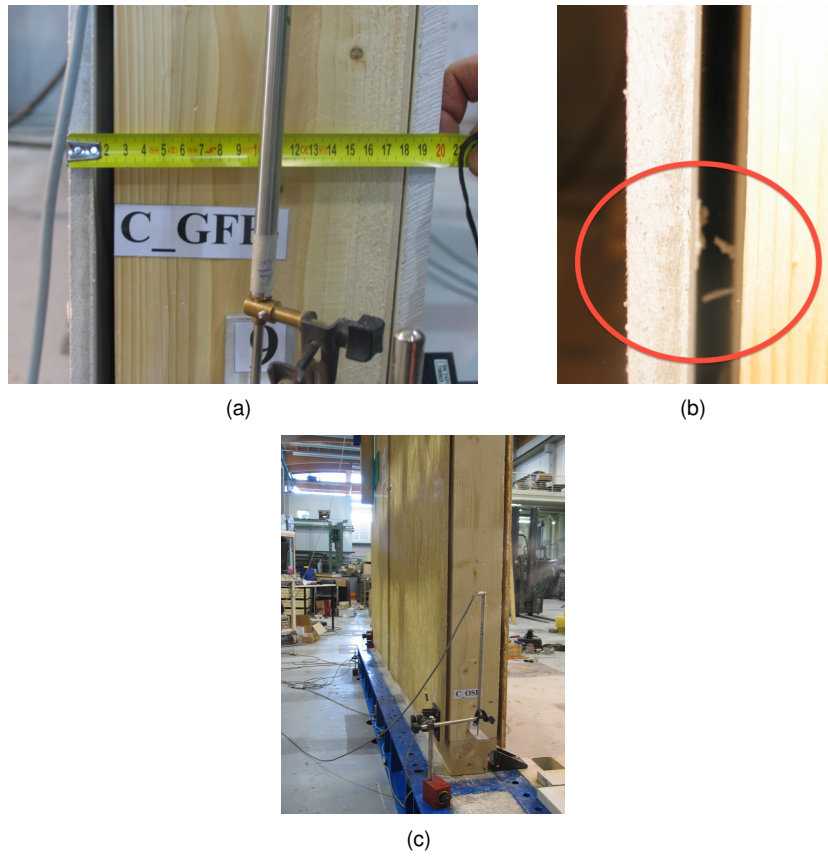


Figure 3.30: *Failure of the connection between timber frame and sheathing panels.*

horizontal force the maximum friction force is about $(50 + 60) \cdot 0.4 = 44kN$.

The displacement of the wall is caused by the force that exceed the friction force ($60 - 44 = 16kN$) therefore, assuming a constant distribution on the three devices, the force on the single angle bracket is about $16/3 = 5.3kN$. On the force vs displacement curve acquired during the test described in the previous section the value of slip corresponding to this value ($5.3kN$) is close to the value observed in the test on shear wall.

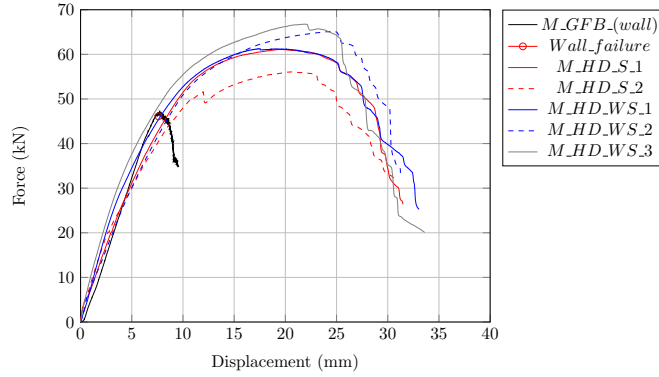


Figure 3.31: Load vs displacement curve of the hold-down from different tests (test on full scale wall M_GFB - transducer (8) and load cell (6) and from monotonic tests on single component (LVDT) (MTS))

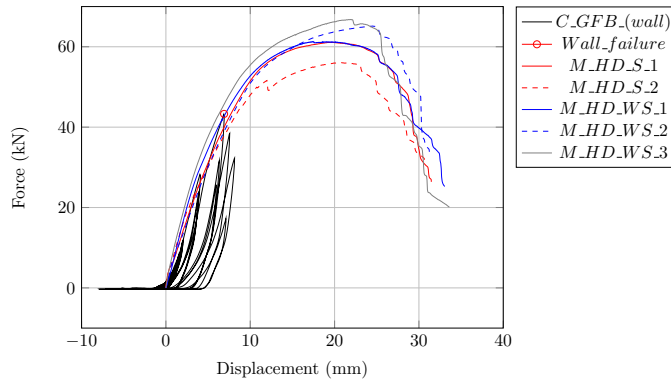


Figure 3.32: Load vs displacement curve of the hold-down from different tests (test on full scale wall C_GFB - transducer (8) and load cell (6) and from monotonic and cyclic tests on single component (LVDT) (MTS))

As shown in the previous picture a good agreement was found between the results of the test on small specimens (hold-down and angle bracket) and the outcome of the full scale tests.

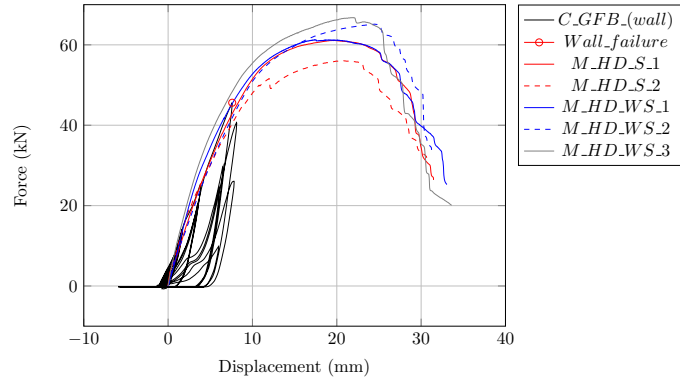


Figure 3.33: Load vs displacement curve of the hold-down from different tests (test on full scale wall C_GFB - transducer (9) and load cell (11) and from monotonic and cyclic tests on single component (LVDT) (MTS))

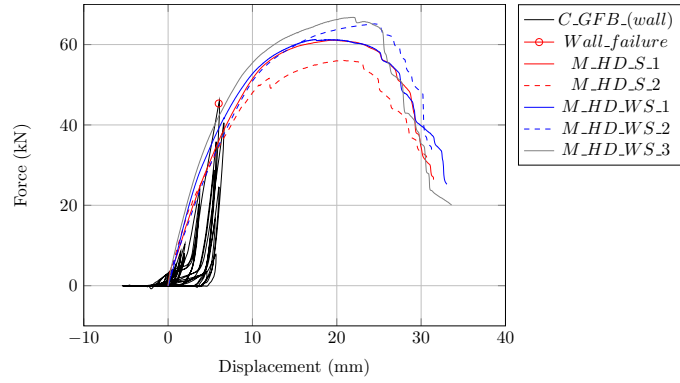


Figure 3.34: Load vs displacement curve of the hold-down from different tests (test on full scale wall C_OSB - transducer (8) and load cell (6) and from monotonic and cyclic tests on single component (LVDT) (MTS))

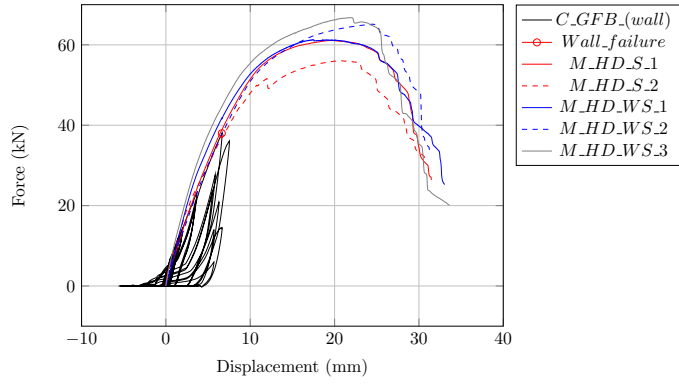


Figure 3.35: Load vs displacement curve of the hold-down from different tests (test on full scale wall C_OSB - transducer (9) and load cell (11) and from monotonic and cyclic tests on single component (LVDT) (MTS))

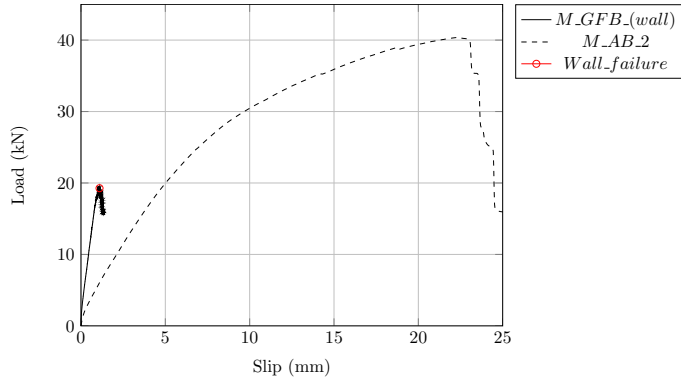


Figure 3.36: Load vs displacement curve of the angle brackets from different tests (test on full scale wall M_GFB - transducer (10) and load cell (2- divided by the number of angle brackets) and from monotonic tests on single component (MTS))

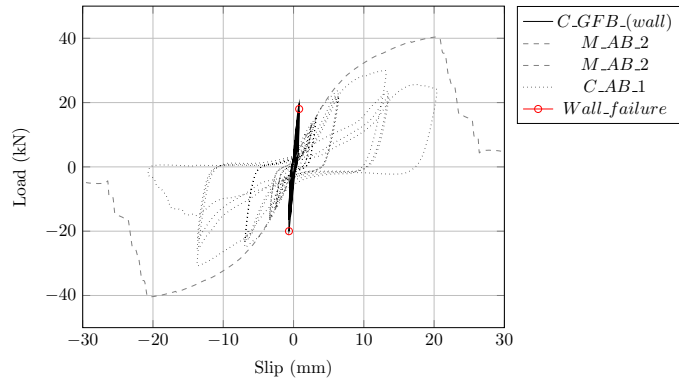


Figure 3.37: Load vs displacement curve of the angle brackets from different tests (test on full scale wall *C_GFB* - transducer (10) and load cell (2- divided by teh number of angle brackets) and from monotonic and cyclic tests on single component (MTS)

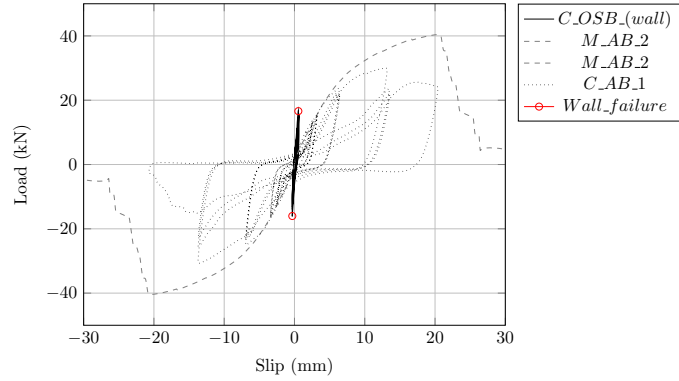


Figure 3.38: Load vs displacement curve of the angle brackets from different tests (test on full scale wall *C_OSB* - transducer (10) and load cell (2- divided by teh number of angle brackets) and from monotonic and cyclic tests on single component (MTS)

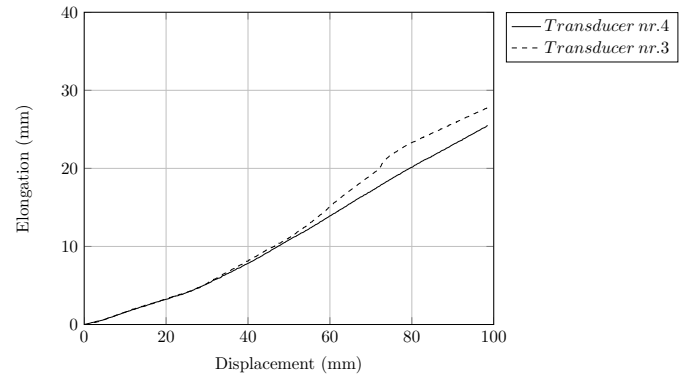


Figure 3.39: Elongation of the main diagonals vs the horizontal imposed displacement

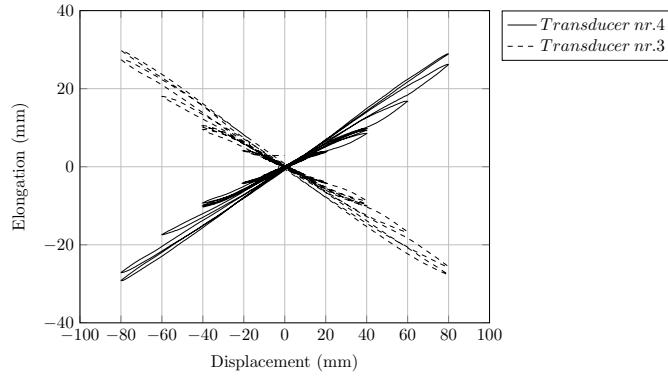


Figure 3.40: *Elongation of the main diagonals vs the horizontal imposed displacement*

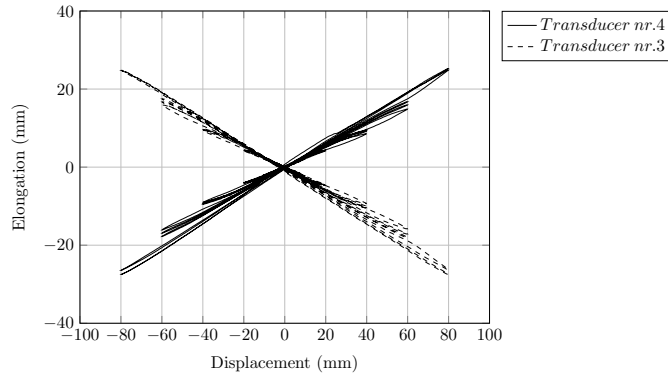


Figure 3.41: *Elongation of the main diagonals vs the horizontal imposed displacement*

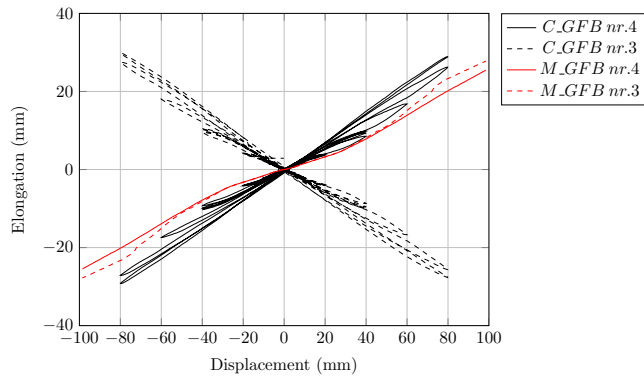


Figure 3.42: *Comparison between M_GFB and C_GFB - elongation of the main diagonals vs the horizontal imposed displacement*

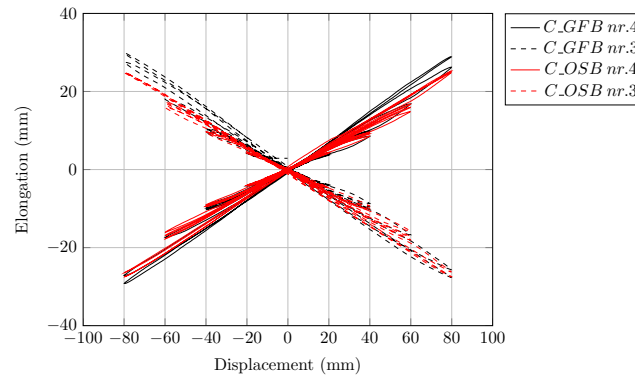


Figure 3.43: Comparison between C_GFB and C_OSB - elongation of the main diagonals vs the horizontal imposed displacement

3.1 Theoretical considerations

3.1.1 Hold-down

Load bearing capacity

The hold down components were designed according to the European design codes EN 1995-1 [1] and the Italian code D.M. 14/01/2008 [15]. The load bearing capacity of the system is calculated as the minimum value between the failure modes that can occur in:

- steel to timber nailed connection;
- steel plate;
- connection between pre-drilled plate and base (bolt);
- anchor system between the foundation and the steel base.

In the following paragraphs an analytical provisions of the capacity in terms of resistance and stiffness will be presented. The load bearing capacity of the steel to timber connection was calculated according to the "European yield model". This method, originally proposed in 1949 by K.W. Johansen, nowadays is one of the most reliable and widespread methods to estimate the load bearing capacity of dowel type connection. This model take into account the contribution of the yield strength, the embedment strength, and the withdrawal strength of the fastener. This strength, according to the failure mode that depend from the geometry of the connection, is fully

exploited only if brittle failure (plug shear, block shear) are prevented. Thus the general formulae is:

$$F_{v,Rk} = \min (F_{v,ef,Rk,1}; F_{bs,Rk})$$

The first term on the right side of the previous equation is the total capacity of the fasteners. The characteristic nails load-carrying capacity per shear plane per fastener, depend on the mechanical parameters (timber embedment strength $f_{h,k}$, fastener yield moment $M_{y,Rk}$ and withdrawal capacity $F_{ax,Rk}$) and from the geometry of the steel plate (thickness and the tolerance on hole diameters). Concerning the influence of the steel plate geometry on the mechanical behaviour two different cases can be identified. The first one "thin plate" occur when the thickness is less than or equal to 0,5 times the fastener diameter. The second "thick plate" occur when the thickness is greater than or equal to the diameter of the fasteners. Nevertheless when the tolerance on hole diameters is greater than 0,1 of the diameter of the fasteners the behaviour of the connection should be considered as "thin plate". For the two case the load bearing capacity of a ringed shank nail (diameter, d - penetration depth, t_1) is calculated as the minimum value found from expressions:

$$F_{v,Rk,1} = \min \begin{cases} f_{h,k} t_1 d & \text{(c)} \\ f_{h,t} t_1 d \left[\sqrt{2 + \frac{4 M_{y,Rk}}{f_{h,k} d t_1^2}} - 1 \right] + \frac{F_{ax,Rk}}{4} & \text{(d) Thick plate} \\ 2,3 \sqrt{M_{y,Rk} f_{h,k} d} + \frac{F_{ax,Rk}}{4} & \text{(e)} \end{cases}$$

$$F_{v,Rk,1} = \min \begin{cases} 0,4 \cdot f_{h,k} \cdot t_1 \cdot d & \text{(a)} \\ 1,15 \cdot \sqrt{2 \cdot M_{y,Rk} \cdot f_{h,k} \cdot d} + \frac{F_{ax,Rk}}{4} & \text{(b) Thin plate} \end{cases}$$

Where the characteristic fastener yield moment and the characteristic withdrawal capacity are given by the product data-sheet $M_{y,Rk} = 6550 Nmm$ $F_{ax,Rk} = 1.22 kN$ and the characteristic embedment strength in the timber member, assuming a $\rho_k = 350 kg/m^3$ according to the timber C24 grading, is calculated as:

$$f_{h,k} = 0.082 \cdot \rho_k \cdot d^{-0.3} = 18.9 MPa$$

The different failure modes according to the two formulations are illustrated in Figure 3.44. For the "thick plate" the fastener support is considered as a fixed constrain.

The steel plate provide sufficient rotation resistance, thus the formation of the plastic hinge occur immediately at the surface of the steel plate (failure mode d,e). In the "thin plate" the support of the fastener is assumed as pin-jointed constrain. The steel plate allow free rotation and so no plastic hinge can be formed on the end of the fastener (a,b). In the author opinion the more reliable condition is the "thick plate" because the ringed shank nails geometry, and in particular the conical under-head $\phi_{min} = 4mm$ and $\phi_{max} = 5.4mm$ is optimized for the steel to timber connections. As a consequence the load bearing capacity of a single nail is $1.92kN$

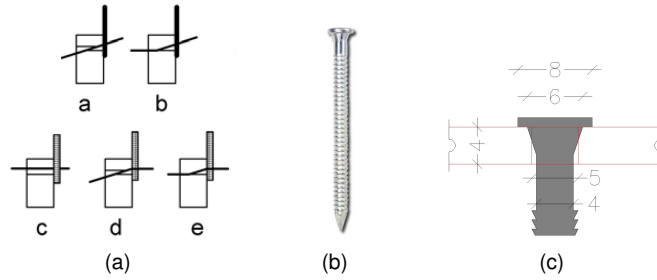


Figure 3.44: Steel to timber connection - a) failure mode according to the [1] formulation - b) ringed shank nail - c) under-head geometry.

The total strength of the nailed joint should be calculated using the effective number of fasteners n_{ef} . The possible reduction of the number of fasteners take into account the stress distribution, according to EN1995 the reduction is calculated as:

$$n_{ef} = n^{K_{ef}}$$

Where n_{ef} is the effective number of nails in the row, n is the number of nails in a row and K_{ef} is a coefficient (from 1 to 0.5) which depend from the fasteners spacing along the row. For the geometry of the hold-down element K_{ef} is equal to 0,897 and the effective nails is 22 (6 nails per row - 4 rows plus 2 additional nails on the bottom of the flange). The rules proposed by the European yielding model (EYM) are based on the plastic limit state analysis assuming an ideal rigid plastic material-law both for timber and steel. Nevertheless this theory is valid only if brittle failure in the timber elements are prevented. Consequently the rules adopted for the minimum spacing between the fasteners and the edge/end-distance have been implemented to prevent the - "splitting", "plug shear" and "group tear out". The load bearing capacity for the "block shear" and "plug shear" failure can be estimated by the rules reported in appendix A of [1]. *The characteristic load carrying capacity of fracture along the*

perimeter of the fastener area, as shown in Figure 3.45(a) (block shear failure) and Figure 3.45(b) (plug shear failure), should be taken as:

$$F_{bs,Rk} = \max \begin{cases} 1,5 A_{net,t} f_{t,0,k} \\ 0,7 A_{net,v} f_{v,k} \end{cases}$$

Where $A_{net,t} = 1495 \text{ mm}^2$ is the net cross-sectional area perpendicular to the grain, $A_{net,v} = 27269 \text{ mm}^2$ is the net shear area in the parallel to grain direction, $t_{ef} = 18,6 \text{ mm}$ is the effective depth depending of the failure mode of the fastener in this case (e), $f_{t,0,k} = 14 \text{ MPa}$ is the characteristic tensile strength of the timber member - C24 [16], $f_{v,k} = 4 \text{ MPa}$ is the characteristic shear strength of the timber member - C24 [16].

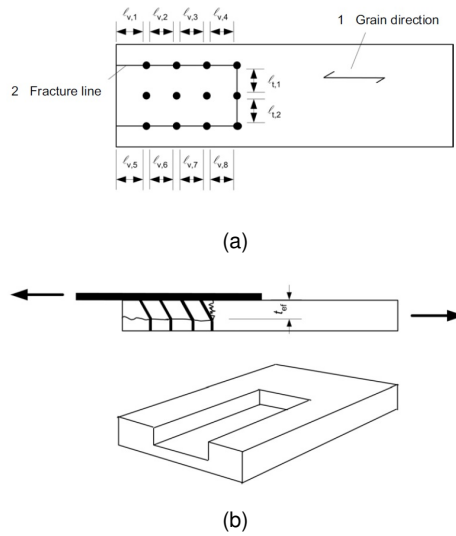


Figure 3.45: Brittle timber failure modes [1] - a) block shear failure - b) plug shear failure.

The value $F_{bs,Rk}$ for the geometry presented in the previous section is 76 kN , hence the resistance of the connection is related to the fasteners load bearing capacity $F_{v,ef,Rk,1} = n_{eff} \cdot F_{v,Rk,1} = 42,3 \text{ kN}$. This value correspond to a design resistance, for the fundamental combinations, of 35.7 kN ($\gamma_m = 1.3$; $k_{mod} = 1.1$) according to EN1995 and 28.2 kN ($\gamma_m = 1.5$; $k_{mod} = 1.0$) according to [15]. For the accidental combination the values are respectively 46.7 kN ($\gamma_m = 1$; $k_{mod} = 1.1$) and 28.2 kN ($\gamma_m = 1.5$; $k_{mod} = 1.0$). The partial factor adopted in the ULS according to the [15] is higher than the [1] although a value equal to 1 is reported for the accidental

combinations because the detailed rules for the oligo-cyclic loads influence are not provided.

The the strength of the steel plate and the load bearing capacity of the connection between pre-drilled plate and base (bolt) are verified according to the rules of the [17]. The flange can fail by reaching one of the limit condition "net section" fracture or the "gross section" yielding.

$$N_{t,Rd} = \min \left\{ \begin{array}{l} N_{pl,Rd} = \frac{A f_{y,k}}{\gamma_{M0}} \\ N_{u,Rd} = \frac{0,9 A_{net} f_{t,k}}{\gamma_{M2}} \end{array} \right.$$

Where:

$f_{y,k} = 235 \text{ MPa}$ is the yield strength S235;

$f_{t,k} = 360 \text{ MPa}$ is the ultimate strength S235;

$A = 224 \text{ mm}^2$ is the gross section area;

$A_{net} = 184 \text{ mm}^2$ is the net section area;

$\gamma_{M0} = 1,05$ is the partial factor for resistance of cross-sections whatever the class is;

$\gamma_{M2} = 1,25$ is the partial factor for resistance of cross-sections in tension to fracture.

The resistance of the steel plate is 47.7 kN both for EN 1993 [17] and the Italian code D.M. 14/01/2008 [15] the only difference between these two code is the partial factor $\gamma_{M0} = 1,0$ instead of 1.05 as proposed by D.M. 14/01/2008.

The failure of the connection between the pre-drilled flange and the steel base occur if the load bearing capacity of the bolt ($\phi 16 \text{ mm cl } 8.8$) is exceeded, according to EN 1993-1-8 this capacity is calculated as:

$$F_{v,Rd} = \frac{0,6 f_{t,b} A_{res}}{\gamma_{M2}} = 60,3 \text{ kN}$$

Where $f_{t,b} = 800 \text{ MPa}$ is the ultimate tensile strength of the bolt, $A_{res} = 157 \text{ mm}^2$ is the tensile stress area of the bolt A_s and $\gamma_{M2} = 1,25$ is the partial safety factors for joints. The bearing resistance $F_{b,Rd}$ is:

$$F_{b,Rd} = \frac{k \alpha f_{t,k} d t}{\gamma_{M2}} = 79,0 \text{ kN}$$

Where:

$$k = \min \left[2, 8 \frac{e_2}{d_0} - 1, 7; 2, 5 \right] = 2, 5;$$

$$\alpha = \min \left[\frac{e_1}{3 d_0}; \frac{f_{t,b}}{f_{t,k}}; 1 \right] = 0, 49;$$

$t = 4 + 10 = 14 \text{ mm}$ is the thickness of the plate.

The last component of the connection is the anchor bolt. The eccentricity between the anchor bolt and the steel flange introduce an additional force on the fastener as reported in Figure 3.46.

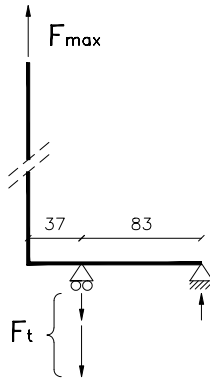


Figure 3.46: Effect of the eccentricity between bolt and pre-drilled plate.

The tension resistance of a 8.8 graded bolt, according to the notation list of the previous case, is:

$$F_{t,Rd} = \frac{0,9 f_{t,b} A_{res}}{\gamma_{M2}} = 90,4 \text{ KN} > F_t$$

However the actual force on the hold down element (on the same alignment of the nails) can be estimated as:

$$F_t = F_{max} \left(\frac{83 + 37}{83} \right)$$

The tensile force that introduce the failure of the anchor bolt is 62.5 kN . The minimum between the values calculated for each component of the device is the design load Table 3.22. This value, if the hold-down device is assumed as "dissipative joint", should ensure a good ductility without brittle failure rupture. Furthermore the other components should exhibit adequate over-strength.

Component	Characteristic values [kN]		Mechanisms			
			Design values [kN]			
Steel to timber	Nails	Block failure	Nails (EC5)	(DM2008)	Block failure	(DM2008)
	42.2	76.3	46.5	28.2	84.0	50.9
Steel plate	Net area	Gross area	Net area		Gross area	
	59.6	52.6	47.7		52.6	
Connection	Shear	Bearing	Shear		Bearing	
	75.4	98.8	60.3		79.0	
Anchor	Tension		Tension			
	78.1		62.5		62.5	

Table 3.22: Characteristic and design values of the hold-down connection.

The mean value of the load bearing capacity of the connection, necessary to perform the comparison with the mean experimental values, are calculated according to the rules provided by EN 14358:2007 [18].

$$\bar{y} = \frac{F_k}{1 - k \cdot CoV}$$

where:

- \bar{y} is a stochastic mean value;
- k is a factor which depend from the number of test specimens;
- CoV coefficient of variation;

For tests with infinite number of specimens, a p-percentile of $p = 5\%$ and a confidence level of $\alpha = 75\%$ the factor k is given as 1.65 [18]. The variation for wood is reported to be 15-25 % in dependence on the grading class. Not knowing the actual grading class of the used timber, it seems reasonable to assume $CoV = 0.2$, thus the reference value results to be:

$$\bar{y} = \frac{F_k}{1 - 1.65 \cdot 0.2} = 1.493 \cdot F_k$$

However in dependence on the actual timber quality \bar{y} can range from 1.3 and 1.7 times the characteristic resistance value F_k . The comparison between the results are summarized in Table 3.23.

Characteristic value (k)	Mean value (m)		
	CoV = 0.15	CoV = 0.2	CoV = 0.25
42.2	56.1	63.0	71.9

Table 3.23: Mean values of the hold-down connection.

As shown in Figure 3.47 the maximum values of the load vs displacement curves are well approximated by the line that correspond to the mean values calculate from the EYM and the equation proposed in EN 14358:2007.

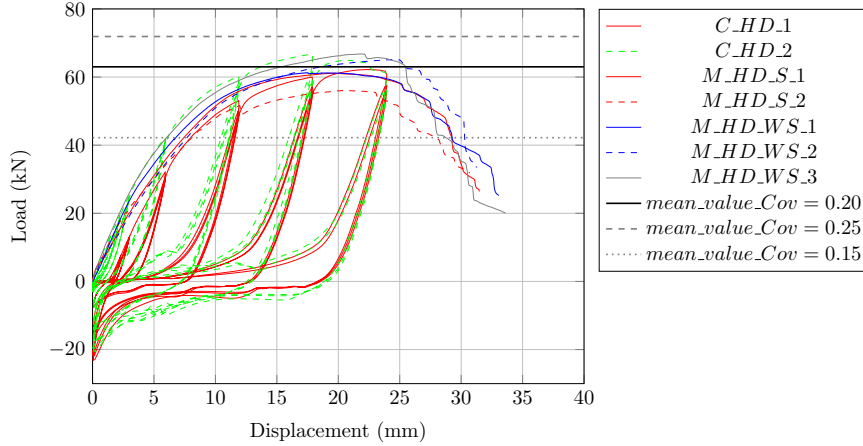


Figure 3.47: Comparison between mean value form analytical models and experimental results .

Stiffness

The device can be idealized as a three main springs connected according the "in series" connection. The first spring represent the connection between the pre-drilled plate and the timber stud. The second one represent the pre-drilled steel plate whereas the third represent the base Figure 3.48. The mechanical characterization of the springs is carried out by analytical model and experimental value.

The stiffness of the steel to timber connection is obtained from the formulae introduced in section 3.0.1 and, as discussed in that paragraph, for the nailed connection the results overestimate the actual values (1740N/mm instead of 550N/mm). However also the experimental values obtained in "pure-shear" test configuration overestimate the actual stiffness of this part of the device. The actual stiffness for single fastener equal to 291N/mm , is calculated from the analysis of the results (transducer AEP-LVDT). The comparison between the result is reported in Figure 3.49

As discussed in the previous section the stiffness of a joint is strongly influenced by the test setup and by the loading condition. Small variations on the layout can lead to different values. In the author opinion the difference in terms of stiffness is attributable to the withdrawal effect introduced by the eccentricity between the steel

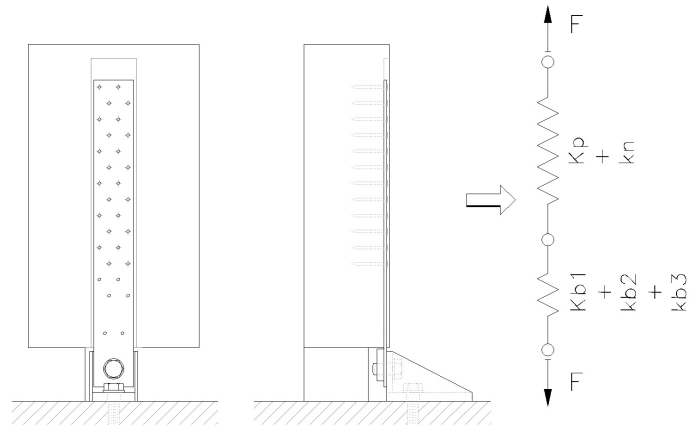


Figure 3.48: Component of the hold down device .

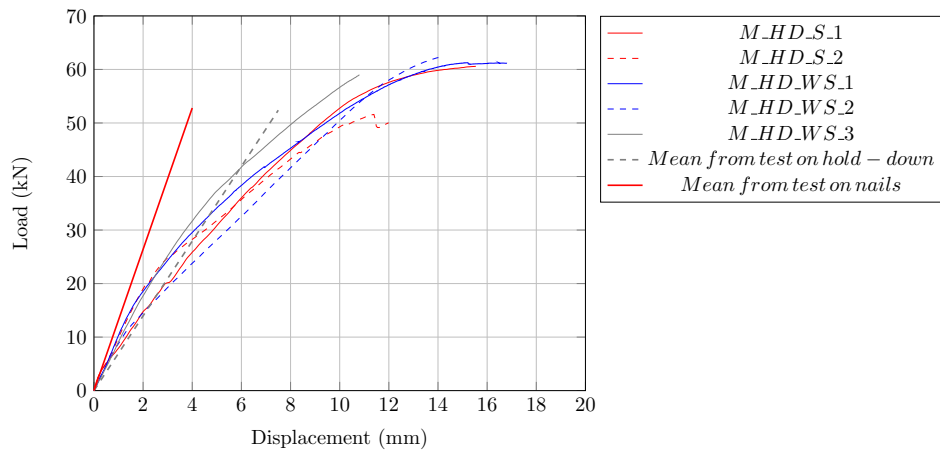


Figure 3.49: Comparison between stiffness mean of the steel to timber connection .

plate and the anchor bolt. As reported in the technical approvals of similar commercial devices the load bearing capacity of the lower nails of the connection is not take into account. Moreover the value k_{ser} is strongly influenced by the shape of the load vs displacement curve. Another parameter influenced by the shape of the curve is the yielding point. Different formulations have been proposed by various authors to obtain a reliable procedure for a load-slip curve without two well-defined linear parts (otherwise the definition is unique). In this thesis the formulation proposed by the EN 12512 were adopted in order to perform comparison between the results and the prescription presented in the code. A detailed review about this argument is reported in [19].

The second spring represent the deformation of the steel plate. The analytical model is based on the analysis of a steel plate loaded by a "triangular" force distribution as shown in Figure 3.50. Each load step correspond to the total load F divided by the number of rows(12).

$$K_p = \frac{F}{\Delta L}$$

where:

$$\Delta L = \int_0^L \varepsilon(x) dx = \int_0^L \frac{\sigma(x)}{E} dx$$

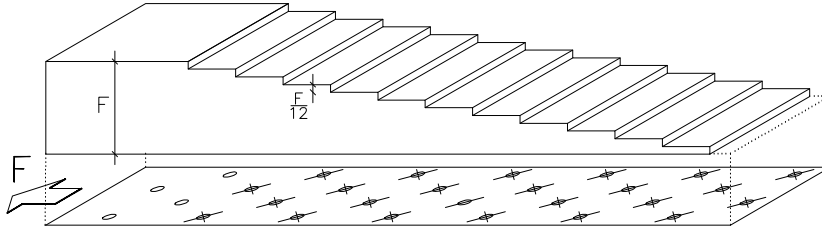


Figure 3.50: Force distribution in the pre-drilled plate.

Assuming the spacing between the row $sp = 22.5mm$, the diameter of the holes $\phi = 5mm$, thickness $t = 4mm$, width $b = 56mm$ and the module of elasticity $E = 210000MPa$ the total elongation of the element is:

$$\Delta L = \frac{F}{A_{net} E} \left[\frac{1}{12} sp + \frac{2}{12} sp + \dots + sp \right] = F \cdot 3,78 \cdot 10^{-6} mm$$

$$K_p = \frac{F}{\Delta L} = 264205 N/mm$$

The equivalent stiffness calculated assuming the net area of the cross section ($A_{net} = 4 \cdot (56 - 5 - 5) = 184 \text{ mm}^2$) is a lower limit of the stiffness; Considering the gross area ($A_{net} = 4 \cdot 56 = 224 \text{ mm}^2$) the stiffness is 321641 MPa . The actual stiffness may consider the plate as a sum of the contribution of gross area and net area elongation. However compared to the stiffness of the previous contribution the assumption of a simplified net area equivalent stiffness is reasonable. Moreover a good agreement with the experimental results of the tests on the steel to timber connection is reached.

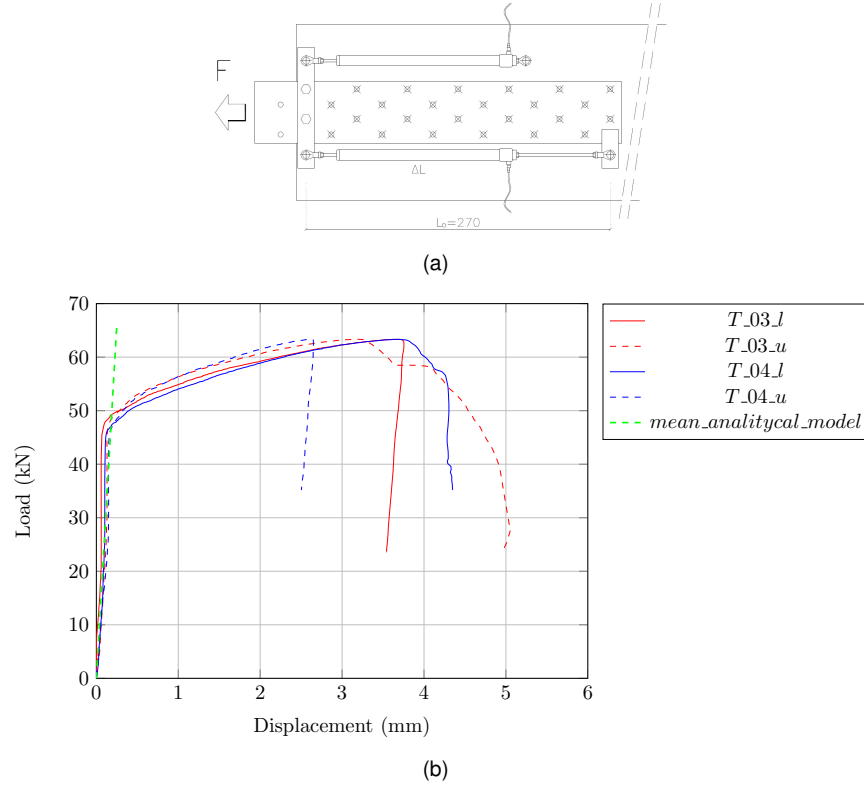


Figure 3.51: Pre-drilled steel plate - a) Test setup adopted in the previous tests - b) results of experimental tests and analytical model.

The last spring represent the steel base (b1), the anchor bolt (b2) and the lower part of the steel flange(b3). In order to calculate the deflection of this component a simplified "c" cross section was assumed Figure 3.52.

$$K_{eq,b1} = \frac{F}{\Delta L} = \frac{10000}{0.17} = 58823 \text{ N/mm}$$

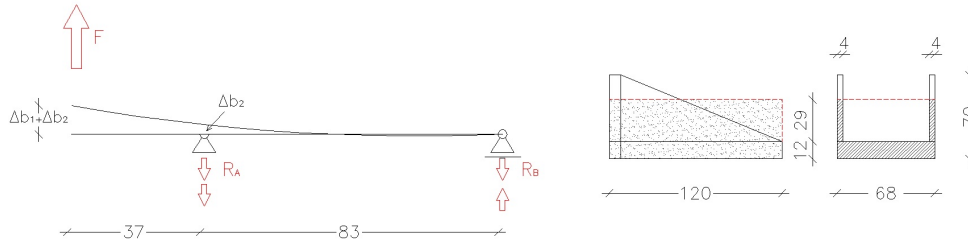


Figure 3.52: Deflection of the steel base.

$$K_{eq,b2} = \frac{E \cdot A_B}{L} \cdot \frac{83}{83 + 37} = \frac{210000 \cdot 0.9 \cdot \pi \cdot d^2}{4 \cdot 20} \cdot 0.69 = 1.31 \cdot 10^6 \text{ N/mm}$$

$$K_{eq,b3} = \frac{E \cdot A_f}{L} = \frac{210000 \cdot 4 \cdot 56}{52.5 + 50} = 418133 \text{ N/mm}$$

$$K_b = \frac{1}{\frac{1}{K_{b1}} + \frac{1}{K_{b2}} + \frac{1}{K_{b3}}} = \frac{1}{\frac{1}{58823} + \frac{1}{1310000} + \frac{1}{418133}} = 49615.2 \text{ N/mm}$$

As for the previous components the stiffness value is compared with the test results presented in section 3.0.2. In order to estimate the influence of the steel part elongation two monotonic tests were carried out Figure 3.53. The uplift of the anchor bolt and the total uplift of the steel base were measured (the total elongation was strongly influenced by the load application system). The test results are showed in Figure 3.54.

The bolt influence of the system is calculated taking into account the effect of the bending moment due to the eccentricity. When a total load of $20kN$ is applied by the test machine the Idt measure a total bolt head uplift of $0.05mm$. However the bolt length ($56mm$) is different from the hold down tests ($20mm$), so the total stiffness is multiplied by a corrective coefficient and also the effect of the lever arm is taken into account through a corrective coefficient.

$$K_{eq,b2} = \frac{F \cdot \frac{83+37}{120}}{\Delta L} \cdot \frac{56}{20} = 1.62 \cdot 10^6 \text{ N/mm}$$

The stiffness of the steel base is calculated by the measure acquired from the linear transducer connected on the back of the sample as shown in Figure 3.53(b). However the displacement is affected also by the rigid rotation due to the bolt elonga-

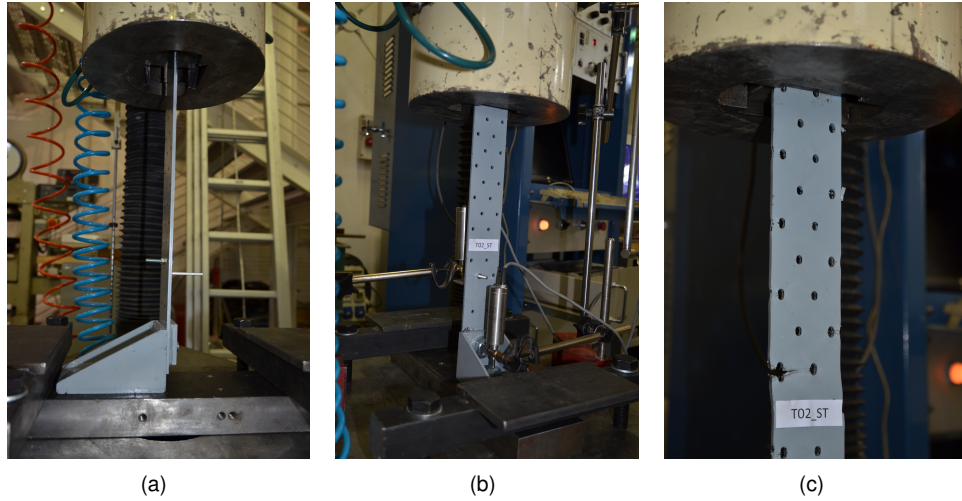


Figure 3.53: Test on the steel components - a) sample - b) measurement instruments arrangement - c) failure.

tion. The deflection of the steel base is calculated according to the "in series spring" scheme as:

$$K_{eq,b1+b2} = 18000 \text{ N/mm}$$

$$K_{eq,b1+b2} = \frac{1}{\frac{1}{k_{b1}} + \frac{1}{k_{b2}}} \text{ N/mm}$$

$$K_{eq,b1} = 18201 \text{ N/mm}$$

The value of stiffness from the analysis of the outcome of the test seems reasonable only for the bolt contribution. Probably, in the author opinion, the influence of the rotation of the steel flange (compared to the measurement range) make the measurement is unreliable. The stiffness of the system (b_1 , b_2 , b_3) is also measured directly by during the test on the hold down devices 3.0.2. The displacement acquired through the transducer "AEP" represent the sum of the elongation of the steel plate and the base. Figure 3.55 show the comparison between the analytical simplified approach and the experimental results.

The comparison between the analytical approach and the experimental results is shown in Figure 3.56.

As visible when the "fully analytical" approach is adopted both for steel to timber

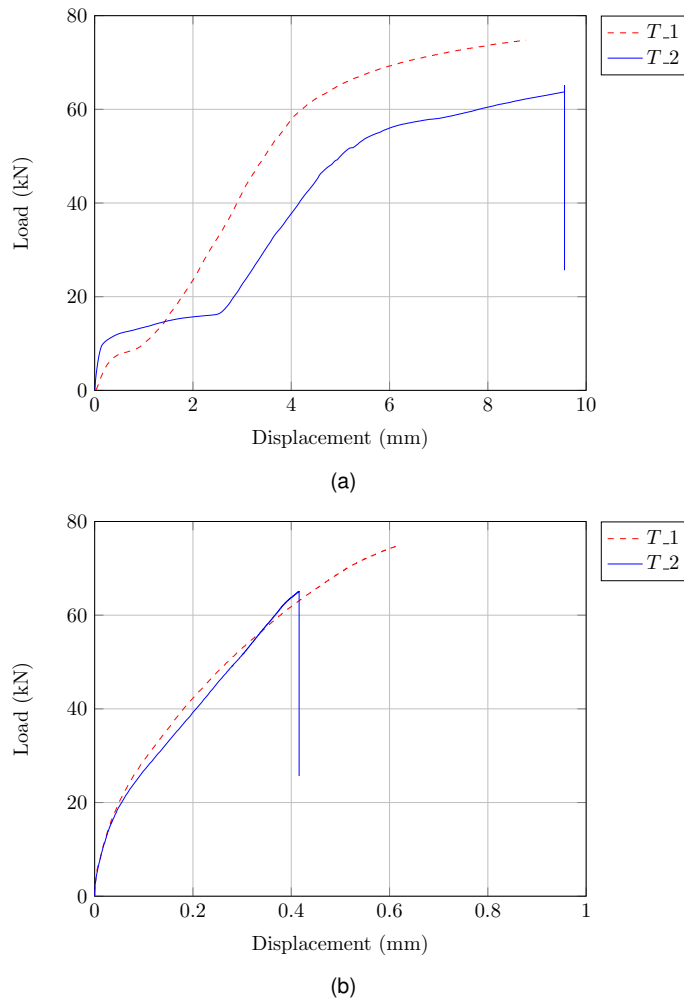


Figure 3.54: Test on the steel components - a) base - b) bolt.

connection and steel parts the elastic stiffness of the system is overestimated. Using a "hybrid" approach where the mean experimental value for k_{ser} from the test presented in 3.0.1 is assumed for the steel to timber component the results is clearly more reasonable.

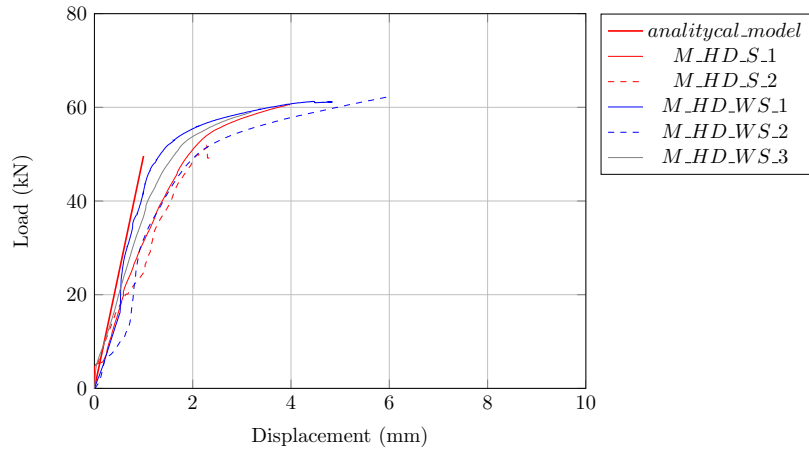


Figure 3.55: Steel base and anchor bolt contribution to the system stiffness-comparison between the experimental values and the elastic stiffness calculated by analytical simplified models.

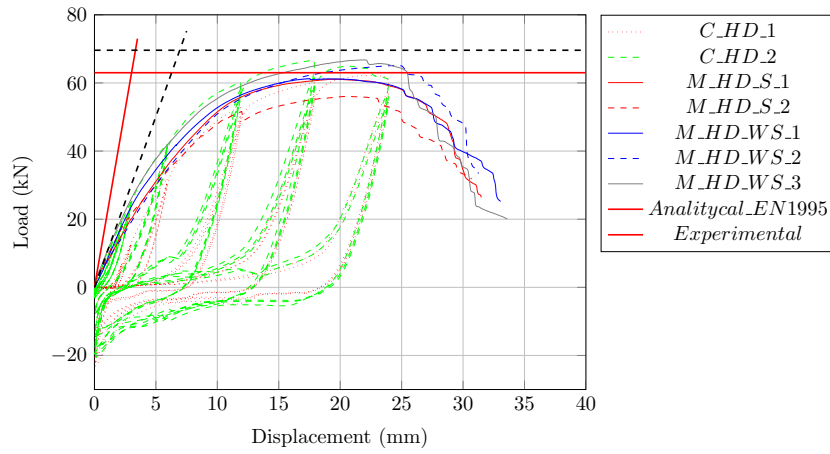


Figure 3.56: Comparison between the analytical and experimental stiffness / load bearing capacity.

3.1.2 Angle brackets

Load bearing capacity

The angle brackets were designed according to the European design codes EN 1995-1 [1] and the Italian code D.M. 14/01/2008 [15]. The load bearing capacity of the system is calculated as the minimum value between the failure modes that can occur in:

- steel to timber nailed connection;

- connection between the two steel parts (two M10 bolts);
- anchor system between the foundation and the steel base (two M12 bolts).

The evaluation of the load bearing capacity of the steel to timber connection, has already been discussed in the previous paragraph. The angle bracket adopt the same fasteners (ringed shank nails $\phi = 4mm$) and the same material (steel S235, timber C24) and approximately the same thickness ($t = 5mm$ instead of $4mm$) of the tension tie described in the previous section. The connection is composed by 11 nails on three rows parallel to the load direction (along the grain for the timber element). The effective number of fasteners per row is:

$$n_{ef} = n^{K_{ef}}$$

The connection is composed by two rows with four nails and one central row with 3 nails. Thus for a constant nails spacing of $40mm$ ($K_{ef} = 0.85$) the effective number is equal to 9 ($2 \cdot 4^{0.85} + 3^{0.85}$).

Assuming a load bearing capacity of $1.99kN$ the characteristic resistance of the steel to timber connection is $17.9kN$. The design value depends from the partial safety factor adopted in the different codes. For the fundamental load combination according to EN 1995 $F_{v,Rd} = 15.2kN$ ($\gamma_m = 1.3$; $k_{mod} = 1.1$) while for DM 2008 is $F_{v,Rd} = 11.9kN$ ($\gamma_m = 1.5$; $k_{mod} = 1.0$). For the accidental combination the values are respectively $19.7kN$ ($\gamma_m = 1$; $k_{mod} = 1.1$) and $11.9kN$ ($\gamma_m = 1.5$; $k_{mod} = 1.0$). The partial factor adopted in the ULS according to the DM.2008 is higher than the EC5 although a value equal to 1 is reported for the accidental combinations because the detailed rules for the oligo-cyclic loads influence are not provided.

In this case the brittle "group" failure is negligible because the ends of the sill beam are usually far from the angle brackets and the minimum spacing between the fasteners is respected.

The second component is the connection between the pre-drilled flange and the angle part. This connection is realized by means of two M10 bolts. The load bearing capacity of the bolts is calculated according to EN1993 as:

$$F_{t,Rd} = \frac{0,6 f_{t,b} A_{res}}{\gamma_{M2}} = 22.3 KN$$

Where $f_{t,b}$ is the steel ultimate strength ($800MPa$), A_{res} is the cross section area $58mm^2$, γ_{M2} is the partial factor 1,25. The bearing resistance of the steel plate $F_{b,Rd}$ is:

$$F_{b,Rd} = \frac{k \alpha f_{t,k} d t}{\gamma_{M2}} = 16.6 \text{ KN}$$

Where:

$$k = \min \left[2, 8 \frac{e_2}{d_0} - 1, 7; 2, 5 \right] = 2, 18;$$

$$\alpha = \min \left[\frac{e_1}{3 d_0}; \frac{f_{t,b}}{f_{t,k}}; 1 \right] = 0, 0.53;$$

$t = 4 + 10 = 14 \text{ mm}$ is the thickness of the plate.

Moreover the minimum distance between the bolts and the edge of the plate must be verified:

$$e_1 = 17, 5 \text{ mm} > 1, 2 d_0 = 13, 2 \text{ mm}$$

$$e_2 = 15 \text{ mm} > 1, 2 d_0 = 13, 2 \text{ mm}$$

$$p_1 = 110 \text{ mm} > 2, 2 d_0 = 24, 2 \text{ mm}$$

The last component is the anchor between the steel angle and the foundation. The eccentricity between the nailed connection and the fasteners produces two bending moment in the vertical (M_x) and horizontal plane (M_y).

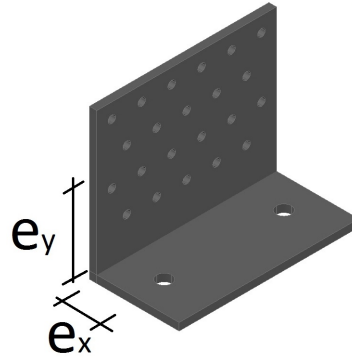


Figure 3.57: Angle bracket eccentricities.

$$M_x = F \cdot e_y$$

$$M_y = F \cdot e_x$$

Where F is the load on the centroid of the nails e_x and e_y are the eccentricities according to Figure 3.57. The total force on the anchor bolt (shear + tension) is calculated as the sum of the two lateral forces $F_{v,\parallel}$ and $F_{v,\perp}$ and the tension force:

$$F_{v,\parallel} = \frac{F}{2}$$

$$F_{v,\perp} = \frac{M_y}{C}$$

$$F_{v,Ed} = \sqrt{(F_{v,\parallel})^2 + (F_{v,\perp})^2}$$

$$F_{t,Ed} = \frac{M_x}{C}$$

Where C is the spacing between the anchor bolts. The failure load for combined tension and lateral forces is calculated from the formulae:

$$\frac{F_{v,Ed}}{F_{v,Rd}} + \frac{F_{t,Ed}}{1,4 F_{t,Rd}} \leq 1$$

$$\frac{\sqrt{(\frac{F}{2})^2 + (\frac{F \cdot e_x}{C})^2}}{F_{v,Rd}} + \frac{\frac{F \cdot e_y}{C}}{1,4 F_{t,Rd}} = 1$$

For a 12mm bolt graded 8.8 the design strength for lateral load and axial load is:

$$F_{v,Rd} = \frac{0,6 f_{t,b} A_{res}}{\gamma_{M2}} = 32,4 \text{ KN}$$

$$F_{t,Rd} = \frac{0,9 f_{t,b} A_{res}}{\gamma_{M2}} = 48,6 \text{ KN}$$

The maximum load which corresponds to the breaking of the bolt is 39.5kN. As for the hold-down case the resistance mechanism of the system is the steel to timber connection failure. In order to compare the analytical model results with the experimental values, in accordance to the previous section, a coefficient calculated through the rules of the EN 14358:2007 [18] is introduced.

$$\bar{y} = \frac{F_k}{1 - k \cdot CoV}$$

where:

\bar{y} is a stochastic mean value;

k is a factor;

CoV coefficient of variation;

For tests with infinite number of specimens, a p-percentile of $p = 5\%$ and a confidence level of $\alpha = 75\%$ the factor k is given as 1.65 [18]. The variation for wood is reported to be 15-25 % in dependence on the grading class. Not knowing the actual grading class of the used timber, it seems reasonable to assume $CoV = 0.2$, thus the reference value results to be:

$$\bar{y} = \frac{F_k}{1 - 1.65 \cdot 0.2} = 1.493 \cdot F_k$$

However in dependence on the actual timber quality \bar{y} can range from 1.3 and 1.7 times the characteristic resistance value F_k . The comparison between the results are summarized in Table 3.24.

Characteristic value	Mean value		
	CoV = 0.15	CoV = 0.2	CoV = 0.25
17.9	23.3	26.7	30.4

Table 3.24: Mean values of the angle bracket connection.

As shown in Figure 3.58 the maximum value of the load vs displacement curves of the cyclic test protocol is close to the value predicted by the analytical model (EYM). Nevertheless the value obtained during the monotonic protocol is higher ($40kN$ instead of $22 - 29kN$). However as illustrated by the test results on the steel to timber connection described in section 3.0.1 the material related variability is obviously higher than other material.

Section 3.0.1 summarize the result of tests on steel to timber connection. Two of those tests were carried out on a nailed joint with two different timber density ($\rho = 466.5kg/m^3$ $\rho = 373.6kg/m^3$). The results in terms of load bearing capacity are wide different, the connection with higher density timber shows a resistance 38% higher than the other case.

The maximum value obtained in these tests ($3.6kN$) multiplied by the number of fasteners in the angle bracket ($39.3kN$) is compatible with the results of the monotonic tests ($40.4kN$). Is worth notice that the experimental campaign was carried out on a small number of specimens especially on the higher density layout. However considering the gap between the value one of the reason could be the material related variability.

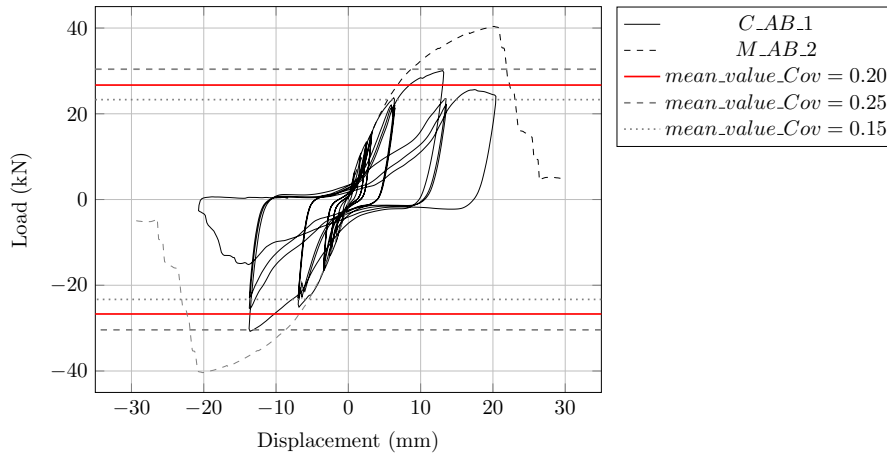


Figure 3.58: Comparison between the analytical and experimental bearing capacity.

Stiffness

The direct comparison between the experimental and analytical stiffness of the angle bracket is difficult. First because no transducers were installed to measure directly the load - slip curve of the nails and the mounting allowance between the two parts and the anchor bolts had an influence on the results especially in the cyclic test. However assuming that, thanks to the geometry of the element, the main contribution to the total displacement is attributable to the nailed connection. The analytical stiffness of this component is:

$$K_{tot} = k_{ser} \cdot n$$

The analytical device stiffness calculated according to EN1995 is $19140N/mm$ by using the actual number of fasteners ($n=11$) and $15660N/mm$ using the effective number $n_{ef} = 9$. As pointed out the $k_{ser} = 1740$ value proposed by the EN 1995 overestimate the effective stiffness of the joint. A more reliable value could be defined using the experimental mean stiffness of the tests presented in section 3.0.1. The slip modulus for a single fastener is $(550N/mm)$ and the total stiffness is $6050N/mm$ and $4950N/mm$ respectively for n and n_{ef} . The comparison between the result is reported in Figure 3.59.

The mean stiffness calculated using the experimental values of section 3.0.1 are close to the mean stiffness of the cyclic load-slip curve $4731N/mm$ (calculated by the envelope). This result, in the author opinion confirm that the geometry of the angle

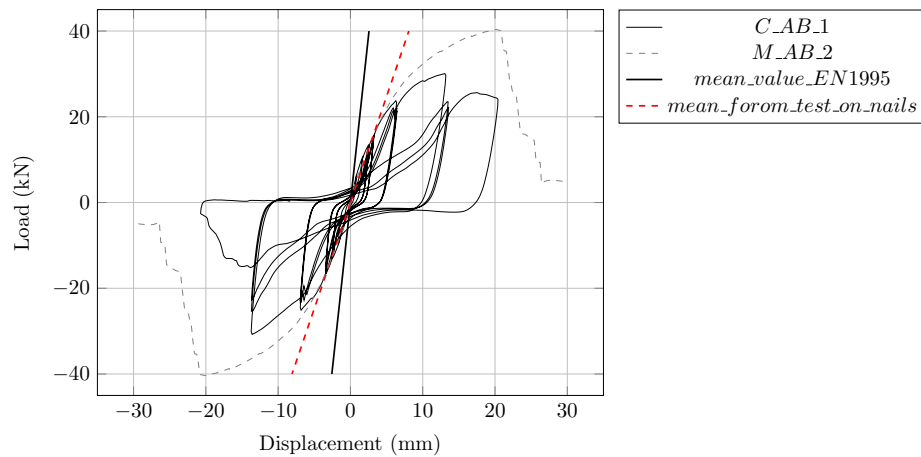


Figure 3.59: Comparison between the analytical and experimental stiffness.

brackets minimize the effect of the eccentricities on the elements (torsional effect on the nails and tensile forces on the anchor bolts).

3.1.3 Shear walls

Load bearing capacity

The load bearing capacity of the shear wall system is calculated as the minimum between:

- the sheathing to frame connection (staples);
- the tension tie connection against uplift (hold-down);
- the connection against the sliding (angle brackets).

The first item of the previous bullet-list is the resistance of the "fully-anchored" walls. The approach proposed by the EN 1995 is based on the limit analysis of the mechanical system. The hypothesis of the method prescribe that the failure should occur in the connection between frame and sheathing (adequate board resistance) and the wall should be fixed at both end by tension ties. Moreover the fasteners spacing should be constant along the perimeter of every sheet and the width of each sheet should be at least $h/4$. Other geometric limits are suggested in order to provide adequate stability (width/thickness ratio of the panel) and to consider the centre stud

consider as support for a sheet (the spacing of fasteners in the centre stud should not be greater than twice the spacing of the fasteners along the edges of the sheet).

The input data of the model are the dimension, the total numbers of sheathing panels, the fasteners spacing along the edge of the panel and the load bearing capacity of the fasteners Table 3.25.

Wall geometry				
Total length	l	2500	[mm]	
Height	h	2485	[mm]	
Material (sheathing)	OSB	GFB		
Panel width	b	1250	[mm]	
Panel thickness	t	(GFB) 12,5/15	[mm]	
Panel thickness	t	(OSB) 15	[mm]	
Number of sheathed	n_s	2	[-]	
Fasteners spacing	s	125	[mm]	

Table 3.25: Input data for the analytical EN1995 model suitable to predict the racking resistance of a shear wall (A-method).

Description	Staples 1.35 x 1.59 x 45 mm according to the German technical approval Z-9-1-37 (26/03/2007)		
Material	Steel rod according to EN 10016-2.		
Dimension	1.35x1.59	Characteristic tensile strength $f_{u,k,min} = 900\text{N/mm}^2$	
Load bearing capacity			
Equivalent diameter	d_{eq}	1.47	
Characteristic yield moment	$M_{y,k}$	647.8	
Characteristic density	ρ_k	380	
Characteristic embedment strength (panel)	$f_{h,1}$	65.2	
Characteristic embedment strength (timber)	$f_{h,2}$	27.8	
Head-side thickness	β	0.4	
point-side penetration	t_1	15	12.5
	t_2	30	32.5
		$t_1 = 15\text{mm}$	$t = 12.5\text{mm}$
Characteristic load-carrying capacity according to EN 1995	a	[kN]	[kN]
	b	2.35	2.87
	c	2.65	2.44
	d	1.06	1.07
Mean load carrying capacity according to EN 1995 and EN 14358:2007	e	0.77	0.91
	f	1.08	1.01
	mina,b,c,d,e,f:	0.62	0.63
	$f_{f,mean}$	0.62	0.63
		0.93	0.93

Table 3.26: Characteristic and mean value of the load bearing capacity of the staples.

		EN1995	Mean (EN14358)
Fastener load bearing capacity	$F_{f,k}$	0.63	1.4
	$F_f = 1.2 \cdot F_{f,k}$	0.756	-
Panel width	b_i	1250	1250
Panel height	h	2485	2485
	s	125	125
Shape coefficient	$c_i = \begin{cases} 1 & \text{if } b_i \geq b_0 \\ \frac{b_i}{b_0} & \text{if } b_i < b_0 \end{cases}$	1	1
	$b_0 = \frac{h}{2}$	1	1
Number of sheathing panels	2 on the front and 2 on the back side	4	4
Characteristic racking resistance of single wall panel	$F_{i,v,k} = \frac{F_{f,k} \cdot b_i \cdot c_i}{s}$	7.56	14
Characteristic racking resistance	$F_{v,k} = \sum_{i=1}^n F_{i,v,k}$	30.24	-
Mean racking resistance (according to EN 14358:2007)	$F_{v,k} \cdot 1.49$	45.1	56.0

Table 3.27: Racking resistance of the wall.

The mean load bearing capacity of the staples calculated according to the EYM and multiplied by the coefficient described in the previous section (1.493 for CoV 20%) is $0.93kN$. However from a previous experimental campaign [6] a higher mean value was found $1.4kN$. The total racking resistance of the wall is respectively $45.1kN$ and $56kN$.

The second item of the bullet-list, corresponding to the rocking mechanism, is related to the failure of the hold-down. Concerning this failure mode the vertical load at the top of the wall had a strong influence. The vertical force introduce a component opposite to the tensile load in the hold down. In other words the hold down device is activated only when the stabilizing moment due to the vertical load is overcome.

The total horizontal force at the top of the wall which correspond to the failure of the tension tie is calculated by the rotational equilibrium equation as:

$$F_{max,HD} = (R_{HD} + \frac{q \cdot l}{2}) \cdot \frac{l}{h}$$

The axial resistance calculated in section 3.0.2 is $63kN$ thus the maximum horizontal load that correspond to the rocking mechanism is $88.5kN$.

The last item of the bullet-list correspond to the sliding mechanism. In this case the vertical load introduce a horizontal component due to friction force. The horizontal load at the top of the wall which causes the failure of the connection is calculated by the translational equilibrium as:

$$F_{max,AB} = n_{AB} \cdot R_{AB} + \mu \cdot q \cdot l$$

For a total load of $50kN$ ($20kN/m \cdot 2.5m$) a friction coefficient of 0.4 and three angle brackets with a maximum load bearing capacity of $30kN$ the maximum horizontal force is $110kN$.

The resistance of the system composed by sheathing panels/frame connection, hold-down and angle brackets is calculated as the minimum between the three values $F_{max,SH} = 56kN$; $F_{max,HD} = 88.5kN$; $F_{max,AB} = 110kN$. In Figure 3.60 are shown the results. The total resistance of the system is well approximated by the mean value obtained from the model proposed by EN1995.

Stiffness

The elastic stiffness of light timber framed walls, as for the racking resistance, depends from different contribution. However in the national Italian standard (DM.

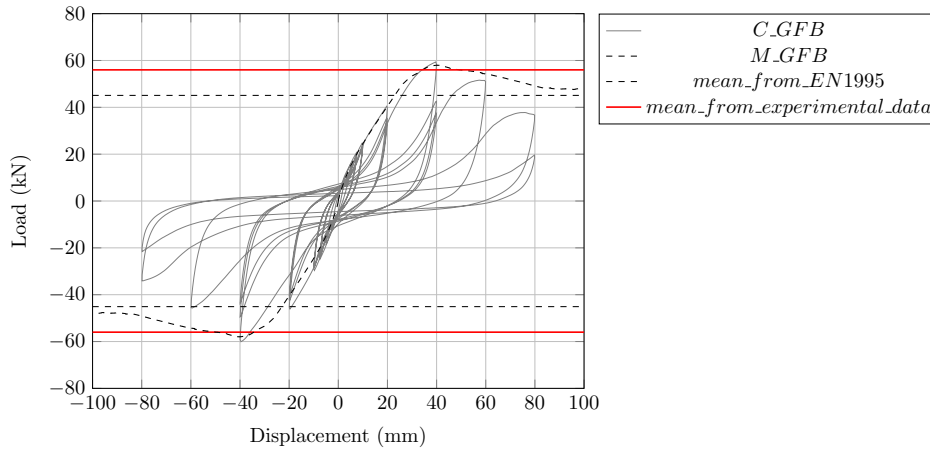


Figure 3.60: Comparison between the analytical and experimental racking resistance.

2008) as well as in European code (EN1995) no specific rules are reported.

In other document different approaches are introduced to predict the elastic stiffness of the walls. Three national standard formulations (German, New-Zealand, Canadian/US) and an analytical method proposed by Kälssner and Girhammar were proposed with this aim. A brief review of these approaches is summarized in the next paragraphs.

In the last part of this section, the elastic stiffness of the wall will be calculated according to a complete model developed from the literature proposal. This model was studied during several works carried out by the timber research group of the University of Trento ([20]).

German approach: In a companion document of the national German code for timber construction DIN 1052:2004 [21] "Erläuterung zu DIN 1052:2004-08" [22] has been proposed a analytical method. Four main contribution are taken into account, for a single panel length wall:

- panel to frame contribution- u_K
- shear deflection of the sheathing panels - u_G
- frame deflection - u_E

- contribution of the compression orthogonal to the grain at the support- u_v

$$u_{tot} = u_K + u_G + u_E + u_v$$

The displacement u_K is calculated using the "virtual work principle". The input data of the formulae are: the geometry of the panel (width l , height h and nail spacing a_v) and the stiffness of the single fastener k_{ser} .

$$\begin{aligned} u_K &= \sum \frac{S_{v,0} \cdot \bar{S}_{v,0}}{K_{ser}} = \left(\frac{2 \cdot l}{a_v} + \frac{2 \cdot h}{a_v} \right) \cdot \frac{S_{v,0} \cdot \bar{S}_{v,0}}{K_{ser}} \\ &= \left(\frac{2 \cdot l}{a_v} + \frac{2 \cdot h}{a_v} \right) \cdot \frac{F \cdot a_v^2}{k_{ser} \cdot l^2} = (2 \cdot l + 2 \cdot h) \cdot \frac{a_v}{k_{ser} \cdot l^2} \cdot F \end{aligned}$$

The second contribution u_G is calculated according to the analytical formulae for the shear deformation:

$$u_G = \frac{F}{G \cdot t} \cdot \frac{h}{l}$$

Where G is the shear modulus of the sheathing panel, t , l and h are respectively thickness-width and height of the panel. If the frame is braced on both side the total force is divided in two panels and the deflection is an half of the single panel case.

The frame deflection u_e is calculated according to the "virtual work principle" as:

$$u_E = \sum_i \int_{l_i} \frac{N_i \cdot \bar{N}_i}{E_i \cdot A_i} dx = \frac{2}{3} \cdot \frac{F}{E_0 \cdot A} \cdot \left(l + \frac{h^2}{l^2} \cdot h \right)$$

Where E_0 is the timber elastic modulus and A is the cross section area of the frame members. As for the previous case l and h are the dimension of the wall.

The last contribution to the horizontal wall displacement is caused by the compression perpendicular to the grain in the sill beam u_v .

$$u_v = \nu_{90} \cdot \frac{h}{l} \cdot \frac{\sigma_{c,90,k}}{1,2 \cdot k_{c,90} \cdot f_{c,90,k} \cdot k_{mod}}$$

Where ν_{90} is an non-dimensional parameter, $\sigma_{c,90,k}$ is the actual compression orthogonal to the grain, $f_{c,90,k}$ is the characteristic value of compressive strength and $k_{c,90}$ is a factor taking into account the load configuration, the possibility of splitting and the degree of compressive deformation.

New-Zealand approach: The national timber structures standard [23] report an analytical method to estimate the inter storey deflection based on a research work undertaken at the University of Canterbury. According to the total displacement is composed by four main contribution:

- Δ_4 - inter storey deflection due to chord relaxation at the base connection;
- Δ_5 - inter storey deflection due to shear deformation of plywood sheathing;
- Δ_6 - inter storey deflection due to nail slip, en, between sheathing and framing;
- Δ_7 - inter storey flexural deflection as a cantilever.

$$\Delta_w = \Delta_4 + \Delta_5 + \Delta_6 + \Delta_7$$

The first contribution δ_4 represent the compression of the sill beam (δ_c) and the elongation of the hold-down (δ_t) .

$$\Delta_4 = (\delta_c + \delta_t) \cdot \frac{H}{B}$$

The in the previous formulae the vertical displacement are converted into horizontal displacement by means of the ratio between height (H) and length (B) of the wall. The first members (δ_c) defined as "Vertical downward movement (mm) at the base of the compression end of the wall due to compression perpendicular to grain deformation in the bottom plate". The second δ_t defined as "Vertical upward movement (mm) at the base of the tension end of the wall due to deformations in a nailed fastener and the members to which it is anchored)".

The second contribution δ_5 represent the inter storey deflection due to the deformation of the sheathing panels.

$$\Delta_5 = \frac{V \cdot H}{G \cdot B \cdot t}$$

Where P is the inter storey shear force (N), G and t are respectively shear modulus (MPa) and thickness (mm) of the sheathing.

The third contribution δ_6 represent the inter storey deflection due to nail slip, e_n , between sheathing and framing.

$$\Delta_6 = 2 \cdot (1 + a) \cdot m \cdot e_n$$

The aspect ratio between the dimension of the panel is take into account using the coefficient a . This parameter is equal to 0 when relative movement along sheet edges is prevented, 1 when square sheathing panels are used, 2 when $2.4 \times 1.2m$ panels are orientated with the $2.4m$ length parallel with the diaphragm chords (= 0.5 alternative orientation).

The nail slip is calculated according to a quite complex method. The slip in a nailed joint is determined through a initial slope, between 0 and $0.5mm$ and a line passing through fixed points. The initial slope is calculated as:

$$e_n = \delta = \frac{k_{37} \cdot 0,8 \cdot P^2}{Q_n^2}$$

Where k_{37} is a model parameter, depending from the type of fasteners and from the load duration, P is the applied nail load and Q_n is the nominal strength for a single nail with short term loading (depending from timber grading).

The first point correspond to "a load equal to 1.25 times the nominal short term strength of a single nail gives an average slip of $2.5mm$ ". The second point correspond to 1.2 times the nominal strength with a slip of $6mm$ and the third point to a load level of 1.4 times the nominal strength with a slip of $10mm$.

The last contribution to the total displacement at the top of the wall, δ_7 , represent the flexural deflection of the frame. The deflection is calculated as the deflection of cantilever beam. The moment of inertia of the shear-wall is calculate neglecting the contribution of the internal framing members and sheathing to the flexural stiffness. Thus the total moment of inertia is $2 \cdot I_c + 2 \cdot A \cdot (B/2)^2$ where B is the distance between

the two chords. The flexural deformation is greater for slender walls while is almost negligible for squat walls (single storey).

$$\Delta_7 = \frac{2 \cdot V \cdot H^3}{3 \cdot E \cdot A \cdot B^2} + H \cdot \Theta$$

Where: V is the shear force in the storey under consideration (N), E is the elastic modulus of the chord members (MPa), A is the sectional area of one chord (m^2), B is the distance between diaphragm chord members (mm), H is the height of the storey under consideration (mm), Θ is the flexural rotation at the base of the storey under consideration (*radians*) arising from the tie-rod elongation (if this device is installed).

Canadian/US approach: The Canadian code CSA-086-14 [24] and the International Building code (IBC 2009) [25] suggest a method to predict the horizontal displacement of timber framed shear walls similar to the NZL approach. The formulae is composed by four main contributions: the flexural deformations, the sheet shear deformation, the sheathing nail-slip and the anchorage system deformation.

$$\Delta_{sw} = \frac{2 \cdot \nu \cdot H_s^3}{3 \cdot E \cdot A \cdot L_s} + \frac{\nu \cdot H_s}{B_v} + 0.0025 \cdot H_s \cdot e_n + \frac{H_s \cdot d_a}{L_s}$$

Where:

- ν = maximum shear due to specified loads at the top of the wall, N/mm
- H_s = height of shear-wall segment, mm
- E = elastic modulus of boundary element (vertical member at shear-wall segment boundary), N/mm^2
- A = cross-sectional area of the boundary member, mm^2
- L_s = length of shear-wall segment, mm
- B_v = shear-through-thickness rigidity of the sheathing, N/mm
- e_n = nail deformation, mm
- d_a = total vertical elongation of the wall anchorage system (including fastener slip, device elongation, anchor or rod elongation, etc.) at the induced shear load.

	d	l	for maximum loads-up to		e_n
	[mm]	[mm]	[lbf]	[N]	[in]
6d common nail (0.113"x2")	2.9	50.8	180	800.64	$(V_n/456)^3 \cdot 1.144$
8d common nail (0.131"x2-1/2")	3.2	63.5	220	978.56	$(V_n/616)^3 \cdot 0.018$
10d common nail (0.148"x3")	3.8	76.2	260	1156.48	$(V_n/769)^3 \cdot 0.276$
14ga staple			140	622.72	$(V_n/596)^1 \cdot 0.999$
14ga staple			170	756.16	$(V_n/461)^2 \cdot 0.776$

Table 3.28: Fasteners slip equation according to IBC2009 (v_m is the load per nail)

Nail slip (e_n) used in the shear wall deflection equation is calculated according to the value proposed in Table 3.28.

A similar formulation, specified for shear wall and diaphragm, is proposed by [24]:

$$e_n = \left(\frac{0.013 \cdot v s}{d_f^2} \right)^2$$

Where v is the the maximum specified shear force per unit length along the diaphragm boundary or top of shear-wall, [N/mm] and s is the nail spacing at panel edges of shearwalls or diaphragms, [mm].

About the last term of the previous equation (d_a) the CSA [24] introduce two sub-cases concerning the timber framing design strategies when the factored dead loads are not sufficient to prevent overturning. The first layout "Shear-wall segments with hold-downs" is characterized by the hold down elements that provide a continuous direct load path, typically between upper storey wall chords and lower storey chords, beams, or foundations. According to the second layout "shear-wall segments without hold-downs" the tension force due to the uplift is transfer from the shear-wall segment to the other element by means of anchor bolts connected to the bottom beam of the frame.

For shear-wall segments without hold-downs, the total vertical elongation, d_a , may be taken as follows:

$$d_a = 2.5 \cdot d \cdot k_m \left(\frac{(\nu \cdot H_s - P) \frac{s_n}{L_s}}{n_u} \right)^{1.7}$$

Where:

- d = nail diameter, mm
- K_m = service creep factor
- ν = maximum shear due to specified load at the top of the wall, N/mm

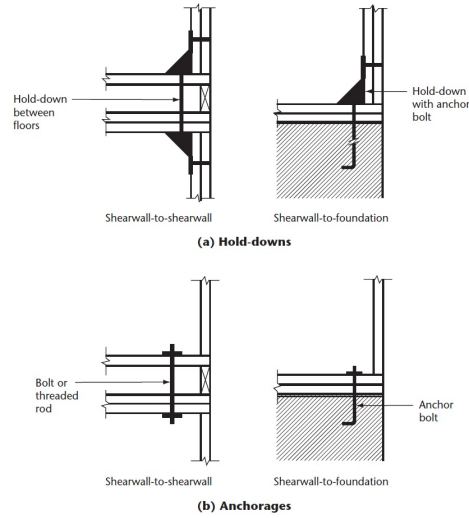


Figure 3.61: Examples of hold-downs and anchorage from CSA-086-09 [24].

- H_s = height of shear-wall segment, mm
- P = specified load per nail, N
- s_n = nail spacing around panel edge, mm
- L_s = length of shear-wall segment, mm
- n_u = unit lateral nail strength resistance, N

For the shear-wall segment with hold-downs the standard do not provide any detailed formulae.

Swedish approach: The paragraph hereinafter summarize a model proposed by Kallsner and Girhammar [26] for the elastic analysis of fully anchored walls. On the contrary of the methods proposed in the previous sections this formulation is not reported in a design code. Nevertheless, in the author opinion, the work developed by Kallsner and Girhammar is characterized by a fully-theoretical simple and reliable approach. This method is based on the analysis of the sheathing to frame connection and on the shear deformation of the sheathing panels under the following hypothesis:

- Displacements of the wall are small compared to the width and height of the sheets;

- Sheathing-to-framing joints have linear elastic load-slip characteristics up to failure. Slip modulus is constant and the same in all joints. Joint stiffness is independent of the force direction and of the mutual orientation of the sheets and framing members;
- Framing joints act as hinges;
- No contact between adjacent sheets or between sheets and surrounding structure (sheets are free to rotate);
- Edge distances of sheathing-to-framing joints are small compared to the width and height of the sheets, i.e. the fasteners are approximately located along the edges of the sheets.

The authors propose a complete formulation for the evaluation of the lateral load bearing capacity and the displacement of the top of the wall based on the elastic theory (minimum of the potential energy method). The method was proposed assuming rigid frame members and rigid sheathing panels. In a second step the model was modified to taking into account the shear deflection of sheets and the flexible framing members influence (only the "fully flexible condition").

The horizontal displacement of the top rail of the wall is calculated as:

$$u_{frame} = \gamma \cdot h = \frac{H \cdot h^2}{k} \left[\frac{1}{\sum_{i=1}^n \hat{x}_i^2} + \frac{1}{\sum_{i=1}^n \hat{y}_i^2} \right]$$

Where h and b are respectively the height and the width of the sheathing panel, H is the force applied at the top of the wall and k is the slip-modulus of the fasteners. The quantity $\sum_{i=1}^n \hat{x}_i^2$ and $\sum_{i=1}^n \hat{y}_i^2$ depends from the geometry of the connection between sheathing and frame. In particular form the nail spacing along the external studs (s_{ps}), on the internal stud (s_{is}), on the top and bottom rails (s_r) and from the distance of each fastener from the center of the wall. For a common configuration with $h = 2 \cdot b$ (commercial panels size) and for a nail spacing $s_{ps} = s_r = 2 \cdot s_{is}$ the previous equation gives:

$$u_{frame} \approx \frac{348}{77} \cdot \frac{s_r}{b} \cdot \frac{H}{k} = 4,52 \cdot \frac{s_r}{b} \cdot \frac{H}{k} = 4,52 \cdot \frac{H}{K_r \cdot b}$$

The deflection of the wall taking into account the contribution of the shear deformation of the panels is:

$$u_{frame} = \gamma \cdot h = \frac{H}{k} \left[h^2 \cdot \left(\frac{1}{\sum_{i=1}^n \hat{x}_i^2} + \frac{1}{\sum_{i=1}^n \hat{y}_i^2} \right) + \frac{h}{b} \cdot \frac{k}{G \cdot t} \right]$$

Complete approach: As mentioned in the introductory part of this subsection a complete model, where both the deflection of the wall-panel and the connection to the foundation are taken into account, was proposed by Casagrande et al ([27]). The reliability of this model was verified through several research campaigns on light-timber framed and cross-laminated timber walls carried out by Timber research group of the University of Trento. The model is based on the elastic analysis of the displacement caused by different contribution such as the sheathing-to-framing connection slip (Δ_{sh}), the rigid-body rotation (Δ_h), the rigid-body translation (Δ_a) and the sheathing-panels shear deflection (Δ_p). However also other component can be considered if a more accurate analysis is required (as an example deflection due to the compression of the sill beam and bottom rail, friction). One of the key point of the presented model is that all the main contribution are considered as well as the influence of the vertical loads on the top rail of the wall.

The analytical general expression of the displacement is:

$$\Delta = \frac{F \cdot h}{l} \frac{1}{G_p \cdot n_{bs} \cdot t_p} + \frac{F \cdot l}{n_{bs}} \cdot \lambda \cdot \frac{s_c}{k_c} + \frac{F}{k_a \cdot n_a} + \frac{1}{k_h} \cdot \left(\frac{F \cdot h}{l} - \frac{q \cdot l}{2} \right) \cdot \frac{h}{l}$$

Where F is the horizontal force applied at the top of the wall, q is the vertical load and the geometrical parameters are:

- h is the panel's height;
- l is the total wall length;
- τ is a no-dimensional factor that take into account the position of the rotation center of the wall;
- n_{bs} is the number of sheathed size (1 or 2);
- λ is a shape factor;

- α is an no-dimensional parameter of the sheathing panel equal to h/b ;
- s_c is the spacing of the connectors placed on the edge of each panels;

The material and connection proprieties introduced as:

- G_p is the shear modulus of the sheathing;
- k_c is the stiffness of the sheathing to frame fasteners;
- k_a is the stiffness of the anchor against the wall slippage (i.e. angle brackets);
- n_a is the number of the anchor against the wall slippage;
- k_h is the stiffness of the tension tie.

The vertical load q introduce a "breaking point" in the elastic response of the wall. As shown in Figure 3.62, in the first part of the load vs displacement curve, the rigid body rotation of the wall due to the external force F is prevented by the stabilizing moment caused by the vertical load. When the stabilizing moment is overcome the rocking mechanism is activated and the contribution of the hold-down (uplift) increase the displacement. As clearly visible by Figure 3.62 the slope of the initial part of the curve is higher than the second because the flexibility of an equivalent spring (k_h) is added to the model.

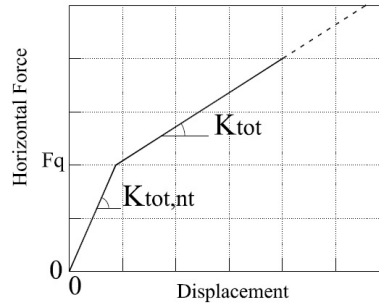


Figure 3.62: Load vs displacement curve - the first regime (no-uplift, $M_q > M_f$) is characterized by higher stiffness ($k_{tot,nt}$) while the second regime (uplift, $M_q < M_f$) is characterized by lower stiffness (k_{tot}) [27].

As pointed out by Casagrande in ([27]) the consequences of this non linearity affect the stiffness distribution between the walls of the building because the horizontal load distribution is no longer proportional to the wall length. If the rocking mechanism is activated after the first phase the stiffness of the wall is proportional to the square of the wall length.

The model proposed by Casagrande is a simple and reliable model that can be useful for the accurate analysis of both light-frame and CL timber buildings. To analyse cross-laminated timber walls displacement only minor changes have to be done on the equations about the stiffness of the panel itself. Obviously no sheathing to framing connection have to be consider and the shear deformation of the panels in this case represent the total shear deformation of the CLT diaphragm.

In order to compare the results of the different approaches some consideration have to be discussed. First the different codes proposal about the nail-slip are different and, depending on the fastener type, lead to different degree of accuracy with the experimental results. The "semi-empirical" formulations are based on the local constructive system and on the material/geometry used in each single region. Therefore a direct extension at other situation may be not a trivial issue. Figure 3.63 show the load-slip curves for nails ($\phi 2, 8mm$) and for staples ($1.35 \times 1.59mm$).

The results of the different relationship are visible in Figure 3.64 where the results of the test on shear wall are expressed in terms of the "fully anchored" conditions (the influence of the rocking mechanism are subtracted from the total displacement).

As described in the previous paragraphs the influence of some contribution may be neglected. As an example, for the presented geometry summarized in Table 3.29, the influence of the sill beam, the bending deformation and the influence of the friction force between foundation slab and sill beam are negligible compared to the main contribution due to nail-slip and rocking caused by hold down element. Nevertheless the influence of these component may be important when the stiffness ratio between the equivalent spring is different from the analysed case. As an example for the CLT walls the main contribution is due to the elongation of the tension tie and the horizontal slip due to the angle brackets. In this case the shear deformation of the panel itself is lower compared to the rocking and slip of the wall, and maybe the compression of the sill beam/panel could be important.

Figure 3.66 show the variation of the load-displacement curves for different input values set for the gypsum fibre and OSB layouts (experimental data about the behaviour of frame to sheathing connection using OSB and staples were not available). The first set is characterized by the experimental values aquired during the preliminary tests (angle brackets - section 3.0.3, hold down - section 3.0.2, panel to frame connection - [28] , [6]). In the second set the values are calculated from the formulae proposed by the EN1995. The third set is based on the analytical formulations adopting mean experimental values of stiffness where the codes proposal led to an excessive estimations. In detail the hold down and the angle brackets stiffness are

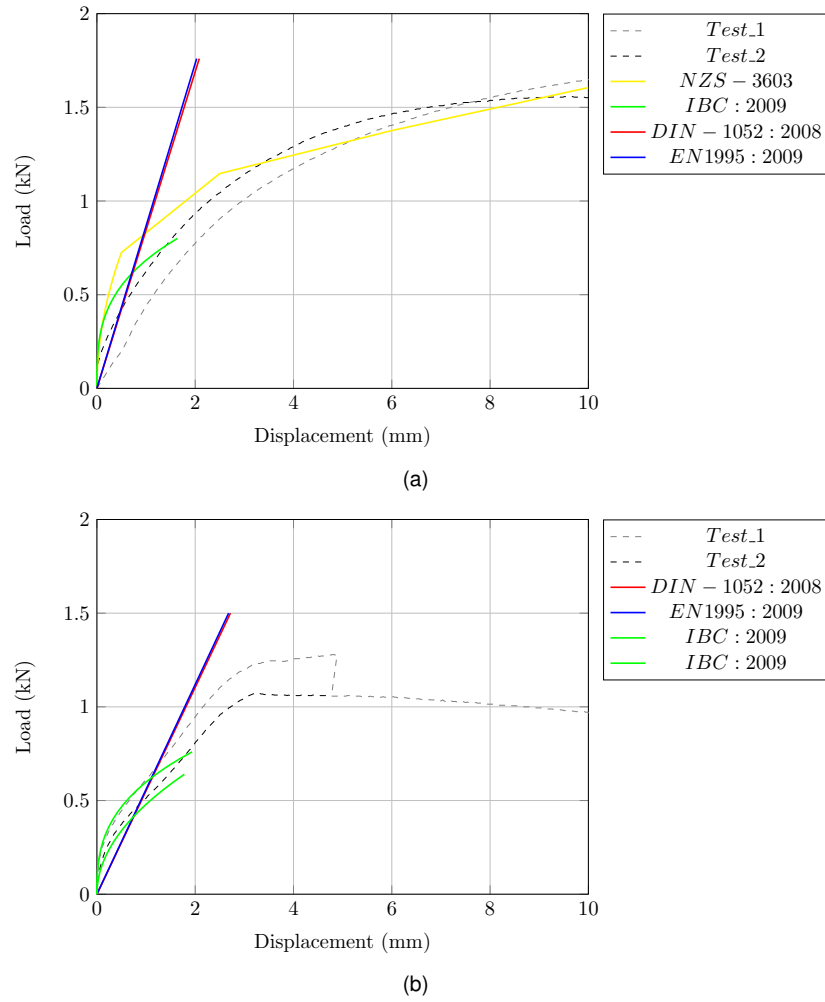
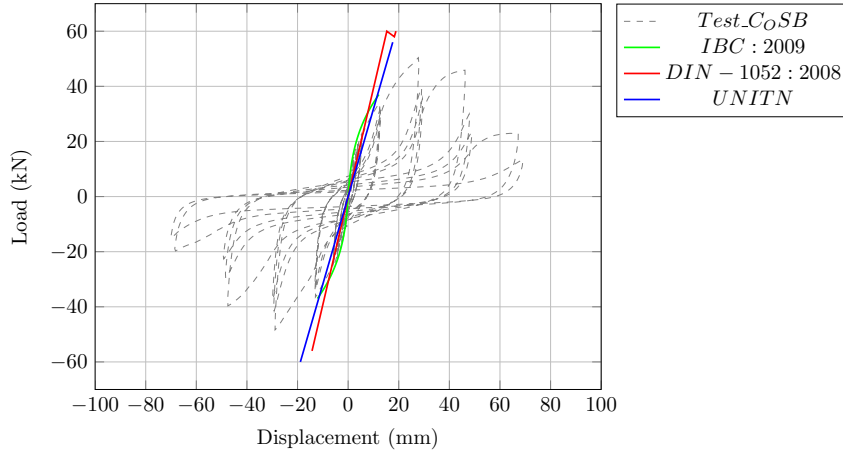


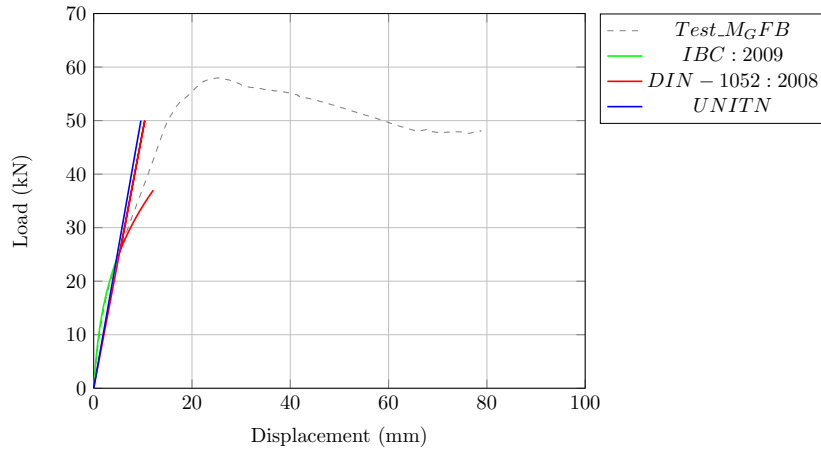
Figure 3.63: Load vs slip curve - a) nails $\phi 2, 8mm$ - b) Staples $1.35 \times 1.59mm$.

calculated, according to sections 3.0.2 and 3.0.3, as a series of elastic springs where the only experimental value is the stiffness of the timber to steel connection (mean value of the tests in section 3.0.1).

The elastic behaviour of the wall predicted by the complete model, using the experimental values of stiffness of each single equivalent spring, show a good agreement with the experimental results.



(a)



(b)

Figure 3.64: Load vs displacement curve for fully anchored wall a) (M_{GFB}) gypsum-fibre sheathing/staples $1.35 \times 1.59 \text{ mm}$ - b) (C_{OSB}) OSB sheathing/staples $1.35 \times 1.59 \text{ mm}$.

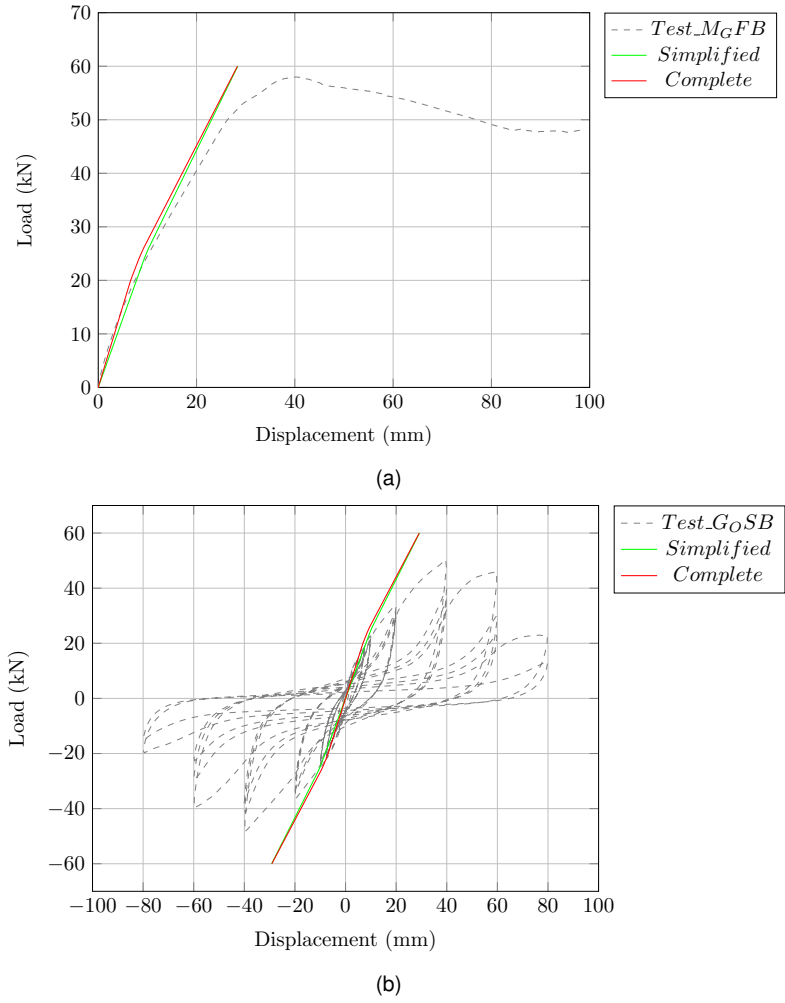
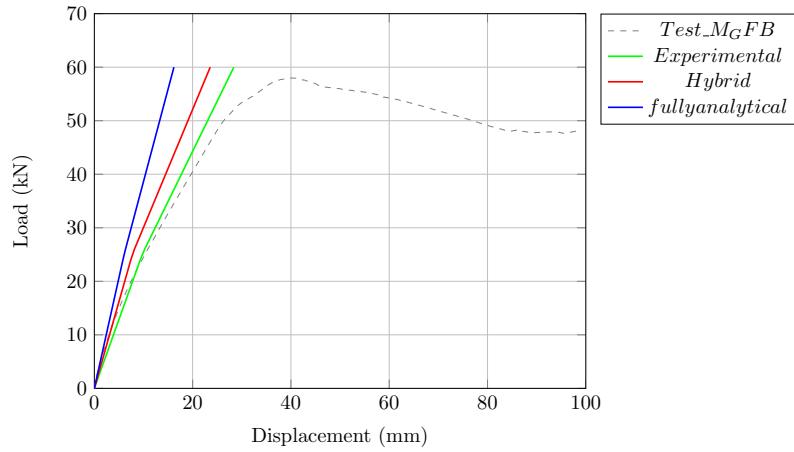
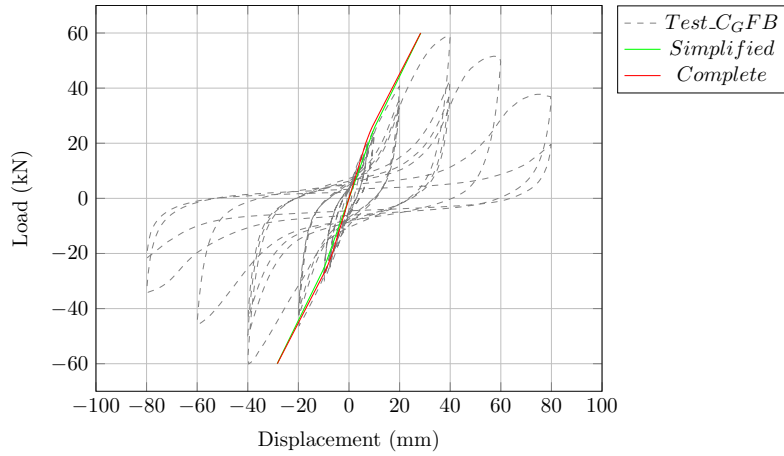


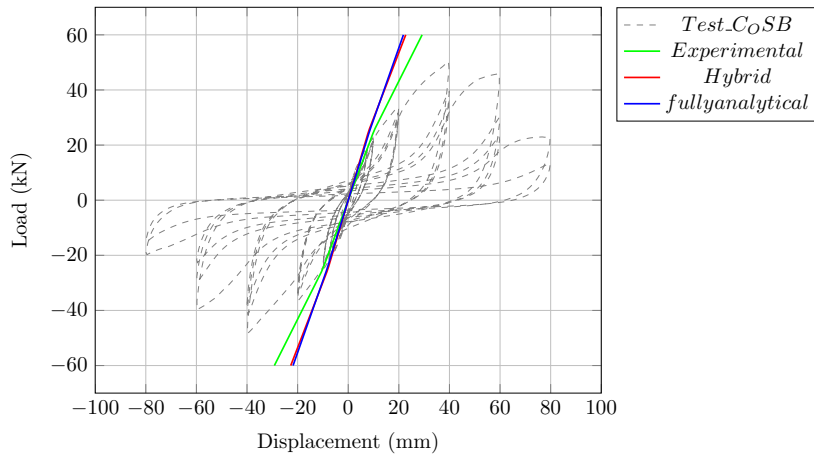
Figure 3.65: Load vs displacement curve for fully anchored wall a) (M_{GFB}) gypsum-fibre sheathing/staples 1.35x1.59mm - b) (C_{OSB}) OSB sheathing/staples 1.35x1.59mm.



(a)



(b)



(c)

Figure 3.66: Influence of the input data - Load vs displacement curve for fully anchored wall a) (M_{GFB}) gypsum-fibre sheathing/staples 1.35x1.59mm - b) (C_{GFB}) GFB sheathing/staples 1.35x1.59mm - c) (C_{OSB}) OSB sheathing/staples 1.35x1.59mm.

Component	Description	Label	Value	Unit
Geometry	Length of the wall segment	l	2500	[mm]
	Height of the wall segment	h	2560	[mm]
	Width of the single sheathing	b	1250	[mm]
	Height of the single sheathing	h	2560	[mm]
	Thickness of the panels	t	15/12.5	[mm]
	Number of sides	n_{bs}	2	
	Number of angle brackets	n_a	3	
	Friction coefficient	μ	0.4	
	Nail-spacing	s	125	[mm]
	Cross section	$1.35 \cdot 1.59$		[mm]
Staples	Equivalent diameter single	d	1.47	[mm]
Timber (C24)	Mean density	ρ_m	420	[kg/m ³]
	Characteristic density	ρ_k	350	[kg/m ³]
	Mean modulus of elasticity parallel	E_0	11000	[MPa]
	Mean modulus of elasticity perpendicular	E_{90}	370	[MPa]
Oriented strand board (OSB/3)	Mean density	ρ_m	600	[kg/m ³]
	Characteristic density	ρ_k	550	[kg/m ³]
	Mean shear modulus	G	1080	[MPa]
Gypsum fibre board (GFB)	Mean density	ρ_m	1000	[kg/m ³]
	Characteristic density	ρ_k	800	[kg/m ³]
	Mean shear modulus	G	1600	[MPa]
Mechanical proprieties	Staples experimental mean stiffness (GFB)	$k_{c,exp}$	411	[N/mm]
	Hold-down experimental mean stiffness	$k_{h,exp}$	6854.8	[N/mm]
	Angle bracket experimental mean stiffness	$k_{A,exp}$	3781.5	[N/mm]
	Staples analytical mean stiffness (OSB)	$k_{c,an}$	382	[N/mm]
	Staples analytical mean stiffness (GFB)	$k_{c,an}$	560	[N/mm]
	Hold-down analytical mean stiffness	$k_{h,an}$	20882	[N/mm]
	Angle bracket analytical mean stiffness	$k_{A,an}$	15660	[N/mm]
	Staples analytical mean stiffness (OSB)	$k_{c,hy}$	382	[N/mm]
	Staples analytical mean stiffness (GFB)	$k_{c,hy}$	560	[N/mm]
	Hold-down hybrid stiffness	$k_{h,hy}$	20882	[N/mm]
	Angle bracket hybrid stiffness	$k_{A,hy}$	15660	[N/mm]

Table 3.29: Input data.

3.2 Component method

In this section is presented a model suitable to predict the elasto-plastic behaviour of the wall segment. The plastic behaviour and the ultimate displacement are calculated through a model based on the analysis of the system as a series of springs.

According to the general equations hereinafter presented, the overall behaviour of the wall is strongly related to the interaction between the springs. The stiffness, ultimate displacement and the ductility, strength and the energy dissipation are mainly related to the weaker failure mode of the system. In other words if the wall is considered as a "dissipative system" in order to achieve the maximum performances in terms of energy dissipation the weaker spring of the system shall be the most ductile and the others have to be over-designed both for resistance and stiffness.

This topic is introduced in the codes as "capacity design" through adequate over-strength factors. This procedure ensure that the most ductile failure modes of each part of the structure (hence also the overall building) avoiding the brittle failure mode.

The European code [2], as mentioned in the introductory section, report detailed rules for the method application for steel - reinforced concrete - hybrid structures but for timber construction the prescriptions are not detailed enough.

However the first step in order to analyse the seismic performance of the vertical shear wall bracing system is the study of the interaction of the connection with the foundation and the frame to panel connections. The walls can be idealized as a series of springs, in this case with a non linear law, as shown in Figure 3.67.

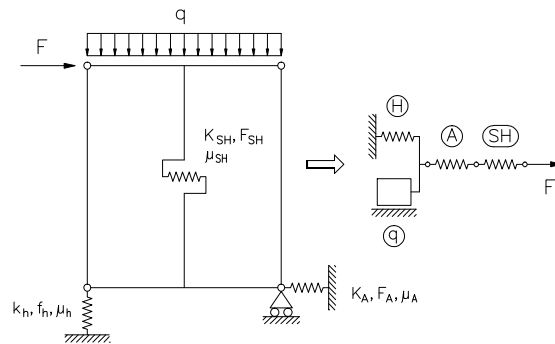


Figure 3.67: Analytical model spring layout.

This model take into account three springs. The first, H, represent the equivalent horizontal spring which correspond to the rocking effect due to the tension tie elongation. As discussed in the previous section the effect of the vertical dead load on

the stiffness and load carrying capacity of the wall should be take into account. For this purpose a "friction block" is connected in parallel to the the non-linear spring H. The second spring, A, represent the systems against the horizontal slippage (angle brackets or screws). Also in this case a friction block can be linked in parallel to take into account the friction force. The last spring, SH, represent the "fully anchored" wall deformation (sheathing to frame connection and panel shear deformation).

Each of the previous spring ¹ is defined by three main parameters: stiffness, load bearing capacity and ductility. These value are calculated by the bi-linearisation of the load versus displacement curves acquired during the experimental tests and from an analytical model based on a incremental-step analysis. The result of the model, based on the experimental values, is the equivalent non-linear behaviour of the wall in terms of mean value of stiffness, resistance and displacement.

3.2.1 Bi-linearisation of the experimental curves

The bi-linear curves of the connection (angle brackets, hold-down, frame to sheathing fasteners) are the input data for the model proposed in the next paragraphs. Using experimental data the output of the model is more reliable and it is consistent with the experimental results. The reason, as pointed out in the previous part of this document, is that the value calculated according to the building codes overestimate the experimental results (especially in terms of stiffness).

Especially for the angle brackets and hold downs this issue is crucial. On the other hand, the stiffness the resistance and the ultimate displacement of the fully anchored wall can be well-predicted through non linear analysis ([29]).

This approach is suitable for the common design practice because the anchor system provided by the producers are standard devices (material, number and type of fasteners, mounting tolerances, use etc.) whereas for the wall segment geometries different solution can be adopted (geometry, aspect ratio, sheathing materials, number of panels/sides, nail-spacing, etc.).

The next pictures shows the bi-linear load vs displacement curves and the fundamental parameters (maximum load f_i , yielding displacement $\delta_{y,i}$, ultimate displacement $\delta_{u,i}$, stiffness k_i and the ductility μ_i).

These curves/parameters were calculated according to a common procedure. The first part of the curve is defined as the secant line between the origin of the axis

¹the capital letters means "horizontal equivalent springs" while the lower-case letters indicates the behaviour along the actual loaded direction (ie: hold down vertical displacement)

and the point of the curve corresponding to the 70% of the maximum load. The horizontal slope part position is defined through a "area balance" criterion and the ultimate displacement correspond to a impairment of the maximum load of 20%. Both monotonic and cyclic test results were analysed to take into account the effect of the different protocol on the ultimate displacement and on the impairment of strength.

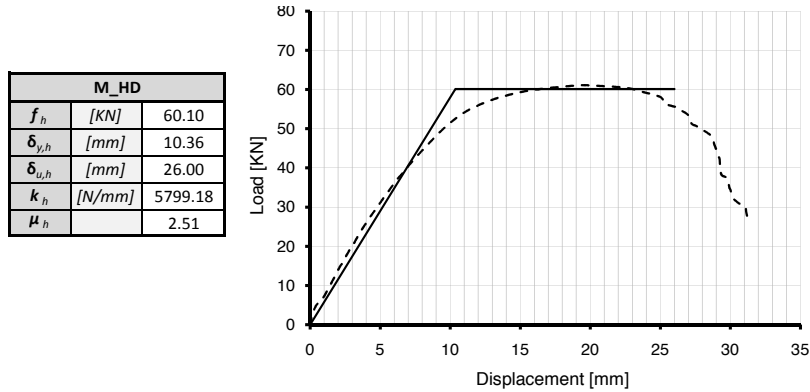


Figure 3.68: Bi-linear curve: monotonic tests Hold-down.

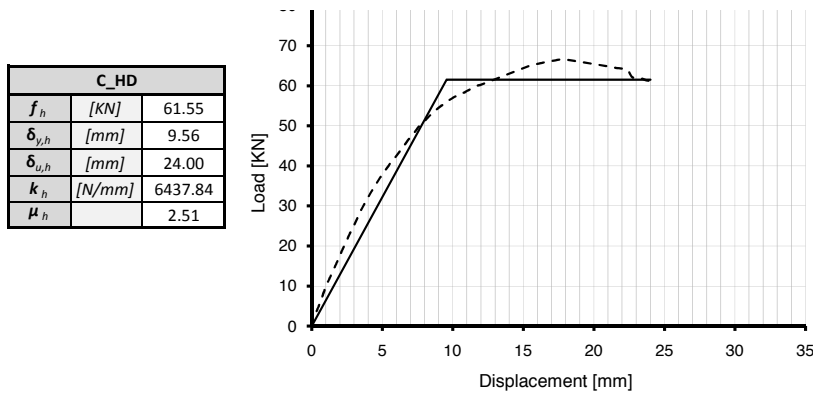


Figure 3.69: Bi-linear curve: cyclic tests Hold-down.

M_AB		
f_a	[kN]	38.37
$\delta_{y,a}$	[mm]	11.60
$\delta_{u,a}$	[mm]	22.00
k_a	[N/mm]	3307.36
μ_a		1.90

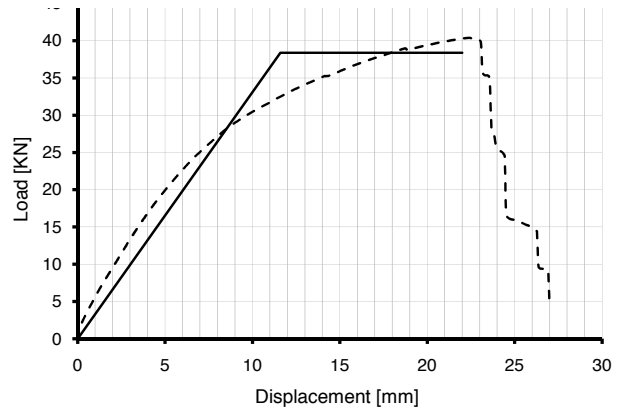


Figure 3.70: Bi-linear curve: monotonic tests angle brackets.

C_AB		
f_a	[kN]	27.97
$\delta_{y,a}$	[mm]	7.14
$\delta_{u,a}$	[mm]	21.00
k_a	[N/mm]	3916.13
μ_a		2.94

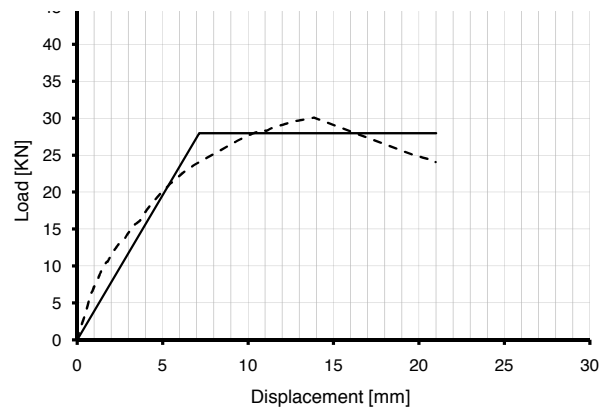


Figure 3.71: Bi-linear curve: cyclic tests angle brackets.

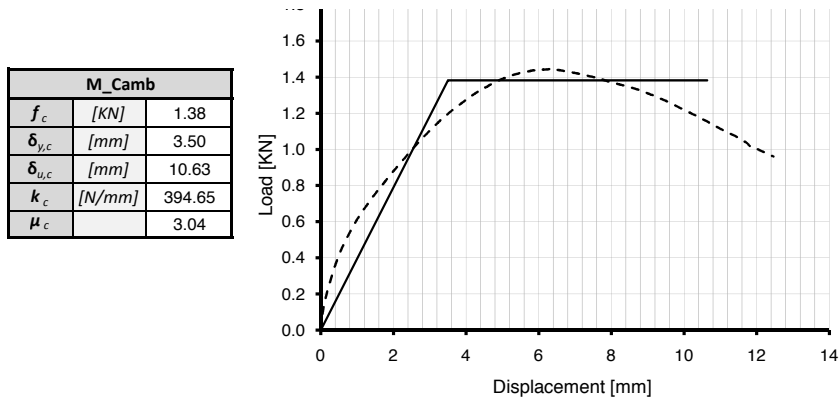


Figure 3.72: Bi-linear curve: monotonic tests sheathing to frame connection (staples).

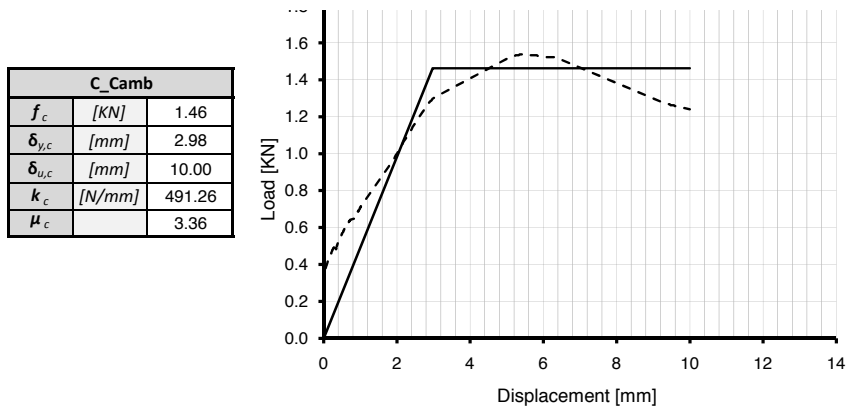


Figure 3.73: Bi-linear curve: cyclic tests sheathing to frame connection (staples).

3.2.2 Hold-down equivalent spring - H

From the input data obtained through the experimental results analysis is possible to obtain the "equivalent horizontal" spring. As pointed in the previous subsection the effect of the vertical load introduce two different static regime of the wall segment.

The first one is characterized by higher stiffness because the uplift is prevented by the vertical dead load, while the second is characterized by a lower stiffness because the hold-down spring is "activated". The model proposed take into account this issue by means of a "friction block" connected to the spring as shown in Figure 3.74.

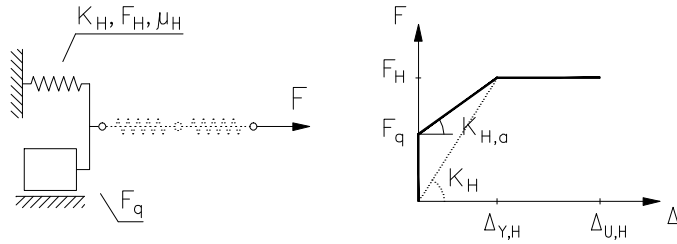


Figure 3.74: Tension tie (hold-down) element.

The magnitude of the horizontal force corresponding to the activation of the hold-down device F_q is obtained through the rotational equilibrium (rigid body rotation around the point P in Figure 3.75).

$$F_q = \frac{q l^2}{2 h}$$

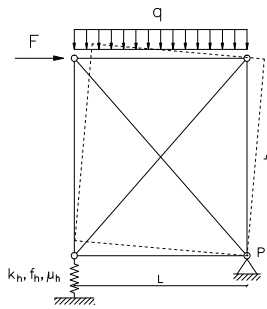


Figure 3.75: Rocking mechanism (rigid body rotation).

Through geometrical consideration about the rigid body rotation, summarized in the next equations, is showed that the ductility of the horizontal spring (μ_H) is the same of the hold-down ductility (μ_h).

$$\Delta_{Y,H} = \frac{\delta_{y,h}}{l} h \quad \Delta_{U,H} = \frac{\delta_{u,h}}{l} h$$

$$\mu_H = \frac{\Delta_{U,H}}{\Delta_{Y,H}} = \frac{\delta_{u,h}}{\delta_{y,h}} = \mu_h$$

The vertical load increase the load bearing capacity of the overturning mechanism. In other word thanks to the stabilizing effect of the vertical load an additional component have to be overcome before the H spring reach the yielding load. The horizontal force magnitude that cause the yielding of the vertical spring is:

$$F_H = \left(f_h n_h + \frac{q l}{2} \right) \frac{l}{h}$$

The stiffness of the system is:

$$\begin{cases} K_{H,na} \rightarrow \infty \\ K_{H,a} = \frac{(F_H - F_q)}{\Delta_{Y,H}} = k_h n_h \left(\frac{l}{h} \right)^2 \end{cases}$$

Where $K_{H,na}$ is the stiffness when the uplift is prevented by the dead load ($F < F_q$) and $K_{H,a}$ is the stiffness when the uplift of the wall is greater than zero ($F_q < F < F_H$). Another useful mechanical parameter is the "secant stiffness" k_H (Figure 3.74) defined as:

$$K_H = \frac{F_H}{\Delta_{Y,H}} = k_h n_h \left(\frac{l}{h} \right)^2 + \frac{q l^3}{2 \delta_{y,h} h^2} = K_{H,a} + \frac{q l^3}{2 \delta_{y,h} h^2}$$

The results are summarized in Table 3.30

Tests:	Hold-down (H)		
	Monotonic	Cyclic	
F_H	[kN]	85.6	87.1
F_q	[kN]	25.2	25.2
$\Delta_{Y,H}$	[mm]	10.3	9.5
$\Delta_{U,H}$	[mm]	25.8	23.9
$K_{H,na}$	[N/mm]	∞	∞
$K_{H,a}$	[N/mm]	5869.4	6515.8
μ_H		2.51	2.51
K_H	[N/mm]	8311	9162.5

Table 3.30: Connection against rocking - equivalent bi-linear curve parameters.

3.2.3 Angle brackets equivalent spring - A

The effect of the connection against the slippage are depend on the number of angle brackets n_a (or other devices i.e. screws), from the mechanical characteristics of the elements and from the friction force due to the vertical loads.

As a general consideration the friction force is not taken into account as resisting mechanism by the current standards. So according to these prescription the contribution could be neglected in the equation, assuming a lower resistance an a more flexible system. However the influence of the friction could be take into account through a "friction block".

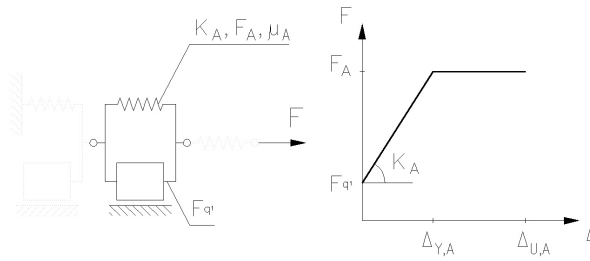


Figure 3.76: Angle brackets + friction element.

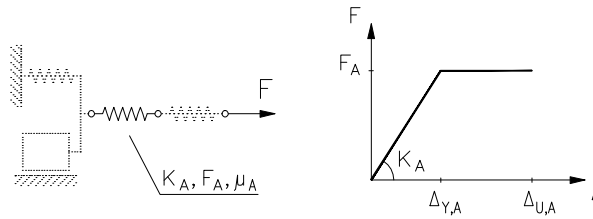


Figure 3.77: Angle brackets.

According to the "in parallel" connection the overall behaviour of the system is defined as:

$$\Delta_{Y,A} = \delta_{y,a} \quad \Delta_{U,A} = \delta_{u,a}$$

$$\mu_A = \frac{\Delta_{U,A}}{\Delta_{Y,A}} = \mu_a$$

If the friction contribution is taken into account in the model the equation becomes:

$$F_A = f_a n_a \quad K_A = \frac{F_A}{\Delta_{Y,A}} = k_a n_a$$

$$F_A = F_q + f_a \cdot n_a = \mu \cdot q \cdot l + f_a \cdot n_a$$

$$\left\{ \begin{array}{l} K_{A,na} \rightarrow \infty \\ K_{A,a} = \frac{(F_A - F_q)}{\Delta_{Y,A}} \end{array} \right.$$

The input data are summarized in Table 3.31:

		Angle brackets (A)	
Tests:		Monotonic	Cyclic
F_A	[kN]	115.1	83.9
$\Delta_{Y,A}$	[mm]	11.6	7.1
$\Delta_{U,A}$	[mm]	22	21
K_A	[N/mm]	9922.1	11748.4
μ_A	-	1.9	2.94

Table 3.31: Connection against horizontal slippage - equivalent bi-linear curve parameters.

3.2.4 Sheathing to frame connection - SH

The mechanical characterization of the frame to sheathing connection spring was carried out according to analytical models proposed in literature. These proposal have shown good results using experimental input data.

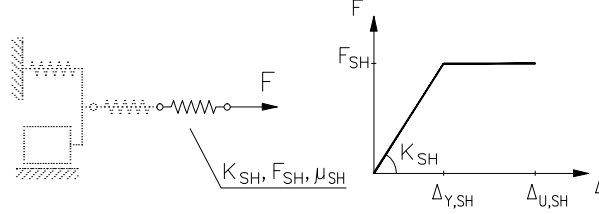


Figure 3.78: Sheathing to frame connection.

The proprieties of the SH spring depends from the fasteners proprieties (resistance f_c , stiffness k_c , ductility μ_c) and from the geometry of the wall segment (height h , length l , panel width b , nail-spacing s , number of sheathing sides n_{sides}).

The first parameter is the slope of the first part of the load versus displacement curve, calculated according to the model proposed in the previous section as:

$$K_{SH} = \frac{F_{SH}}{\Delta_{Y,SH}} = \frac{n_{sides}}{\frac{1}{k_c} \lambda(\alpha) \frac{s}{l}}$$

Where $\lambda(\alpha)$ is a geometrical parameter depend from the aspect ratio of the panel $\alpha = h/b$:

$$\lambda(\alpha) = 0,810 + 1,855 \alpha$$

The second parameter is the load bearing capacity F_{SH} , calculated according to the model proposed in EN1995:

$$F_{SH} = n_{sides} f_c c \frac{l}{s}$$

Where:

$$c = \begin{cases} 1 & \text{se } \alpha < 2 \\ \frac{\alpha}{2} & \text{se } \alpha > 2 \end{cases}$$

From the previous data F_{SH} K_{SH} can be derived the displacement that correspond to the elastic limit:

$$\Delta_{Y,SH} = \frac{F_{SH}}{K_{SH}}$$

The third parameter, μ_{SH} , could be defined from the model proposed by Casagrande. This model is based on a incremental analysis of the fully anchored wall segment. According to this analysis the horizontal load increase step by step, and when the most stressed fastener reach the yielding point the stiffness matrix is updated, considering the internal redistribution of the stress. The "updating" procedure consist in the re-definition of the stiffness matrix neglecting the presence of the yielded fastener (because the slope of the plastic branch is zero). The ultimate displacement (and thus the ductility) correspond to the bracing system failure (kinematic mechanism). Further detail about the analysis can be found in [29].

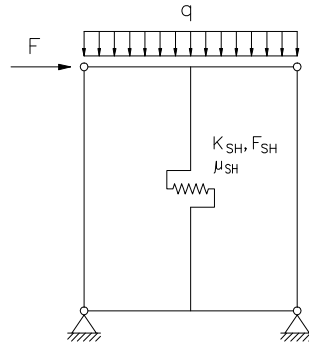


Figure 3.79: Fully-anchored wall

The results of the analysis is an explicit formulation that link the ductility of the single fastener μ_c with the ductility of the fully anchored wall μ_{SH} :

$$\mu_{SH} = \rho_{(\alpha)} \mu_c + v_{(\alpha)}$$

Where:

$$\begin{cases} \rho_{(\alpha)} = -0,054 \alpha^2 + 0,350 \alpha + 0,305 \\ v_{(\alpha)} = 0,068 \alpha^2 - 0,415 \alpha + 0,753 \end{cases}$$

From the expressions is worth noting that the ductility is not influenced by the fasteners spacing, but the only variable is the ductility of the fastener and the aspect ratio of the panels α . The results are summarized in Table 3.32:

Sheathing to frame connection (SH)			
Tests:		Monotonic	Cyclic
F_{SH}	[kN]	55.3	58.5
$\Delta_{Y,SH}$	[mm]	15.8	13.4
$\Delta_{U,SH}$	[mm]	40.8	38.1
K_{SH}	[N/mm]	3509.8	4368.9
μ_{SH}	-	2.6	2.8

Table 3.32: Sheathing to framing connection - SH - equivalent bi-linear curve parameters.

3.2.5 Complete model - H-A-SH interaction

As presented in the introductory part of this section the model is based on the "in-series" assembly of non linear springs (Figure 3.80).

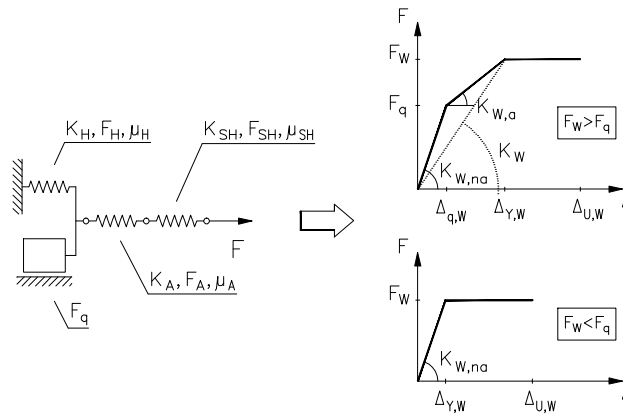


Figure 3.80: Rheological model.

Table 3.33 and Figure 3.81 report the load versus displacement parameters and the curves of the single springs.

Bi-linear curve parameters						
Connection	H(S)	H(C)	A(S)	A(C)	SH(S)	SH(C)
F_i [kN]	85.6	87.1	115.1	83.9	55.3	58.5
$\Delta_{Y,i}$ [mm]	10.3	9.5	11.6	7.1	15.8	13.4
$\Delta_{U,i}$ [mm]	25.8	23.9	22	21	40.8	38.1
K_i [N/mm]	8311	9162.5	9922.1	11748.4	3509.8	4368.9
μ_i -	2.5	2.5	1.9	2.94	2.6	2.8
$K_{i,na}$ [N/mm]	∞	∞				
$K_{i,a}$ [N/mm]	5869.4	6515.8				
F_q [kN]	25.2	25.2				

Table 3.33: Parameters: Comparison between the single component of the rheological model.

The label "S" define the parameters obtained from the monotonic tests while the

label "C" indicates the parameters obtained from cyclic tests.

The load bearing capacity of the wall correspond to the lower yielding value between the single springs, because the wall segment is an isostatic structure.

$$F_W = \min(F_H; F_A; F_{SH}) = F_i$$

The stiffness is influenced by the stabilizing effect due to the vertical load. The shear block introduce two separate fields, the first where the overturning moment is greater than the stabilizing moment (no-uplift, $F_W < F_q$) and a second where the overturning moment is greater then the stabilizing moment (uplift, $F_W > F_q$).

Case 1: $F_W < F_q$

In this sub-case the vertical dead loads prevent the uplift of the wall. This condition occurs in case of hight vertical dead load (q) and long-shearwall segment. The spring "H" which correspond to the rigid body rotation is unloaded and the equation using $K_{H,na} \rightarrow \infty$ become:

$$K_{W,na} = \frac{1}{\frac{1}{K_{H,na}} + \frac{1}{K_A} + \frac{1}{K_{SH}}} = \frac{1}{\frac{1}{K_A} + \frac{1}{K_{SH}}}$$

The yielding displacement $\Delta_{Y,W}$ is defined as:

$$\Delta_{Y,W} = \frac{F_W}{K_{W,na}}$$

When the maximum load is reached by the weaker component of the model the increment of displacement can only take place in this element. According to a elastic-perfectly plastic constitutive law the increment of displacement at constant level of load can occur only in the plastic branch. Thus the maximum plastic displacement is equal to the length of the plastic branch of the weaker spring:

$$\Delta_{pl,W} = \Delta_{pl,i} = \Delta_{U,i} - \Delta_{Y,i}$$

The ductility of the system becomes :

$$\Delta_{U,W} = \Delta_{Y,W} + \Delta_{pl,W}$$

$$\mu_W = \frac{\Delta_{U,W}}{\Delta_{Y,W}} = 1 + \frac{\Delta_{pl,W}}{\Delta_{Y,W}} = 1 + \frac{\Delta_{pl,i}}{\Delta_{Y,W}}$$

The plastic displacement of the weaker link can be expressed as:

$$\Delta_{pl,i} = \Delta_{U,i} - \Delta_{Y,i} = \Delta_{Y,i} (\mu_i - 1) = \frac{F_i}{K_i} (\mu_i - 1) = \frac{F_W}{K_i} (\mu_i - 1)$$

The relationship between the system ductility μ and the weaker link ductility is:

$$\mu_W = 1 + \frac{K_{W,na}}{K_i} (\mu_i - 1)$$

The equation set for if $F_W < F_q$:

$$\begin{cases} K_{W,na} = \frac{1}{\frac{1}{K_A} + \frac{1}{K_{SH}}} \\ F_W = \min(F_H; F_A; F_{SH}) = F_i \\ \mu_W = 1 + \frac{K_{W,na}}{K_i} (\mu_i - 1) \end{cases}$$

Case 2: $F_W > F_q$

When the overturning moment due to the horizontal load at the top of the wall exceed the moment due to the vertical dead load the hold-down is activated. Hence the overall behaviour of the wall is defined by three linear parts with a progressive stiffness reduction (Figure 3.80). For values of horizontal load lower than F_q only the contribution of A and SH are exploited. When the horizontal force overcome F_q all the contribution are activated.

For $0 < F < F_q$ the stiffness is equal to the previous case:

$$K_{W,na} = \frac{1}{\frac{1}{K_{H,na}} + \frac{1}{K_A} + \frac{1}{K_{SH}}} = \frac{1}{\frac{1}{K_A} + \frac{1}{K_{SH}}}$$

The displacement which correspond to the load level " F_q " is:

$$\Delta_{q,W} = \frac{F_q}{K_{W,na}}$$

After this value also the H spring is active. For $F_q < F < F_W$ the slope of the elastic branch is lower:

$$K_{W,a} = \frac{1}{\frac{1}{K_{H,a}} + \frac{1}{K_A} + \frac{1}{K_{SH}}}$$

The horizontal displacement at the elastic limit is:

$$\Delta_{Y,W} = \frac{F_q}{K_{W,na}} + \frac{(F_W - F_q)}{K_{W,a}} = \frac{F_W}{K_{W,a}} - \frac{F_q}{K_{H,a}}$$

Also for this sub-case the ductility of the system is related to the proprieties of the weaker link (H o A o SH).

$$\Delta_{pl,W} = \Delta_{pl,i} = \Delta_{U,i} - \Delta_{Y,i}$$

$$\Delta_{U,W} = \Delta_{Y,W} + \Delta_{pl,W}$$

$$\mu_W = \frac{\Delta_{U,W}}{\Delta_{Y,W}}$$

The secant stiffness of the wall segment at the elastic limit is:

$$K_W = \frac{F_W}{\Delta_{Y,W}} = \frac{F_W}{F_W \left(\frac{1}{K_{W,a}} - \frac{F_q}{F_W K_{H,a}} \right)} = \frac{1}{\frac{1}{K_{W,a}} - \beta \frac{1}{K_{H,a}}}$$

where:

$$\beta = \frac{F_q}{F_W} < 1$$

Summarizing the sub case $F_W > F_q$ equation are:

$$\left\{ \begin{array}{l} K_{W,na} = \frac{1}{\frac{1}{K_a} + \frac{1}{K_{SH}}} \\ K_{W,a} = \frac{1}{\frac{1}{K_{W,a}} + \frac{1}{K_a} + \frac{1}{K_{SH}}} \\ F_q = \frac{q l^2}{2 h} \\ F_W = \min(F_H; F_A; F_{SH}) = F_i \\ \mu_W = 1 + \frac{K_W}{K_i} (\mu_i - 1) \end{array} \right.$$

For the tested geometry and for the vertical load magnitude ($q = 20kN/m$) the second set of equation shall be used because the overturning moment overcome the stabilizing moment. The weaker element was the sheathing to frame connection (SH) thus $F_W = F_i = F_{SH}$. The numerical results are summarized in Figure 3.82.

Rheological model of the wall (W)			
Tests		M	C
$K_{W,na}$	[N/mm]	2592.7	3184.6
$K_{W,a}$	[N/mm]	1798.3	2139.1
K_W	[N/mm]	2089.6	2490.8
F_W	[N/mm]	55.3	58.5
F_q	[kN]	25.2	25.2
μ_W	-	1.95	2.05
$\Delta_{Y,W}$	[mm]	26.5	23.5
$\Delta U, W$	[mm]	51.5	48.1
$\Delta q, W$	[mm]	9.7	7.9

Table 3.34: Model outcome - table of the parameters - for cyclic input data set (C) and monotonic data set (S).

In Figure 3.83 and 3.84 are shown the comparisons between the analytical results of the model and the experimental results of the full-scale tests. Figure 3.83 show the results of the monotonic test M_GFB whereas the Figure 3.84 show the results of the cyclic test C_GFB. The results of the cyclic test exhibit a good agreement with the model outcome.

In order to obtain a more "clear" graphic comparison in Figure 3.85 the first cycle envelope curve load-versus-displacement curve was bi-linearised with the same criteria adopted for the single springs. The cyclic protocol is the most severe in terms of ultimate displacement. The fully reverse cycles led to a premature failure of the connection between frame and sheathing, thus this situation is considered as most representative case. Moreover to achieve a clear numerical comparison the stiffness value of the model is expressed as secant yield value:

$$K_W = \frac{F_W}{\Delta_{Y,W}} = \frac{1}{\frac{1}{K_{W,a}} - \beta \frac{1}{K_{H,a}}}$$

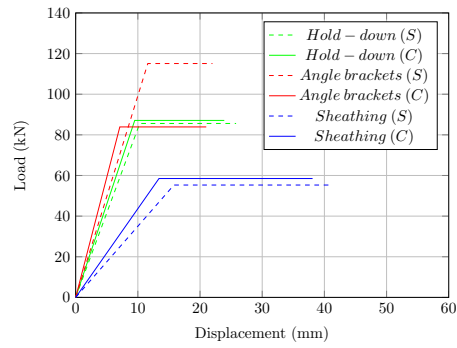


Figure 3.81: Bi-linear curves: Comparison between the single component of the rheological model.

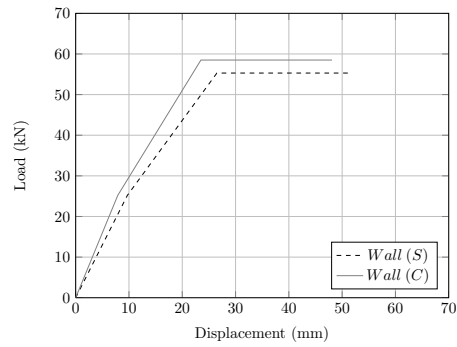


Figure 3.82: Model outcome - load vs displacement curves for cyclic input data set (C) and monotonic data set (S).

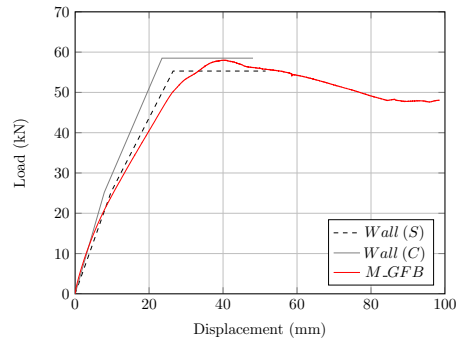


Figure 3.83: Comparison between the model outcome and the monotonic test result (M_GFB)

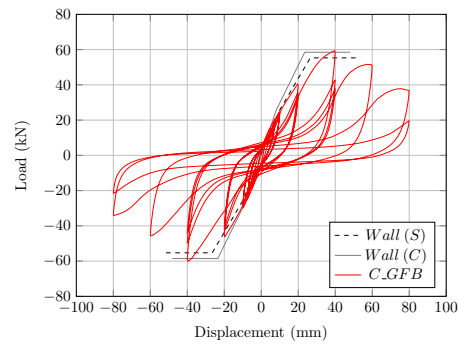


Figure 3.84: Comparison between the model outcome and the cyclic test result (C_GFB)

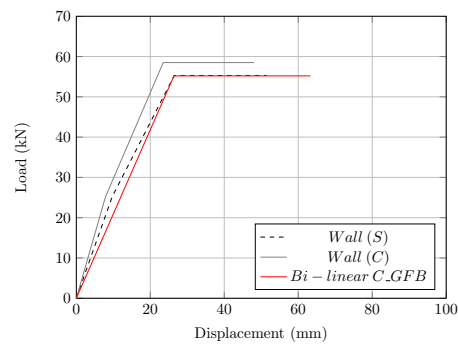


Figure 3.85: Comparison between the model outcome and the first loop backbone curve of the cyclic test (C_GFB)

Comparison: Experimental tests - rheological model output						
Tests		Experimental	Model		Model	
		C_{GFB}	S		C	
K_W	[N/mm]	2088.5	2089.6	(-0.05%)	2490.8	(+19.3%)
F_W	[N/mm]	55.2	55.3	(+0.11%)	58.5	(+5.9%)
$\Delta_{Y,W}$	[mm]	26.4	26.4	(+0.06%)	23.5	(-11.2%)
μ_W	-	2.4	1.95	(-20.14%)	2.05	(-15.8%)

Table 3.35: Comparison between experimental and analytical data.

3.2.6 Comment

The model shows a good agreement, in terms of strength and stiffness, with the experimental results obtained from the experimental tests (monotonic and first cycle backbone curves of cyclic test). The load bearing capacity of the wall segment was predicted with a maximum difference that range between 0.1% and 5.6%. A wider range was found for the secant stiffness 0.05% and 19% and for the yielding point displacement (0.06% and 11%). However as pointed out several times in this document the stiffness and the yielding point estimation are influenced by the shape of the curve, hence to achieve a complete characterization a high number of test is necessary to achieve a representative statistical population.

The ultimate displacement of the first cycle backbone complete curve is overestimated both from the "C" and "S" data set.

Nevertheless the failure of the wall according to the impairment of strength criterion have been occurred at $40mm$ in terms of total displacement (Figure 3.84) and therefore the model overestimate about the 16% of the actual experimental value.

The gap between the test result and the model output are attributable to the low number of tests carried out on the staples and on the influence of the boundary condition on the test. Probably with a large number of cyclic and monotonic tests, with a more representative input parameters, the experimental curves would be approximated better in terms of ultimate displacement

3.3 Conclusions

The previous chapter report the outcome of laboratory tests carried out on light-timber framed components. This part of the research have been focused on the mechanical characterization of the anchor systems and walls segments sheathed by gypsum fibre boards connected to the frame by means of staples. The results have been analysed to investigate the mechanical proprieties of the system and to assess the main difference with the wood framed walls sheathed with oriented strand boards or plywood. The interaction between the components (hold-down, angle brackets, sheathing) was implemented in a simplified model to assess the reliability of the analytical prevision.

The plastic behaviour and energy dissipation of the structures according to the recent design methods and literature are fundamental parameters of the seismic response. The high reduction factor (q) proposed in [2] and in other international codes

attest that timber-framed walls buildings could reach at the ultimate limit states a high energy dissipation with a large amount of damages (non-linear plastic behaviour) without a global collapse.

However as introduced in the introduction of this section the seismic response of timber building is strongly related to the behaviour of the connections between the elements (joints). In the platform buildings the main sources of energy dissipation are related to the anchor system between the walls and foundation (hold-down and angle brackets) and the connection between timber frame and sheathing panels. Concerning these aspects, three main sub-cases (failure modes) could occur at the ultimate limit state (ULS):

- the first, related to the anchor system failure, ensure the lower performance in terms of ductility. The failure of hold-down or angle brackets could be caused by steel to timber connection - steel flange or anchor failure that correspond, according to the experimental tests, to the most brittle mode.
- the second, related to the sheathing to frame connection, ensure the best performance in terms of ductility and energy dissipation. The small diameter of the fasteners develop a great number of plastic hinges moreover this mechanism allows an efficient control of the failure mode.
- the third, related to a mixed failure mode, ensure a good seismic response but the mechanism is not well defined also because the material related properties have a strong influence on the mechanical properties of the connections (design hypothesis, over-strength, load distribution).

Therefore, according to the modern design criteria, the failure mechanism control is extremely important in the definition of the basic parameters of the design. The ratio between the mechanical proprieties (strength, stiffness and ductility) of the single component is strongly related to the overall behaviour of the system. High level of force reduction factors have to be coherent with the most convenient failure mode that should developed in the dissipative zone assuming adequate over strength factors for the non-dissipative zone and for the brittle elements.

The performance in terms of energy dissipation of these zones is related to the hysteresis loops area of the cyclic test protocol. In this contest, the tests carried out on the connection system and on the shear walls, are fundamental.

Hold-downs and angle brackets during the tests reaches the ultimate condition of the steel to timber connection (nails) whereas the steel components have never reached the failure mechanisms.

The cyclic tests on anchor devices highlight the typical steel-to-timber hysteresis loop characterized by a pinching effect. The impairment of strength between the 1st and the 3rd cycle results below the 10% in case of hold-down. On the contrary, an impairment of 26% was obtained for angle brackets for a displacement of 14 mm. The second and third hysteresis loop, especially for the hold down device, exhibit a significant lower energy dissipation due to the embedment of the timber fibres.

In order to reproduce the boundary condition of shear walls tests were carried out on two samples. The first one was sheathed by gypsum fibres boards whereas the second was sheathed by oriented strand boards, both the sheathing were connected by means of the same staples (1.35x1.59x45mm).

The comparison between the test results highlight a lower stiffness (-6.4%) and a lower resistance (-15%) of the wall sheathed by OSB, with a similar yielding displacement and ductility. Good agreement between monotonic and cyclic tests was found, the first loop backbone curve of the cyclic test and the monotonic test exhibit similar results in terms of stiffness and maximum load. However, according to the failure criterion, the impairment of strength between the first and the third loop ($v = 40mm$ amplitude), indicate a premature failure of the system. The mechanism failure of the wall was related to the oligo-cyclic fatigue failure of the staple legs. Therefore, in tested wall, the sheathing-to-framing connection represents the weakest component of the structural system.

The wall sheathed by GFB and connected by staples show lower values of ductility compared to other systems such as OSB+nails reported in [7].

This fact was confirmed also by a previous experimental campaign [29] and from the literature. However the results of the tests and the predictive models based on input values from the single component (stiffness, strength, ductility) shows that the sheathing to frame connection represent the most convenient dissipative element of the system.

Concerning this issue the design rules and the detailed procedures, as pointed out in the introduction, have not been developed in the European codes yet. The need of a deeper discussion and assessment of these issues is nowadays the leitmotif of different researches carries out in the last years on the timber constructions. Hence the goal of these studies is the definition of a design strategy supported by the rules of the capacity design ([30]). The efforts shall be concentrated on the single devices in order to obtain efficient anchor systems, where the failure modes involve only the ductile mechanisms, and the shear walls that are connected with these component.

Chapter 4

Full scale shake table tests

4.1 Introduction

This section presents two shake table tests carried out on light timber framed wall buildings. These experimental tests were a part of an extensive research project promoted by an European programme for research and technological development SERIES. The acronym stands for "Seismic Engineering Research Infrastructures for European Synergies", the aim of the activity is the promotion of the cooperation between researchers from different European countries and the dissemination of the results.

Through the transnational access financing a lead user (University of Trento) proposed an experimental analysis of the most widespread timber constructive system. In this context three Universities, Trento (Italy) - Minho (Portugal) and Graz (Austria), and the Portuguese National Laboratory of Civil Engineering have done tests on three constructive systems. University of Trento had performed two tests on light timber framed buildings, University of Minho on a log-house and Graz University of Technology on a cross laminated timber panels building. All specimens, as deeper discussed in the next sections, had the same geometry (plan dimensions 7 x 5 meters) and architectural layout.

This research is probably one of the first organic test campaigns on the most European widespread constructive systems. In the next subsection are summarized the main test campaigns carried out in the last fifteen years on shake table, which constitutes an essential basis for planning and carrying out the test project SERIES. After this brief introduction of the state of the art the description of the SERIES tests

and main conclusions and outcomes will be discussed.

4.1.1 State of the art

The growing popularity of the timber constructive system in the southern countries of the European area are related to different key issues. First the attention paid to the energetic consumption and the eco-sustainability of the construction. Second the fast constructive process thanks to the prefabrication. However another important driving force for this system was, especially for the most seismic prone areas, the load bearing capacity when Earthquake occur.

Italy as other southern European countries was subjected to catastrophic earthquake in the last decades where the limits of the most vulnerable buildings such as masonry and older reinforce concrete building were highlighted.

These events had promoted research in the assessment of the existing buildings and the development new techniques to reinforce and improve the capacity of the historic building heritage, while on the other start the development of more efficient buildings systems such as timber framed and CLT construction.

Concerning the light timber framed constructions the recent studies are based on the experience of previous experimental campaign developed in the United States between 2000 and 2010. In particular two key works are the CUREE-Caltech (Consortium of Universities for Research in Earthquake Engineering) and the NEESWOOD research projects.

The first was probably one of the earlier dynamic full-scale test campaign on a full scale-woodframe building ¹. The aim of the project, coordinated by the Californian Institute of Technology (Caltech), was the analysis of the performance of north American-type woodframe building which after the Northridge earthquake (17/01/1994) shown high level of damages due to seismic loads. The project was funded by the Federal Emergency Management Agency (FEMA) and was planned to analyse different critical point through large-scale tests and preliminary tests on single component.

Three full scale shake table tests were carried out on different samples (from Curee documentation [31]):

- **"Shake Table Tests of a Simplified Two-Story Single-Family House":**The main objective of this task is to perform shake table testing on a simplified full-scale two-story single-family house to measure and quantify the overall dynamic

¹ Before this test campaign different tests were performed on the Japanese traditional constructive system, but this construction were typically build as post and beam frame

responses for various construction configurations and to document how the distribution of forces within the structure may change between the various configurations. [André Filiatrault; Chia-Ming Uang and Frieder Seible (UC San Diego)]

- **"Shake Table Test of Multi-Story Apartment Building with Tuck-under Parking"**: The main objective is to conduct multi-directional shake table tests of a full-scale three-story multi-family building with tuck-under parking. The building is designed and constructed to represent 1960's engineering practice in Northern California. In addition to testing the original building, a rehabilitated building will be tested using a special moment resisting steel frame in the open front to improve the seismic performance of the first story. [Khalid M. Mosalam (University of California, Berkeley)]
- **"Shake Table Tests Simplified Model"**: The main objective of this task is to perform shake table testing on a simplified model to verify the reliability of the non-linear finite element dynamic analysis model [R.O Foschi, F. Lam, H. Prion, and C. Ventura (University of British Columbia)].

The first task was divided in "sub-sections" to address different topics about the structural and non structural behaviour. The sample was a single family house with a footprint of "4.8x6 meters. The material and the members cross sections were the commonly adopted in the Us (10mm Oriented strands boards, 2.8x65 mm nails) and also the typical connection of the North American woodframe were adopted (internal hold down, external steel strap). The design of the structure was carried out according to the 1994 edition of the Uniform Building Code (ICBO) to assess the engineering design provisions that were followed after the Northridge earthquake. The architectural layout was planned to introduce a significant eccentricity of the lateral load bearing walls along the shake table motion direction to emphasize the torsional effects. The walls opening distribution in the orthogonal direction was kept symmetric in order to aid the outcomes interpretation.

Quasi-static and dynamic tests were carried out on the samples in different configuration (one floor / two floors, different nail patterns, openings, different connection type, finish materials) and using different input signals (two recorded time history with different PGA scaling).

The seismic test procedure was planned to investigate the "two stories with roof" building behaviour under different layouts:

- two sides fully sheathed, two sides sheathed with openings [Phase 5]

- two sides sheathed with window and small door openings, two sides sheathed with openings [Phase 6]
- two sides sheathed with window and small door openings with "wastewall" sheathing removed (panels above and under the openings), two sides sheathed with openings [Phase 6A]
- two sides sheathed with window and small door openings using perforated shearwall design, two sides sheathed with openings [Phase 7]
- two sides sheathed with window and small door openings using perforated shearwall design with anchor bolt adjacent to door openings, two sides sheathed with openings [Phase 7A]
- two sides sheathed with window and small door openings using conventional construction, two sides sheathed with openings [Phase 8]
- two sides sheathed with window openings and small door opening on west wall and large door opening on east wall, two sides sheathed with openings [Phase 9]
- two sides sheathed with window openings and small door opening on west wall and large door opening on east wall, two sides sheathed with openings, finished with exterior stucco and interior gypsum wallboard [Phase 10]

Seismic Test Level	Ground Motion signal	Hazard Level	PGA [g]
1	Northridge Canoga Park	99.99%/50 years	0.05
2	Northridge Canoga Park	50%/50 years	0.22
3	Northridge Canoga Park	20%/50 years	0.36
4	Northridge Canoga Park	10%/50 years	0.5
5	Northridge Rinaldi	2%/50 years	0.89

Table 4.1: *Test Phases - tests and PGA from [31]*

As shown in Table 4.1 two different input signals were used. The first one - recorded at Canoga park, scaled to represent different probability of exceedance in the reference period, was selected as "ordinary ground motion" to reproduce signal recorded at distance greater than 10km from the epicentre of the earthquake. The second signal recorded at Rinaldi was selected as "near-field ground motion" .

The test procedure as summarized in the previous paragraphs was organized in different steps with a sequence of quasi-static, modal parameters identification

and dynamic tests. After each test described in the Table 4.1 the damages was visually inspected and recorded. This approach requires repair operation to restore the structural damages in order to get the initial capacity and stiffness of the sample.

The outcome were focused on the definition of the dynamic characteristics and the overall response of the building. Moreover another fundamental results was the experimental analysis of the relationship between the ground motion severity and the structural and non-structural damages. The major findings of this extensive and detailed investigation, well described in [31], are summarized below:

- windows and doors openings have influenced the overall behaviour of the building both in the stiffness (lateral displacement) and increase of overturning. This outcome was highlighted from the comparison of the fully sheathed structure and the structure with symmetrical openings;
- torsional moment introduced by the non-symmetrical opening distribution caused a significant differences in the deformation and in the force distribution on the tension ties;
- the sheathing panels above and below the windows/doors provide a significant contribution to the stiffness of the system;
- the use of hold down devices, nailed directly on the studs, reduce the displacement of the walls;
- the use of non structural layers increase the stiffness and load bearing capacity of the system (the gypsum panel were nailed above the OSB panels).

Another research project which was concentrated on the light timber framed building, once again the Us typology, is the NEESWood carried out by the consortium of University (Network for Earthquake Engineering Simulation).

The project layout, was slightly different from the CUREE, because the efforts in this case were focused on gap between the current design provisions and the actual performance of timber mid-rise buildings (five or six-story). Therefore the research was focused mainly on the development of a new logical performance-based seismic design for mid-rise buildings and not only on the assessment of the current regulation or on the mitigation of the weaker point of the seismic response of the typical North American framed houses (2" by 4").

Also this test campaign was organized in more than one step. The first, indicated as "benchmark" test, was carried out to provide of an existing building under different

seismic intensity levels and to obtain a database for the numerical model improvement [32]. The test was performed on a two-story building with a footprint of 17 by 7 meters for a total height at the ridge of 5.5 meters. It represents one unit of a two-story townhouse containing three units with an attached two-car garage, designed according to the code of the latest '80.

The structural system was based on "two by four" and "two by six" inches frame elements sheathed by OSB panels (10mm) connected by means of $2.8 \times 65 \text{ mm}$ smooth nails. The test procedure of this first part of the test was planned to investigate:

- engineered wood structural (shear) walls alone [Phase 1];
- wood structural walls incorporating viscous fluid dampers [Phase 2];
- installation of gypsum wallboard to engineered wood structural walls [Phase 3];
- installation of gypsum wallboard to interior partition walls and ceilings [Phase 4];
- installation of stucco as exterior wall finish and the structure was fully furnished [Phase 5].

The outcome of the benchmark tests highlight the good response of the timber framed building regard safety level.

According to the other studies the influence of the drywall and exterior stucco finish on the stiffness and strength were not negligible. A significant reduction of the natural period was observed through the dynamic identification of the building before and after the installation of the finishing on the structural walls. The stucco was an important component, on the contrary of the European construction, because it consisted of a mesh of wire lath (16 gauge steel wire mesh) and 3 coats of Portland cement-based plaster instead of a thin layer of plaster.

As a consequence the equivalent lateral stiffness of the "only-structural" layout deteriorate more rapidly through the seismic tests than the configuration stiffened by the finishing (the ground floor is the critical level). The damage level of the structure was significant only for the most severe seismic input. At lower level minor damages (hairline cracking) had occurred on the corner of the opening.

After the most severe test the splitting of the 2x4" and 2x6" sill plates around the entire perimeter of the building was observed. As pointed out by the authors this failure would be very costly to repair in a real building.

The maximum inter-storey drift was about 3.5% in the first level. Another interesting measure was the tension force on the hold-down elements. A maximum anchor bolt force of approximately 27 kN (approximately 44% of ultimate capacity), was recorded in a hold-down device during the Phase 5 building.

During a second step, which represent the core of the project, a six storey building with a steel moment frame structure at ground floor was tested on a large tri-directional shake table (E-Defence, Kobe Japan). The structure was made with 2x6" wall frame element (multiple element for the boundary members) braced by OSB panels. The horizontal diaphragms were realized through I-joist and glue laminated beams sheathed by OSB panels. The overturning was prevented through vertical steel rods connected by shrinkage compensating devices. The structure was tested with and without the moment frame steel structure (the ground floor was fixed to test only the timber structure). Once again the structure demonstrate an good seismic behaviour without significant structural damages. Nevertheless the results of this second part is beyond the scope of this document.

A direct extension of the results and outcomes of the tests on other geometry, materials and anchor systems is difficult and could be misleading. The traditional 2x4" (or 2x6") American systems analysed in these experimental campaign is quite different from the European system. The main differences deals with the sheathing system (one side instead of two sides), the fasteners (smooth nails instead of ring nails) and the anchor system (internal hold-downs instead of external hold-downs). Moreover other parts of the building often are realized with different techniques compared to the Us type. As an example the floors are often made with timber box element or timber beams with a in-plane and out of plane stiffness greater than the US traditional I-joist floor. However, despite the differences, these "on field" experience were the fundamental references for a recent test campaign carried out by the University of Trento. This research was performed in the framework of the "chi-quadro" project, financed by the local govern (Provincia autonoma di Trento), which in the past has promoted other important activity on other timber constructive system (multi-storey 3 and 6 cross laminated timber shake table tests SOFIE [33]).

The project, as for the previously mentioned experiences, was organized in two steps. The first was the analysis of the connection through experimental quasi-static monotonic and cyclic tests (sheathing to frame connection [6] - angle brackets and hold down [5] - full scale shear walls [14]). In these preliminary test different commonly used solution of timber framing have been analysed. The aim of the project was the characterization of the seismic performance of a European building design according

to the current technical standards. The specimen of the capstone test, carried out on the shaking table of the TreesLab laboratory (Pavia, Italy), was a 7x5 m residential three storey building with an overall height at the ridge of 7.5 meters.

Only the structural component of the building was tested (no-finishing layers) under a unidirectional ground motion along the main direction of the building. The ground motion was selected among the most severe earthquake compatible with the meridional European geophysical situation. The frequency content of the selected signal (Montenegro 15/04/1979) was significant in the range of the natural periods of the structure and the constant part of the spectrum was large enough to ensure the same acceleration even if the periods increase. The scaling of the reference input signal have been increased from 0.07g up to 1.0g with intermediate tests at 0.27g, 0.5g, 0.7g.

The outcome of the tests highlight the excellent response of the tested building. No significant damages were detected until the 1.0g PGA. After this input level, the measured fundamental period was changed, confirm that the structure behave beyond the elastic limits. However the visual inspection of the structure did not show any relevant damage.

4.1.2 SERIES project

The SERIES project, "Seismic Engineering Research Infrastructures for European Synergies", was an organic project focused on the research cooperation between the institutions of different countries carried out in the framework of a European research funding.

The "timber buildings" task of this research deal with the seismic behaviour of different timber structural systems.

Traditionally the seismic engineering have been addressed in the earthquake prone areas such as Italy, Spain, and Portugal where the use of timber as structural material is younger whereas in the northern European countries, which have a long timber construction history, the seismic load is not important as wind and vertical loads.

The aim of this proposal is the analysis of the performance of four common structural systems in order to investigate deeply several aspect of the structural response and the behaviour of the non structural components during earthquake.

Thanks to the transnational access financing, three University - Trento (Italy) - Minho (Portugal) and Graz (Austria), and a research laboratory (National Laboratory of Civil Engineering) have carried out test on three constructive systems. For each

system, one full-scale specimen of a multi-storey timber house was to tested on the shaking table:

- log house system (LH) - university of Minho;
- platform frame system braced by OSB sheathing (LTF-OSB) - University of Trento;
- platform frame system braced by gypsum fibre panel (LTF-GF) - University of Trento;
- cross-laminated system (CLT) - University of Graz.

The buildings geometry, characterized by 7x5 meters footprint, and the architectural layout were exactly the same for all the tests. The only exception was the log house, because according to the current state of the art, a three-storey building is unusual. Therefore, the number of storey was limited to two.

In order to compare the seismic response of the different constructive system the first phase of each test was carried out with the same input signals following a common test protocol. The signal were scaled up to the maximum capacity of the shake table capacity.

A second step of the test procedure was dedicated, for each sample, to specific tests such as different input signals, different structural layouts and anchor system.

Despite of the common geometry and the same test procedure each test has been planned to investigate peculiar aspect of the seismic response which in the past have not been sufficiently discussed.

Often the seismic response of timber building during earthquake is associated only to the material proprieties (weight to strength ratio) and to the mechanical fasteners used to connect the members, nevertheless these two features represents necessary but not sufficient conditions to achieve this goal. High values of "seismic-performance" such as energy dissipation and displacement capacity can be reached only if the brittle failure are avoided and the collapse is related to ductile mechanisms. The European design codes provides only few prescriptions about the seismic design according to capacity design especially for the multi-storey buildings. These design rules are general remarks, certainly valid, but sketchy from the practical application perspective. Moreover prescription and design rules for new-developed materials such as CLT and gypsum fibre sheathing boards as well as traditional log-house system are not reported in the current codes.



(a)



(b)



(d)

Figure 4.1: Series project tests - a) Log-house - b) timber light-frame braced by OSB - c) timber light-frame braced by GFB - d) CLT building.

The traditional Log house system, to the best author knowledge, had been investigated only by few authors especially regard the vertical load bearing capacity. The lateral load bearing behaviour was analysed for the traditional round log and for handcrafted Saddle Notch that are not comparable with the modern system.

Cross laminated timber, as other new materials developed in the last decades, was deeply investigated by tests campaigns promoted by different research groups Europe. Nevertheless different aspects of the global behaviour of the constructive system should be tested and the design hypothesis about the dissipative behaviour of the system should be confirmed.

Light-timber framed houses had been widely investigated but some aspect of the seismic behaviour still need to be investigated. The differences between the European timber frame system and the American system on which a wide literature about the seismic is already available should be discussed. The European system load bearing capacity was investigated by another tests on shake table ([34]) where the excellent resistance was highlighted. However the performance of other materials such as gypsum fibre, the influence of the non-structural elements and the level of damage related to the inter-storey drift are interesting arguments that need to be investigated.

The next chapters of the thesis are focused on the test results and on the analysis of the main outcome of the tests on the timber framed building

4.2 Shake table tests on full-scale TFS buildings

The timber research group of the University of Trento in the last five years have been involved in several tests campaigns to characterize the mechanical behaviour of the single components and the overall behaviour of the building. One of the most representative steps of these programs were the shake table tests carried out in the framework of the SERIES project.

Two light-timber framed building have been tested using the common technical solution and materials. The first specimen was assembled using OSB (Oriented Strand Boards) structural sheathing panels connected to the wall timber frame by means of nails. It was completed with external and internal claddings. One room, at the first level, was also equipped with a laminate floor, drywall and ceilings, doors, windows and technical implants. The second timber frame house was assembled using gypsum fibre structural sheathing panels connected to the wall timber frame by means of steel staples (PF-GF). In this case, only the structural skeleton was tested, without

the presence of external finishing.

These tests were planned to achieve different information about the seismic performance of the TFS, in the next sections the goal of the tests and the geometry of the building will be described.

4.2.1 Scope of the tests

The first test series has been planned to analyse the behaviour of the building subjected to bi-directional ground motion and to assess effect of the inter-storey drift on the non structural components. The load bearing capacity of the structural system has been already tested by Sartori et al. [35] during the seismic tests performed in the framework of the "chi-quadrato" project. In fact, the two buildings are characterized by the same geometry, materials and weight. Nevertheless in the test performed at TreesLab only the structural components have been tested, whereas in Lisbon the building was completed with non-structural layers. The previous shake table test showed an excellent seismic behaviour of the tested building. No structural damage was detected neither by the dynamic identification or by the visual inspection until a Peak Ground Acceleration (PGA) of 0.7 g. The first variation of the frequency was only observed after the last test with a maximum PGA of 1 g. For this reason no damages were expected on the structural components (sheathing, connections). Nevertheless only the symmetric direction of the building was subjected to the ground motion therefore no torsional contribution affected the building during the test. Moreover no information about the damages on non-structural parts couldn't be gathered. For these reasons the presented experimental test was planned (SERIES). The aim of this investigation was focused on the topics which have not been analysed in previous tests. Thanks to the LNEC facilities a bidirectional seismic input signal was applied to the building, collecting precious information about the behaviour along both directions. Moreover it was decided to equip the specimen with finishing layers and internal/external claddings, to get information about the behaviour of the building at the serviceability limit states.

The second test was planned to investigate the performance of the gypsum fibre-boards structural sheathing. The European construction companies often adopt this solution especially for the hygro-thermal properties and acoustic performances. Compared to other common sheathing materials, such as oriented strand boards (OSB) or plywood (PWD), GFB demonstrate interesting proprieties in terms of sound insulation, vapour permeability and the thermal inertia. Moreover, these products could be

used to ensure an adequate fire protection of the walls. On the contrary of the common gypsum based products, thanks to the cellulose fibres, these panels are also suitable as structural sheathings on the walls of LTF buildings.

Since the mid-90s different experimental campaigns have been carried out on LTF with gypsum (GB) wallboards. These tests were carried out mainly in the north American countries because according to technical codes such as the CSA (2014) and IBC (2009) allows, according to specified requirements and limitations, to consider the GB sheathing panels as structural elements and hence to take account of the GB contribution to the total racking resistance of wall segments.

The tests were mainly focused on the interaction between structural panels (OSB, Plywood, Hardboard) and the gypsum wallboards as summarized [36]. Other authors have performed dynamic tests on shake table where the contribution of the gypsum board are analysed in terms of dynamic proprieties variation (stiffening) and non-structural damages, [12] - [32]. On the other hand, especially in the European areas the mechanical behaviour of timber-framed walls braced by GFB was not analysed deeply as other traditional materials (nailed OSB or plywood) especially under lateral seismic loads. Moreover, only few authors had tested the influence of the cyclic behaviour of the connection between frame and sheathing

Recent European researches, [7] - [37], have compared the mechanical behaviour of fully-GFB-sheathed walls, traditional system (OSB) and mixed solution (GFB-OSB) in order to compare the performances under common boundary condition. The experimental tests were focused on the structural behaviour of the connection between the timber frame and the sheathing panels. Some analytical and numerical predictive models were proposed as well. Shake table tests, Finn R. (2006), on wall segments were carried out to investigate the load bearing capacity under a seismic dynamic input.

In this context the second test on LTF presents a further step in the investigation of seismic structural behaviour of wood framed walls sheathed with GFB panels, since no full-scale tests have never been carried out on an entire LTF building.

4.2.2 Geometry

The architectural layout showed in Figure 4.2 was adopted for all the tested specimens (LH-TF1-TF2-CLT). The mock-up was a compact squared-shape plan building ($7 \times 5m$) with a gable-shaped roof (slope 18°) to an overall height of $7.65m$ organized on three storeys (ground level - first level - attic). The plan of the ground and the first

floor were identical with the exception of the presence of two window along the grid line 3 of the building Figure 4.2 and the balcony at the first floor. The walls distribution was symmetrical along the main axes of the building (y) and un-symmetrical along the orthogonal axes (x). Moreover the walls runs without discontinuity from the ground level up to the roof level, thus the building can be considered regular in elevation according to a regular stiffness distribution.

According to the aim of the project the samples represented the actual common practice for two or three storey single family home both for material and design procedures.

The companies involved in the SERIES tests have used the construction details and geometries that are commonly used to build houses for their clients, reflecting in this way the current housing market. In the next subsections a brief description of the design parameters and geometry of the two buildings will be presented.

4.2.3 Design of the buildings

The design of the structural load bearing component was performed, for all the specimens, following the current procedures adopted by the designers. Regarding the static loads combination (self-weight, live-loads, snow and wind) the rules prescribed by the partial factor method (EN 1995-1-1) have been used whereas for the accidental combination (earthquake) the design was performed according to the current Italian (NTC 2008) and European Standards (EN1998-1 and EN 1995-1-1). The seismic design of a structure was carried out referring to a force-based seismic design method, as reported in European Standard (EN 1998-1/A1, 2013), assuming the following hypothesis:

- the forces were distributed proportionally to the wall length according to the rigid diaphragm assumption;
- the overall box like behaviour was neglected in the calculation and all the single walls were assumed to behave like a cantilever;
- the verification in terms of resistance of the timber elements and the load bearing capacity of the fasteners were conducted using the design values suggested in the (EN 1995-1-1).
- the safety factor (γ_m) equal to 1 was used for all structural verifications for both materials and connections according to Eurocode 8.

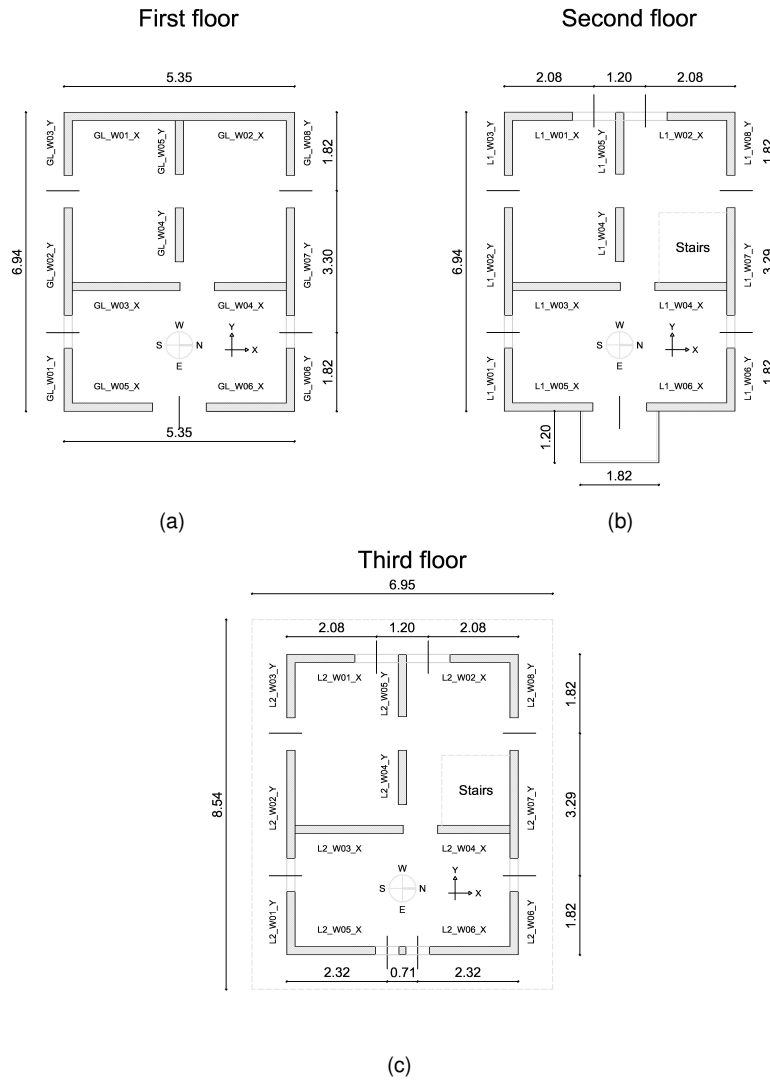


Figure 4.2: Plans of the building - a) ground floor - b) first floor - b) second floor.

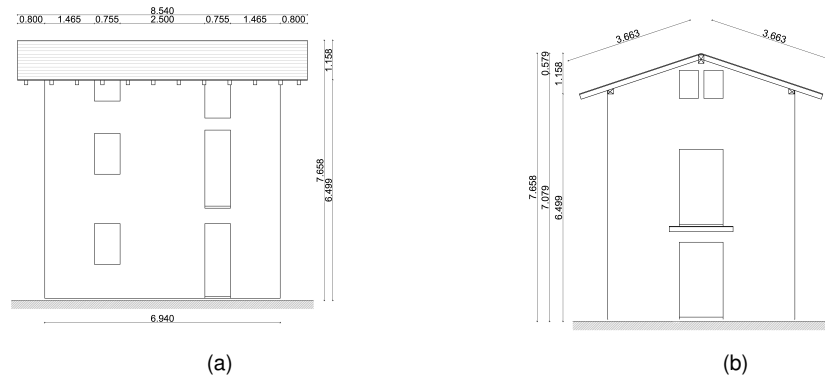


Figure 4.3: Lateral views - a) x-ditection - b) y-direction .

In order to reproduce the most severe condition it was supposed to build the house in the area with the higher seismic hazard according to the national Italian standards (Ferla, Sicily). The design peak ground acceleration was equal to $0.28g$ for a return period of 475 years. Also the design of the sample regard the vertical loads was carried out according to this hypothesis assuming a dead load of $2.5kN/m^2$, a live load of $2kN/m^2$ and a snow load of $0.95kN/m^2$.

The first building was designed assuming a behaviour factor q equal to 4^2 , which corresponds to a high energy dissipation class of the building. The use of this reductive factor, according to the current versions of the technical codes, is related to the proprieties of the fasteners (ductility, impairment of strength) and the sheathing panels (load bearing capacity). The fasteners used in joints regarded as dissipative zones should be able to resist to cyclic forces (appropriate low cycle fatigue behaviour). This condition is defined as the capacity: "to deform plastically for at least three fully reversed cycles at a static ductility ratio of 4 for ductility class M structures and at a static ductility ratio of 6 for ductility class H structures, without more than a 20% reduction of their resistance". This proprieties should be checked through experimental tests or, for the most common solution fulfilling geometrical limits. For timber framed walls and timber diaphragm the nails diameter (d), related to the failure mode, should be lower than $3.1mm$ and the sheathing panels should be ticker than $4d$. Moreover the behaviour factor is related to the regularity proprieties of the building: the reference behaviour factor is decreased for buildings non-regular in elevation. For the presented

²This value is lower than the maximum value proposed by the coses (Eurocode 8). This reduction, on the safe side for the structural check, was choose according to different prudential suggestion in the literature for the European light timber framed typologies.

structural layout the requirement in terms of regularity of the mass distribution and the stiffness distribution were satisfied.

The second building was realized using a sheathing material (GF) not covered by any harmonised technical specification (EN). The current version of the EN1995 does not provide any information about the design rules of this material, thus the certification for the structural use and the technical details necessary for the implementation of the project are reported in a specific product document. This European Technical Approvals ([38]) reports specifications and details for designing and installation, such as connector typology and connector spacing, are to be satisfied. In this case the design was carried out assuming a behaviour factor q equal to 2.5 according to the German national extension of the European technical approval [39].

Light-timber framed-sample 1

As introduced in the previous sections although the two light-timber framed buildings were geometrically identical different technical solutions were adopted both for the materials and connection. The main difference for the seismic behaviour was the sheathing material and the frame to panel connection. The load bearing walls were braced on both sides by OSB/3 panels nailed onto the timber studs and beam by means of ringed shank nails ($2.8 \times 60 \text{ mm}$). The timber frame was composed by solid wood studs ($60 \times 160 \text{ mm}$ and $100 \times 160 \text{ mm}$ with a constant spacing of 625 mm) and solid wood plate ($60 \times 160 \text{ mm}$). A constant spacing between the fasteners was maintained for all the walls (100 mm) and on the three levels Figure 4.4. The wall segments in the corner of the building and the intersection of the inner with the external walls were connected by means of fully threaded self-tapping screws. Thanks to these fasteners the walls in the two orthogonal direction were connected, making possible a collaboration between two orthogonal walls making effective a interaction between the load bearing structures in the two direction of the building.

The walls were connected to the foundation through inclined screws (against rigid body translation Figure 4.5(a)) and hold-down (rigid body rotation Figure 4.5(d)). The same mechanism at the upper levels were prevented by steel plates and tie-down (Figure 4.6(a)). The walls were positioned above a sill beam that, according to the common practice, is often used to facilitate the mounting operation and to increase the durability of the construction. Nevertheless these sill beams were used to transfer the shear force from the walls to the foundation through the inclined screws ($8 \times 180 \text{ mm}$).

The floors were composed by modular box element ($140 \times 600 \text{ mm}$) connected by

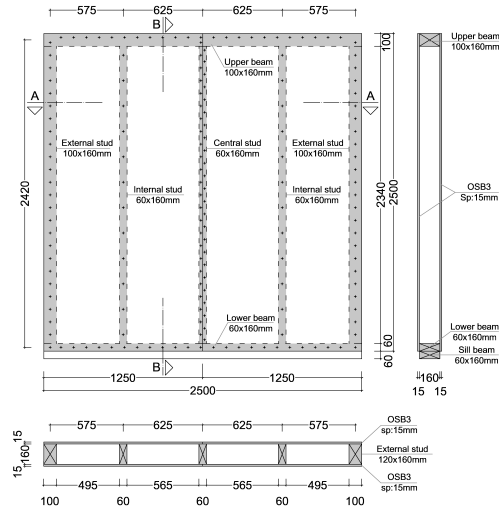


Figure 4.4: Geometry of the standard wall.

means of ring nails to the sheathing panels (OSB) to ensure a rigid diaphragm behaviour. Each element was made two external plates (31 mm) glued to three ribs joist (78x31 mm). The floors were connected to the top beam of the walls by means of self-tapping screws. The roof was made by solid wood rafters (100x140/760 mm) and glued laminated timber beam (160x240 mm ridge beam and 160x160 mm). The boarding (20 mm) was connected to the rafters by means of ring and, to ensure a shear stiffness of the two pitches, nailed strips were connected to the rafters (cross bracing).

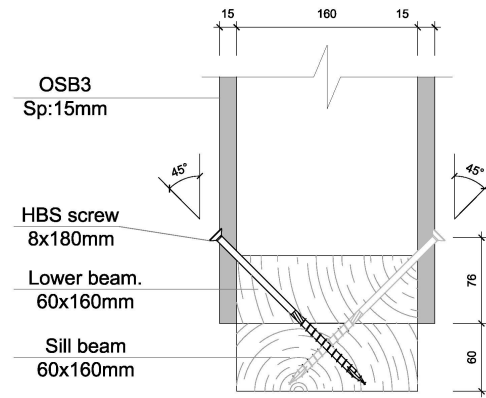
The external walls of the building were completed, according to an advanced pre-fabrication process, with external insulation panels, plaster and internal gypsum wall-boards. Moreover a room at the first floor was equipped with laminate floor, ceiling gypsum boards, doors and windows.

Light-timber framed-sample 2

The second sample was build using different materials and connection devices. The main difference compared to the previous case was the sheathing material and the sheathing to frame fasteners. In this second case gypsum fibres panels (GFB) and staples (1.59x1.35x45 mm) have been used instead of OSB and ring nails. The studs, positioned with a spacing of 605 mm, had a cross-section of 80x160 mm and 80x120 mm in the outer and in the inner walls respectively. The bottom rails were ticker



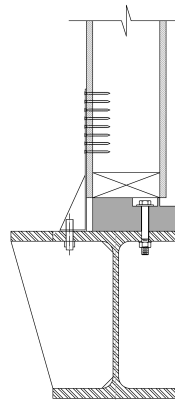
(a)



(b)



(c)

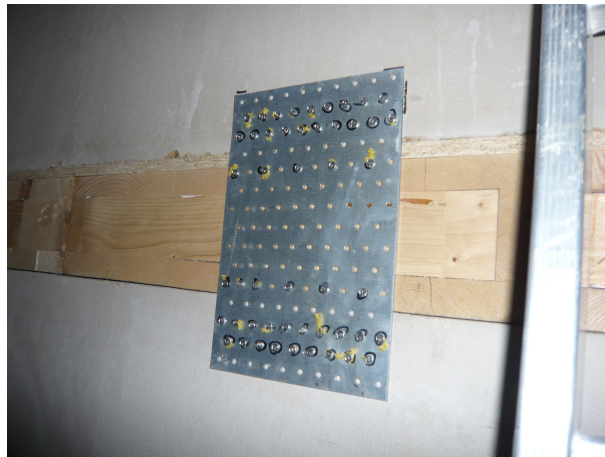


(d)

Figure 4.5: *Ground level connection - a,b) inclined screws - c,d) hold-down.*



(a)



(b)

Figure 4.6: First level connection - a) tie-down and steel plate - b) steel plate on the internal wall.

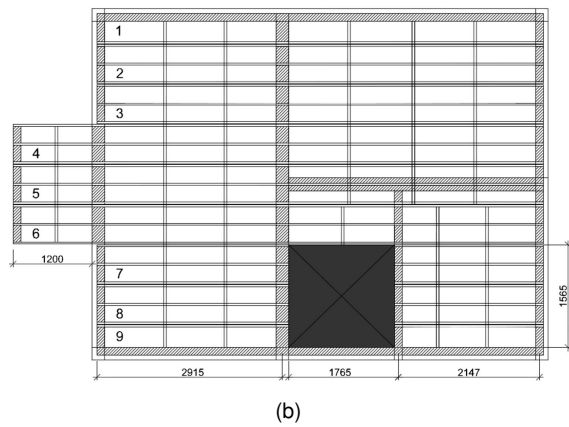
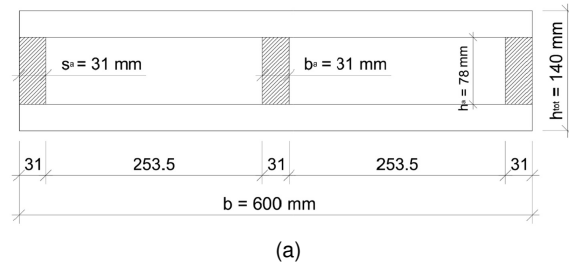
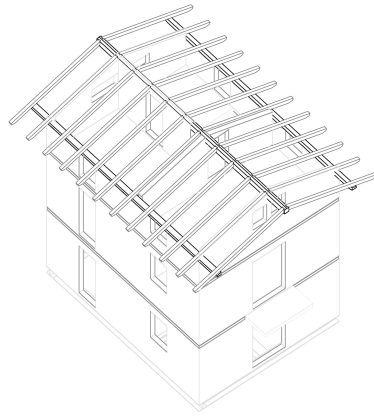


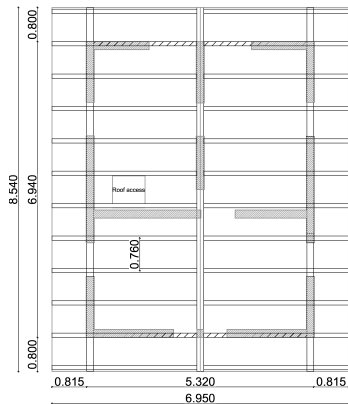
Figure 4.7: Floors structure - a) box modular element - b) plan distribution.



(a)



(b)

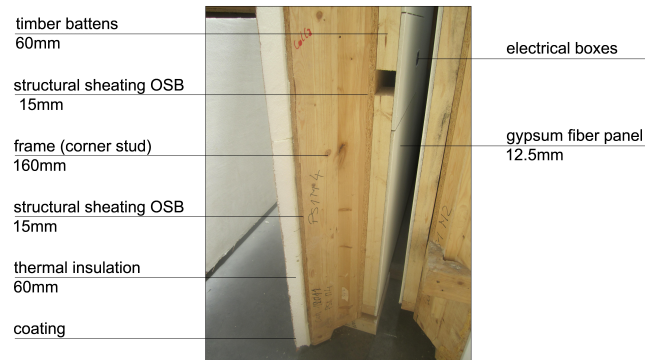


(c)

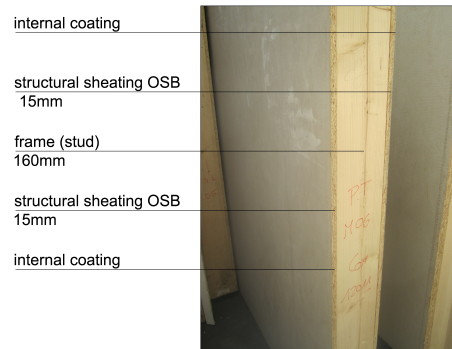


(d)

Figure 4.8: *Groun level connection - a) tridimensional view of the roof structure - b) construction phases - c) plan - d) x-brace.*



(a)



(b)



(c)

Figure 4.9: Walls finishing layers - a) external walls layout - b) internal walls layout- c) ceiling.



Figure 4.10: Room equipped with furniture.

in order to connect the anchor systems already described in the previous sections 3.0.2 and 3.0.3. A constant spacing between the fasteners was maintained for all the walls (125mm) and on the three levels. The wall segments in the corner of the building and the intersection of the inner with the external walls were connected by means of self-tapping screws.

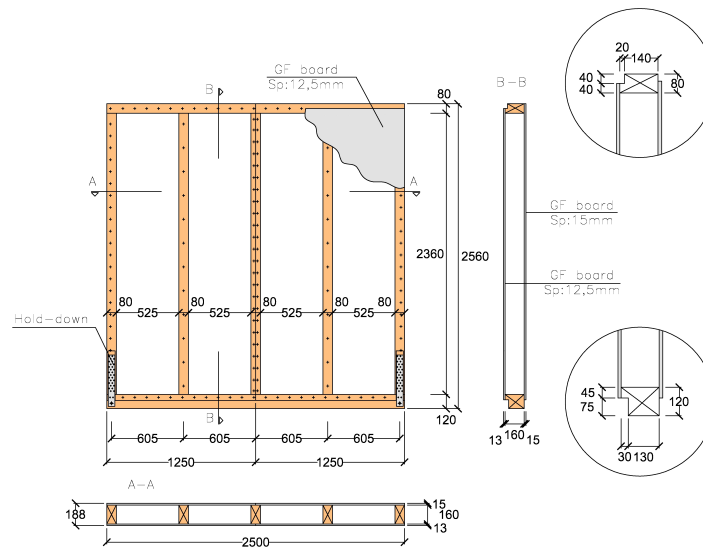


Figure 4.11: Geometry of the standard wall (external).

The rigid body rotation and slippage were prevented, at the ground level, by hold-down and angle brackets (Figure 4.12). The shear forces at the upper storey was

transmitted by means of angle brackets from the walls to the floor and then to the lower walls, whereas the tensile force was transmitted by tension ties (tie-down).

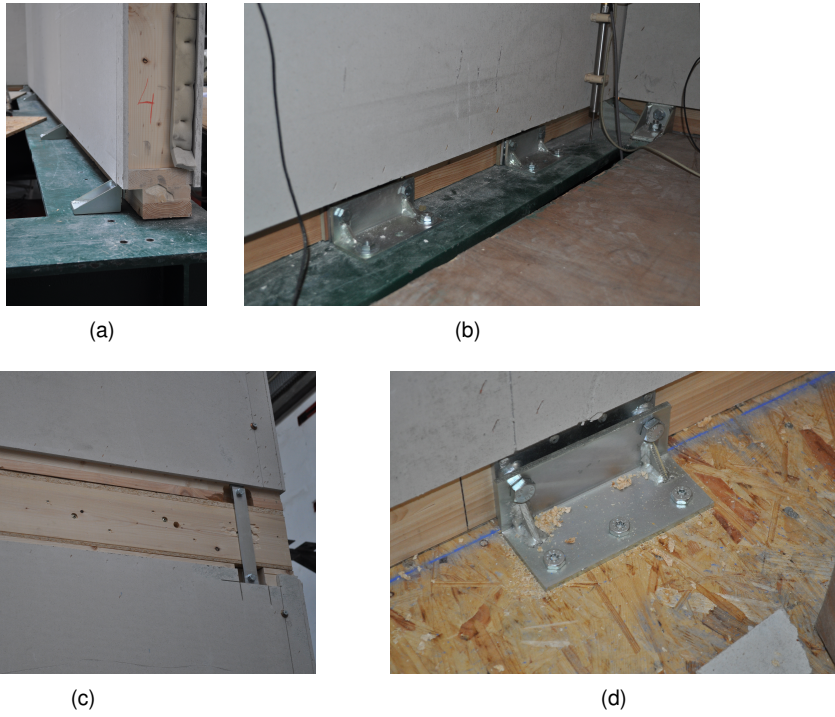


Figure 4.12: Walls connections - a) hold-down (ground level) - b) angle brackets (ground level)- c) tie-down (first/second level) - d) angle brackets (first/second level).

The floor structure was composed by solid wood joists with height of 200mm and a width of 80mm . The horizontal diaphragm behaviour of the floor was ensured by 18mm thick OSB panels nailed to the timber beams. To achieve a higher level of prefabrication the joist were organized as modular box element using an additional layer of OSB. The floors were connected to the top beam of the walls by means of self-tapping screws. The structural plans of the two floors were reported in Figure 4.13.

The roof was characterized by a traditional gable shaped wood joist structure with a floorboard stiffened by metal strips exactly as for the previous building. The structural plan of the roof is showed in Figure 4.13.

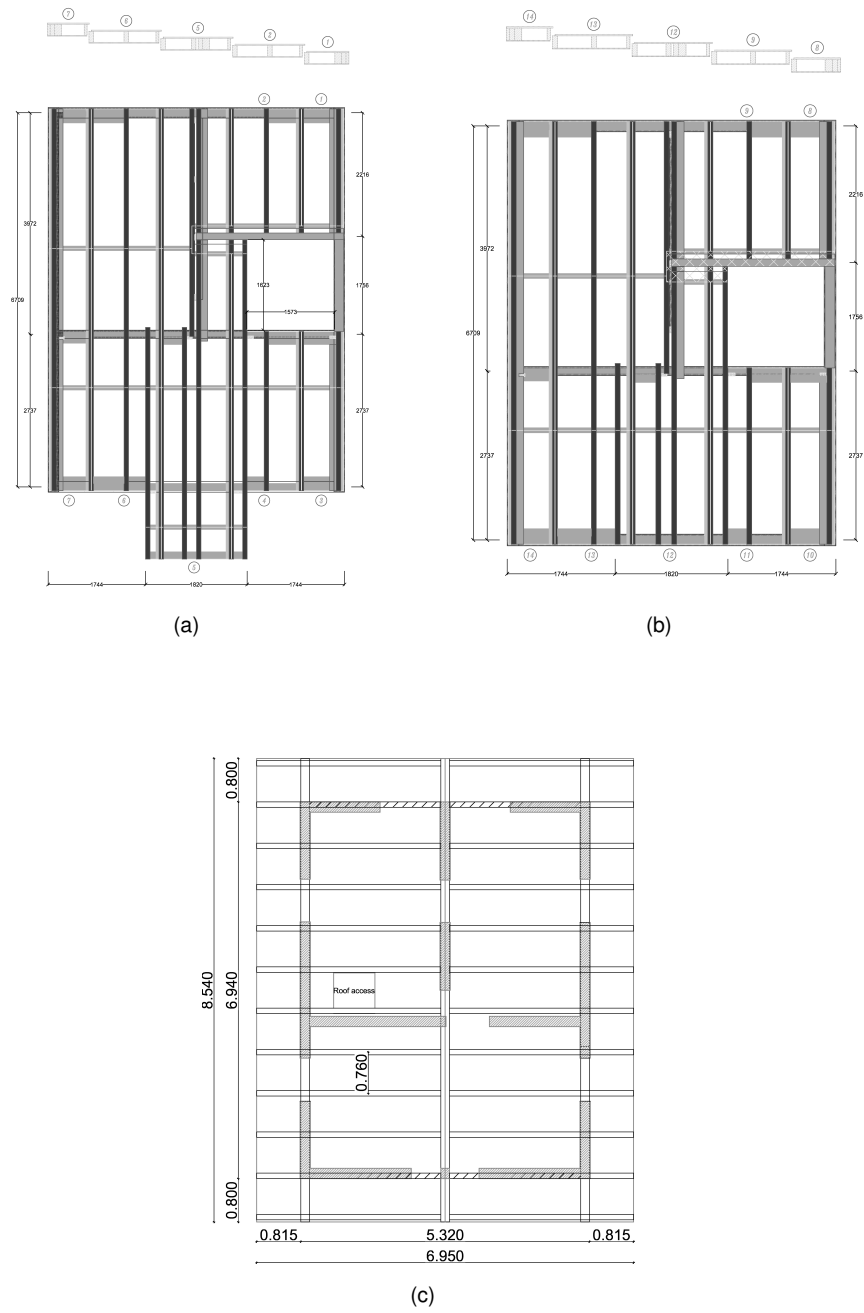


Figure 4.13: Structural layout of the floors - a) first floor - b) second floor - roof.

4.2.4 Test set-up

The seismic tests were performed on the shake table of the Earthquake Engineering Research Centre (NESDE) at "National Laboratory of Civil Engineering" in Lisbon (Portugal). The oleo-dynamic system of the platform allows three independent ground motions up to a maximum acceleration of 1.1, 1.8 and 0.5 g for the transverse, longitudinal and vertical axis respectively, and maximum displacements in the range 175mm for all the three axes (bare table). The ground motion is provided by servo-controlled hydraulic actuators (2 in the transverse, one in the longitudinal and one in the vertical direction) powered by three pump groups, each of 110 kW (plus an additional 22 kW for boost purpose). The power pack is connected to an additional bank of nitrogen accumulators [40]. The rotational degrees of freedom restrained by a passive system based on a set of high torsion stiffness tubes. The maximum payload of the device is about 400kN (Table 4.2).

As presented in the previous paragraphs the footprint of the timber buildings tested during the SERIES project was 7x5 meters, therefore a steel enlargement structure was connected to the platform. This parts of the set-up was composed by two separate portion, symmetrical along the main direction (y), made of steel beams (HEA 400 and IPE 400 profiles) reinforced by gusset plates. The specimens were connected directly onto this lattice through the anchor devices (hold-downs, angle brackets, bolts). The total mock-up masses, which includes the self weight and the additional loads and the steel basement self weight, were very close to the nominal maximum payload of the table.

Characteristics	Units	Longitudinal	Transverse	Vertical
Force	<i>kN</i>	1250	20E375	375
Stroke (effective/maximum)	<i>mmpp</i>	290/400	290/400	290/400
Max velocity (nominal/limit)	<i>cm/s</i>	70.1/121.5	42.4/73.5	41.9/72.6
Max acceleration (bare table)	<i>m/s²</i>	18.75	31.25	9.38
Frequency Range	<i>Hz</i>			0.1-40

Table 4.2: Main characteristics of the large LNEC-3D shaking table

Two reference systems were used to identify the main direction of the building or the principal axes of the houses:

- L,T,V is the absolute reference system of the LNEC laboratory, each letter correspond to a degrees of freedom of the table. Moreover another reference system is introduced according to the compass points N,S,W,E of the laboratory;
- X,Y refer to the main direction of the building. Another reference system is used

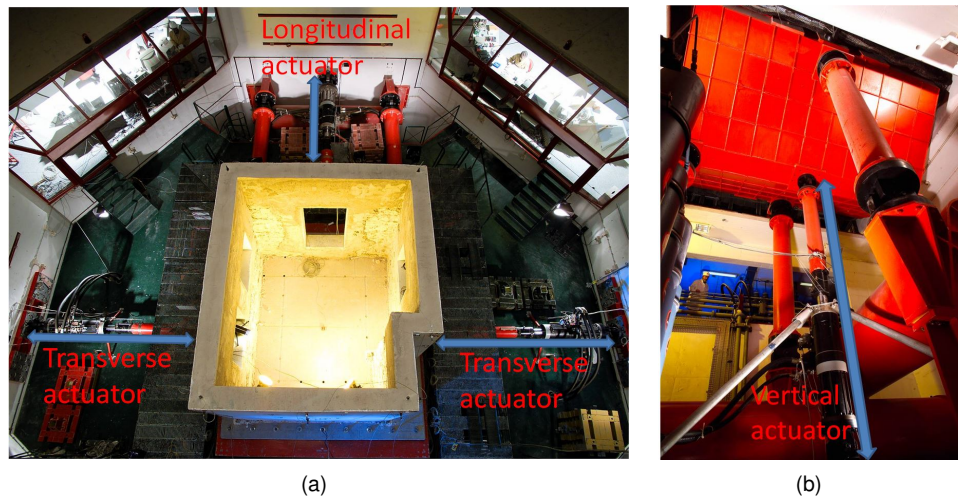


Figure 4.14: 3D shaking table - a) plan view (transverse and longitudinal actuators) - b) vertical actuator and torque tube system.

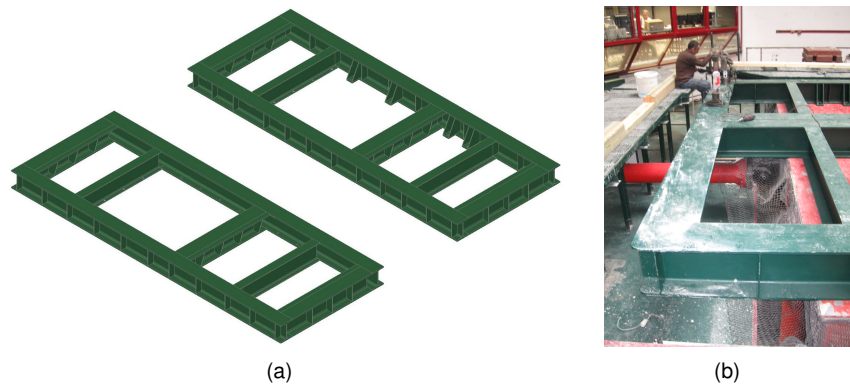


Figure 4.15: Steel enlargement structure.

to name the alignments of the grid (a, b, c for the short side and 1, 2, 3 for the long side of the building).

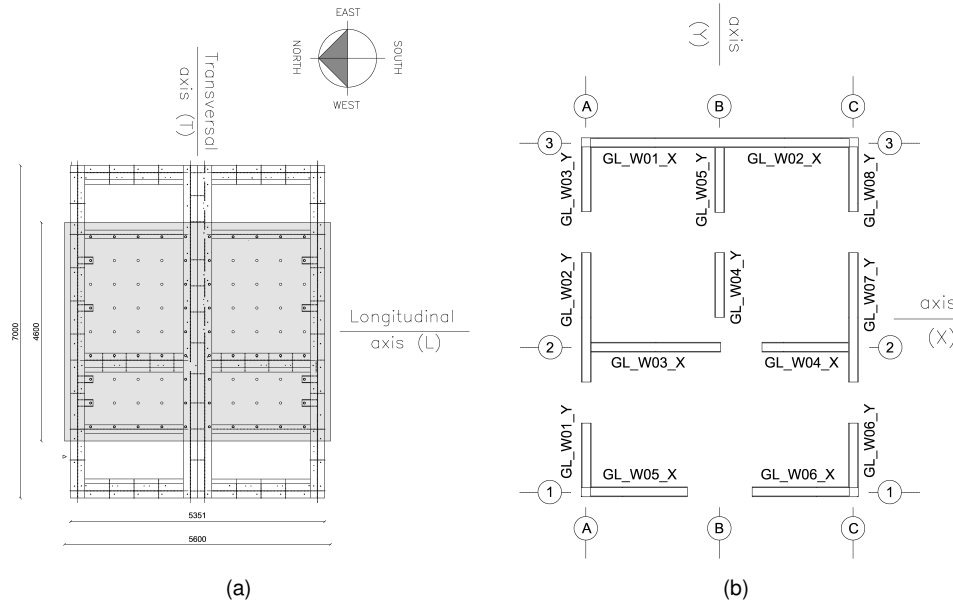


Figure 4.16: Reference system: a) laboratory table directions (L,T,V); b) building reference system and grid (X,Y).

Steel masses (each one of 600 or 1200 kg) were connected to the first and second floor of the building to simulate the non structural finishing weight and the variable loads, whereas the weight of the non-structural components of the roof (e.g. boards and insulations) was taken into account using weightier tiles. For the first specimen a total of 10 additional masses were installed both at the first and second level. The second specimen was equipped with $12 \times 600 \text{ kg}$ masses at the first floor and $14 \times 600 \text{ kg}$ at the second.

4.2.5 Instrument layout

The mock-up was monitored through 105 transducers (accelerometers, linear displacement transducers, load cells) as reported in Table 4.3. The data were acquired by a data acquisition system with a sampling rate of 125 Hz .

Two additional optical systems were used to measure the absolute displacement of the building. The first, based on the Hamamatsu system (comprising lens, sensor



148

head and led target, conditioning device), was installed on the the north-west corner (C3) with a camera on each level and on the south-east corner only on the roof (A1). The second, based on a Krypton (Nikon K-series) characterized by 20 markers and infra-red cameras, was adopted to measure the 3D-displacement of the South-East corner of the building at the second level. A complete description and further figures of the measurement set-up are reported in [41].

	Instrument	Q.ty	Phisical property
Linear variable displacement transducer (Lvd)		4	Intrere storey drift
Linear variable displacement transducer (Lvd)		8	wall sliding
Linear variable displacement transducer (Lvd)		10	wall uplift
Uniaxial accelerometers		39	acceleration at different levels
Uniaxial accelerometers		5	acceleration at the shaking table level
Load cells		10	forces on hold down anchoring elements
Optical displacement measurement system 1		5	point absolute displacemnets (5 points x,y)
Optical displacement measurement system 2		20	point absolute displacemnent

Table 4.3: Measurement instruments.

The wall uplift, slippage and the tension force on the hold-down were monitored for five walls at ground and first level. Transducer layout and the lateral view of the instruments is reported in Figure 4.18 and Figure 4.19.

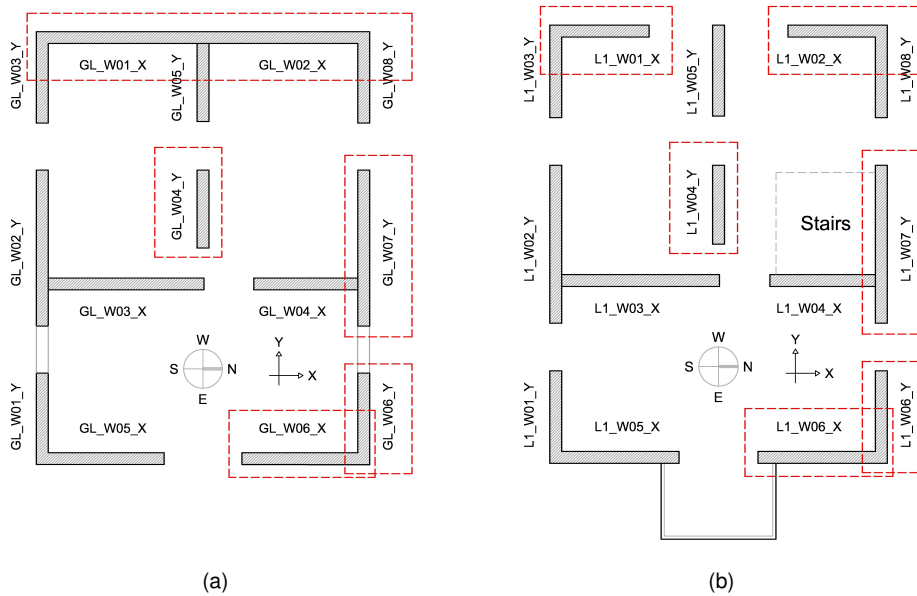
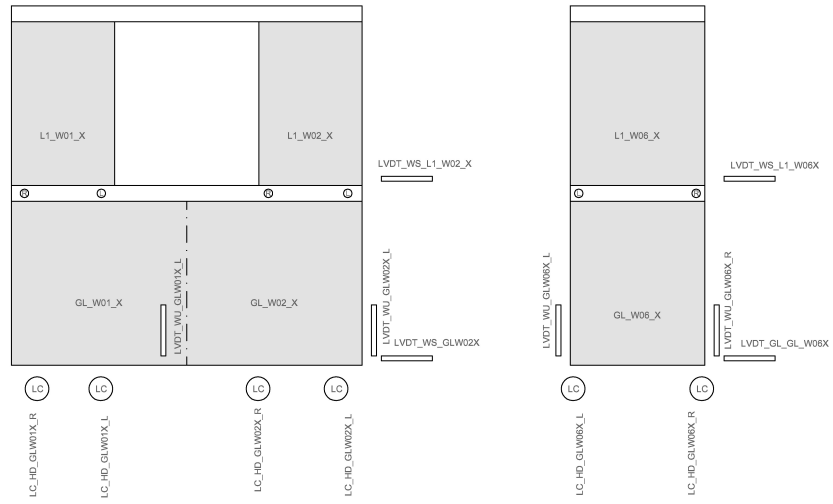
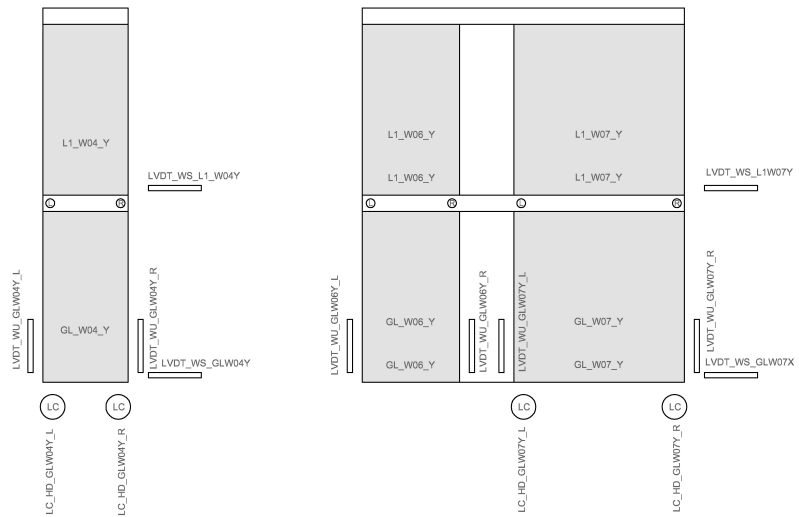


Figure 4.18: Displacement and force transducers - a) ground level- b) first level.



(a)



(b)

Figure 4.19: Displacement and force transducers - a) Longitudinal direction - b) transverse direction.

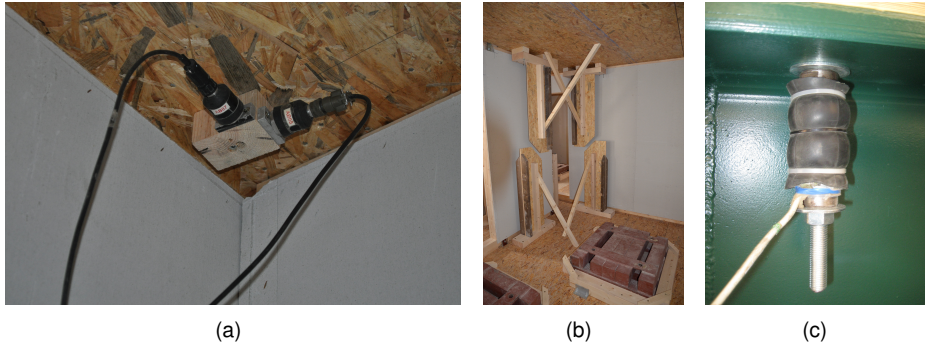


Figure 4.20: Displacement and force transducers - a) accelerometers - b) interstorey-drift - c) load cell .

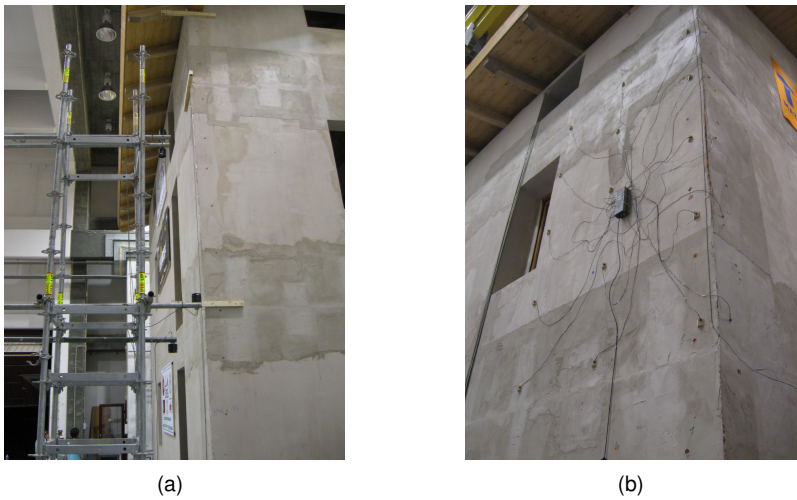


Figure 4.21: Optical displacement measurement system - a) system 1 (Hamamatsutm) - b) system 2 (Kryptontm) .

4.2.6 Test procedure

The shake table tests, part of the European SERIES project, were planned to compare the seismic capacity of four different timber-buildings characterized by the same geometry, design parameters but different constructive systems. For this reason, the specimens were subjected to the same seismic test sequence adopted for other buildings.

The ground motion recorded at Ulcinj (station Hotel Albatros - ST64, time UTC 06:19:41), during the Montenegro earthquake (Mw 6.9) occurred on 15/04/1979, was used as input signal. This signal was selected since it represents a seismic event compatible with the geophysical mechanism of southern Europe and it is characterized by a large extension of the constant acceleration part of the elastic pseudo-acceleration response spectrum (from 0.25 s to 0.80 s) as shown in Figure 4.23. This bi-directional signal was scaled to increase the PGA and reaching different limit states of the building. An adaptive control algorithm was adopted to match each target signal (T) through a set of drive signals (D). Each target motion was achieved through intermediate stages by increasing the input signals of the shake table, [42], up to the target PGA.

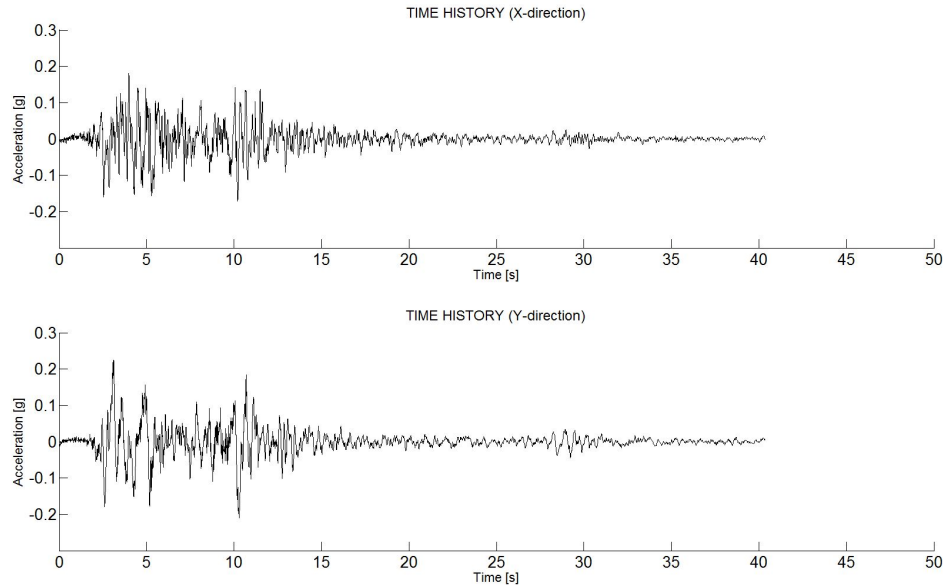
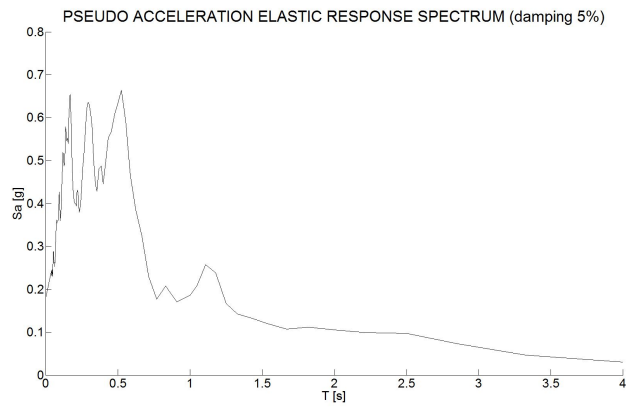
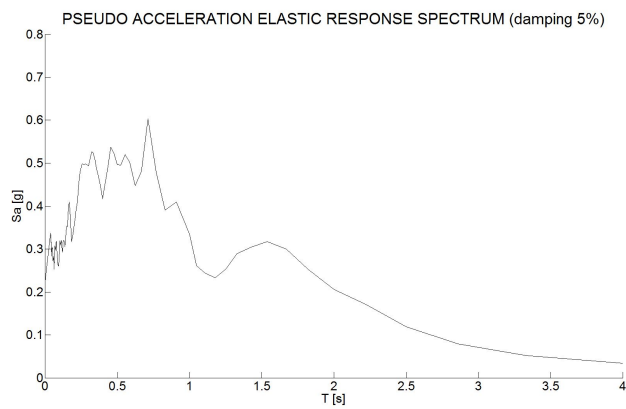


Figure 4.22: Accelerogram recorded during the Montenegro earthquake: X-component ($PGA = 1.774m/s^2$); Y-component ($PGA = 2.199m/s^2$).



(a)



(b)

Figure 4.23: Pseudo acceleration response spectrum of Montenegro earthquake, a) signal imposed in the x direction - b) signal imposed in the y direction of the sample.

Since no significant visible damage was detected after the common sequence (stage 1) the first light-timber framed specimen was subjected to a different input signal (Tohoku 2011 modified signals) whereas the second building was weakened (weakened building).

The Tohoku signal was characterized by a longer duration and a greater energy content and the stronger motion of the signal was applied in the longitudinal direction.

Table 4.4 report the test sequence for the first buildings whereas - Table 4.5 for the second building.

Label	Typology	Targ-x	Targ-y
I0	Dynamic id.	-	-
D1	Seismic test	0.06g	0.07g
T1	Seismic test		
I1	Dynamic id.	-	-
D3	Seismic test	0.12g	0.15g
T2	Seismic test		
I2	Dynamic id.	-	-
D5	Seismic test		
D6	Seismic test	0.23g	0.28g
T3	Seismic test		
I3	Dynamic id.	-	-
D7	Seismic test		
D8	Seismic test		
D9	Seismic test	0.40g	0.50g
D10	Seismic test		
T4	Seismic test		
I4	Dynamic id.	-	-

Label	Typology	Targ-x	Targ-y
I5	Dynamic id.	-	-
D9	Seismic test		
D10	Seismic test	0.27g	0.15g
T5	Seismic test		
I6	Dynamic id.	-	-
D12	Seismic test		
D13	Seismic test	0.54g	0.30g
T6	Seismic test		
I7	Dynamic id.	-	-

Table 4.4: Test procedure for the first timber framed building: Montenegro earthquake (Stage 1) - Tohoku earthquake (Stage 2).

As reported in the tables a dynamic identification of the sample was performed after each test . The input signal, imposed by the shaking table for an overall duration of 180 sec, was a low intensity random signal (white noise characterized by a Gaussian distribution of root mean square - RMS - of 0.05 g with a frequency ranging between 0.1 Hz and 30 Hz Figure 4.24).

Un-weakened building (stage 1)				Weakened building (stage 1)			
Label	Typology	Targ-x	Targ-y	Label	Typology	Targ-x	Targ-y
I0	Dynamic id.	-	-	I5	Dynamic id.	-	-
D1	Seismic test			D9	Seismic test		
D2	Seismic test	0.06g	0.07g	D10	Seismic test		
T1	Seismic test			D11	Seismic test	0.06g	0.07g
I1	Dynamic id.	-	-	T5	Seismic test		
D3	Seismic test			I6	Dynamic id.	-	-
D4	Seismic test	0.12g	0.15g	D12	Seismic test		
T2	Seismic test			D13	Seismic test	0.12g	0.15g
I2	Dynamic id.	-	-	T6	Seismic test		
D5	Seismic test			I7	Dynamic id.	-	-
D6	Seismic test	0.23g	0.28g	D14	Seismic test		
T3	Seismic test			D15	Seismic test	0.23g	0.28g
I3	Dynamic id.	-	-	D16	Seismic test		
D7	Seismic test			T7	Seismic test		
D8	Seismic test	0.40g	0.50g	I8	Dynamic id.	-	-
T4	Seismic test			D17	Seismic test		
I4	Dynamic id.	-	-	D18	Seismic test	0.40g	0.50g
				D19	Seismic test		
				I9	Dynamic id.	-	-
				T8	Seismic test	0.40g	0.50g
				I10	Seismic test		
				T9	Seismic test	0.53g	0.66g
				I11	Dynamic id.	-	-

Table 4.5: Test procedure for the second timber framed building: un-weakened building (Stage 1) - weakened building (Stage 2) .

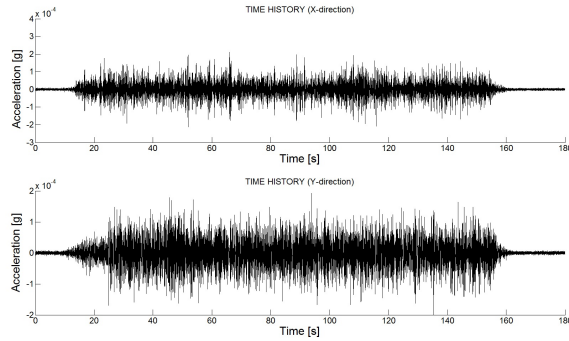


Figure 4.24: Input signal for the dynamic identification.

4.2.7 Results

Light-timber framed-sample 1

The first building (light timber framed sheathed by OSB panels) was tested by several ground motion obtained from the scaling of two accelerograms. A total of 18 tests were carried out according to the adaptive control algorithm each step was repeated to achieve the reference signals. Visual inspection of the structural and non-structural components after each single seismic test showed no significant damage. The checks have been focused on the connections between structural elements (steel flanges/nails of the hold-downs) and on the relative displacement or cracking of the sheathing panels (a thin layer of plaster was prepared on the internal side of the walls). Also the damages on the installed windows and doors were carefully verified. The damage level of the structure was verified by modal testing techniques, recording the variation of the system dynamic properties, which is strongly correlated to the stiffness of the structural elements. The frequency obtained did not vary until the last test of the "Montenegro procedure". Only after test (T4) was a minimal decrease of frequency apparent: see Table 4.6.

Mode	stage 1						
	I0	I1	I2	I3	I4	I6	I7
I mode shape in x	3.63	3.63	3.63	3.63	3.63	3.63	3.45
I modeshape in y	4.18	4.18	4.18	4.18	4.03	4.03	4.03
Torsional mode shape	5.89	5.89	5.89	5.89	5.89	5.89	5.89
II mode shape in x	14.37	14.37	14.37	14.56	14.37	14.37	14.37
II mode shape in y	15.63	15.63	15.63	15.63	15.63	15.63	15.63
III mode shape in y	20.6	20.6	20.6	20.6	20.14	20.14	20.14

Table 4.6: Frequencies [Hz] obtained by identification tests.

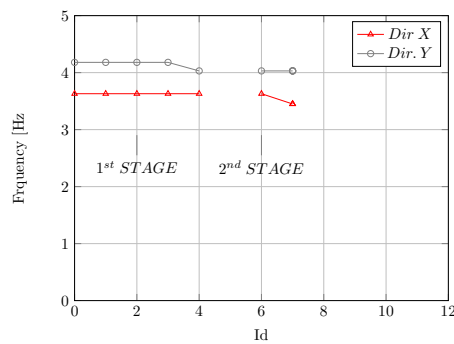


Figure 4.25: Frequency variation.

The results of Table 4.6 show that the frequency of the torsional mode is higher than those of the two first translational modes in the X and Y directions. Furthermore the translational modal shapes show no significant torsional components. Hence, the building can be assumed as in-plan regular for mass and stiffness distributions.

The first frequency variation in the longitudinal direction (x) was equal to zero until the T4 level; between T4 and T5 a variation of 4.95% was recorded. In the transverse direction no variations were registered until level T3, whilst a variation of 3.63% between T3 and T4 occurred. The frequency corresponding to the torsional modal shape remained constant (Table 4.6). The negligible variation of the dynamic properties of the building indicates no significant damage on the structural parts of the building (walls and connections). Thus the elastic limit of the structure was not reached during the seismic test (both for the Montenegro and modified Tohoku earthquakes). These findings were confirmed by the visual inspection and by the results of the previous test ([34]).

As reported in Figure 4.27, thirty nine uni-axial accelerometers were installed on the building and five on the steel basement. Moreover, the imposed acceleration was monitored in both directions by the control system of the shaking table. Table 4.7 shows the absolute values of the peak acceleration at different levels in the centroid of the structure.

Dir.	pos	stage 1					stage 2	
		T1	T2	T3	D10	T4	T5	T6
X	Ref. Acc. Table	0.06	0.12	0.25	0.80	0.67	0.29	0.73
	1st floor	0.12	0.2	0.33	0.60	0.74	0.34	0.82
	2nd floor	0.20	0.36	0.52	0.70	0.89	0.51	1
Y	Ref. Acc. Table	0.08	0.16	0.34	0.75	1.15	0.18	0.34
	1st floor	0.10	0.21	0.41	0.71	1.04	0.19	0.4
	2nd floor	0.17	0.32	0.48	0.88	1.08	0.30	0.58

Table 4.7: Peak acceleration values [g] recorded in the center of mass at each floor.

Figure 4.28 represents the profile of the peak acceleration along the height of the structure (assuming a normalization respect the maximum values). The shape of the profile is influenced by the horizontal inertial forces because, as discussed in the previous chapters, the anchor system affect the structural response only when the stabilizing moment (for the hold-down) and the friction forces are overcome.

One of the key-parameters of the analysis of the seismic structural response is the inter-storey drift, (defined as ratio between the relative displacement of two adjacent levels and the storey height) which the different limit states of the structure may related to. The maximum inter-storey drift recorded during the test is shown in Table 4.8.

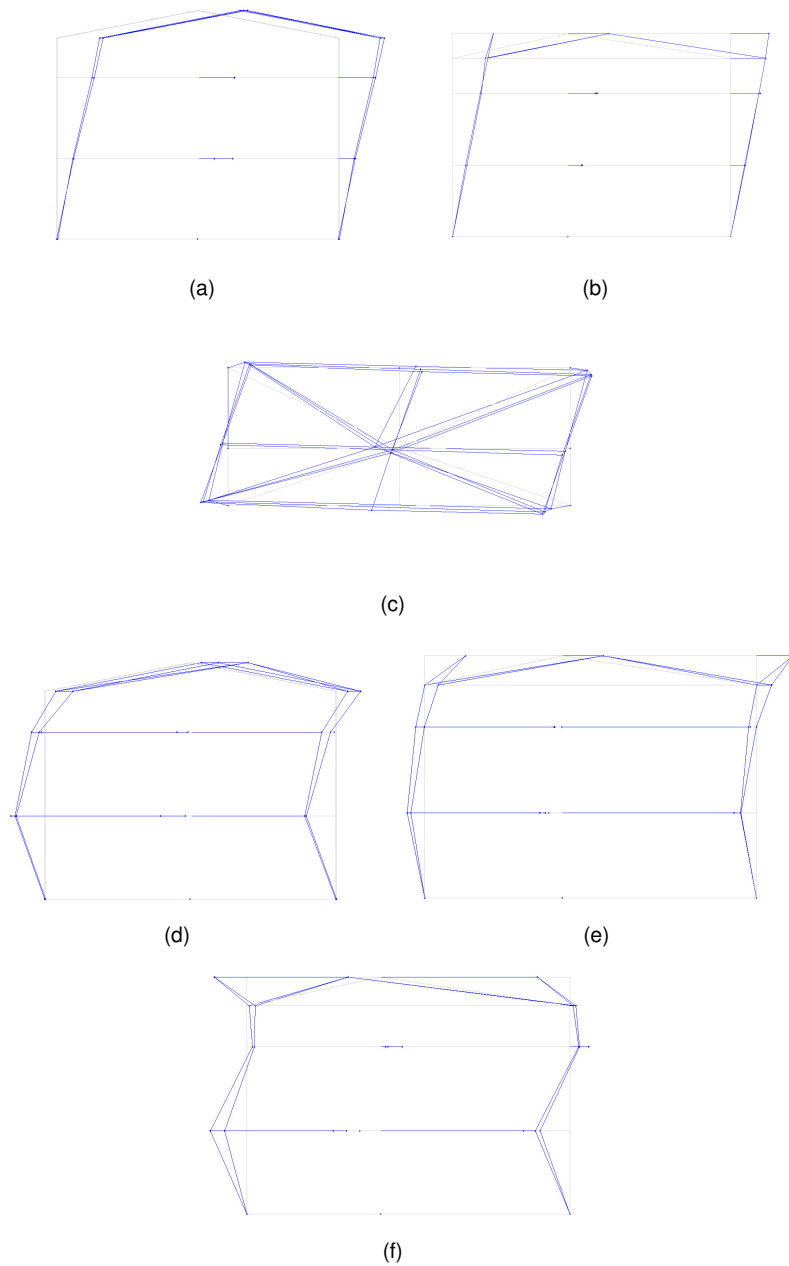


Figure 4.26: Mode shapes - a) 1st mode shape in x-direction (3.63 Hz); b) 1st mode shape in y-direction (4.18 Hz); c) 1st torsional mode shape (5.89 Hz); d) 2nd mode shape in x-direction (14.37 Hz); e) 2nd mode shape in y-direction (15.63 Hz); f) 3rd mode shape in y-direction (20.6 Hz).

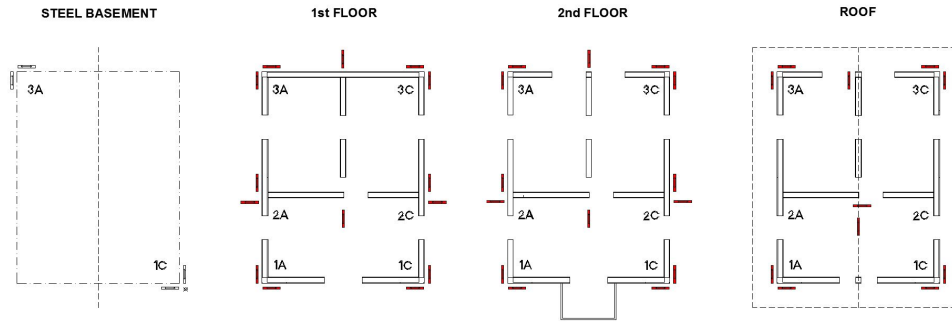


Figure 4.27: Accelerometers used for the dynamic identification of the structure and for the seismic tests.

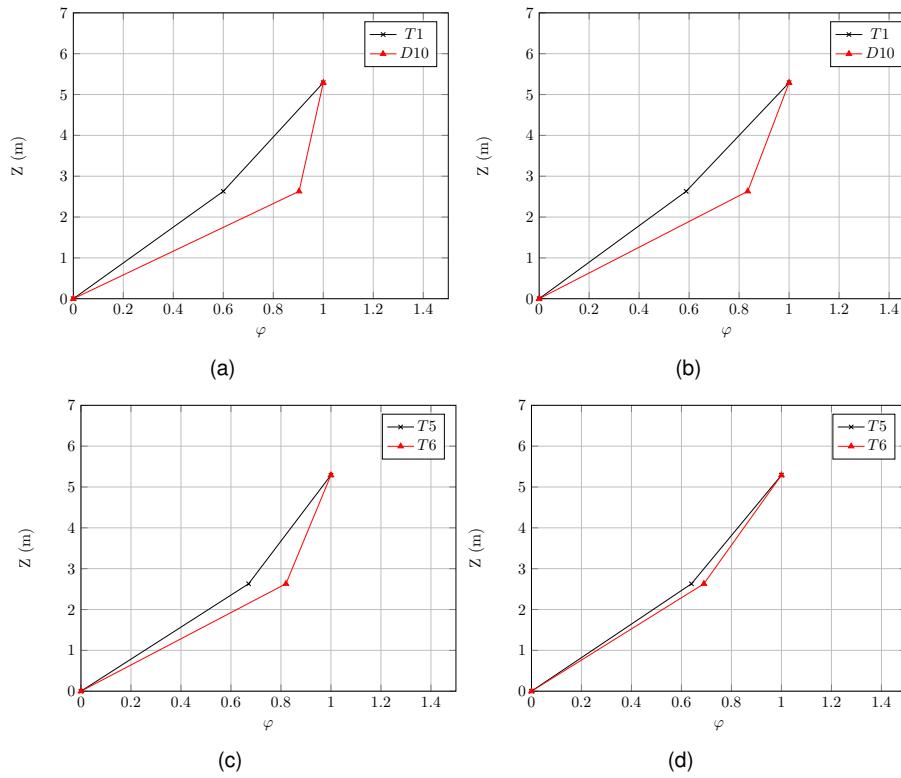


Figure 4.28: Peak acceleration values for test T1, D10 (stage1) and T5, T6 (stage 2)

The optical system was installed on the external corner of the building (C3) whereas the inter-storey displacement differ from the data acquired from the lvdt transducers because the effect of the rotation of the building were more significant. The maximum inter-storey drift for all tests was reached in x-direction during the T5 test (0.61%) at the first floor whereas a value of 0.66% was obtained in y-direction during the T4 test at the ground floor. These percentages as well as reported by the studies in the literature ([31]) and ([43]) are compatible with the absence of damage to the structure and the finishing that we observed. This fact is also demonstrated by the tests carried out in the preliminary tests ([7]).

	Ground - first dir. X				Ground first dir. Y			
	Lvdt		opt.		Lvdt		opt.	
	δ	θ	δ	θ	δ	θ	δ	θ
	[mm]		[mm]	[%]	[mm]		[mm]	[%]
T1	-	-	2.13	0.08	0.5	0.02	2.15	0.08
T2	-	-	2.76	0.11	1.0	0.04	3.42	0.13
T3	7.9	0.31	3.79	0.15	1.9	0.07	5.44	0.21
D10	15.6	0.61	7.46	0.29	4.4	0.17	10.15	0.40
T4	17.2	0.67	8.36	0.33	5.0	0.20	16.01	0.63
T5	8.0	0.31	6.61	0.26	1.6	0.06	4.57	0.18
T6	16.9	0.66	12.45	0.49	2.9	0.11	6.75	0.26

Table 4.8: Inter-storey displacement between ground and first level [mm] measured by the lvdt and optical transducers.

	First - second dir. X				First - second dir. Y			
	Lvdt		opt.		Lvdt		opt.	
	δ	θ	δ	θ	δ	θ	δ	θ
	[mm]		[mm]	[%]	[mm]		[mm]	[%]
T1	1.4	0.06	2.50	0.10	1.0	0.04	2.03	0.08
T2	3.2	0.13	2.45	0.10	2.4	0.09	2.42	0.09
T3	5.2	0.20	3.77	0.15	4.0	0.15	4.54	0.18
D10	8.7	0.34	9.88	0.39	8.0	0.31	8.96	0.35
T4	9.5	0.37	-	-	8.8	0.34	-	-
T5	4.8	0.19	5.58	0.22	2.3	0.09	5.11	0.20
T6	8.4	0.33	15.72	0.61	5.1	0.20	7.78	0.30

Table 4.9: Inter-storey displacement between first and second [mm] measured by the lvdt and optical transducers.

Figure 4.32 reports the inter-storey drift versus peak ground acceleration. The correlation between inter-storey drift and peak ground acceleration recorded at each stage was linearly proportional in both the main directions. This assumption was confirmed by the analysis of the peak values of the hysteresis loop in terms of total inertial forces and relative displacement between the second level and the steel basement. Each point of the curve reported in Figure 4.29, in terms of force, correspond to the

sum of the products of the mass of each storey multiplied by the mean value of the acceleration at the corner.

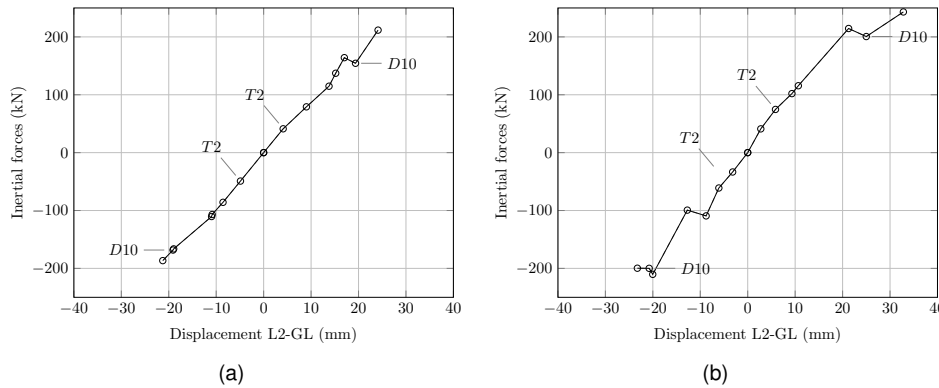


Figure 4.29

Table 4.11 reports the simultaneous forces on the load cells on the monitored walls for the last test (T4). The diagonal cells of the table show the maximum values of each channel, while the remaining cells of the rows show the values recorded in other devices at the same time instant. This table is crucial for understanding the force distribution on the walls and for the actual effectiveness of the "box-like behaviour" ensured by the connections among the structural elements. As clearly visible in Figure 4.33, which reports the peak load cell values, at the same time instant one of the two load cells at the wall corners records a higher tensile force, while the other one records a null value or smaller tensile force. Hence discussed in the next section a predominant "box-like" behaviour cannot be identified and each walls act mainly as a cantilever. The contribution of the orthogonal walls, connected by means of self-tapping screws, ensure a reduction of the tensile force on the hold-down nevertheless the overall response was not a full global box behaviour. This extreme situation occurs when the rotation involves the entire building thanks to the connection between the walls. In this configuration, all the hold-down on one side of the building should be in tension with the maximum value while on the other should be unloaded (rigid block rotation).

Similar consideration could be done also for the uplift of the two opposite corner of each single wall segment Table 4.12.

The values of force and uplift for the test with low intensity (T1-T2) were negligible because the stabilizing moment due to the self-weight of the structure and the additional masses were enough to balance the overturning moment of the inertial

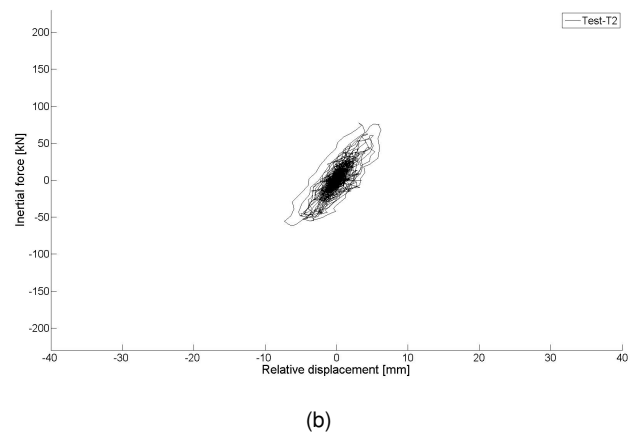
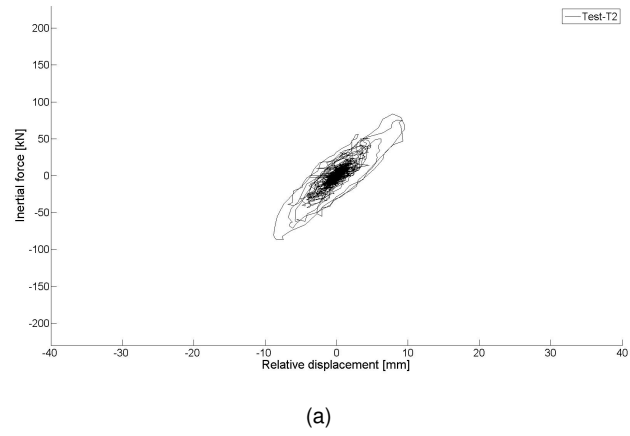
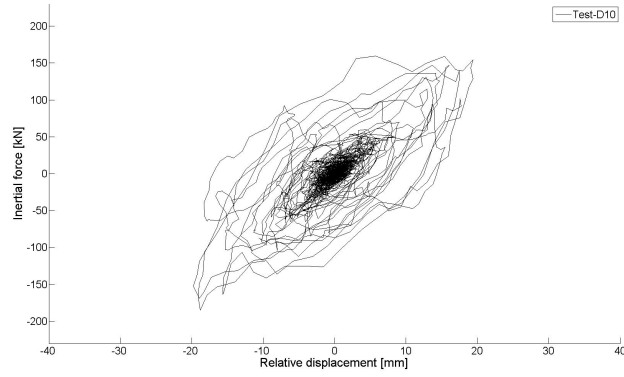
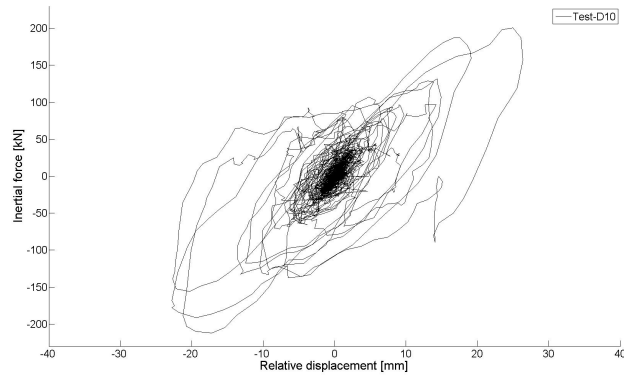


Figure 4.30: *Test T2 - inertial forces vs displacement*



(a)



(b)

Figure 4.31: *Test D10 - inertial forces vs displacement*

forces. The maximum tensile force recorded in the load cells of the hold-downs was $23.3kN$. This value was recorded in the 07_Y_R hold-down during test T4. At the same time, also the hold-down reached its maximum ($20.2kN$) in 04_Y_R hold-down. In the orthogonal direction, the maximum load was recorded in the 06_X_L ($12.4kN$) (see Table 4.11).

Furthermore, the comparisons between the maximum values of the tensile force in the hold-downs during the most severe seismic test ($23.9kN$) and the results of the cyclic and monotonic test on the same hold-down elements ([5]) show that the maximum force was smaller than the yielding point of the connection.

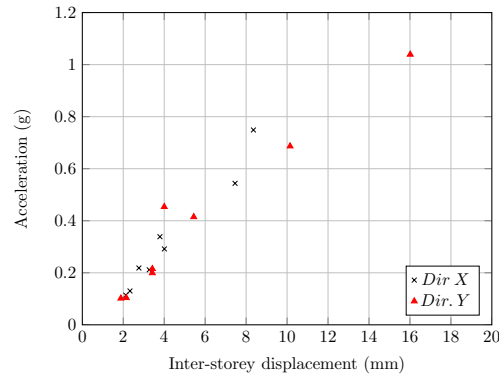


Figure 4.32: Acceleration (p.t 3C-first storey) versus inter-storey displacement between the ground and first floor (optical system).

	Stage 1					Stage 2	
	T1	T2	T3	D10	T4	T5	T6
06X_L	0.8	2.2	4.7	11.1	12.4	2.7	11
06X_R	0.5	1	1.9	6	7.7	2.3	11.4
07Y_L	0.5	1	2	5.2	6.1	1.5	3.6
07Y_R	1.1	2.4	7.2	21.4	23.3	0.7	4
01X_L	0.8	1.7	3.9	8.6	9.5	2.6	7
01X_R	0.2	0.2	0.8	2.7	2.9	0.7	2.4
04Y_L	0.7	1.2	2.1	7.3	8.1	1.9	4.9
04Y_R	2.4	4.6	9.4	18.7	20.2	5.2	9.9

Table 4.10: Peak tensile force values [kN].

The maximum relative displacement between the sill beam and the lower beam of the framed walls was $3.9mm$ at the ground level on the wall GL_02_X and $2.8mm$ at the wall at the second floor L1_07_Y. For the other walls, the sliding was less than $1.5mm$ (Table 4.14).

	06X_L	06X_R	07Y_L	07Y_R	01X_L	01X_R	04Y_L	04Y_R
06X_L	12.4	0.0	4.2	0.0	0.0	0.0	5.1	0.0
06X_R	0.0	7.7	1.6	21.1	9.4	2.9	1.0	19.0
07Y_L	6.4	0.0	6.1	0.3	0.0	0.4	8.1	0.0
07Y_R	0.0	7.1	1.6	23.3	9.3	2.8	0.8	20.2
01X_L	0.0	7.6	1.6	22.6	9.5	2.9	0.9	19.5
01X_R	0.0	7.7	1.6	21.1	9.4	2.9	1.0	19.0
04Y_L	5.6	0.0	6.0	0.2	0.0	0.4	8.1	0.0
04Y_R	0.0	7.1	1.6	23.3	9.3	2.8	0.8	20.2

Table 4.11: Simultaneous values of tensile force values [kN].

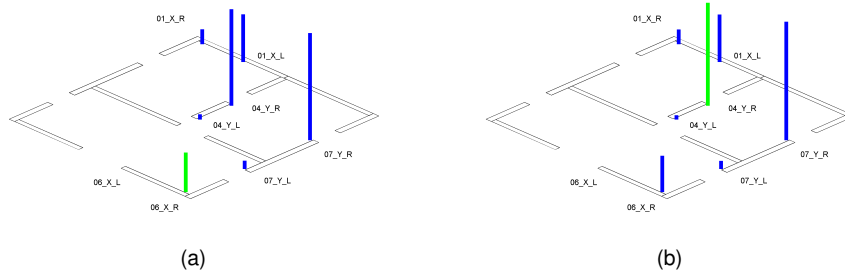


Figure 4.33: Simultaneous values of tensile force values

	Stage 1					Stage 2	
	T1	T2	T3	D10	T4	T5	T6
06X_L	-	-	1.0	2.2	2.3	0.7	2.0
06X_R	-	-	0.4	1.0	1.1	0.7	2.1
06Y_L	-	-	0.1	0.1	0.0	0.0	0.1
06Y_R	-	-	0.3	0.6	0.7	0.3	0.6
07Y_L	-	-	0.4	1.0	1.2	0.5	1.0
07Y_R	-	-	1.5	4.4	5.2	4.4	2.4
04Y_L	-	-	0.4	1.6	1.9	0.6	1.3
04Y_R	-	-	1.2	2.9	3.2	0.8	1.5
02X_R	-	-	0.0	0.0	0.0	0.0	0.0
01X_L	-	-	0.4	0.8	0.8	0.4	0.7

Table 4.12: Peak uplift values [mm].

	06X_L	06X_R	06Y_L	06Y_R	07Y_L	07Y_R	04Y_L	04Y_R	02X_R	01X_L
06X_L	2.2	0.2	0.0	0.1	0.6	-1.5	0.6	-1.0	0.1	-0.2
06X_R	-0.2	1.0	0.1	0.6	0.2	4.2	-0.3	2.8	0.1	0.8
06Y_L	0.3	0.5	0.1	0.3	0.4	-0.9	0.4	-0.5	0.3	0.3
06Y_R	-0.2	1.0	0.1	0.6	0.2	4.2	-0.3	2.8	0.1	0.8
07Y_L	1.3	0.4	0.1	0.1	1.0	-2.4	1.6	-1.0	0.1	-0.2
07Y_R	-0.5	0.6	0.0	0.5	0.0	4.4	-0.5	2.9	0.0	0.7
04Y_L	0.9	0.3	0.0	0.0	1.0	-2.4	1.6	-1.0	-0.1	-0.2
04Y_R	-0.5	0.8	0.0	0.5	0.1	4.4	-0.4	2.9	0.0	0.7
02X_R	-0.2	-0.5	0.0	-0.5	-0.3	0.0	0.0	-0.1	-0.4	-0.2
01X_L	-0.2	1.0	0.1	0.6	0.2	4.2	-0.3	2.8	0.1	0.8

Table 4.13: Simultaneous values of the uplift values [mm].

	Stage 1					Stage 2	
	T1	T2	T3	D10	T4	T5	T6
GL06_X	0.3	0.4	0.6	1.2	1.2	0.7	1.3
GL07_Y	0.3	0.4	0.6	1.4	1.5	0.4	0.6
GL02_X	0.1	0.3	1.3	3.6	3.9	1.3	3.6
GL04_Y	0.1	0.1	0.2	0.2	0.1	0.1	0.4
L106_X	0.1	0.1	0.2	0.2	0.2	0.2	0.2
L107_Y	0.2	0.6	1.1	2.7	2.8	1.0	2.0
L102_X	0.2	0.2	0.3	0.2	0.2	0.2	0.2
L104_Y	0.1	0.2	0.2	0.2	0.2	0.2	0.1

Table 4.14: Peak slippage values at the ground and first level [mm].

Light-timber framed-sample 2

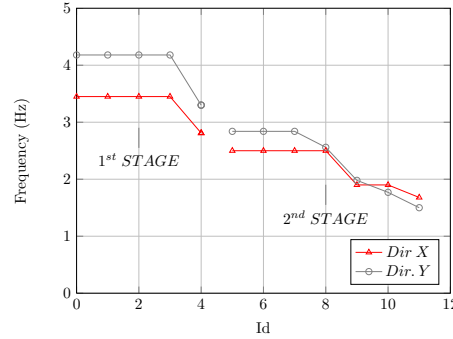
The second building, as discussed in the previous sections, was made with gypsum fibre sheathing panels. The literature and the preliminary tests about this technical solution highlighted relevant differences with the common solution based on strand boards or plywood. The main differences concern the resistance of the material (out of plane failure) and the mechanical behaviour of the connection between the sheathing panels and the timber frame (oligo-cyclic fatigue, tear out, pull off).

With the aim of detecting any damage of the structure a dynamic identification test was carried out after every target T seismic test. Three additional dynamic tests were carried out before D1 and D9 and after D19. Since a variation of modal properties was observed after the seismic tests of the stage 1 (test I4), we can assume that the dynamic behaviour of the building in the stage 2 had been influenced by the stage 1 seismic tests. The modal properties were calculated with an input/output technique in the frequency domain using the data recorded by the accelerometers at each level (output signals) and on the shake table (input signal). The Frequency Response Functions (FRFs) were calculated by means of the Welch method with a Hanning window and an overlap of 66.67%. The Peak Peaking amplitude method (PP) was adopted - to get frequencies and mode shapes. In Table 4.15 the frequencies for the 1st bending mode shape along the X and Y direction are reported respectively. The same values are plotted in Figure 4.34.

The building in stage 1 was not characterized by any frequency variation until I3 whereas at I4 (performed after the seismic test with nominal PGA along y-direction of 0.50 g, T4) a variation of 19% and 21% along the x and y direction was detected respectively. Despite of no structural damage was observed during the visual inspection after this test, a reduction of the stiffness occurred due to some internal damage related to a non-linear behaviour of the structure during the previous test. From stage 1 (test I4) to stage 2 (test I5) a significant reduction of frequency was shown in both directions due to the sheathing panel cutting: 11% in x and 14% in y. For stage 2, no variation was observed until the test I9 and I8 for the X and Y directions respectively. A significant reduction of frequencies was observed in the three last tests. Referring to the initial values for stage 2 (I5) a reduction of 43% (X) and 76% (Y) was observed during the last modal test (I11). These results highlight a substantial variation in the structure stiffness due to a strong non-linear behaviour.

The mode shapes of 1st mode in X and Y direction are shown in Figure 4.35. Only the 1st and 2nd storey are represented because accelerometers of the roof did

	I0	I1	I2	I3	I4	I5	I6	I7	I8	I9	I10	I11
1st x	3.45	3.45	3.45	3.45	2.81	2.5	2.5	2.5	2.5	1.9	1.9	1.68
1st y	4.18	4.18	4.18	4.18	3.3	2.84	2.84	2.84	2.56	1.98	1.77	1.5

Table 4.15: Frequencies [Hz] obtained by identification tests.**Figure 4.34:** Frequency variation.

not work correctly. A significant difference can be observed between the stage 1 and the stage 2. The un-weakened building is in fact characterized by a deformed shape linear along the height of the building and by no significant torsional contribution. For the weakened building, conversely, the mode shapes show a clear soft-storey mode and an important torsional component along X. The soft-storey mode is emphasised when damage occurred in the last seismic tests.

The peak acceleration values, recorded by the uni-axial accelerometers located on the proximity of the centre of mass at 1st and 2nd floors during the seismic tests, are reported in Table 4.16. Higher values of acceleration were obtained in the weakened building for the same reference PGA (e.g. T3 and T7, T4 and T8). In all tests the peak acceleration increased along the height of the building but in case of the weakened buildings similar peak values of acceleration were obtained at the 1st and the 2nd storey, showing a clear soft-storey behaviour of the building in stage 2. This can be confirmed plotting the fundamental peak acceleration values along the height of the building. As for the previous building, the profile of the peak ground acceleration amplification along the height of the building is presented (Figure 4.36).

In the figure are shown test T1, T4 for the stage 1 (un-weakened) and T5, T8 for the stage 2 (weakened). These results are very similar to the mode shapes obtained from the modal testing analysis: the un-weakened building is characterized by modal displacement which increase linearly along the height of building, whereas a soft-storey mode is shown for weakened building.

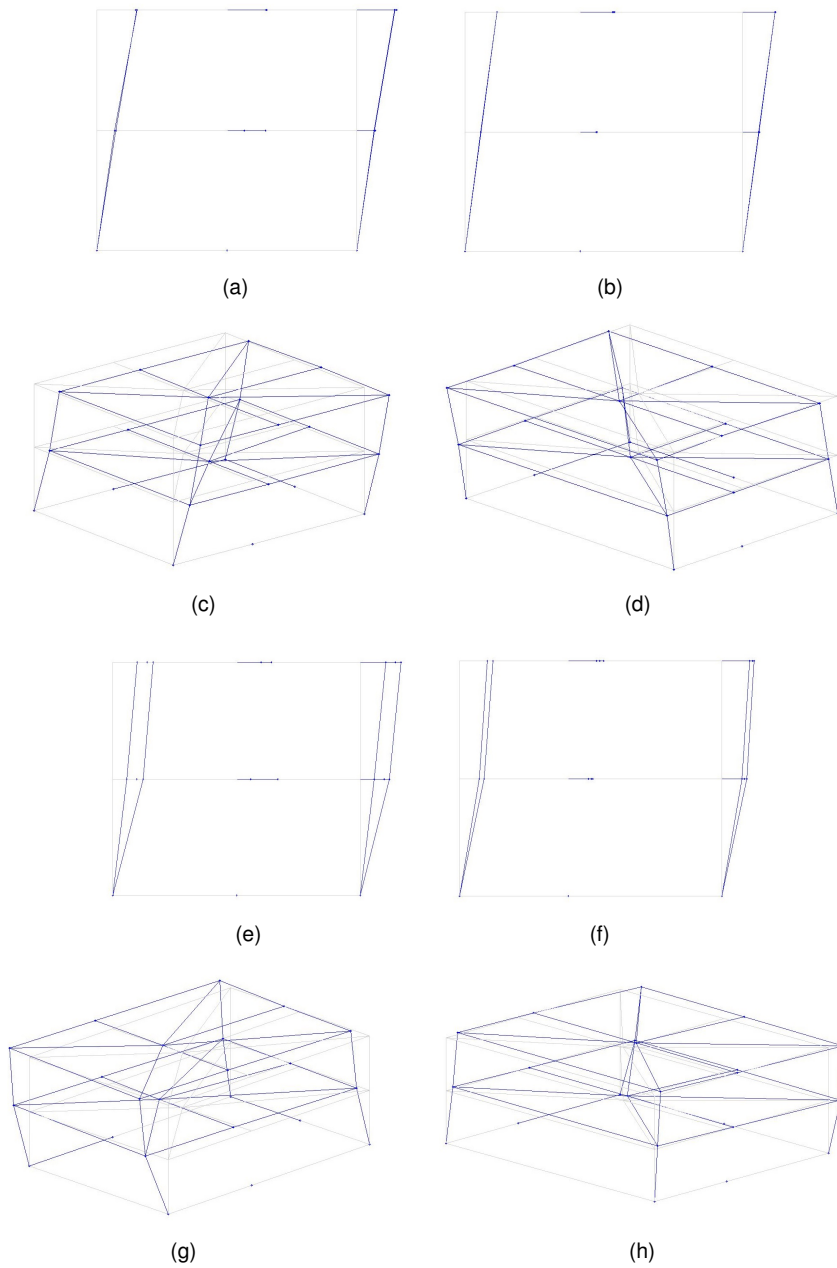


Figure 4.35: First mode shapes - 2D view x-direction test I0 a) - 2D view y-direction test I0 b) - 3D view x-direction test I0 c) - 3D view y-direction test I0 d) - 2D view x-direction test I5 e) - 2D view y-direction test I5 f) - 3D view x-direction test I5 g) - 3D view y-direction test I5 h).

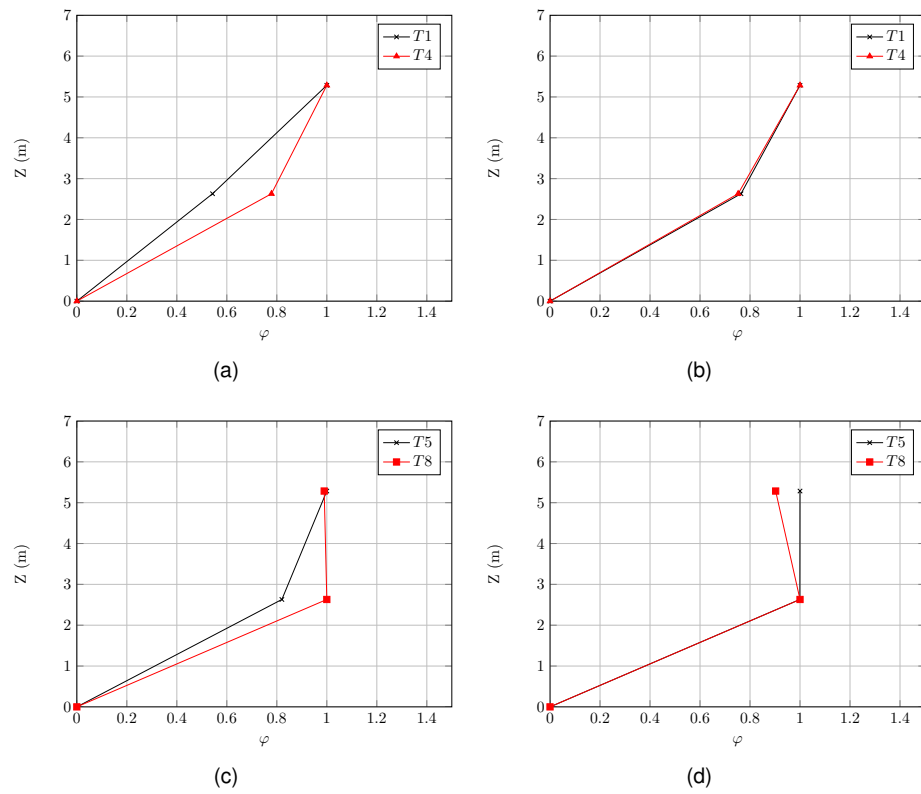


Figure 4.36: Mode shapes obtained from peak acceleration values for test T1, T4 (stage 1) and T5,T8 (stage 2).

Dir.	Test Pos.	Un-weakened (stage 1)				Weakened (stage 2)					
		T1	T2	T3	T4	T5	T6	T7	D19	T8	T9
X	Ref.acc.										
	Table	0.06	0.12	0.22	0.57	0.06	0.1	0.22	0.42	0.43	0.44
	1st floor	0.1	0.17	0.35	0.69	0.08	0.2	0.57	1.01	0.97	0.84
	2nd floor	0.19	0.3	0.49	0.89	0.1	0.24	0.57	0.99	0.96	0.93
Y	Ref.acc.										
	Table	0.07	0.13	0.28	0.51	0.07	0.14	0.29	0.47	0.73	0.73
	1st floor	0.1	0.18	0.39	0.62	0.13	0.25	0.52	0.89	1.03	1.1
	2nd floor	0.13	0.25	0.44	0.82	0.13	0.23	0.45	0.87	0.93	0.96

Table 4.16: Peak acceleration values [g] recorded in centre of mass at each floor.

The inter-storey displacement Δ and the inter-storey drift ϑ , defined as the ratio between Δ and the inter-storey height of the building (in this case equal to 2560mm), are key factors for understanding the mechanical behaviour of a structure under a seismic event. The damage-level and the seismic capacity of the structure are in fact strongly related to these two parameters, [31] - [43] and [34]. In Table 4.17 the peak values of Δ and ϑ are reported for all seismic tests recorded by LVDTs, in the centre of the building, and by the optical system on the corner north-west. At stage 1, values of ϑ lower than 0.8 % were obtained. At stage 2, as expected, much higher values were found, especially in Y direction of the building where a peak value of 2.46 % was recorded for the T9 tests. A lower value (0.61%) was recorded for the same test at the first level, confirming a soft-storey behaviour.

	Ground-first dir. X				Ground-first dir. Y			
	Lvdt		opt.		Lvdt		opt.	
	Δ [mm]	ϑ [%]	Δ [mm]	ϑ [%]	Δ [mm]	ϑ [%]	Δ [mm]	ϑ [%]
T1	0.5	0.02	1.9	0.08	0.9	0.04	2.2	0.09
T2	1	0.04	2.8	0.11	2.2	0.09	4.1	0.16
T3	2.6	0.1	5.6	0.22	7.1	0.28	6.4	0.25
T4	6.6	0.26	15.3	0.6	19.6	0.77	14.1	0.55
T5	1.1	0.04	2.6	0.1	3.5	0.14	4.5	0.18
T6	2.5	0.1	5.5	0.22	7.9	0.31	7.1	0.28
T7	5.6	0.22	10.8	0.42	16.7	0.65	15.3	0.6
D19	11	0.43	16.7	0.65	34.1	1.33	30	1.17
T8	12	0.47	15.3	0.6	40.8	1.6	38.6	1.51
T9	12.5	0.49	16	0.62	60	2.35	62.9	2.46

Table 4.17: Inter-storey displacement [mm] measured by the Lvdt and optical system.

The peak acceleration values, recorded at the 1st storey on the corner C1, vs the peak inter-storey drift values (optical), between the ground and the first level, both for stage 1 and stage 2, are reported in Figure 4.37 for all seismic tests (target and drive). For stage 2 along the Y direction a significant reduction of the curve slope

shown for displacement greater than 30mm , confirming a strong non-linear behaviour of the structure in the last tests.

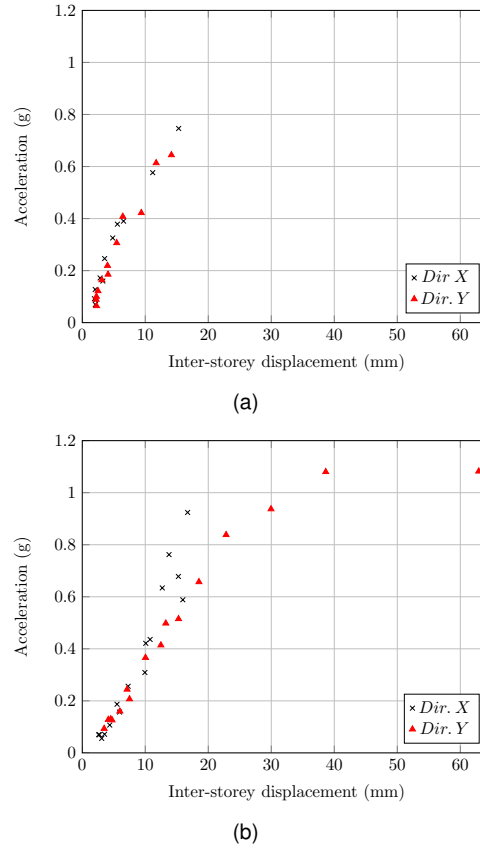


Figure 4.37: Acceleration (*p.t 3C - 1st storey*) vs inter-storey displacement (*Optical system*) between the ground and 1st level for stage 1 (a) and stage 2(b).

After each seismic test visual damage inspections were made, Figure 4.38. No damage was detected during stage 1 and until test D19 for stage 2. On the contrary numerous occurrences of cracking of GFB around the openings and in the proximity of hold-down anchors were observed after test D19, T8 and T9. After T9 test spalling at the corner of the window of wall W06_Y was observed. A list of all damages detected are reported in Table 4.17. All damages occurred at the ground level.

With the aim to assess the effect of the over-turning moment on each wall, load cells were used to record the tensile force in the hold-downs. In Table 4.19 the peak tensile force values are reported. A maximum value of 25.1kN and 39.3kN were

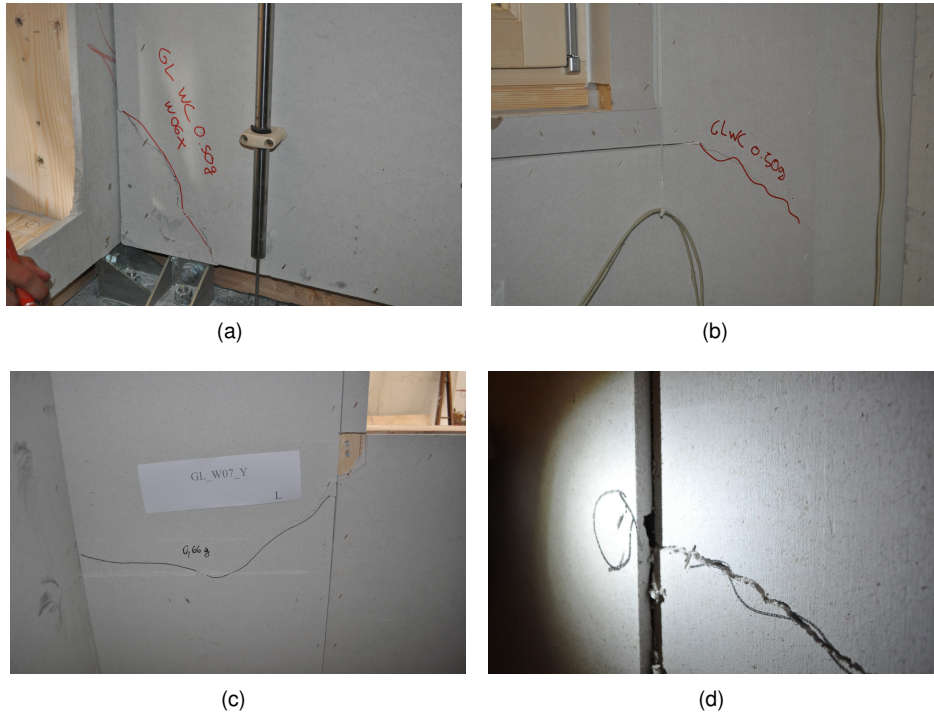


Figure 4.38: Cracking of GFB in the proximity of the hold down anchor on wall W06_X (a) after test D19 (a), cracking on gypsum wallboards at corners of openings at the ground level on wall W02_Y after test D19 (b), cracking on the GFB on W07_Y after test T9 (c), Spalling at the corner of the window on wall W06_Y, north after test T9.

Test	Detected damage
D19	Cracking of GFB in the proximity of the hold down anchor (W06_X, north east bottom corner), cracking on gypsum wallboards at corners of openings at the ground level (W01_Y, south east - W02_Y, south - W06_X, north east), cracking on the GFB at the ground level (W06_X, north), spalling of the bottom edge of the GFB (W07_Y, north) at the ground level.
T8	Cracking on the GFB at the ground level (W07_Y, north - W04_X, central), cracking of the bottom corner of the GFB (W07_Y, north) at the ground level.
T9	Spalling at the corner of the window (W06_Y, north), staples pull through (W07_Y, north), cracking of GFB in the proximity of the hold down anchor (W04_X, north east bottom corner), cracking on the GFB at the ground level (W07_Y, north)

Table 4.18: List of visual damages for stage 2.

recorded at stage 1 (test T4) and at stage 2 (test T8) respectively. These values are quite lower than the strength obtained from laboratory test (equal to $62kN$), confirming that the structural damage was related to the sheathing-to-framing connections and GFB. In Figure 4.39 the simultaneous tensile forces at the instant when the maximum value was achieved in X and Y direction for tests T4 and T8 (nominal PGA y of $0.50g$). The hold-down force distribution, as for the test on the OSB-sheathed building, shows that each wall behaved like a cantilever. When the left corner of a wall is subjected to a high tensile force, in the right corner a negligible tensile force is recorded.

	Un-weakened (stage 1)				Weakened (stage 2)					
	T1	T2	T3	T4	T5	T6	T7	D19	T8	T9
06X_L	0.2	0.2	0.2	5.3	0.1	0.2	0.2	3.6	4.1	4.9
06X_R	0.1	0.2	0.3	13.4	0.2	1	13.5	37.2	39.3	32
07Y_L	0.2	0.3	0.6	5.9	0.2	0.5	1.1	6.5	8.4	8.1
07Y_R	0.8	1.3	1.8	19.2	0.6	0.9	13.4	43.4	32	16.9
01X_L	0.2	0.2	0.2	1.2	0.2	0.2	0.2	2.2	4.8	10.7
01X_R	0.1	0.1	0.4	5.6	0.1	0.2	0.3	8	7.8	2.2
04Y_L	0.2	0.4	1.1	2.1	0.3	0.6	1.2	5.8	11.9	21.3
04Y_R	1.2	1	1.4	6.1	0.5	0.4	1.8	14.3	18.5	24.2
02X_L	0.1	0.2	5	25.1	0.2	0.4	8.7	25.6	21.8	10.3
02X_R	0.1	0.2	0.4	3.3	0.1	0.1	0.2	0.7	0.9	1

Table 4.19: Peak tensile force values [kN].

In Table 4.23 the peak values of the wall slippages at ground level are reported. A maximum value of 4.8 mm and 3.4 mm was recorded at test T4 for stage 1 in X and Y direction. As expected, higher values were obtained for the same nominal PGA of $0.50g$ at stage 2 at T8 test. A maximum value of 8.8 mm was recorded at GLW04Y wall during the last test (T9) along the Y direction. From the comparison of this value with the total inter-storey drift between the ground and the first level measured by the LVDT (equal to $60mm$), it was shown that the slippage deformation contribution results significant (around 15% of the global inter-storey displacement).

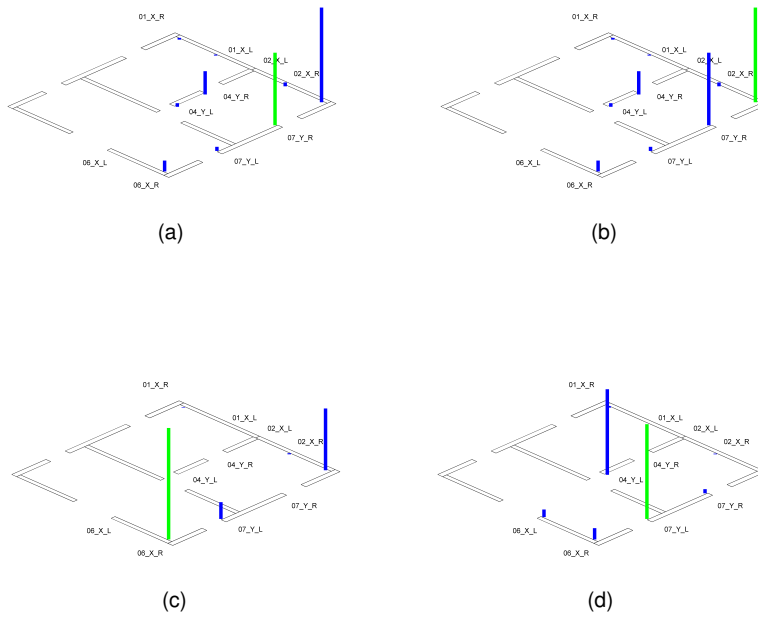


Figure 4.39: Simultaneous values of HD tensile forces: peak value in X direction for test T4 a), peak value in Y direction for test T4 b), peak value in X direction for test T8 c), peak value in Y direction for test T8 d).

	Un-weakened (stage 1)					Weakened (stage 2)					
	T1	T2	T3	D8	T4	T5	T6	T7	D19	T8	T9
07Y_R	0.2	0.3	1.3	2.4	3.0	0.4	1.2	2.8	5.6	6.0	5.3
07Y_L	0.1	0.3	0.9	2.1	2.8	0.5	0.8	2.2	5.8	7.6	12.4
06X_R	0.2	0.4	1.0	2.4	3.9	0.6	1.5	4.0	8.4	10.1	12.8
06X_L	0.3	0.6	0.9	2.0	3.3	0.3	0.7	1.9	5.4	5.4	5.1
04Y_R	0.1	0.4	1.3	2.9	3.6	0.5	1.2	2.8	6.4	7.3	6.8
04Y_L	0.2	0.4	1.2	2.1	2.3	0.5	0.7	2.0	4.4	6.0	10.2
06Y_R	0.2	0.4	1.1	1.9	2.9	0.3	0.4	1.7	3.4	4.2	5.0
06Y_L	0.1	0.3	0.9	2.1	2.6	0.1	0.5	1.7	2.2	2.2	2.8
02X_L	0.2	0.2	0.4	0.6	0.7	0.2	0.2	0.5	0.9	0.8	0.7
01X_L	0.2	0.2	0.5	1.0	1.7	0.2	0.3	1.0	1.7	2.0	1.6

Table 4.20: Peak uplift values [mm].

	07Y_R	07Y_L	06X_R	06X_L	04Y_R	04Y_L	06Y_R	06Y_L	02X_L	01X_L
07Y_R	6.0	-5.5	5.8	1.0	7.1	-4.9	-3.4	-1.0	0.5	0.1
07Y_L	-2.8	7.6	-4.0	1.1	-3.8	5.9	3.9	2.2	-0.2	1.0
06X_R	3.7	-2.2	10.1	-0.3	5.0	-0.7	-0.1	1.8	0.8	-0.9
06X_L	0.1	1.7	-5.8	5.4	0.1	-1.4	1.5	0.7	-0.2	1.4
04Y_R	5.5	-5.3	4.2	0.8	7.3	-4.8	-3.4	-0.9	0.3	-0.2
04Y_L	-2.7	7.5	-4.1	0.8	-3.8	6.0	4.0	2.0	0.0	1.1
06Y_R	-2.4	7.5	-3.6	2.0	-3.7	5.8	4.2	2.1	0.2	1.3
06Y_L	-2.8	7.6	-4.0	1.1	-3.8	5.9	3.9	2.2	-0.2	1.0
02X_L	3.7	-2.2	10.1	-0.3	5.0	-0.7	-0.1	1.8	0.8	-0.9
01X_L	-0.9	3.9	-6.1	4.1	-1.8	0.5	2.2	0.8	-0.1	2.0

Table 4.21: Simultaneous values of the uplift values [mm] test T8.

With the aim to analyse the global behaviour of the building along the Y direction (this is the direction where the higher displacements were recorded and the higher modification of period was obtained), the global hysteretic response was represented in Figure 4.40. These were obtained plotting the building inertial force vs the relative displacement of the second level. The building inertial force was calculated as the sum of the contributions of inertial force of each storey obtained multiplying the storey mass (126.2kN - 1st st., 109.6kN - 2nd st. and 66.3kN roof) by the average of the acceleration signals measured by the four accelerometers positioned in the four corners at. The relative displacement between the second storey and the ground level was calculated as the difference between the absolute displacement of the second storey and of the steel basement, obtained through a double integration of the acceleration signals, filtered in the frequency band between 0.15Hz and 30Hz, recorded by the accelerometers located in the centre of the building at second storey and on steel basement. In Figure 4.40(a) the global hysteretic responses for the test T2 and test T6 are reported, showing how the un-weakened buildings results stiffer. In both cases the loops appear small and strict, demonstrating an elastic-behaviour of the two buildings. In a comparison of the two buildings for the nominal PGA of 0.50 g

	07Y_R	07Y_L	06X_R	06X_L	04Y_R	04Y_L	06Y_R	06Y_L	02X_L	01X_L
07Y_R	2.4	-0.9	2.1	-0.3	2.9	-1.7	1.9	-0.7	0.5	-0.6
07Y_L	0.1	2.1	2.3	-0.3	0.2	1.6	1.3	2.1	0.4	-0.7
06X_R	0.1	2.0	2.4	0.0	0.2	1.6	1.3	2.0	0.5	-0.5
06X_L	-0.1	0.8	-1.4	2.0	-0.9	0.5	-0.5	0.4	-0.2	1.0
04Y_R	2.4	-0.9	2.1	-0.4	2.9	-1.7	1.9	-0.7	0.5	-0.6
04Y_L	-0.8	1.4	0.1	0.7	-1.0	2.1	-0.3	1.5	-0.1	0.1
06Y_R	2.4	-0.9	2.2	-0.4	2.9	-1.8	1.9	-0.7	0.6	-0.6
06Y_L	0.1	2.1	2.3	-0.3	0.2	1.6	1.3	2.1	0.4	-0.7
02X_L	2.4	-0.9	2.2	-0.4	2.9	-1.8	1.9	-0.7	0.6	-0.6
01X_L	-0.3	1.0	-1.4	1.9	-1.0	0.7	-0.5	0.5	-0.3	1.0

Table 4.22: Simultaneous values of the uplift values [mm] test D8.

	Un-weakened (stage 1)				Weakened (stage 2)					
	T1	T2	T3	T4	T5	T6	T7	D19	T8	T9
GLW02X	0.1	0.2	0.6	2.4	0.2	0.5	1.3	2.6	2.6	1.7
GLW06X	0.2	0.2	0.4	4.8	0.2	0.4	1	2.8	3.4	3.9
GLW04Y	0.1	0.1	0.6	2.2	0.2	0.6	1.8	4.6	6.1	8.8
GLW07Y	0.1	0.3	1	3.4	0.4	1	2.4	5.5	6.2	2.8
L1W02X	0.1	0.2	0.7	3.3	0.1	0.5	2	4.2	4.4	3.9
L1W06X	0.2	0.4	0.9	2.6	0.1	0.7	1.6	3.4	3.7	3.7
L1W04Y	0.1	0.1	0.3	2	0.1	0.1	0.8	2.1	2.2	1.8
L1W07Y	0.1	0.2	0.5	1.6	0.2	0.4	1.1	2.1	2.3	2.4

Table 4.23: Peak slippage values at the ground level [mm].

is shown (test T4 and T8). The weakened building cyclic behaviour is characterized by larger loops showing a greater energy dissipation due to non-linear behaviour. A significant hysteretic behaviour is shown for the un-weakened building as well. In Figure 4.40(c) the response for the weakened building at the last tests T8 and T9 is presented, demonstrating a strong non-linear behaviour of the building.

Capacity spectra were developed for all seismic tests. In Figure 4.41(a) and Figure 4.41(b) plots of the maximum inertial force versus the corresponding relative displacement are shown for stage 1 and stage 2 respectively. For the un-weakened building a quasi linear relationship can be defined until last test where a reduction of the slope is observed. For the weakened building, conversely, a clear non-linear behaviour is shown after test T7: the relative displacement significantly increases in spite of a small variation of the peak force.

4.2.8 Conclusions

The previous sections summarize the main results of the tests on two light-timber framed buildings. The two samples were designed following the commonly adopted technical solutions of the European timber-framing typology assuming the maximum

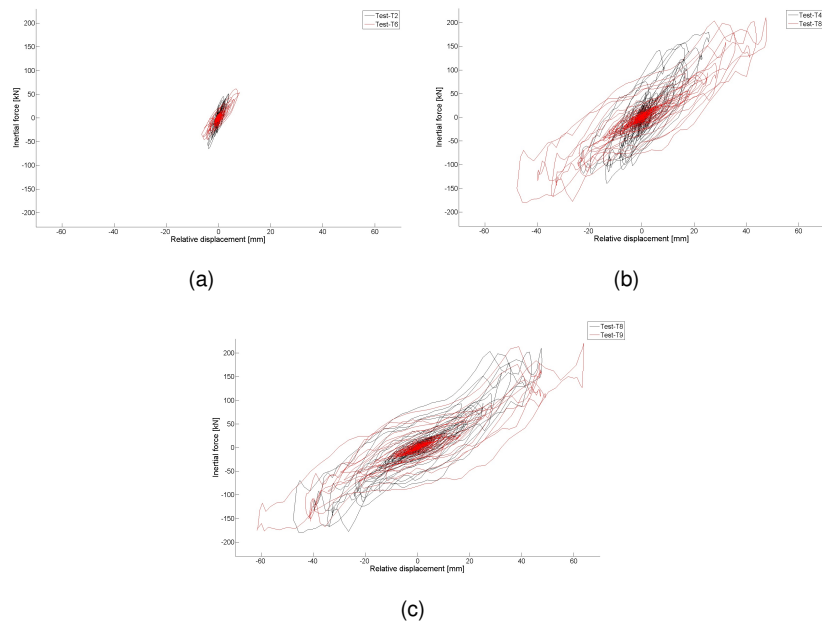


Figure 4.40: Global inertial force vs relative displacement hysteresis loops: tests T2 and T6 a), tests T4 and T8 b), test T8 and T9 c).

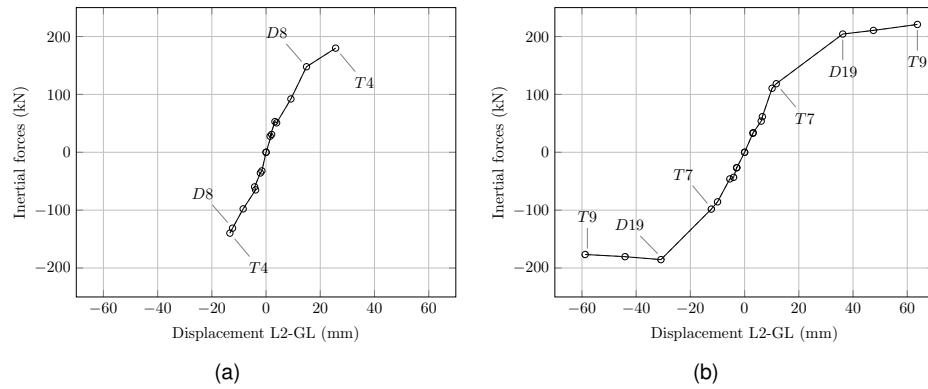


Figure 4.41: Capacity curves along the Y direction for un-weakened (a) and weakened (b) building .

PGA according to the current codes (0.28g) and .

The aim of the shake table tests on the this constructive system was the to evaluate some aspects that, especially for the European prefabricated structure, need to be verified. These tests represent the capstone of an extensive research programme carried out by the university of Trento in the last years which was organized to characterize the lateral load bearing behaviour from the single component to the full scale building.

Several shake table were carried out, using a adaptive control algorithm, with an increasing level of peak ground acceleration (drive + seismic tests) from 0.07g up to 0.50g. Moreover after a common test procedure a second tests series were performed on the same samples to investigate peculiar aspect of the seismic response. The first building was tested under a different accelerogram whereas the second was tested with a different structural layout. The tests demonstrate a good seismic response of the two tested buildings both for the ultimate and serviceability limit states conditions because, as summarized in the following paragraphs, no significant damages had occurred during the tests

From the dynamic identification tests and by the analysis of the trends of the capacity curves obtained from the peak values of the hysteresis loops the building sheathed by oriented strand boards (OSB) behave in the elastic range until the last test of the first test protocol (0.50g). The tensile forces recorded by the hold-down load cells were lower than the elastic limits obtained from the preliminary tests reported in [5]. Also the shear anchor systems, for the slippage recorded during the tests, behave in the elastic range identified by the load-displacement curves [5].

The same parameters and analysis tools have shown a linear behaviour of the structure sheathed by gypsum fibre boards up to the test T3 (0.28g). After the seismic test level T4 a significant reduction of the natural frequencies along the two direction (19% in the x-direction and 21% in the y-direction) was detected. The peak of the hysteresis loop value seems to confirm the non-linear behaviour of the system. However after the first stage the overall response of the building was significantly far from the near collapse condition and no visible damages were recorded during the inspections. Once again the most loaded connection, hold-down and angle brackets, behave in the elastic branch of the load displacement curves obtained from the tests presented in the first part of the theses.

The peak inter-storey drift reached during the first step of the test campaign (common test protocol) were compatible with the absence of cracks or other damages of the structural and non structural components. The maximum value recorded for the

first (0.63%) and the second building (0.77%) confirm the results of the preliminary tests and the values reported in [7] and in [31].

From the analysis of the force distribution on the hold downs element some interesting consideration have been provided. Observing the force distribution between the walls, at the same time instant, it can be deduced that the main resisting mechanism of the wall was a flexural mode with a force distribution "similar" to a cantilever beam. According to this scheme each wall can be considered as working mostly as a "cantilever beam" because for same time instant the hold-down on one side was loaded while the opposite device was unloaded. Thus a predominant "box like behaviour" was not reached in the two tested buildings.

The second stage of the test procedure was planned to analyse different aspect of the structural response. In the in these tests the first building was loaded by the Tohoku input signal. This signal present a different frequency content and higher PGA (0.72g) and a stronger motion along the orthogonal direction with respect to the Montenegro procedure. Despite of the different input the building did not shows any damages and the overall response still remain in the elastic field.

The second building was tested with a new structural layout. In the latter stage, the sheathing panels of five external walls at ground level were removed in order to reduce the racking capacity of the building.

From the modal analysis carried out before the first seismic test in stage 2 (I5) a significant reduction of frequencies was observed due to the stiffness reduction at the ground level. From mode shapes, a clear soft-storey dynamic behaviour is shown. A significant torsional component, due to the panel cutting on the wall in a unsymmetrical position along the x axis, characterized the mode shape along x-direction as well. The building showed a quasi-elastic linear behaviour until test T7 (PGA of 0.22 g along x and 0.28g along y). This was confirmed by modal analysis (a small variation along y-direction occurred), by visual inspection (no visible damage) and by inter-storey drift (0.42 % in x and 0.65% in y). Differently from the un-weakened building, with the increasing of ground acceleration (test D19, T8 and T9), the specimen showed a significant non-linear behaviour and visible structural damage. The high reduction of natural frequencies, the non-linear trend of capacity curve along y-direction and the global hysteresis loop confirmed the achievement of an ultimate limit state condition of structure. The values of peak inter-storey drift (around 2.5%) are in fact compatible with this condition.

These comments about the tests results of different sheathing materials (OSB-GFB), input signal and structural layout lead to some interesting considerations about

the behaviour of the structural system.

The comparisons between the results of the test and the design limit states peak ground acceleration suggest, for this layout, demonstrate a conservative design approach. The outcomes of the test highlight that, although the structural design of the was conducted assuming a non-linear plastic behaviour the structure behaved in the elastic range up to the last test (T4), especially for the OSB sheathed building (behaviour factor equal to 4). The difference between the actual performance and the design prevision, in the author opinion, is related to the analysis model which in many cases is on the safe side because important mechanisms are neglected. For instance the contribution of friction forces, the presence of structural lintels and the connection between walls at the corner of the buildings and the between the orthogonal walls are often not taken into account in the structural design.

However if the geometry and the architectural layouts, such as opening dimensions and plan distribution, allows the creation of these mechanisms a significant reduction of the forces on the anchor devices leads to a stronger behaviour of the system against the horizontal loads.

About this issue, further studies should investigate the influence of these mechanism analysing different structural layout, to achieve a more precise asses of the secondary contribution in order to better understand the global behaviour of the structure.

Part II

LOG-HOUSE

Chapter 5

LOG-HOUSE

5.1 Introduction

Log-house system is a traditional construction technique used in the northern region, where large amounts of straight and tall trees were easily available. The constructive principle of the walls is the superposition of linear elements connected to the orthogonal walls by corner joints. Records show that this construction type has its roots in the late Bronze Age (1100 - 1800 BC), most likely in Northern Europe. Originally, the structures were fairly simple and less architecturally sophisticated, historically constructed with round overlapped logs covering the gaps between logs with moss. Due to the good insulation properties of solid wood, its robust design and to the fact that a log structure can be erected relatively quickly in all weather conditions, it found wide application in many countries such as Scandinavia, Northern Russia and the southern Alpine region.

Today, coniferous wood is used almost exclusively for the walls, roofs and ceilings of log buildings. The only exception are the sill logs in direct contact with the foundation, where larch or oak are preferred for reasons of weather resistance and durability.

The coniferous wood species used are pine, spruce, larch and for a number of years also Douglas fir. Typical for the engineered wood industry, the timber must meet the requirements in line with the validation standard [44]; in other words it must be sorted according to its load-bearing capacity. Structural timber must be made of graded wood and the mean moisture content may not exceed 20 %. In the case of log constructions even stricter requirements are made. In order to avoid shrinkage, de-

formations and cracks, a mean moisture content of 12 to 18 % must not be exceeded. Fungal infections are thereby restricted.

The beams can be produced using solid wood or glued laminated timber. For solid wood structures, spruce wood from Northern Europe with its fine-grained texture is usually chosen. This rather slow-growing wood provides higher strength, a lower degree of vertical shrinkage, a higher resistance to weathering and better insulation properties compared to pine. At the same time, spruce is more cost-effective than larch and Douglas fir. For glued laminated timbers, cheaper and faster-growing pines are commonly used. The cost-increasing process of gluing together a number of graded and seasoned laminates (using permeable glue) with exposed pith along their flat side significantly improves the original characteristics of the wood. For this reason in the modern construction double and triple laminated beams are often preferred.

The logs are locked together with single or multiple groove and tongue systems to ensure an easier montage and to improve the stability of the walls. This milling ensure also a better building airtightness.

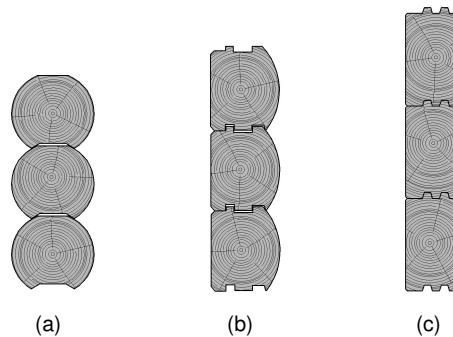


Figure 5.1: Logs section: (a) *Swedish Cope* - (b) *D-shaped* - (c) *Square*

At first glance, the system may seem very simple, but the design of the building and the constructive details must be carefully analysed. The key point is the horizontal orientation of the logs fibres which is one of the main limits of this system because of dimensional variation of the wall due to the moisture content changing. Shrinkage and swelling of the logs in the direction perpendicular to the grain vary between 10 to 20% whereas along the grain is about 1% and consequently the variation of the wall dimension reaches high values when high variation of moisture occurs. The height variation could be even 2 cm each meter [45] in the worst condition. This fact implies a series of details (e.g. connection between windows or door, insulation etc.). This condition is emphasized when other vertical bearing elements are inserted, for

instance when a beam of the floor is supported by two external walls and from an internal column (Figure 5.2). In this case the internal support must be equipped with an adjustment device to bridging or reduce the gap between the two elements. Furthermore the vertical loads are transmitted in the logs weaker direction (perpendicular to the grain) and also the vertical stability of the walls could limit the maximum numbers of stories to two or three.

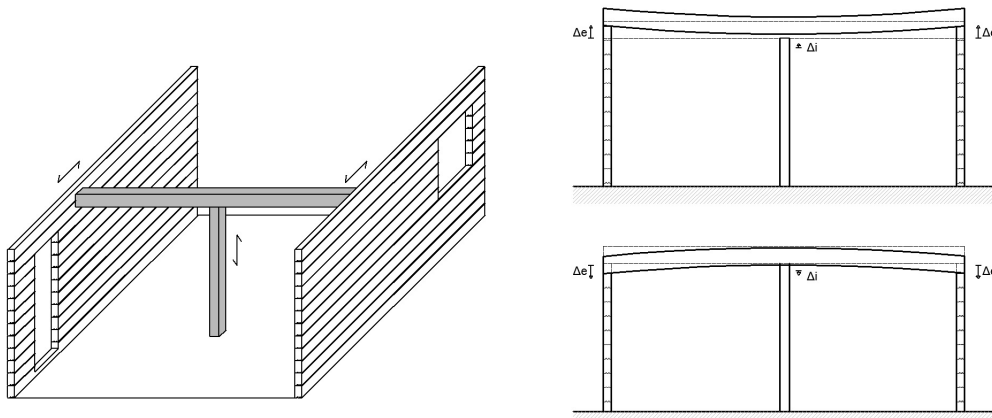


Figure 5.2: Effect of the timber moisture variation on elements with different grain orientation.

The previous consideration must be taken into account also for doors and windows as well as for the technical equipment.

There are no restrictions on choice of window and door constructions, as long as shrinkage or swelling of the surrounding wooden construction are unhindered in order to avoid undesirable stresses and crack formations. The frame of the door or window is inserted using a tongue-and-groove system with sealing strips. This connection, which is covered by an additional frame, guarantees an unhindered deformation of the wall and, at the same time, air tightness and wind impermeability of the joints. In the upper part of the opening, the tolerance for shrinkage and swelling is provided which is closed using compressible thermal insulation material. The necessary free distance between frame and lintel is determined according to the respective degree of shrinkage and swelling of the wood used. In the case of a two meter high door, for example, a settling space of 5 - 6 cm must be provided. Regarding to service installations several important aspects must be considered. The most important ones are:

- no water-carrying pipes on the inside of external walls,

- pipes orientated transversely to the direction of the joints of inner log walls, radiators and sanitary installations must be fixed with fasteners which allow gliding,
- for safety, cables should be installed in empty conduits.

Controlled domestic ventilation systems are especially suitable for wooden structures. They help keep the air moisture content constant and thereby control the shrinkage behaviour of wooden construction components.

5.1.1 Design principle

Log house can be classified as "load bearing walls" structure. The walls usually have both space-defining and static constructive function, for which the characteristic corner styles constitutes one of the main characteristics. Both vertical and horizontal loads are transferred to the foundation through external and internal walls. The vertical load is directly taken by the logs that transfer through stress perpendicular to the grain the load itself to the ground. The vertical stability is guarantee by the intersection with the other walls. Friction between logs and the presence of the corner joints are the two resistance mechanisms that give stiffness and resistance to the walls itself. The overall behaviour is complex because these two mechanisms are exploitable at different displacement level. Between the "initial friction regime" and the interlock "contribution" there is a large semi-horizontal (or low - rise slope) plateau governed by dynamic friction. Thus if no other fasteners are used, the mounting tolerance contribution are fundamental.

This load path is also reflected in the cyclic monotonic and dynamic conditions. The behaviour is clearly visible in Figure 5.3(b) where an idealized representation of a quasi-static cyclic test is presented. In the first cycles the stiffness of the interlocks is not activated and the shape of the hysteresis loops is almost as a perfect "friction dissipator". When the gaps between the surfaces of the joints is exceeded the behaviour is attributable both to dynamic friction dissipation and to the mechanisms correlated to the compression perpendicular to the grain.

The behaviour of the system can be improved using timber (dovetail reinforce) or steel fasteners (self-tapping screws or dowels) Figure 5.4(b). These inter-log connections are often used when the geometry allows a limited number of corner joints or when wide openings interrupt the logs continuity. However, this solution can be used also to achieve a more efficient behaviour (as described in paragraph 5.4). Even in this case a careful analysis of the compatibility with the dimensional variation of the logs must be considered. Another possibility to achieve a higher performance is the

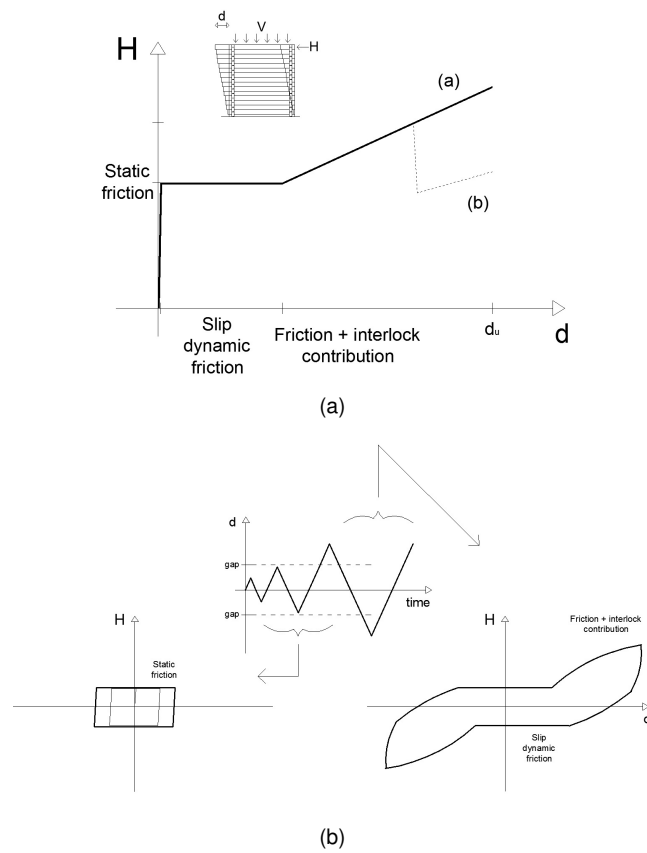


Figure 5.3: Log house shear wall behaviour: (a) monotonic test - (b) cyclic test

use of multi-layer configuration of the corner joints (Figure 5.4(a)). Nevertheless this solution is clearly more complex and expensive. The mounting phases are more difficult and the gain in terms of resistance and stiffness often do not justifies this effort.



(a)



(b)

Figure 5.4: (a) Timber dowels reinforce (from www.lithouse.eu)-(b) multilayer system (from www.logcabinssouthwest.co.uk)

The design of the structural lateral load bearing capacity of the log house is different from the light timber framed walls platform systems. In the LH the force distribution and the resistance is influenced by the number of intersection and by the magnitude of the vertical load (independent from the length of the wall). In the second the resistance and the stiffness is correlated with the numbers of connections between the sheathing panels and studs and from on the hold-down elements (both dependent from the wall length). The behaviour of these systems, as shown in Figure 5.5, is completely different in term of stiffness, maximum load and energy dissipation. The

horizontal load carrying capacity of the TF construction has been deeply investigated and the reliability of the models was investigated and confirmed during the last fifty years by different authors from different countries. The design codes, based on these experiences, provides models to verification of the structural systems. This procedure was not followed for the LH. The current design approach is based on the verification of the resistance of the carpentry joints (compression perpendicular to the grain, tension, shear/rolling-shear). However, few specific rules are provided for the static and seismic case. The system was not explicitly mentioned in the current standards ([2]; [46] - [15]).

5.1.2 State of the art

The studies about log construction, often based on the in-field experience, are mainly focused on the constructive details. About these topic different authors, especially in the German area has published interesting works, in particular on the stability of the walls under vertical loads [47]. In low-seismic areas, the main issues are related to the compression perpendicular to the grain stress and the vertical stability. In these regions where the design peak ground acceleration is low, especially for low-rise lightweight buildings, the inertial forces are often less important than the wind loads. However, several research programs have already been carried out with the goal of better understand the log systems regarding the lateral load bearing behaviour. Popovski and Leichti have done research on the traditional hand-crafted logs system through full-scale tests [48] and tests on connections with the foundation [49]. The object of the study was, inter alia, the influence of soft or hardwood pins on the in-plane behaviour of log walls. In recent years, especially in Italy and Portugal, various research focused on the seismic behaviour were carried out. First, reference should be made to the research of Jorge M. Branco and Joao P. Araujo [50]. This research was organized in four steps. The first was the analysis of the in-plane resistance ensured only by the log-to-log friction and the connection to the foundation. The second was the analysis of the behaviour of the interception between orthogonal walls (no inter-log hardware such as dowels) on small specimens. The last was a shake table test carried out in the framework of the European SERIES project (Seismic Engineering Research Infrastructures for European Synergies). A real scale two storey building with a square plan 7×5.35 m for a total height at the ridge of 5.28 m was tested [51] (Figure 5.6) (overall 12 tests were carried out). The input signal was the recorded accelerogram during the Montenegro earthquake (1979) scaled in the two

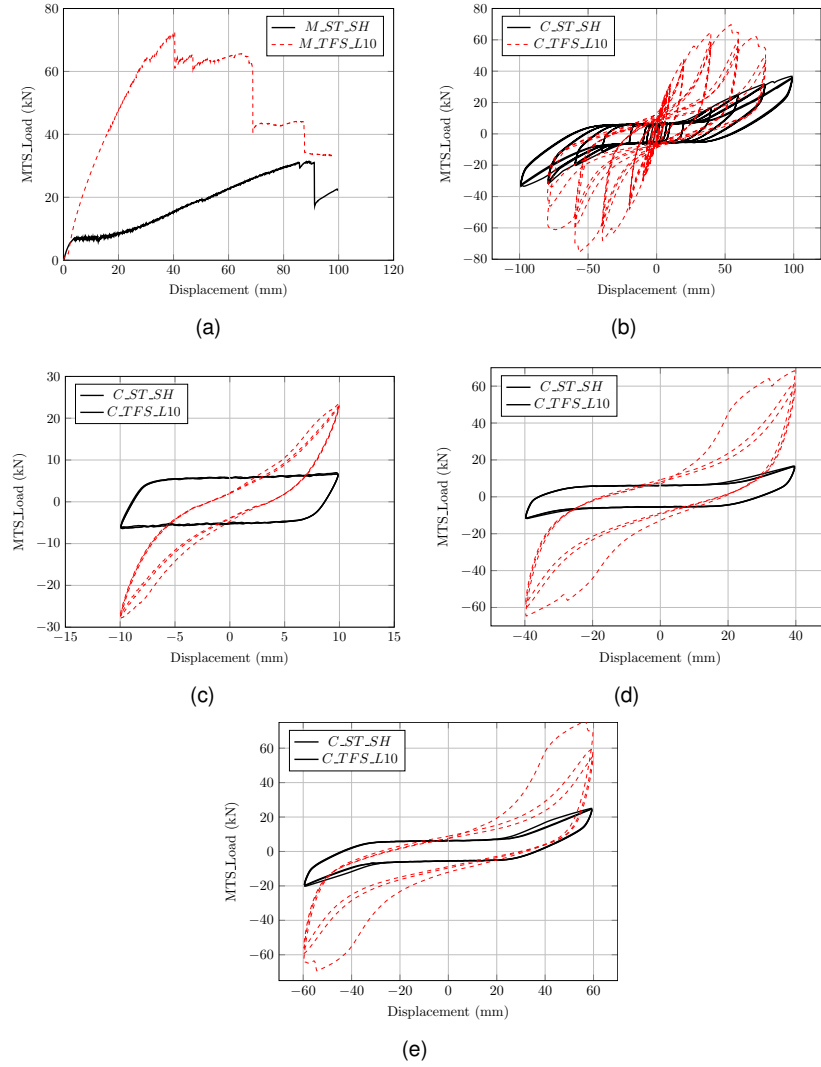


Figure 5.5: Comparison between LH and TFS (see [7]).(a) Monotonic test - (b) cyclic test - (c) 10mm hysteresis loops - (d) 40mm hysteresis loops - (e) 40mm hysteresis loops .

main direction from 0.07g up to 0.50g. At the end of the tests, the analysis of the dynamic identification and the visual inspection did not shows relevant damages. The visible damages consist in the residual deformation on the alignment of the side of the windows holes located in the part between two adjacent windows.



(a)



(b)

Figure 5.6: Building tested in the SERIES project (Branco et al): (a) external view - (b) inner walls

The direct comparison of the results obtained by different authors is difficult because different geometries and different test setup were adopted (corner joints, logs section, vertical loads, reinforce systems, etc). However the review of the data shown a "common" behaviour characterized by three main contributions: friction - mounting tolerance - and interlocks/reinforce contribution. The interaction between these three mechanisms is complex and cannot be modelled with the classical models used for the timber structure design. The results of the tests campaigns have demonstrated, in all the case, a good seismic response in terms of energy dissipation. Nevertheless,

this property is correlated to a high deformability of the structural system.

5.2 Experimental investigation

The goals of the presented experimental investigation is the mechanical characterization of the shear walls used in the log system. The research program approaches the topic from two levels. Since that the corner joints are fundamental for the structural resistance of the system, firstly the characteristic corners have been tested. During a second series of tests walls at a scale of 1:1 were tested regarding the lateral load bearing capacity and stiffness. The outcome of the tests, as often happens in experimental research, depends on the constraint system provided by the test setup. For this reason, two test setup, one for the test on joint and one for the walls were developed. A simplified predictive model was calibrate on the results of the first campaign. The input data of the model were the mounting tolerance (gap), the stiffness and load bearing capacity of the interlocks and the friction coefficient. The reliability of the model was verified by the comparisons of the results of the second part of the experimental campaign. One of the advantages in terms of time consuming and money saving is the possibility of developing new structural details without perform new tests on walls.

5.2.1 Tests on corner joints

The mechanical behaviour of the log-house system is strongly related to the resistance, stiffness and constructive tolerance of the corner joints. The quasi-static tests on the corner joints were planned to obtain the relationship between load and displacement for different geometries according to a common protocol. The test apparatus was designed to ensure realistic boundary conditions (constraints). Both monotonic "compression (push-out)" (C) and "traction (pull-out)" (T) tests were carried out on corner joints. The push-out and pull-out tests were planned to reproduce the two different loading pattern at the opposite corner of the same wall (see Figure 5.7).

Moreover cyclic tests (C) were performed. The last two tests, one monotonic and one cyclic, were carried out on a steel to timber dovetail reinforce element. This system exhibit some interesting advantages. First the possibility of reinforce the walls build with the weaker corner joint style or when wide opening interrupt the logs. Moreover this solution often, especially in low seismic risk zone, is cheaper than the screws or timber pins because it use the same geometry of the intersection between internal

walls (without overlap) and only few elements are inserted instead of a large number of small connectors.

All the tests were performed following a displacement-control procedure.

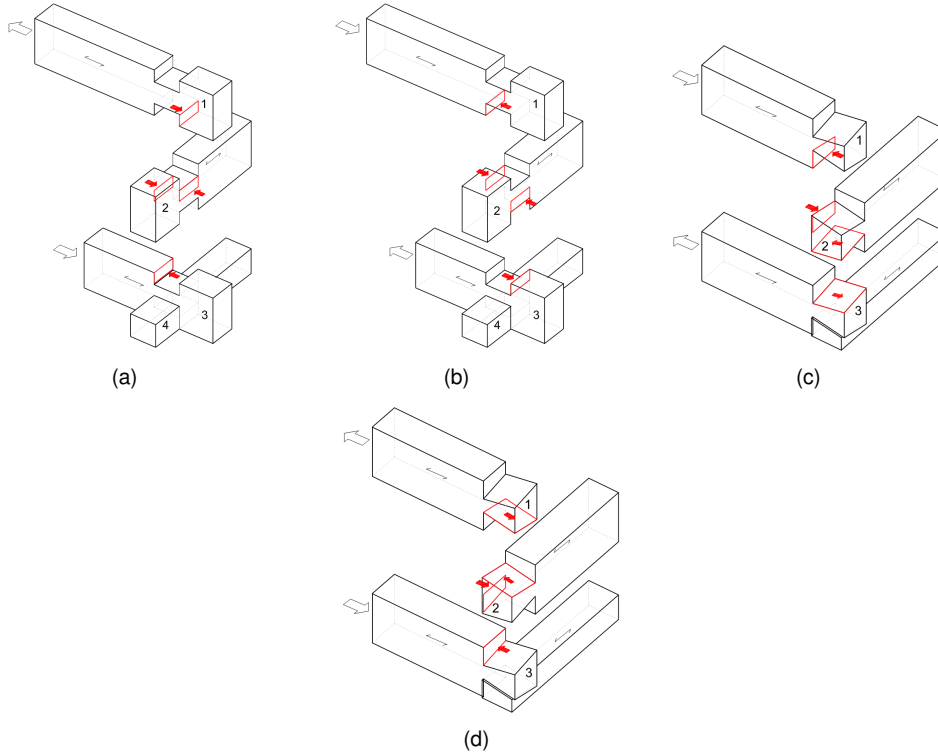


Figure 5.7: Load bearing mechanisms for Standard corner specimen - a) pull out test - b) push out test - c) for Tirolershloss corner specimen pull out test - d) for Tirolershloss corner specimen push out test.

Geometry of the specimens

The samples represent a small portion of the intersection between two orthogonal walls. Along the loading axis there were two logs while in the other there were one log and one-half. The other half piece was not inserted to achieve a more realistic boundary condition characterized by a higher rotation of the horizontal central log (Figure 5.8(b)). This solution was adopted after the first test where the influence of this additional restraint was evident. The effect on the overall behaviour of the joint is visible in Figure 5.8(a). The logs length depends on the corner joint style (from 500 mm to 700 mm).



(a)



(b)

Figure 5.8: *different configuration: a) with three horizontal pieces and b) with two horizontal pieces) .*

Two type of corner joints were tested: a standard saddle notch (ST) and a dovetail corner called Tirolerschloss (TR). Two profile thicknesses have been tested: 90 mm (2 lamellas) and 130 mm (3 lamellas), both with the same depth 160 mm. In addition a dovetail reinforcement sample was tested. It was composed by an "omega" cold formed metal sheet that matches exactly with the shaped grooves on the horizontal timber logs (2 lamellas total thickness 90 mm). In order to allow deformations caused by shrinking, the length of each element is limited on four logs. A hardwood profile has been added within the metal sheet in order to achieve a higher stiffness.

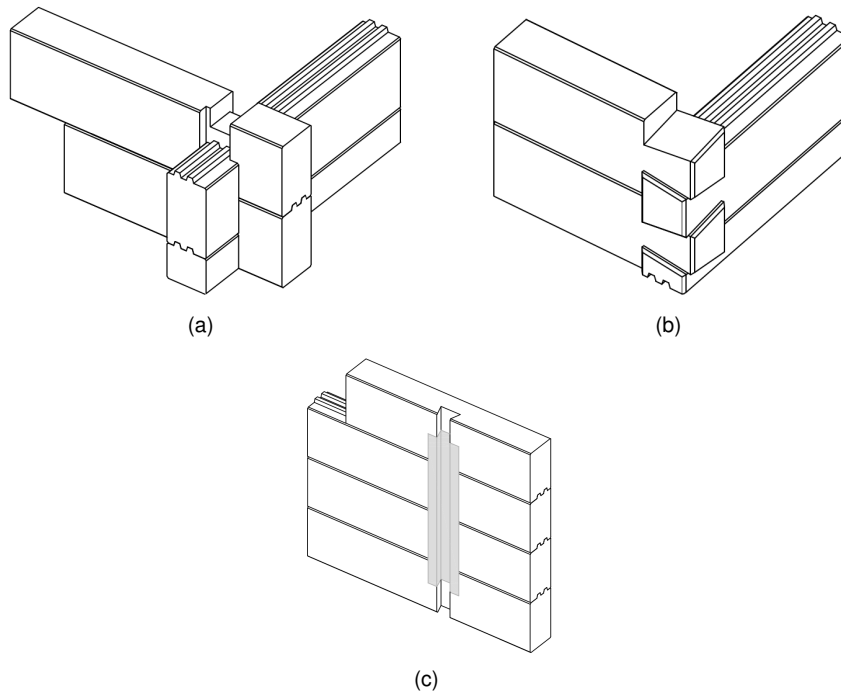


Figure 5.9: Standard (a)- Tirolerschloss (b)- and dovetail reinforce (c) samples.

The timber strength classes for all the specimen was C24 according to [16]. The timber element was connected to the hydraulic jack by means of a glued in threaded bar as showed in Figure 5.10. Using this joint system high stiffness and resistance was achieved.

The experimental setup was specifically designed for this type of test. In particular, it was attempted to reproduce a load state independent of the specimen deformation, allowing the restraint system to slide horizontally on the fixed frame. In so doing a more realistic restraint system is reproduced. In fact, the vertical stress

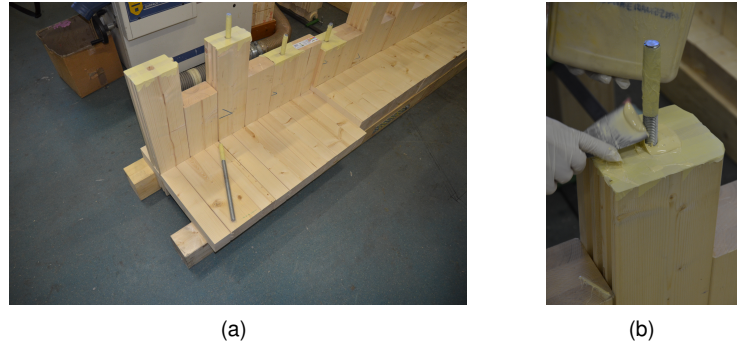


Figure 5.10: *Samples assembly - glued in steel threaded bar (epoxy resin)*

introduced to log house walls normally is limited by the loads transferred by floors (if there are no other constraints between the logs). A rigid mechanical connection would have caused significantly different failure mechanisms than those observed in the real case. The restraint system is linked to the fixed frame by two threaded rods M16, each one with a steel spring at the end, allowing a load increase proportional to the stiffness of the springs (100 N/mm). As an example that the spring system functioned properly, two load-displacement curves for the springs are illustrated in Figure 5.11. A nearly continuous load increase of about 100 N/mm can be observed.

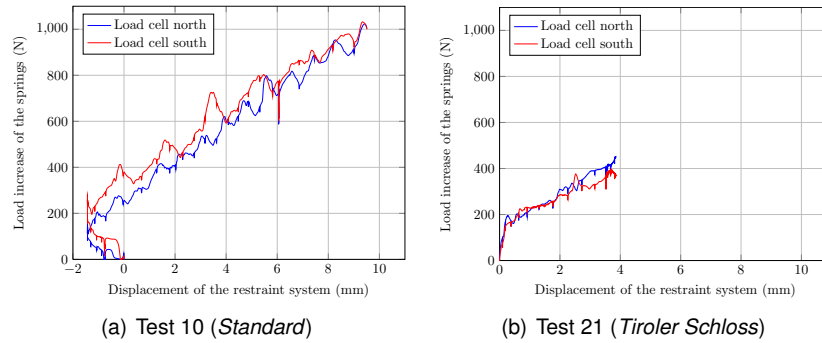


Figure 5.11: *Spring behaviour.*

In this way the specimens are able to expand, maintaining the load level sufficiently for practical applications. Thanks to the low-friction surfaces made of two plastic plates (Polyzene), the restraint system can easily slide. The vertical constraint is defined by four rolling bearings with high mechanical load capacity, which glide on

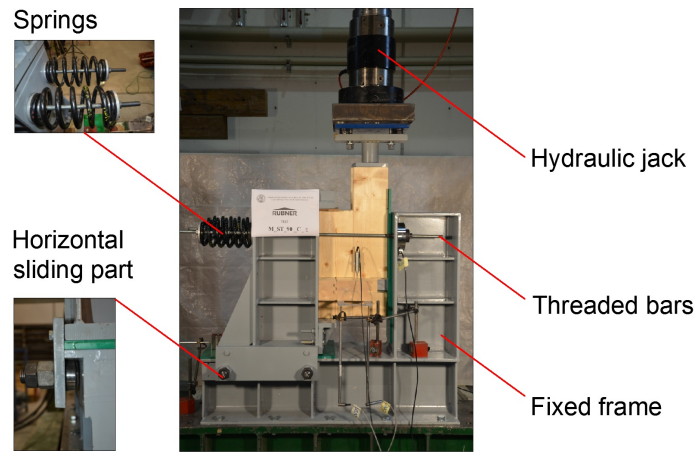
nr	Test ID code	Load	Type	Thickness [mm]
1	M_ST_TP_T	Tension	Standard	90
2	M_ST_TP_C	Compression	Standard	130
3	M_ST_90_C_1	Compression	Standard	90
4	M_ST_90_C_2	Compression	Standard	90
5	M_ST_130_C_1	Compression	Standard	130
6	M_ST_130_C_2	Compression	Standard	130
7	M_ST_90_T_1	Tension	Standard	90
8	M_ST_90_T_2	Tension	Standard	90
9	M_ST_130_T_1	Tension	Standard	130
10	M_ST_130_T_2	Tension	Standard	130
11	C_ST_90	Cyclic	Standard	90
12	C_ST_130	Cyclic	Standard	130
13	M_TR_TP_T	Tension	Tiroler	90
14	M_TR_TP_C	Compression	Tiroler	130
15	M_TR_90_T_1	Tension	Tiroler	90
16	M_TR_90_T_2	Tension	Tiroler	90
17	M_TR_130_T_1	Tension	Tiroler	130
18	M_TR_130_T_2	Tension	Tiroler	130
19	M_TR_90_C_1	Compression	Tiroler	90
20	M_TR_90_C_2	Compression	Tiroler	90
21	M_TR_130_C_1	Compression	Tiroler	130
22	M_TR_130_C_2	Compression	Tiroler	130
23	C_TR_90	Tension	Tiroler	90
24	C_TR_130	Tension	Tiroler	130
25	M_CR_2	Compression	Reinforcement	90
26	C_CR	cyclic	Reinforcement	90

Table 5.1: *List of the test.*

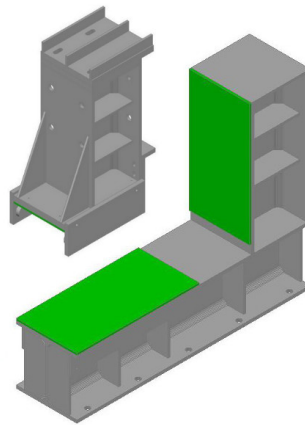
the inferior side of the rigid frames web. Two anchoring reinforced plates attached to the mobile part of the frame guarantee the vertical restraint of the specimen.

Figure 5.13 shows the measurement setup. Five linear displacement transducers (ldt) and three load cells composed the measurement setup. The first displacement transducer was integrated in the hydraulic actuator (displacement control). Two ldt, vertical disposed in a fixed position, allowed the determination of rotation of the central log. Another instrument was fixed on the vertical element connected to the hydraulic jack to measure the relative vertical displacement between horizontal and vertical log. The last ldt was connected to the reaction frame to measure the horizontal sliding of the mobile frame. The first load cell was integrated in the hydraulic jack, while the other were mounted at the end of the two threaded bars opposite to the spring. Thus, the initial pre-load and the variation of the tensile force on the two springs were monitored during the test.

For the dovetail reinforce tests the linear displacement transducers fixed to the sample were fixed on each vertical element in order to measure the slippage between the logs. While another ldt was used to measure the out of plane displacement of the



(a)



(b)

Figure 5.12: *Test setup*

X	YY	ZZ	V
M	ST	TP	T
(Monotonic)	(Standard)	(Pilot test)	(Tension)
C	TR	C (Compression)	
(Cyclic)	(Tiroler)		
CR			
(Reinforce)			

Table 5.2: List of acronyms.

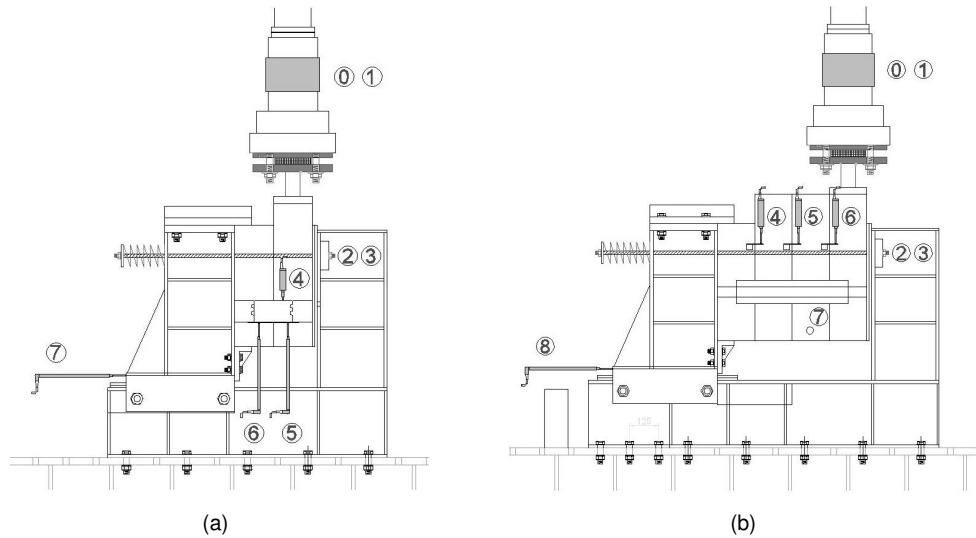


Figure 5.13: Measurement setup: (a) corner joints - (b) dovetail reinforce

second log.

Test results

Twelve tests on the standard corner joint (ten monotonic and two cyclic) and twelve test on the Tirolerschloss (ten monotonic and two cyclic) were done. In the monotonic quasi-static tests two different protocols were applied. The first was a push-out test while the second was a pull-out test. These procedures were implemented to reproduce the stress distribution in the two opposite corner of a wall loaded by a horizontal force. Figure 5.14 shows the load bearing surfaces in the two condition. Because of the unsymmetrical layout the failure mode depends from the loading path. As can be seen in Figure 5.15 the load deformation curve progressions show differences depending on the loading direction. Two issues can explain this difference: - The different transfer mechanisms between the logs just mentioned - The position of the

gap due to the samples assembly as show in Figure 5.14. When the logs are assembled the gaps are distributed in such a way that, when the compression test run, the surfaces are already in contact (due to the self-weight action). Thus the initial gap was almost zero. On the other hand, when the tension test run, the gaps must be overcome before taking force. This consideration allow, especially for the more complex corner joint geometries, the evaluation of the mean value of the tolerance between the elements. This value correspond to the length of the first part of the curve without increase of force after the pre-sliding phase (horizontal plateau in the load-displacement diagram). The initial pre-load was 10 kN for all the tests except for the test C_ST_90_C_2 (test 4) in which it was adopted 5 kN.

Test n_r	Load	T [mm]	Tight. force [kN]	F_{max} [kN]	V_{max} [mm]	F_u [kN]	V_u [mm]
3	Comp.	90	10	39.7	14.1	39.7	14.1
4	Comp.	90	5	27.2	7.1	26.7	7.5
7	Tensile	90	10	37.4	17	37.4	17
8	Tensile	90	10	40	34.6	38.6	30
5	Comp.	130	10	49.5	30.2	49.3	30
6	Comp.	130	10	43.9	30.2	43.4	30
9	Tensile	130	10	44.6	29.7	44.4	30
10	Tensile	130	10	50.2	42.7	45	30

Table 5.3: *Test result-standard joint.*

Test n_r	Load	T [mm]	Tight. force [kN]	F_{max} [kN]	V_{max} [mm]	F_u [kN]	V_u [mm]
15	Tensile	90	10	11.5	14.7	9.2	22.5
16	Tensile	90	10	12	10.2	9.6	25.2
19	Comp.	90	10	13.7	8.6	13.3	25.2
20	Comp.	90	10	12.7	8.3	10.1	27.3
17	Tensile	130	10	10.3	8.9	8.2	27.6
18	Tensile	130	10	11.5	13.9	9.2	27.4
21	Comp.	130	10	16.3	16.3	16.3	16.3
22	Comp.	130	10	17.6	9.1	14.1	16.9

Table 5.4: *Test result-tirolerschloss joint .*

5.2.2 Tests on shear walls

The goal of these tests is to evaluate the behaviour and the resistance of log shear walls. Five monotonic (M) and five cyclic (C) test were performed. These tests were planned to investigate different common configurations in the constructive practice. First two different corner style were analysed (Standard and Tirolerschloss with dovetail reinforcement elements,) with two different thickness (130 mm and 90

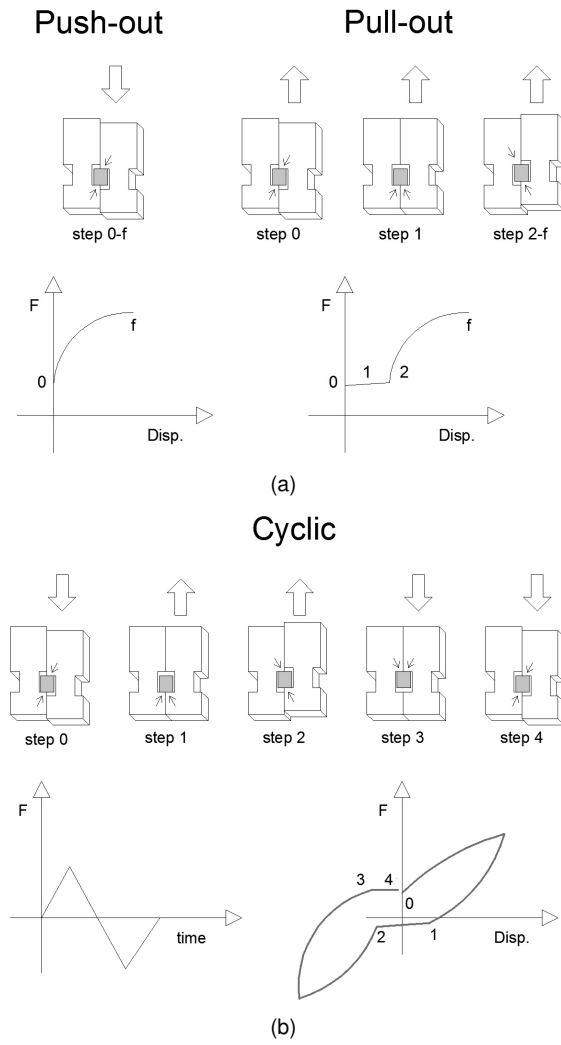
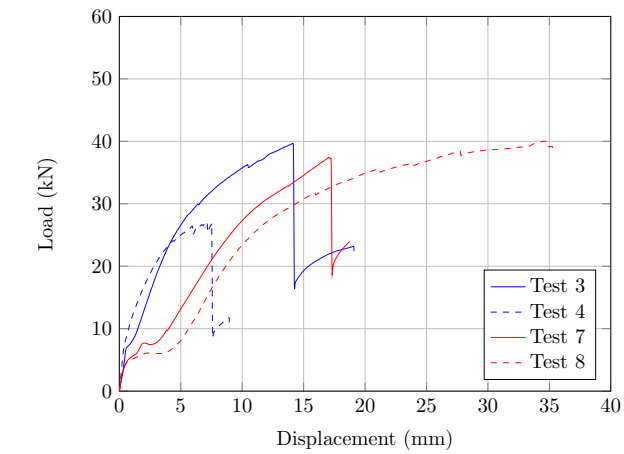
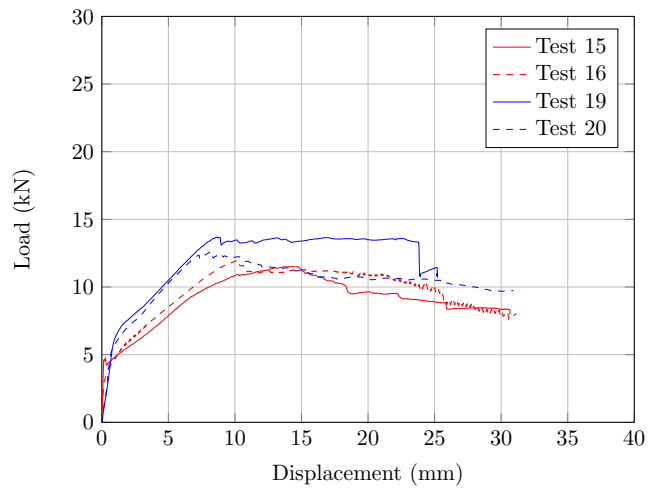


Figure 5.14: Gap distribution for different protocol: (a) monotonic "pull-out" and "push-out" test - (b) cyclic test

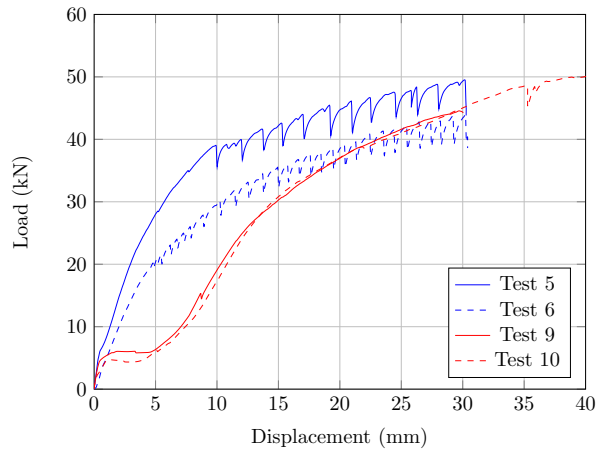


(a)

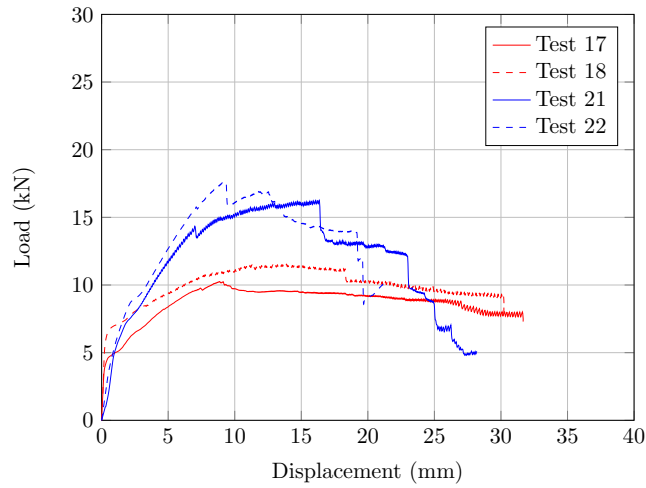


(b)

Figure 5.15: Monotonic tests - standard joint 90 mm (a) - Tirolerschloss 90 mm (b)

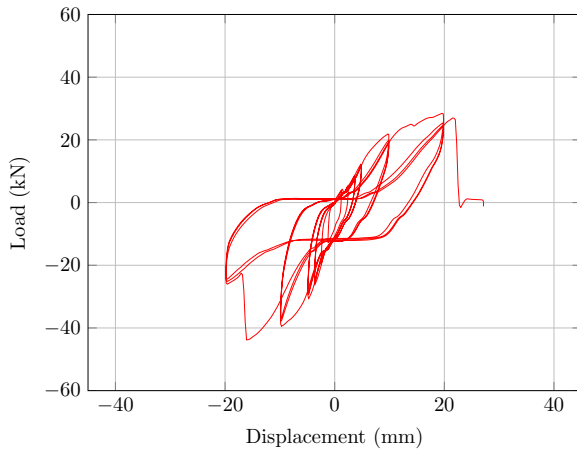


(a)

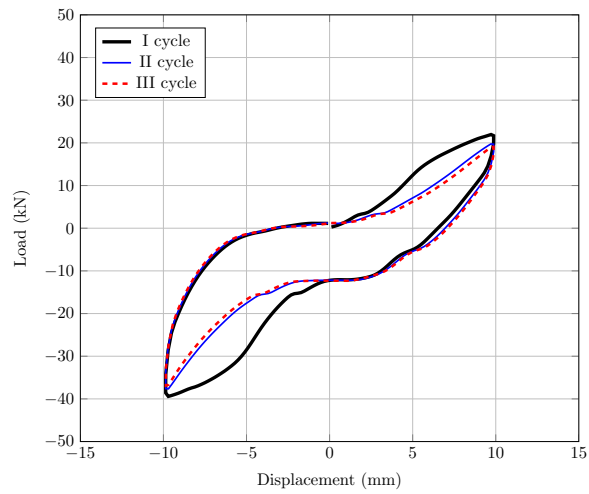


(b)

Figure 5.16: Monotonic tests - standard joint 130 mm (a) tests - Tirolerschloss 130 mm (b)

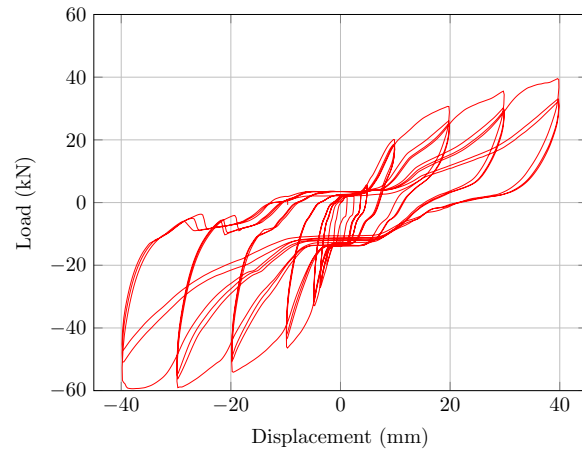


(a)

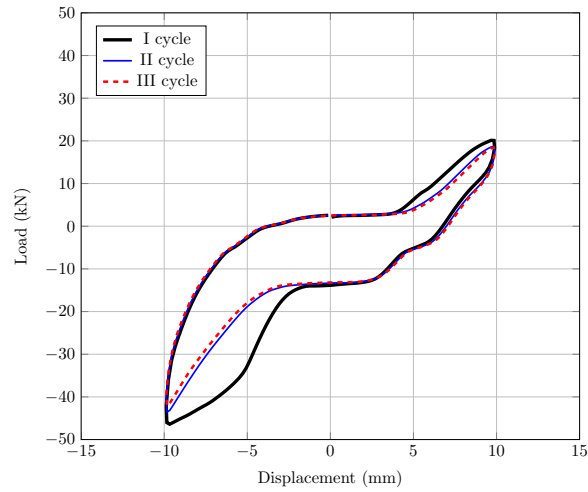


(b)

Figure 5.17: Cyclic test - standard joint 90 mm (a) - hysteresis loop for $v=10$ mm (b)

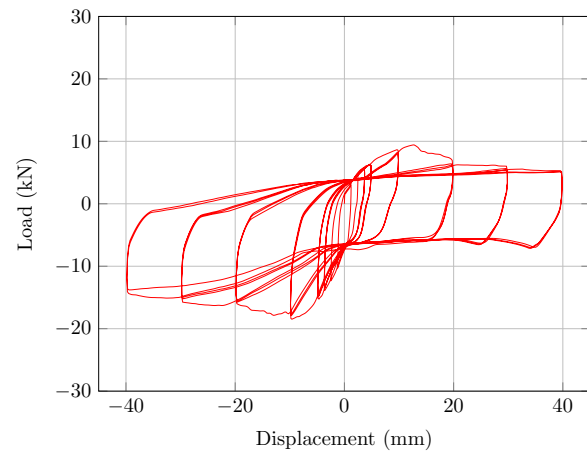


(a)

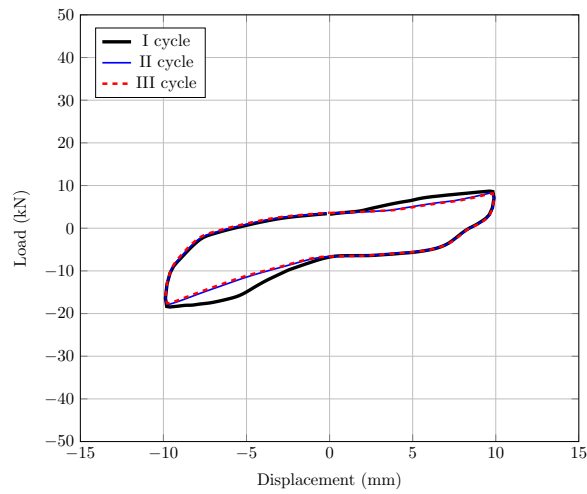


(b)

Figure 5.18: Cyclic test - standard joint 130 mm (a) - hysteresis loop for $v=10$ mm (b)

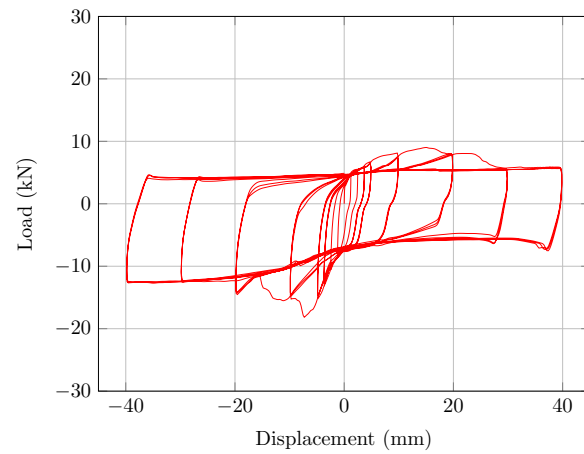


(a)

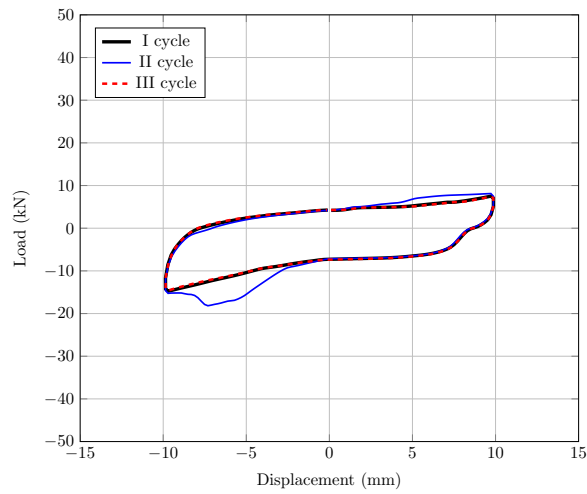


(b)

Figure 5.19: Cyclic test - Tirolerschloss 90 mm (a) - hysteresis loop for $v=10$ mm (b)



(a)



(b)

Figure 5.20: Cyclic test - Tirolerschloss 90 mm (a) - hysteresis loop for $v=10$ mm (b)

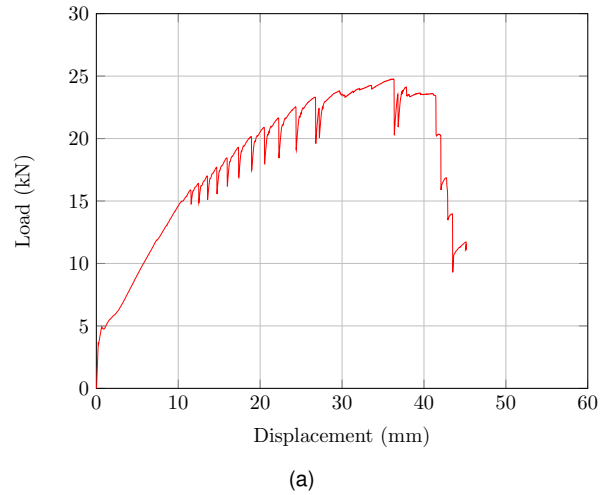


Figure 5.21: Monotonic test on dovetail reinforce - 90 mm

mm). Furthermore, a shorter wall with Standard corners and, a wall with openings (a window and a door), were tested.

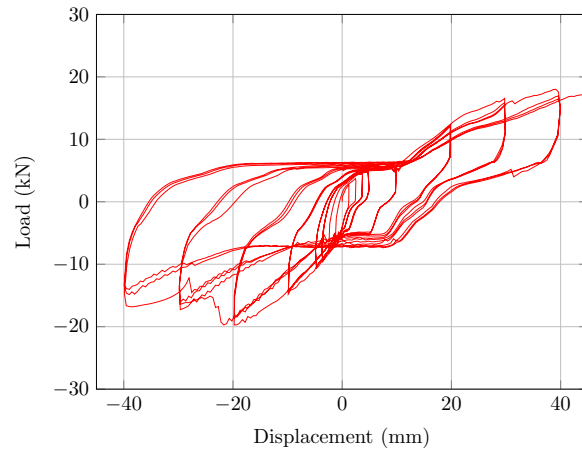
Geometry of the specimens

The geometry of the samples was chosen to reply the load and dimension conditions that usually can be found in log-houses. The specimen were made up by 17 solid laminated timber profiles (double laminated (90 x 160 mm) and triple laminated (130 x 160 mm)). The two bottom elements were fixed each other with 8 x 240 mm screws every 300 mm (see Figure 5.23, 5.24, 5.25, 5.26, 5.27). The load was applied to the top rigid beam fixed to the wall by screws and polyurethane glue. The specimens are 2.8 m height.

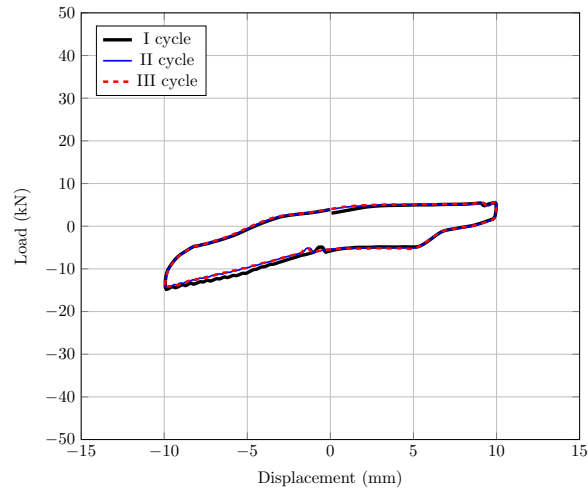
Specimen	i [m]	Length [m]	Thickness [mm]
M/C_ST_90	3.91	4.2	90
M/C_ST_130	3.91	4.31	130
M/C_TR_90	3.91	4.02	90
M/C_ST_SH	2.48	2.78	90
M/C_ST_OP	3.91	4.2	90

Table 5.5: Geometry of the samples; "i" is the centre to centre distance between the corners.

The specimens were subjected to both horizontal and vertical load: the horizontal load was applied by a displacement-controlled hydraulic jack on the rigid top beam.



(a)



(b)

Figure 5.22: Cyclic tests dovetail reinforce - 90 mm (a) - hysteresis loop for $v=10$ mm (b)

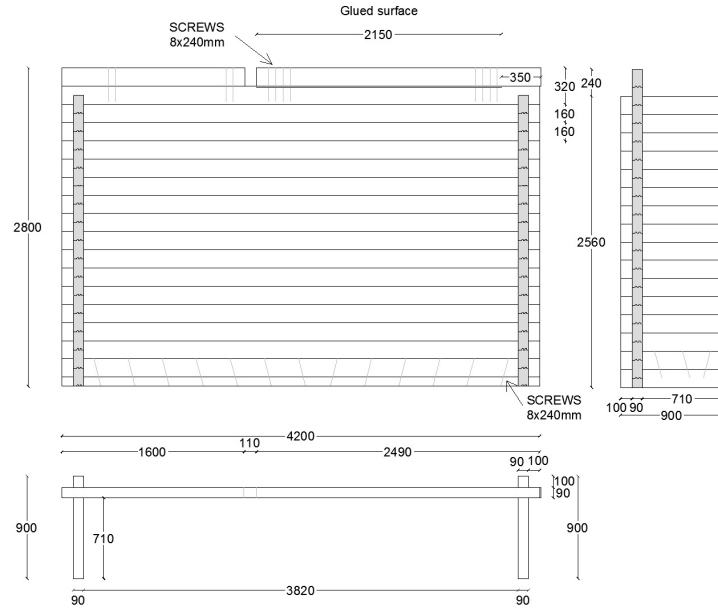


Figure 5.23: Dimension of M/C_ST_90 wall specimen.

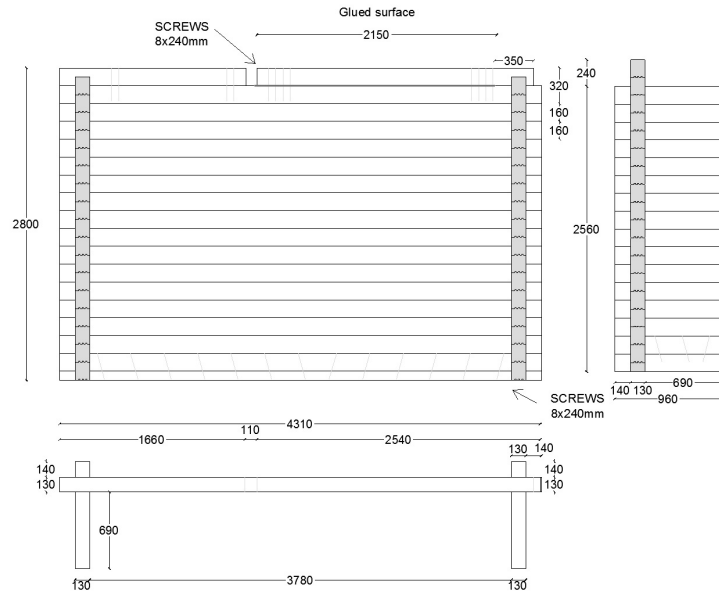


Figure 5.24: Dimension of M/C_ST_130 wall specimen.

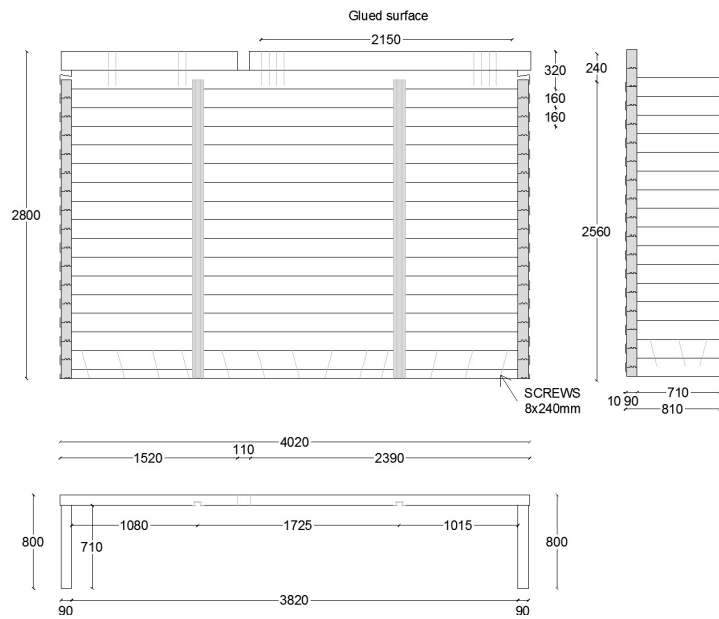


Figure 5.25: *Dimension of M/C_TR wall specimen.*

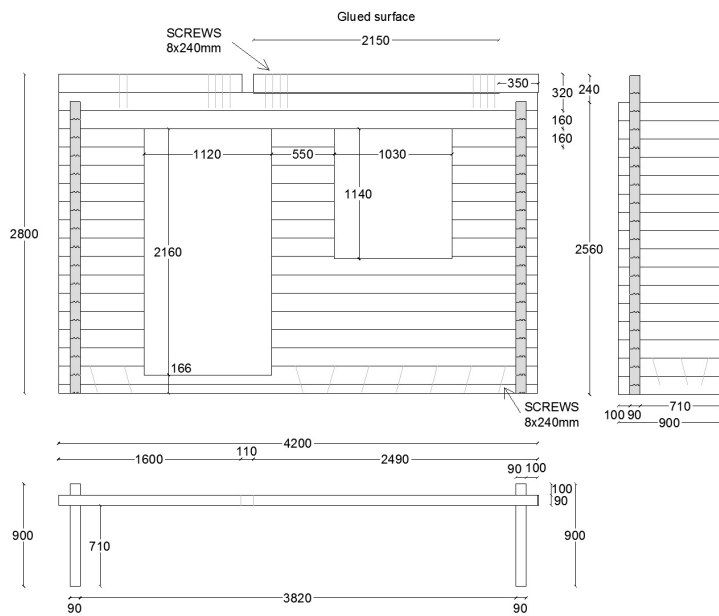


Figure 5.26: *Dimension of M/C_ST_OP wall specimen.*

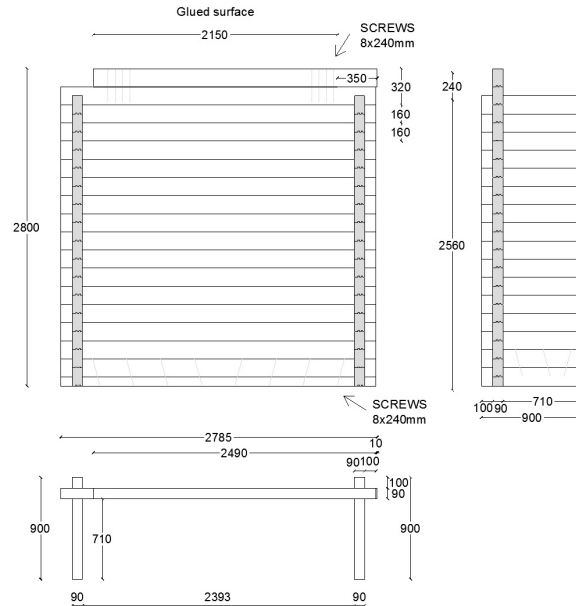


Figure 5.27: Dimension of M/C_ST_SH wall specimen.

The top log was fixed to the lower one only by a rigid glue connection in order to apply the load on the logs without influence on the corner joints behaviour. In the cyclic protocol the actuator pulled the wall through 4 steel bars connected on the top of the sample as shown in Figure 5.28.

The vertical load on walls was applied by a system of levers and counter-weight designed especially for tests on wall specimens (for more informations about the test apparatus see [52]). A vertical load of $44kN$ (about $10.6kN/m$) was applied on samples except for the tests M/C_ST_SH in which the load applied was of $10kN$ (about $5kN/m$).

Each sample was fixed to the ground to withstand the shear force: the bottom log was screwed to a metal profile bolted to the floor. The overturning moment was balanced by two couple of pre-tensioned steel cables ($d = 20mm$) with an initial tightening load of $2 \times 2.5 = 5kN$ each. The cables were connected to special devices (see Figure 20). These solutions were studied to constrain the transversal parts of the "c-shaped" wall without unrealistic contributions arising during the tests. Thus the maximum rotational of the orthogonal elements was ensured. Figure 5.30 show the transducers layouts. During the tests, the horizontal load (1) and the imposed displacement (2) were measured by sensors integrated in the hydraulic actuator while

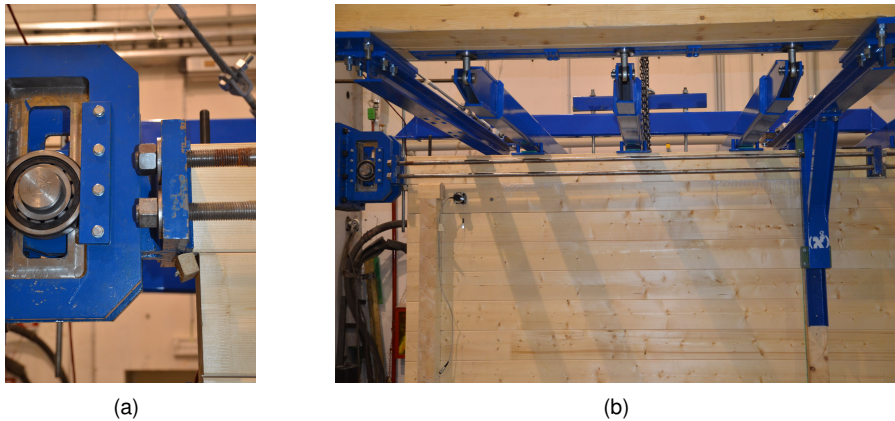


Figure 5.28: System of horizontal load application: a) device mounted to the hydraulic jack that allow vertical sliding and rotation in the vertical plane (along the axe orthogonal to the sample)- b) bars for the cyclic load protocol.

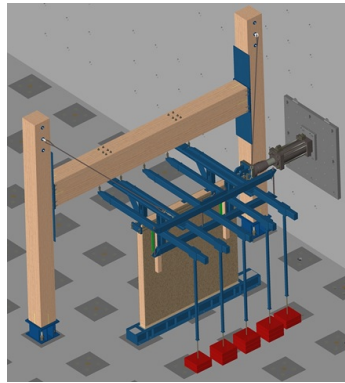
the forces of the tie rods were measured by two load cells (3-4). Four transducers measured the relative horizontal slip between the logs (5-8); three transducers were used to monitor the global horizontal slippage (9) and the global uplift of the logs in the corner (10-11). Two wire displacement transducers (12-13) were used to monitor the uplift between the logs (sum of the logs relative uplift). A transducer was installed on the top logs of the walls, in order to measure the absolute displacement (14).

Test results

Five monotonic and five cyclic test were performed. In the monotonic tests the velocity was maintained constant and equal to 0.05 mm/s till collapse. For the cyclic test the velocities and amplitudes of each cycle are summarized in Table 5.6. A fixed reference value V_r , equal to 10 mm was choose. The results of monotonic tests are summarized in Table 5.7.

In Figure 5.32, Figure 5.33 and Figure 5.35 the results obtained in each monotonic test are reported.

Figure 5.36 and Figure 5.37 shows the force versus displacement curves obtained in the cyclic tests.



(a)



(b)



(c)



(d)

Figure 5.29: Test setup: (a) 3d sketch -(b) front view of the lever system - (c)reaction wall/frame -(d) horizontal load application system

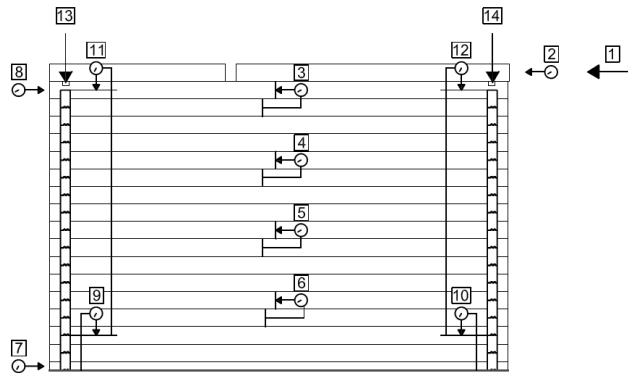


Figure 5.30: Instruments layout - sensor labels

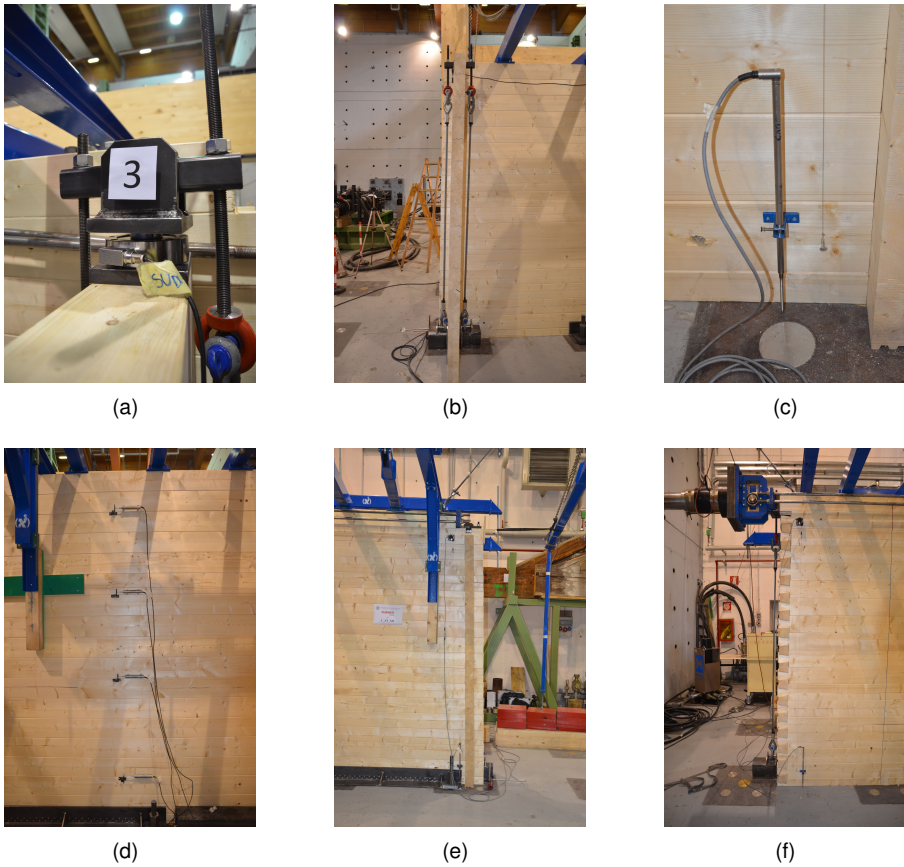
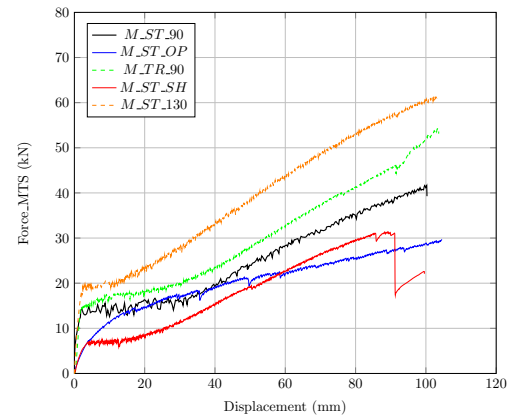
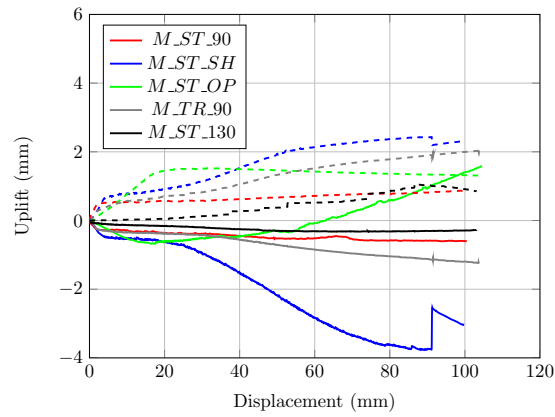


Figure 5.31: Instruments layout - (a,b) load cell at the top of the wall (13) - (c) lvd 10 - (d) ldt 3,4,5,6 - (e) transducer 11 on the top of the wall, 9 7 at the bottom (f) transducers 2,1 (hydraulic jack), ldt 12 and 10 at the bottom.

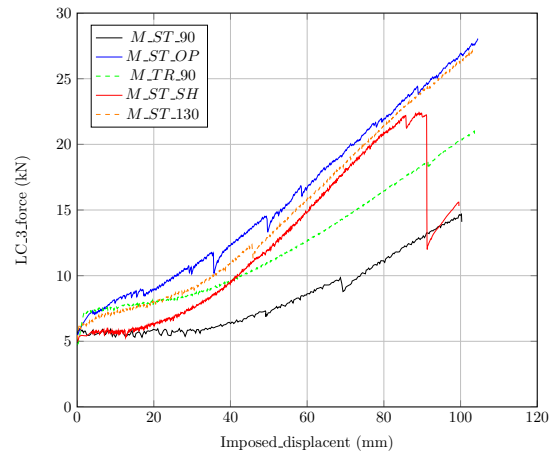


(a)

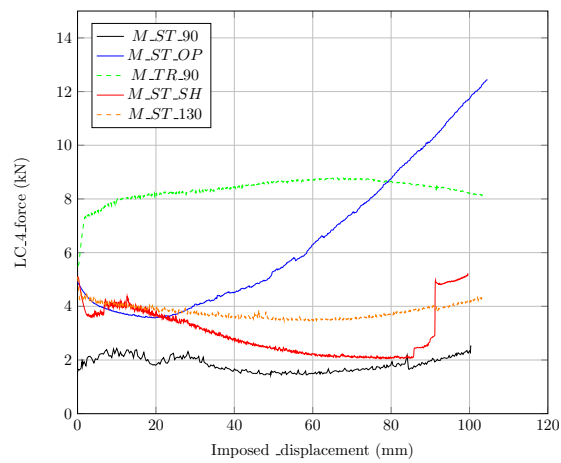


(b)

Figure 5.32: (a) Imposed displacement versus horizontal load for the different monotonic tests - (b) Imposed displacement versus uplift at the top for the different monotonic test.

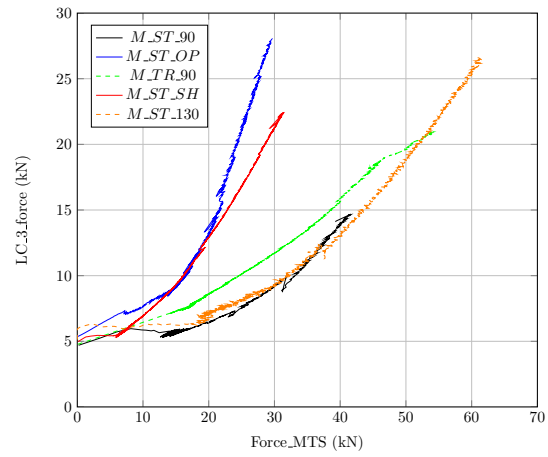


(a)

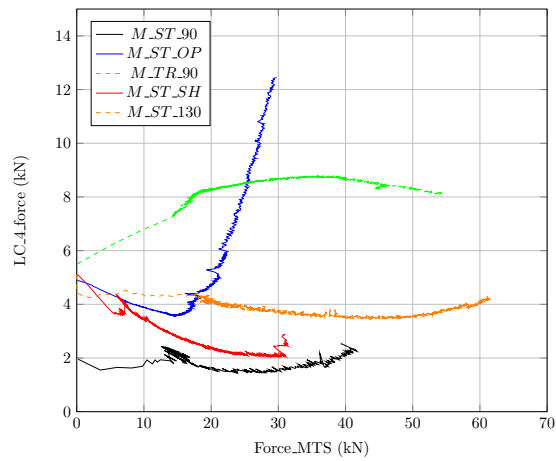


(b)

Figure 5.33: Imposed displacement (2) versus load cell force - 3 (a)-4 (b).

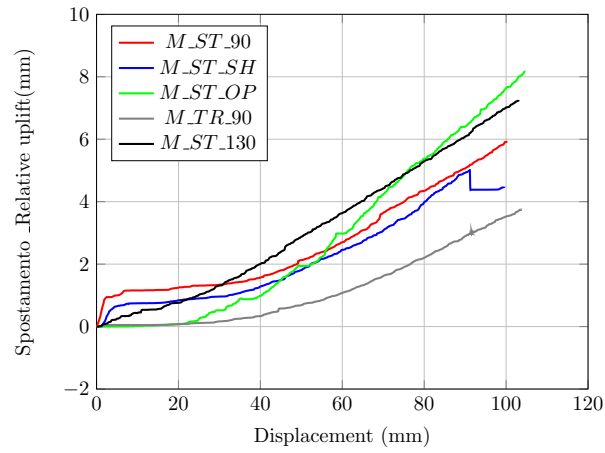


(a)

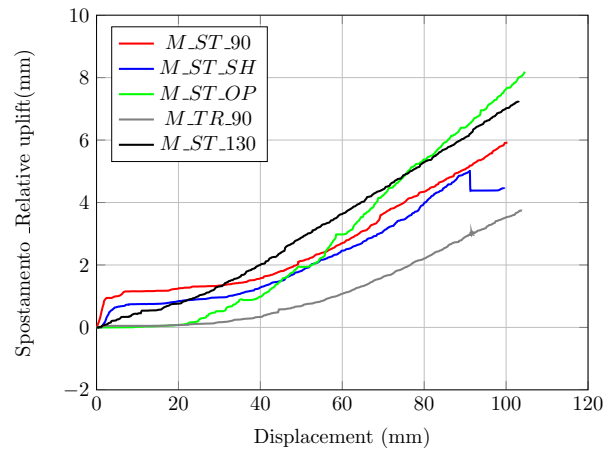


(b)

Figure 5.34: Load on the hydraulic jack (1) versus load cell force - 3 (a)-4 (b).

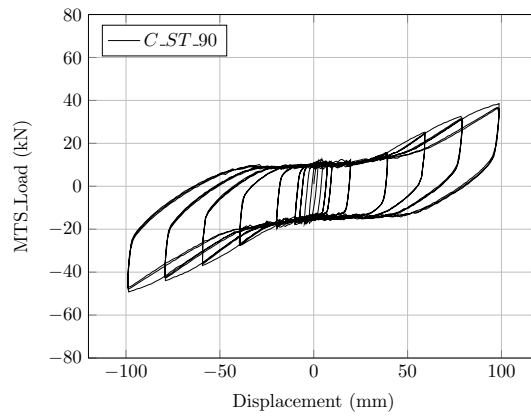


(a)

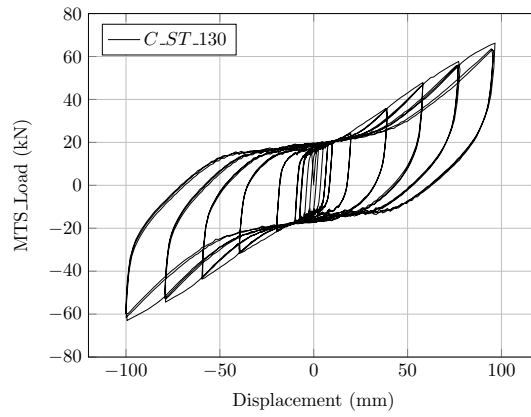


(b)

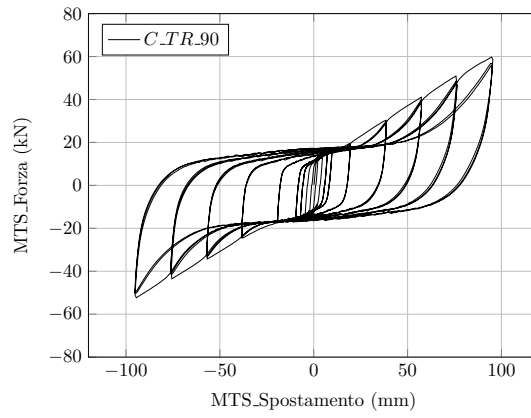
Figure 5.35: *Imposed displacement (2) elongation recorded by the potentiometer - 11 (a)-12 (b).*



(a)

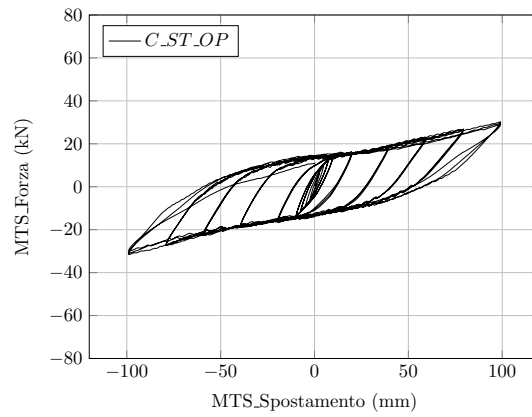


(b)

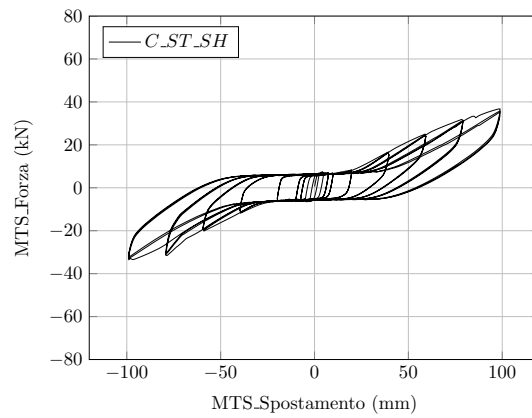


(c)

Figure 5.36: Displacement versus hydraulic jack load (MTS) - (a) C_ST_90 - (b) C_ST_130 - (c) C_TR_90 test.



(a)



(b)

Figure 5.37: Displacement versus hydraulic jack load (MTS) - (a) C_ST_OP - (b) C_ST_SH .

Cycle	Amplitude (mm)	Number of repetitions	Velocity (mm/s)
0.25 Vr	2.5	1	0.05
0.5 Vr	5	1	0.05
0.75Vr	7.5	3	0.1
1Vr	10	3	0.2
2Vr	20	3	0.2
4Vr	40	3	0.5
6Vr	60	3	0.5
8Vr	80	3	0.5
10Vr	100	3	0.5

Table 5.6: *Procedure of cyclic test.*

Test	Fmax [kN]	Vmax [mm]	Fu [kN]	Vu [mm]
M_ST_90	41.6	100.2	41.2	100
M_ST_130	61.5	103.1	60.5	100
M_TR_90	54.3	103.4	52	100
M_ST_SH	31.4	88.3	31.1	91.1
M_ST_OP	29.6	104.6	28.8	100

Table 5.7: *Outocome of the tests.*

5.3 Analysis of the results

5.3.1 Theoretical considerations

Regarding log structures, to the best knowledge of the author, there are no specific design rules in the current valid standards. Therefore, the resistance of the two joint systems will be determined in accordance with the generalities given in Eurocode 5 [46] making reference to technical literature.

For the Standard corner style, there are several design proposals in the literature. Its load-bearing behaviour is rather easy to define, and the in-plane resistance depends primarily on the compression and shear stresses which develop in the corner.

The resistance of the Tirolerschloss corner, however, is more difficult to predict due to the angular cut of the notches. Without a sufficiently high normal load, in the case of the test setup defined by the tightening force of the springs, the performance of the corner is dominated by friction and it is expected that the joint rather opens instead of a failure occurring.

As regards the corner notches, different mechanisms can occur which will be presented afterwards. For each mechanism following expressions shall be satisfied:

$$F_{k,i} \leq X_k \cdot A_{res,i}$$

where:

- $F_{k,i}$ is the characteristic resistance value of a mechanism;
- X_k is the characteristic value of a strength property (see table 5.8);
- A_{res} is the respective resistant surface;

It is important to remark that the ductile failure mode caused by the wood fibre crushing is fixed from a "conventional" strength (corresponding to a fixed deformation) according to EN 408:2012. As pointed out in [53] and [54] the bearing strength capacity of locally loaded timber members depend from the approach adopted from the national codes. Different approaches are used for the strength definition and for test procedure (load condition, size of the specimen). The European approach is based on the model proposed by Blass [55]. The characteristic values are derived from experimental test carried out on small samples (45 x 70 x 180 mm) loaded over its entire surface. The strength value is defined as the intersection between the load-displacement curve and an offset line ($0.01 \times h_0$) of the secant line between the 0.1

and 0.4 of $F_{C,90,max}$ (Figure 5.38). In order to achieve a value of the $F_{C,90,max}$ an iterative procedure must be followed starting from an estimation of the $F_{C,90,max}$.

$$f_{c,90} = \frac{F_{C,90,max}}{b \cdot l}$$

Where $f_{c,90}$ is the compression strength perpendicular to the grain, $F_{C,90,max}$ is the maximum compression load perpendicular to the grain, b and l are the width and the length of the specimens. The aim of the EN 408 definition reflect the choice of defying a material proprieties of the material instead of a load case dependent condition. Thus the resistance of the member is calculated for the different load condition taking into account the effect of the fibre deformation near the loading area (a sort of rope/chain effect) by different additional contribution. First the contact area is increased considering an additional area on the edge of the load surface (where the actual contact length, l , at each side is increased by 30 mm, but not more than a , l or $l/2$). Second a coefficient is introduced to taking into account the load configuration, the possibility of splitting and the degree of compressive deformation $k_{c,90}$.

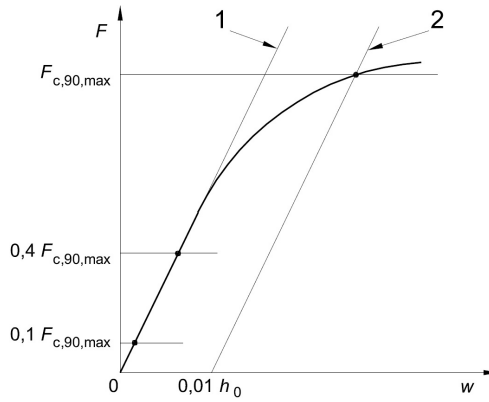


Figure 5.38: Definition of the maximum compressive load perpendicular to the grain according to [56].

In order to err on the right side in case of compression perpendicular to the grain, the factor $k_{c,90}$ used to take into account load configuration, possibility of splitting and degree of compressive deformation is assumed to be 1.0. The relevant characteristic strength values are taken from UNI EN 338:2009 [16] and are listed in table 5.8. Regarding the shear strength perpendicular to the grain, reference is made to the research report [57].

	Symbol	Strength properties [N/mm ²]
Tension perpendicular	$f_{t,0,k}$	0.4
Compression parallel	$f_{c,0,k}$	21
Compression perpendicular	$f_{c,90,k}$	2.5
Shear parallel	$f_{v,0,k}$	4.0 / 2.5 ¹
Shear perpendicular	$f_{v,90,k}$	10.6
Rolling shear	$f_{roll,k}$	0.8 ²

¹ UNI EN 338:2004 (k_{cr})

² The shear strength for rolling shear is approximately equal to twice the tension strength perpendicular to grain [46].

Table 5.8: Characteristic strength values of C24 graded timber.

In order to allow a comparison between pre-calculated characteristic resistances and experimental mean values, the standard UNI EN 14358:2007 [58] provides to calculate characteristic 5-percentile values from the test results. But due to the small number of tests per specimen type, this procedure cannot be applied in this case. Therefore, on basis of the anticipated resistances, reference mean values are calculated as:

$$\bar{y} = \frac{F_k}{1 - k \cdot CoV}$$

where:

- \bar{y} is a stochastic mean value;
- k is a factor;
- CoV coefficient of variation;

For tests with infinite number of specimens, a p-percentile of $p = 5\%$ and a confidence level of $\alpha = 75\%$ the factor k is given as 1.65 [18]. The variation for wood is reported to be 15-25 % in dependence on the grading class. Not knowing the actual grading class of the used timber (at least S10), it seems reasonable to assume $CoV=0.2$, thus the reference value results to be:

$$\bar{y} = \frac{F_k}{1 - 1.65 \cdot 0.2} = 1.493 \cdot F_k$$

In dependence on the actual timber quality \bar{y} can range from 1.3 and 1.7 times the characteristic resistance value F_k .

Although not considered in the current design practice, dry friction is an important resistance mechanism in this kind of timber structural system. Before the resistance of a corner joint, regardless of its type, is activated, the friction between the beams must be overcome. Therefore, the basic friction behaviour shall be briefly outlined

here.

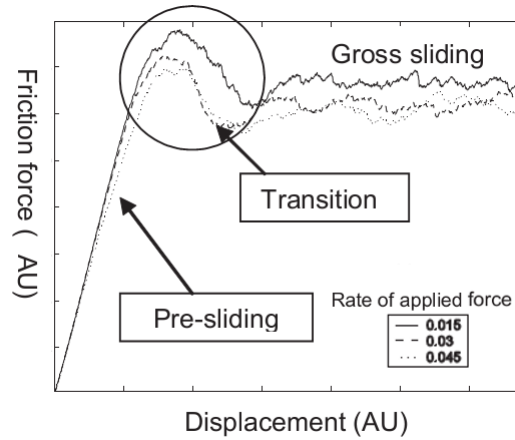


Figure 5.39: The two friction regimes and the transition between them [59].

A tangential force applied on two objects in frictional contact always results in displacement, no matter how small the force is. When the force is below a certain threshold, only preliminary micro-displacements occur. Owing to asperity contacts, adhesive forces are dominant because there are still points of unbroken asperity junctions and points of micro-slip on the contact surfaces [60]. This behaviour is called the *pre-sliding* regime. Assuming that the tangential force is held constant, the displacement will remain constant as well. When the two objects are unloaded, on the other hand, not all displacement will be recovered and there will in general be a residual displacement.

However, if a displacement increase is provided, more and more junctions break and have less time to reform [59]. As the threshold, i.e., the *pre-sliding distance* and/or the static friction force is attained, this behaviour results in true or gross sliding, i.e., kinetic (or dynamic) friction. It is characterized by a continuous process of asperity junction formation and breaking and is regarded as critically stable. In other words, the displacement will not remain constant for a constant applied load, but will suddenly accelerate [60]. The friction force usually has its maximum at the beginning of motion (static friction force). In the gross-sliding regime it decreases and becomes a function of the velocity.

The transition from pre-sliding to gross sliding depends on factors such as the relative velocity (to be envisaged as the displacement rate) and acceleration of the

sliding objects [59].

As the compressive stresses should be nearly uniformly distributed, the static friction force can be taken to be proportional to the normal force acting across the interface [61] and, thus, is governed by the equation:

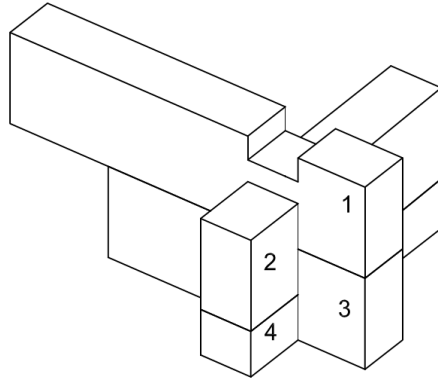
$$F_f \leq \mu \cdot F_n$$

where:

- F_f is the force of friction;
- μ is the coefficient of friction (empirical property);
- F_n normal force exerted by the tightened springs.

For friction of smooth wood on smooth wood with a low moisture content, the coefficient μ is reported to be 0.3-0.6.

Corner joints Standard



The load bearing behaviours of the specimen can be explained by using figure 5.40 and Table 5.9, where potential mechanisms are illustrated. From beam 1, the load is transferred to beam 2 by the lower site of the former's notch (A), which must resist compression stress parallel to the grain (mechanism 1). The two contact surfaces (B) of beam 2 must respectively withstand compression stress perpendicular to the grain (mechanism 2). As the compressive strength perpendicular to the grain is about 10 % of the value along the grain, mechanism 1 can be ignored. So beam 1

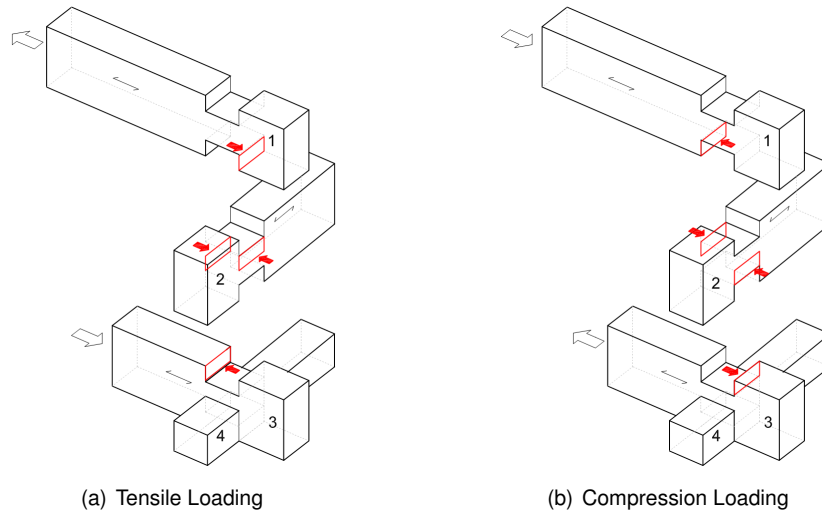


Figure 5.40: Load bearing corner specimen Standard.

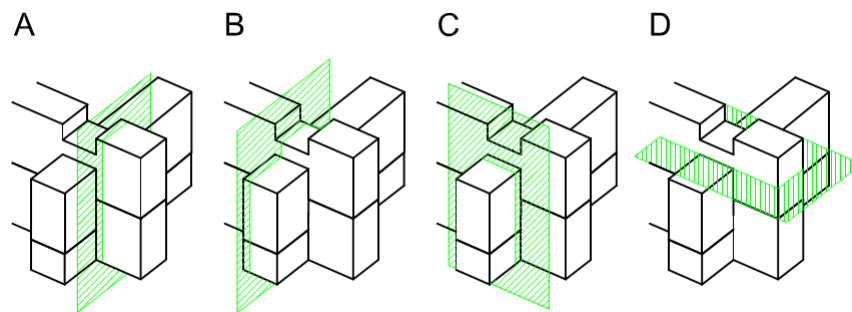


Figure 5.41: Section cuts.

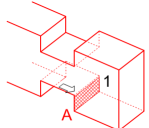
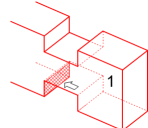
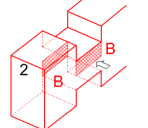
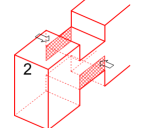
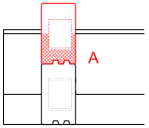
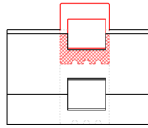
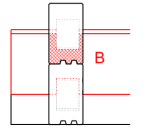
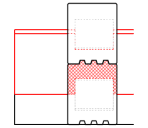
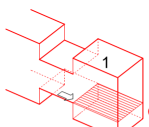
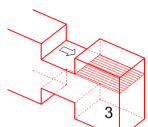
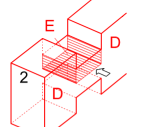
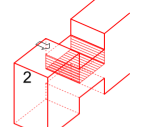
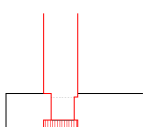
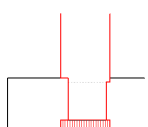
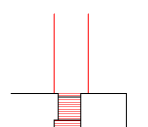
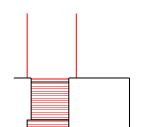
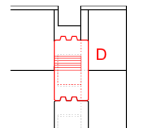
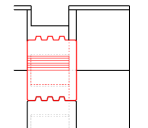
Mechanism 1		Mechanism 2	
Compression loading	Tensile loading	Compression loading	Tensile loading
			
Section cut A	Section cut B	Section cut A	Section cut A
			
Mechanism 3		Mechanism 4	
Compression loading	Tensile loading	Compression loading	Tensile loading
			
Section cut D	Section cut D	Section cut D	Section cut D
			
		Section cut C	Section cut C
			

Table 5.9: Failure mechanisms corner joint Standard.

will rather not govern the resistance, unless a shear failure occurs in its overlap (C) in case of tensile loading. Same could also happen in the overlap of beam 3 having compression loading. The length of the overlap in the corner is thus an important influencing factor (mechanism 3).

Besides being due to compression perpendicular to the grain, a failure in beam 2 could be caused by shear stresses (mechanism 4). Shear acts perpendicular to the grain on the two lateral vertical surfaces (D) and rolling shear on the horizontal surface (E). According to A. Ceccotti et al. (2007) [62] rolling shear does not have to be taken into account, because of its low resistance value. In case of an adverse ratio of resistant surfaces, this argumentation may not be correct. However, as pointed out by different authors, the low rolling shear stiffness rather favours a load transfer by the lateral surfaces anyway (shear modulus is 10 times than the rolling shear modulus).

For the sake of completeness, however, the characteristic resistance values for each mechanism were determined and respectively listed in the Tables 5.10 for the profile thicknesses of 90 and 130 mm.

Mechanism	Stress type	A_{ef} [mm ²]	$F_{k,i}$ [kN]
<i>90mm</i>			
1	Compression parallel to the grain	4391	92.2
2	Compression perpendicular to the grain	4391	11.0
3	Shear parallel to the grain grain	10800	43.2 / 27.0 ¹
4	Shear perpendicular to the grain	4940	52.4
	Rolling shear	5600	4.5
<i>130mm</i>			
1	Compression parallel to the grain	5771	121.2
2	Compression perpendicular to the grain	5771	14.4
3	Shear parallel to the grain	20800	83.2 / 52.0 ¹
4	Shear perpendicular to the grain	7980	84.6
	Rolling shear	13200	10.6

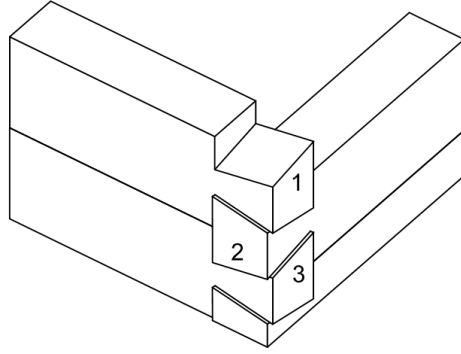
¹ UNI EN 338:2004

Table 5.10: Resistance values corner joint Standard.

As expected, mechanism 1 can be neglected. Probably a crushing of the fibres on the contact surfaces (B) of beam 2 will in each case be observed. Being a type of bearing failure caused by compression stresses perpendicular to the grain, this does not implicate a serious failure. But it can be expected, that the test curve will show a stiffness degradation. So if the test will not be interrupted by achieving a joint slip of 30 mm, a shear failure in the overlap (i.e. mechanism 3) can occur according to the listed results. With a shear strength perpendicular to the grain $f_{v,k} = 2.5$ MPa and a variation coefficient of $CoV = 20$ %, the joints are expected to withstand a maximal load up to 40.3 kN (90 mm) and 77.6 kN (130 mm), not considering the resistance of

4 to 6 kN guaranteed by friction between the logs.

Corner joints Tirolerschloss



The load-bearing behaviour of the corner specimens Tirolerschloss is expected to be governed by dry friction between the angular faces of the notches. As the static friction force depends on the normal force exerted by each surface on the other, the vertical force will be of great importance for the performance of the system. The threshold value above which motion between the notch faces would commence (mechanism 1) can be calculated as follows:

$$F_f = F_{\parallel} - V_{\parallel}$$

With the Coulomb approximation of static friction $F_f = \mu \cdot F_n$ follows:

$$\mu \cdot (F_{\parallel} - V_{\parallel}) = F_{\parallel} - V_{\parallel}$$

$$F = V \cdot \frac{\sin \alpha + \mu \cdot \cos \alpha}{\cos \alpha - \mu \cdot \sin \alpha}$$

Having a friction coefficient μ in the range of 0.3 to 0.6 and an angular cut with a 8° inclination, the resistance of the corner equals about 60 % to 80 % of the normal force. Once this is exceeded the joint will not bear more load, but instead will continuously open. Possible failure mechanism can only be observed below the same

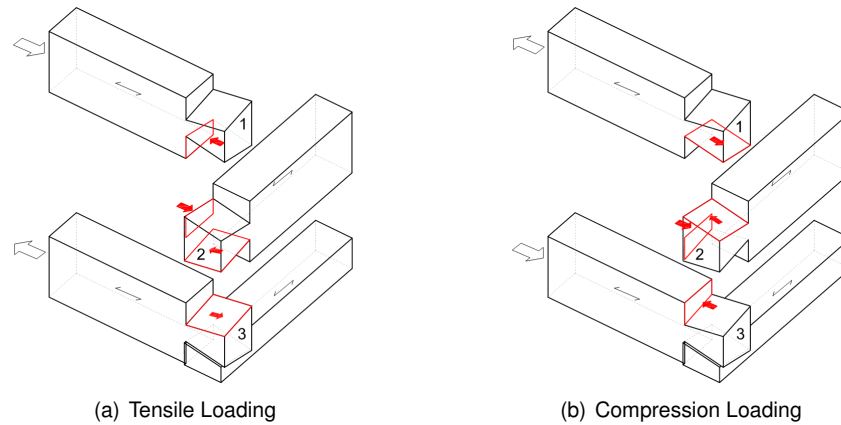


Figure 5.42: Load bearing corner joint *Tirolerschloss*.

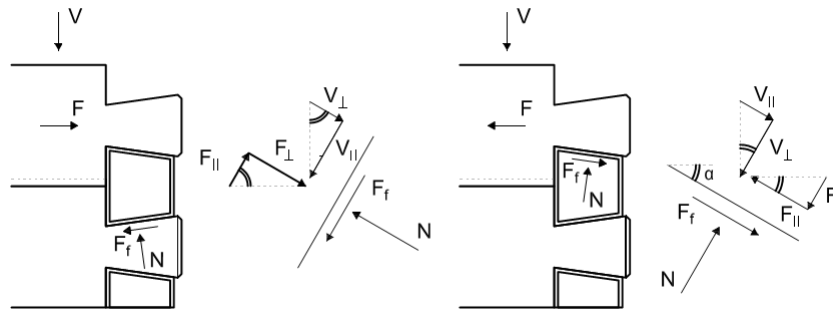


Figure 5.43: Friction forces in the corner joint *Tirolerschloss*.

threshold. It can be reasonably assumed that no failure will occur because of compressive stresses along the grain. Therefore only two possible failure mechanisms which do not require slipping of the abutments must be validated. Besides a bearing failure due to compression stresses perpendicular to the grain, a failure can be caused by shear stresses in beam 2 involving rolling shear. The size of the lateral sides which must withstand shear stresses perpendicular to the grain differs according to the loading direction.

With a total tightening force of the springs of 10 kN, both bearing failure and shear failure of beam 2 can be ruled out, based on the results listed in Table 5.12. As the maximum friction force that can be developed is independent of the contact area, there shall not be a difference in testing the two different profile widths. The load-

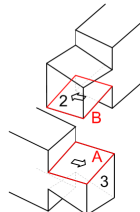
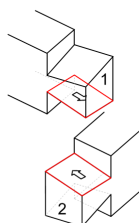
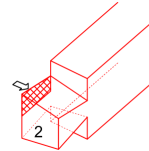
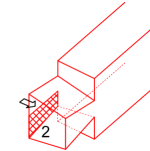
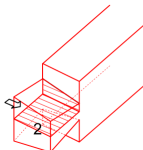
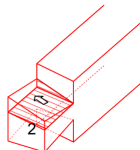
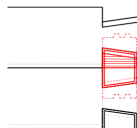
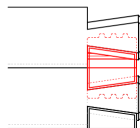
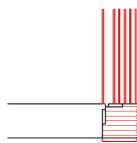
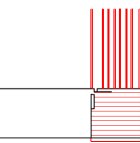
Mechanism 1		Mechanism 2	
Compression loading	Tensile loading	Compression loading	Tensile loading
			
<hr/>			
Mechanism 3			
Compression loading	Tensile loading		
			
			
			

Table 5.11: Failure mechanisms corner joint Tirolerschloss.

Mechanism	Stress type	A_{ef} [mm ²]		$F_{k,i}$ [kN]	
		Comp.	Tension	Comp.	Tension
90 mm					
2	Compression perpendicular to the grain	4007		10.0	
3	Shear perpendicular to the grain	2904	569	30.8	6.0
	Rolling shear	7316		5.9	
130 mm					
2	Compression perpendicular to the grain	6713		16.8	
3	Shear perpendicular to the grain	4058	1233	43.0	13.1
	Rolling shear	16116		12.9	

Table 5.12: Resistance values corner joint Tirolerschloss.

deformation curve will be mainly influenced by the effective friction coefficient. In dependence of this coefficient, the characteristic resistance is of about 10 to 14 kN, of which up to 6 kN result from the interlocking groove-tongue system between the beams. The range of maximum load values obtained from the experiments is expected to correspond to this estimation, as it does not depend on material strength properties, but only on the friction coefficient.

5.3.2 Corner joints: discussion

Thanks to recorded data, it was possible to obtain different useful information. First, according to the standard, the condition corresponding to the weaker failure mode (max load/displacement) or the ultimate "conventional" 30 mm slip condition (load/displacement) if no brittle failure mode was reached.

Regarding the monotonic tests the following conclusion can be made. Both corner styles showed high deformability. The load-bearing behaviour of the specimens 90 mm is characterized by brittle shear failures in the overlap after a considerable slip in the plastic range. Except for test 8, all specimens of 90 mm were subjected to brittle failures caused by shear stresses along the grain in the overlap (see ??). As expected, the failures have occurred at the loaded log in case of tensile loading and the adjacent vertical log in case of compression loading. During test 8, a crack opened in the overlap of the middle horizontal beam due to excessive local tensile stresses along the grain.

Ultimate loads obtained during testing of the 90 mm specimens minus the friction resistance shows a lower resistance compared to the analytical prevision $\bar{y} = 40.3$ kN. With $F_u = 39.7$ kN, the ultimate load which the joint carried during test 3 is

significantly higher than that during test 4 $F_u = 27.2$ kN. The gap of nearly 12 kN cannot be explained by different friction capacities due to the spring forces (tightening forces 5 kN instead of 10 kN). According to the Swiss standard SIA 265:2003 [63], there is a correlation between shear resistance of members in bending and axial force perpendicular to the grain, as illustrated in Figure 5.44. Assuming this could also held true for the joint specimens examined, which were not subjected to bending, the following simple calculation is made:

$$\sigma_{c,90} = \frac{10 \text{ kN}}{(500 - 90) \text{ mm} \cdot 90 \text{ mm}} = 0.27 \frac{\text{N}}{\text{mm}^2} \Rightarrow \frac{\sigma_{c,90}}{f_{c,90,k}} = \frac{0.27}{2.5} = 0.1$$

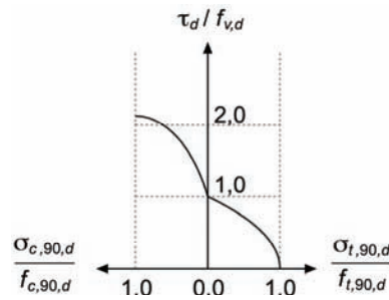


Figure 5.44: Shear and loading perpendicular to the grain [63].

It could be concluded from this, that the tightening force of 10 kN is sufficiently large to provoke an increase in the shear resistance of only 10 %. For a total spring force of 5 kN the resulting increase of shear resistance is correspondingly lower. However, considering the intrinsic characteristics of the material (defects) and the type of connection (carpentry joints), the results the ultimate loads are in line with expectations.

The specimens consisting of 130 mm profiles sustained joint slips of 30 mm. The load-displacement path show a pronounced non-linear behaviour and ultimate loads sustained are about 14 % higher than the values achieved testing the smaller log profiles. Because no brittle failure occurred, the wood crushing was accordingly more severe compared to that observed testing the smaller profiles. Also in this case the analytical models for the load bearing capacity have identified the correct failure mode.

Under cyclic loading the graphs mirror what was observed during the monotonic tests. The maximum loads achieved were higher on the compression side due to the notch's mounting tolerance under tensile loading and, thus, the hysterical loops

are asymmetrical. Wood crushing on the load-transferring notch faces caused a joint slip which increased each time a given amplitude was attained for the 1st time, as can be clearly seen from the growing plateau in the middle of the loops, within the vertical beams were simply sliding on the top of the other. When the notch faces again made contact, the joint became reloaded. Thanks to the rotational freedom of the middle horizontal beam and the resulting irregular stress distribution, the curves show a stiffness degradation until the respective amplitude was achieved and the slope tended towards zero. Completing the hysteresis loop of same amplitude for the 2nd time, a degradation of strength and stiffness was observed and the curve became respectively pinched. Standard corner style showed good energy dissipation characteristics and a rather low impairment of strength.

In conformity with the monotonic test, specimen 11 (90 mm) failed as result of shear stresses in the overlap of the loaded beam. Contrary to standard EN 12512:2006 [64], the test was continued in order to investigate the further load bearing behaviour of the joint. When a tensile failure along the grain occurred in the notch of the loaded beam (see Figure 5.45(b)), during the first cycle corresponding to $6 \cdot V_y$ on the tensile side, the test was interrupted. As expected, no serious failure occurred while testing specimen 12 (130 mm).

Thanks to its characteristic angular notches, the load bearing behaviour of the corner style *Tirolerschloss* is mainly governed by static and kinetic (or dynamic) dry friction and not material-related. Therefore, the profile width did not affected the in-plane resistance. Variations between the experimental curves and results can assumed to be owed to semi-circular leaf and its counter-part. Even though they did not negatively affected the ultimate loads obtained, the caused crack formation is certainly not desirable regarding the serviceability. In summary, the *Tiroler Schloss* sustains a much lower in-plane load in comparison to the previously analysed corner type.

The response obtained from the cyclic tests presents similar characteristics to a friction dissipator. High values of equivalent viscous damping ratios and negligible impairment of strength was observed. The crucial factor for this joint type is the normal force acting on the interlock between two walls. With a superimposed load equal to $10kN$, the lateral resistance is at a much lower level than that measured testing the corner joint Standard.

The cyclic protocol emphasize the contribution of the semi-circular groove on the first cycles. As showed in Figure 5.19 and Figure 5.20 after the failure caused by the tension stress perpendicular to the grain on the central element the shape of the



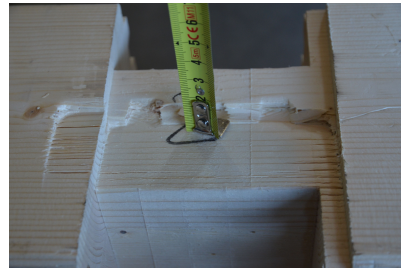
(a)



(b)



(c)



(d)

Figure 5.45: Failure mechanisms: (a) shear failure along the grain (pull out test on 90mm thick element) - (b) tensile failure of the central part of the joint - (c), (d) crushing of the horizontal element (push out test on 130mm thick element).

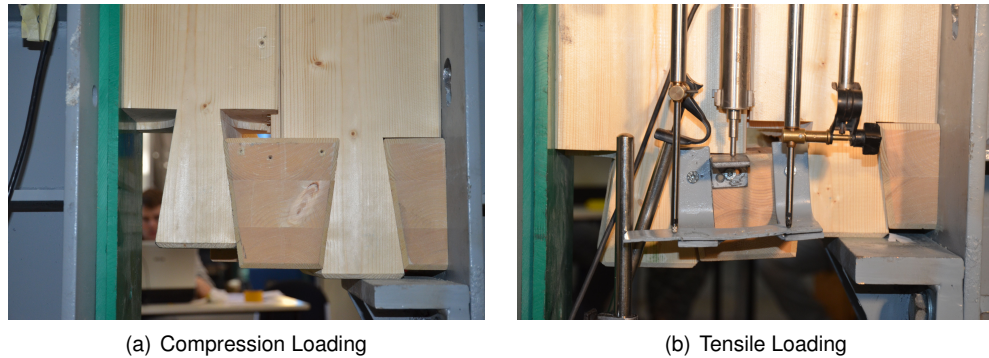


Figure 5.46: *Bearing behaviour of the corner type Tiroler Schloss.*

hysteresis loop changes. After this slip that correspond to the maximum peak, the friction contribution provide the whole resistance of the joint.

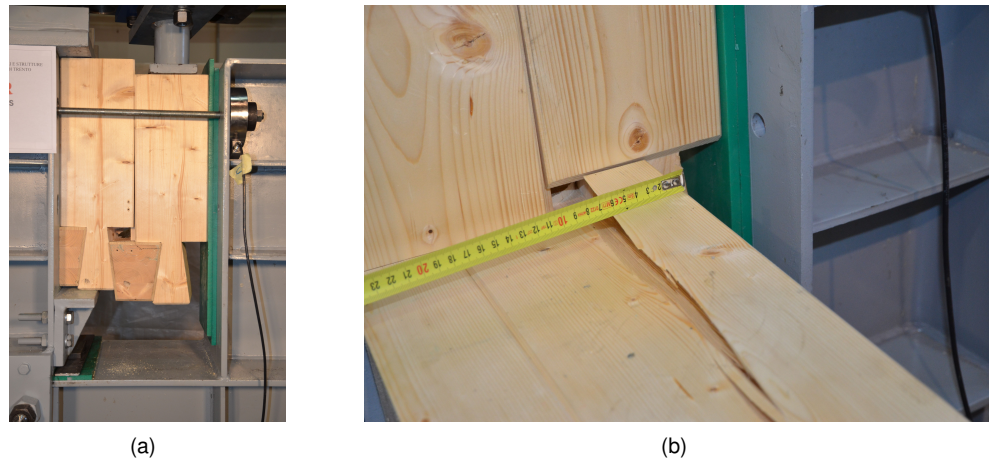


Figure 5.47: *Test on 130 mm thick Tirolerschloss - splitting caused by semi-circular leafs and protrusions.*

The results of the tests on the reinforce system confirm a good overall behaviour. After the static friction force along the groove-tongue system of the logs was exceeded, the reinforcement element persistently remained in the elastic range and, thus, dimensionally stable. A corresponding linear load increase was measured. The brittle shear failure of the external surface occurred only for displacements greater than the conventional ultimate slippage according to UNI EN 12512:2006 (30mm).

For reasons already observed in context of testing the corner style Standard, the hysteresis loops are not symmetric. No considerable strength degradation occurred

while repeating loops of the same amplitude. With increasing amplitude there was a continuous increase in maximum loads and, at the same time, stiffness degradation. During the initial cycle according to a displacement of 30mm a shear failure occurred.

5.3.3 Shear walls: discussion

As mentioned in the introduction chapters the mechanical behaviour of the shear walls is strongly correlated to the interaction of the three main components: friction - gap - joints. For the analysis of the performance, the following general considerations can be itemized. According to the analytical predictive models and as observed in the previous tests three main phases can be identified. The first part of the load-displacement curve is governed by the static friction and depends on the level of vertical load. After the friction regime, the log slip until the load bearing surfaces of the corner (and internal dovetail reinforce for TR) are in contact. The width of this almost horizontal plateau is proportional to the mounting tolerance of the interlocks (different for the two tested log thickness). At the end of the low rise or horizontal slope part the contribution of the load bearing capacity of the corner joints is activated. This peculiar behaviour must be taken into account both for the ultimate limit states (ULS) and serviceability limit states (SLS).

In the ULS verification under seismic loads according to EN1998-1:2005 [2] the friction force cannot be considered as a resistant mechanism in the design models. It might be necessary to verify whether an exception can be made in the case of log house constructions which are provided with anchor mechanisms like internal steel rods fitted with a shrinkage adjustment mechanism. In the SLS the admissible inter-storey drift is 0.5% of the storey height. This requirement, if the friction regime is overcome, cannot be satisfied because the sum of the single mounting tolerance is about $20 - 30\text{mm}$ before reaching the interlock contribution. The number of logs define the total displacement of the wall (gaps + joint deformation). On the other hand, if every joint had the same resistance, this parameter doesn't affect the load bearing capacity. Nevertheless statistic distribution of the system must be taken into account. To a higher number of joints correspond a higher probability to have a weaker one and consequently to affect the wall failure (weakest-link model). The vertical load ensures two main effects. First, it influences the friction forces. Second, it produces the stabilizing moment that acts against the overturning moment introduced by the horizontal load, reducing the total uplift of the logs (relative rotation of the logs).

In order to predict the behaviour of the system a mechanical scheme must be as-

sumed. As shown in Figure 5.48 the total displacement of the wall represent the sum of all the single inter-log slippage. Each couple of logs is connected following the "in parallel" scheme by means of the corner joints. Along the height of the wall these springs are linked following the "in series" scheme. Thus the maximum displacement of the top of the wall ($100mm$) is distributed on the single link with a maximum theoretical slippage of $100/15 = 6.7mm$. According to this assumption, the full resistance of the joint may be not achieved in all the tested specimens especially for the 130 mm thickness. This fact usually is not taken into account for the common design practice. The ultimate condition do not take into account the level of displacement of the wall, therefore the failure of the joints may be occurs at high inter-story drift. If the failure of the interlock is achieved at a displacement level greater than the maximum admissible displacement of the wall divided by the number of joints the full strength of the interlocks is not exploited. The resistance of the corner joint, as mentioned in the previous section, is related to the timber failure modes so the overall resistance is influenced by the defects. In order to get more reliable values of stiffness, strength and ultimate displacement further tests shall be performed to achieve a statistical sample. These considerations will be the basis of the models proposed in section 5.4.

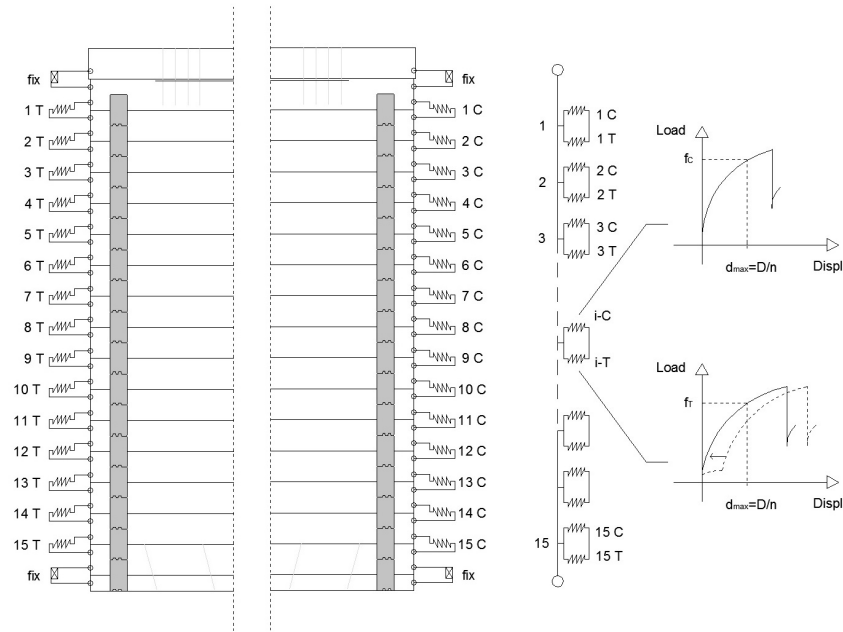


Figure 5.48: Mechanical scheme of the lateral behaviour of the system.

Figure 5.49 shows the load vs displacement curve of two walls with standard corner joint with different length. The shorter wall (M_ST_SH) compared with the longer wall exhibit a lower load bearing capacity because the vertical load is lower (16.7 kN instead of 44 kN). Therefore if an additional part of friction force, corresponding to the difference of vertical load multiplied by the friction coefficient, is added to the curve of the shorter wall the results are similar.

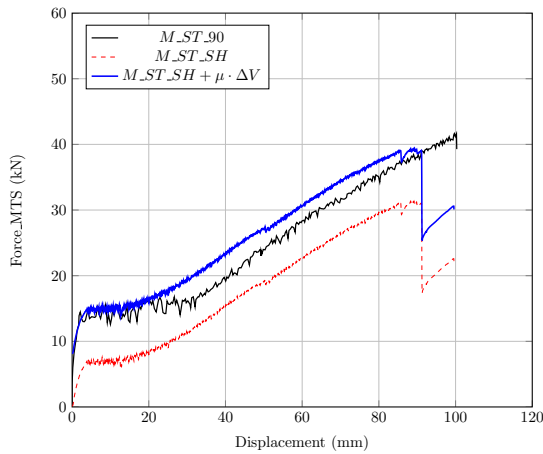


Figure 5.49: Load displacement curves for different wall length. Additional contribution of the vertical load on the friction behaviour.

The presence of large openings (windows or/and doors) reduces significantly the stiffness and the load bearing capacity of the wall (Figure 5.32(a)). The rigid rotation of the parts of the walls on the side of the openings increase the tension on the constrain cables. Moreover this force increase in both the corner according to the mechanism showed in Figure 5.50(a). The tension measured by load cell, in correspondence to the hydraulic jack load equal to 30 kN , increase from 9.2 kN (M_ST_90) to more than 21 kN . The peculiar geometry of the Tirolerschloss corner and consequently its mechanical behaviour (governed by friction) leads to significant uplifts of the logs and increase of both cable forces.

The comparison of the cyclic and monotonic protocol for each test shows a good agreement (Figure 5.51). The load-shear versus displacement curves obtained in the cyclic tests reveal the high capacity of the walls to dissipate energy mainly due to the friction mechanism depending on the vertical load. Thus, the amplitude of the hysteresis loop were correlated mainly to the magnitude of the vertical dead loads. This behaviour is showed in Figure 5.54(b) and Figure 5.49 where the curves of two walls

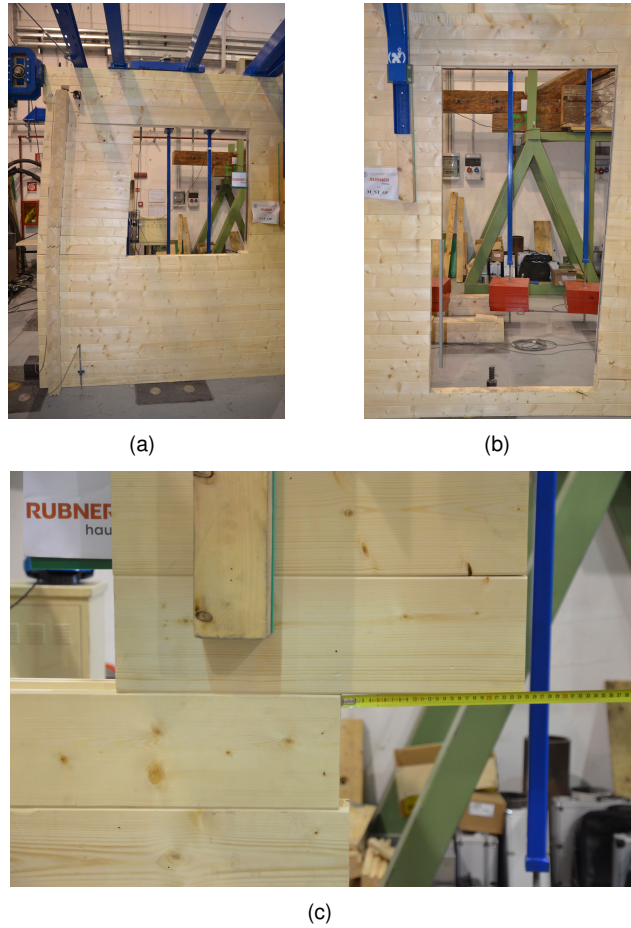
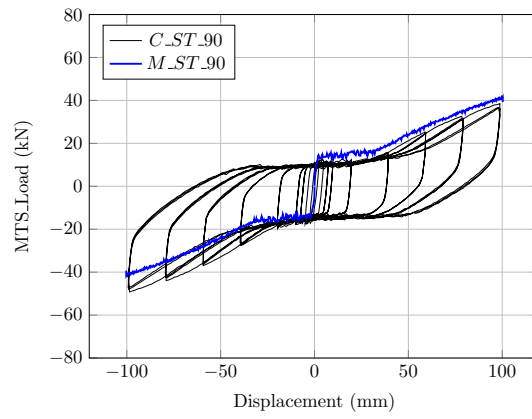
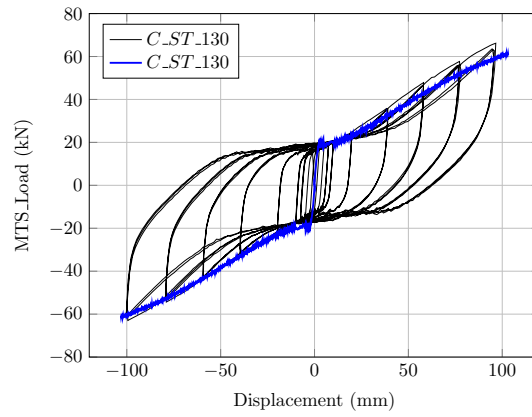


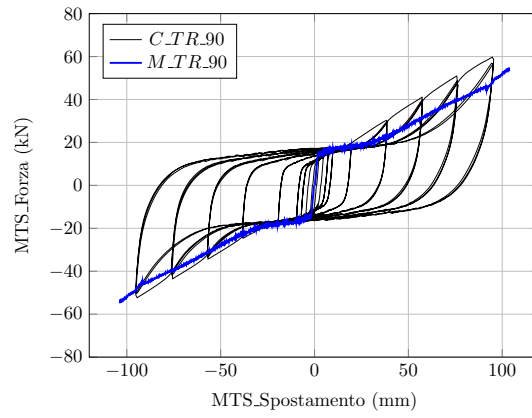
Figure 5.50: Test M_{ST_OP} rocking effect (a) and residual slippage in the wall portion between two openings (b-c)



(a)

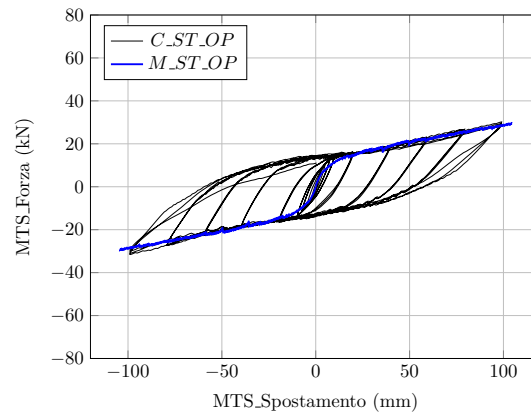


(b)

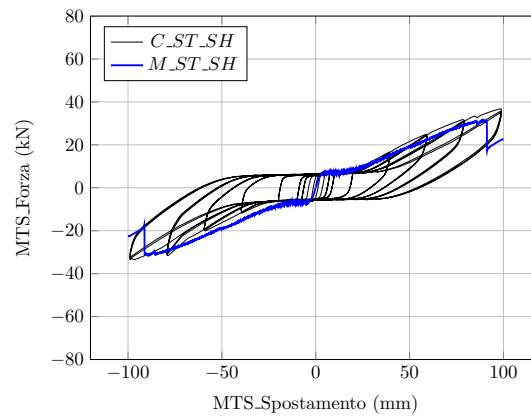


(c)

Figure 5.51: Comparison between cyclic and monotonic test: (a) C/M_ST_90 - (b) C/M_ST_130- (c) C/M_M_TR_90.



(a)



(b)

Figure 5.52: Comparison between cyclic and monotonic test:(d) C/M_M_ST_OP - (e) C/M_M_ST_SH.

with the same corner joints but different vertical load are compared (both in monotonic and cyclic tests). In the authors opinion the results explain the influence of the vertical loads on resistance and energy dissipation through the friction phenomenon. The load bearing capacity of the wall C_ST_90 loaded by a total vertical force $44kN$ ($10.5kN/m \times 4.20m$) was 25% higher than the C_ST_SH loaded by a total vertical force $16.7kN$ ($6kN/m \times 2.785m$). The energy dissipation calculated as mean value of the last three hysteresis loop ($100mm$) in the first case was 52% higher than the second case (C_ST_SH). The corner joints resistance mechanism were activated only after the wide horizontal plateau caused by the mounting tolerance. The stiffness degradation for the medium/high displacement cycles was related to the plastic mechanisms due to the compression perpendicular to the grain. The test C_TR_90 where Tirolerschloss joints and dovetail reinforcement systems were adopted shows a good energy dissipation and a low impairment of strength. Moreover the results were comparable with the standard joints configuration, however, it should be noted that two additional connection were used.

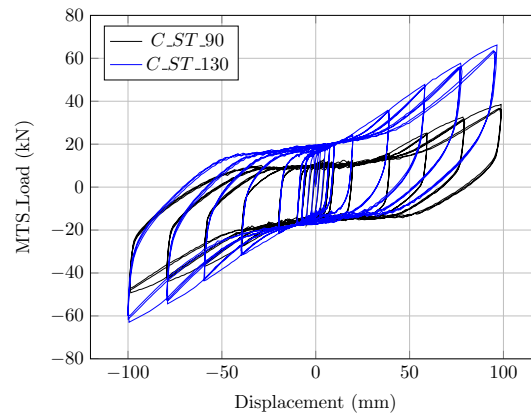
The maximum forces and the mean equivalent viscous damping are reported in Table 5.13. This last measure provides a means with which to describe the energy dissipation characteristics, in other words, the ability to reduce the seismic input energy. It is measured as the ratio between the dissipated energy in one half cycle E_d , also known as hysteretic damping, and the available potential energy E_p , thus, determined by the equation:

$$\nu_{eq} = \frac{E_d}{2 \cdot \pi \cdot E_p}$$

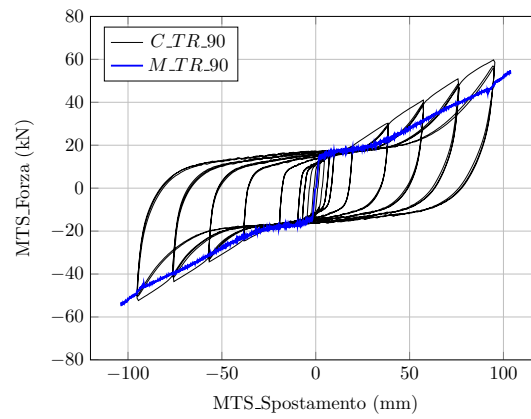
Test	F		ν_{eq}					
	+	-	v_y	$2v_y$	$4v_y$	$6v_y$	$8v_y$	$10v_y$
	kN	kN	%	%	%	%	%	%
C_ST_90	38.5	-49.2	40	39	30	22	20	19
C_ST_130	66.2	-63	43	41	31	23	21	19
C_ST_OP	30.2	-31.6	15	27	33	29	25	18
C_TR_90	59.9	-52.5	41	44	31	24	21	18
C_ST_SH	36.8	-33.5	49	43	23	15	12	11

Table 5.13: Test results - cyclic tests maximum force and equivalent viscous damping at the third cycle.

The maximum theoretical value for the equivalent viscous damping for the "pure - friction" system is 63%. The values obtained from the experimental tests range between 11 and 49% depending on the specimen and the level of displacement. The lower value was observed during the test on the wall with opening.

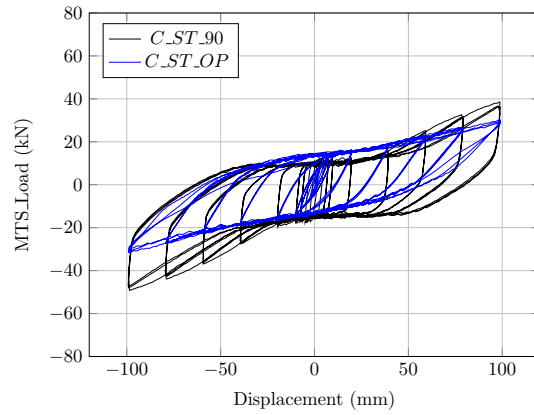


(a)

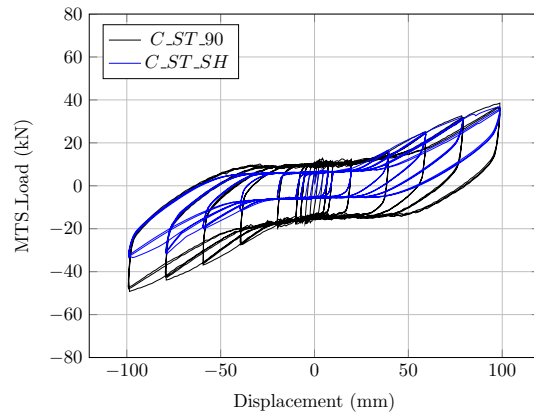


(b)

Figure 5.53: Comparison between cyclic and monotonic test, C_ST_90 vs: (a) C_ST_130 - (b) $C_M_TR_90$.



(a)



(b)

Figure 5.54: Comparison between cyclic and monotonic test, (a) $C_{M_ST_OP}$ - (bb) $C_{M_ST_SH}$.

Regarding the ultimate conditions two failure modes were observed during the test. The first was the "conventional" failure mode caused by the high displacement achieved during the tests (M/C_ST_90 - M/C_TR_90 - M_ST_OP;). The second was the brittle failure of the joints caused by the shear stress on the resisting surfaces of the joints (M/C_ST_SH - C_ST_OP). However the residual strength and stiffness of the system was ensured by a redistribution of the stress on the residual load bearing surfaces of the joints Figure 5.55. In each test was observed the wood crushing, which causes the stiffness degradation.

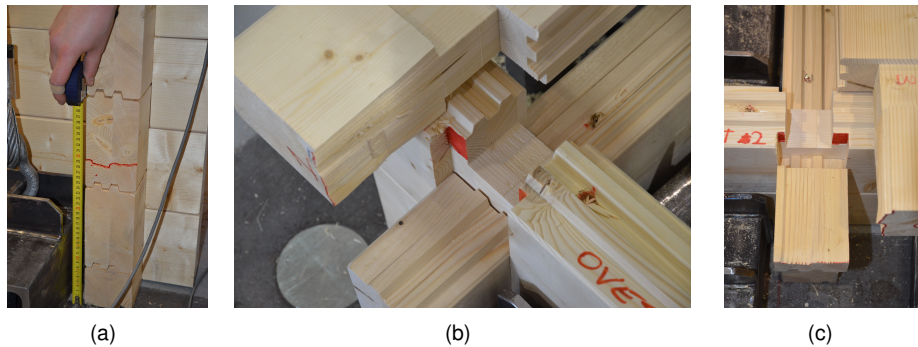


Figure 5.55: *C_ST_SH wall failure - the red color mark the parts of the transversal log that ensure the residual resistance and stiffness after the shear failure of the lower part of the notch.*

5.3.4 Friction and mounting tolerance

The estimation of the actual mounting tolerances is one of the most important operation to achieve a correct model. The quality of the processing of the numerical control machines (C.N.C) is incredibly precise and it is capable of reproducing the same geometry on all the pieces. Then on the contrary of the traditional handicraft works, where every piece is different from the others, the modern working process can be considered as a fixed variable of the system. In order to measure the actual value of the mounting tolerance of the samples, an analysis of the acquired data was performed. The value of the gap can be calculated as the horizontal slope part of the monotonic load curve or as the half sum of the horizontal slope parts of the loops for the cyclic protocol. The total gap was distributed on the two side of the joint.



(a)



(b)

Figure 5.56: Joint worked with CNC machine - (a) standard joint (ST) - (b) Tiroler Schloss (TR)

For the corner joint test a peculiar behaviour was introduced by the test setup. When the samples were assembled the gaps were distributed in such a way that, when the compression test run, the surfaces were already in contact (due to the self-weight of the elements). On the other hand when the tension test run, the gaps had

to be overcome before take force. Thus, the gap is clearly visible only in the "pull out" monotonic test. In the cyclic tests, the gap was calculated in the first hysteresis loop after the amplitude estimated in the monotonic test. For the standard corner joint a total gap of 4 mm was observed during the monotonic tests. Also the cyclic tests shows a total gap of 4 mm ($7.98/2=4$ mm). The samples with ticker logs (130 mm) shows 5 mm in the monotonic tests and 3.5 mm in the cyclic tests ($7.1/2=3.5$ mm).

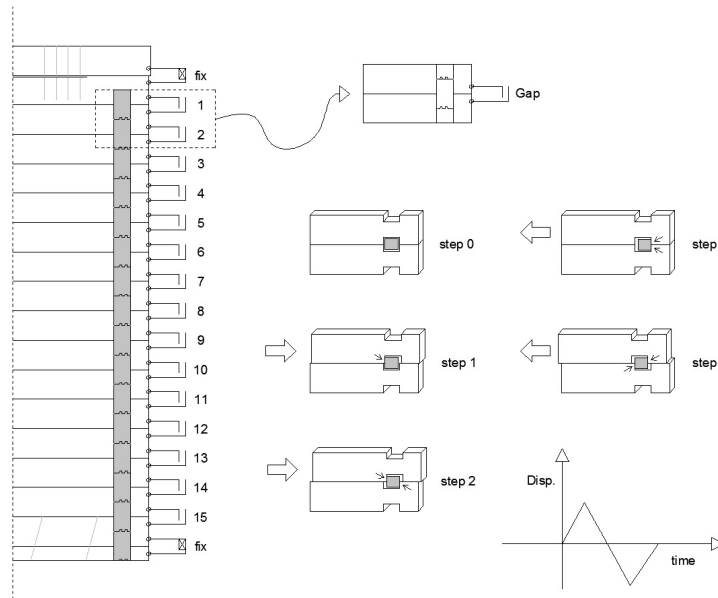


Figure 5.57: Scheme of the distribution of the gap along the wall.

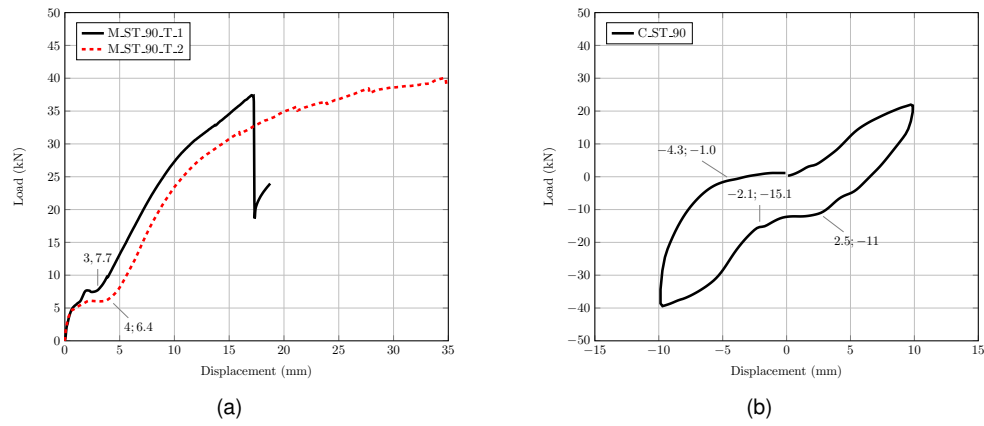


Figure 5.58: Load displacement path of the corner joints tests: monotonic tests 90mm (a) - cyclic test first loop with an amplitude of 10mm (b).

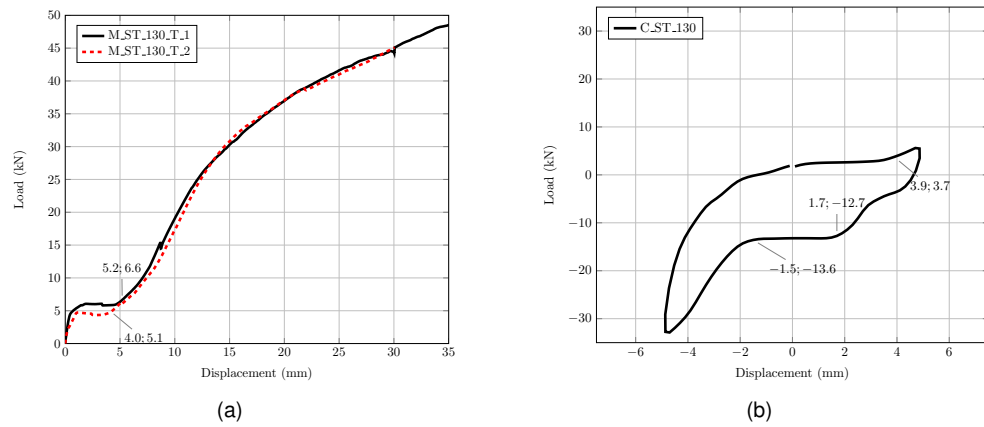


Figure 5.59: Load displacement path of the corner joints tests: monotonic tests 130mm (a) - cyclic test first loop with an amplitude of 5mm (b).

The total horizontal plateau visible in the monotonic test is the sum of the gap between the superimposed logs. As shown in Figure 5.23 the total number of gaps was fifteen. The bottom log was rigidly connected to the second by means of self-tapping screws while the top log on the top of the wall was introduced only for the load application. Four tests were carried out on 90 mm logs with standard joint, two monotonic (M_ST_90 and M_ST_SH) and two cyclic (C_ST_90 and C_ST_SH). The same value was obtained from the tests on the longer walls (M_ST_90 - 31mm) and (C_ST_90 - $60.4/2 = 30.2mm$). The tests on the shorter walls shows different value for the cyclic test (C_ST_SH - $59.96/2 = 30mm$) and for the monotonic test (M_ST_SH - 17.5mm)

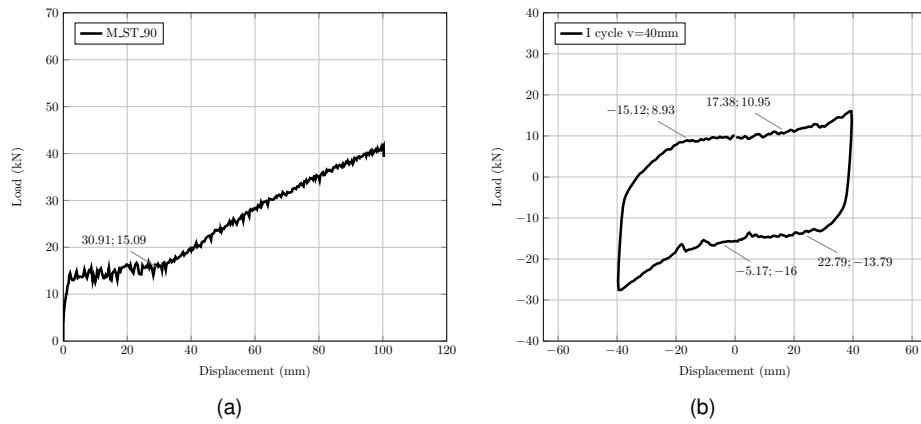


Figure 5.60: Load displacement path of the corner joints tests: monotonic tests 90 mm (a) - cyclic test first loop with an amplitude of 10 mm (b).

Moreover four linear displacement transducers were connected to measure the relative slippage between the logs (inst. 5 - 6 - 7 - 8). These data shows a range of log to log slippage between 1.5mm and 2.5mm (Figure 5.62).

For the layout with thicker logs (130 mm) only two tests were carried out. The total gap with this geometry was hardly detectable both in the monotonic tests and cyclic tests. However, a reasonable value can be estimated as 12 mm.

The mounting tolerance between the surfaces of the tirolerschloss joint is not clearly identifiable in the corner joint tests. While for the test with the additional dovetail reinforce the overall gap was about 30 mm. The gap can be attributed to tolerance between the steel profile and logs. The value of the static friction coefficient implemented in the numerical model was estimated by the analysis of the tests on the corner joints and by the test on the shear walls. The value are summarized in

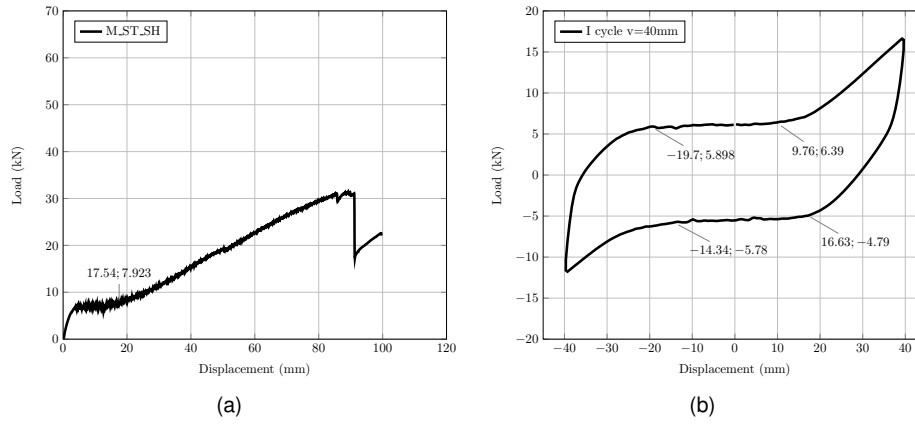


Figure 5.61: Load displacement path of the corner joints tests: monotonic tests - monotonic tests 130 mm (a) - cyclic test first loop with an amplitude of 5 mm (b).

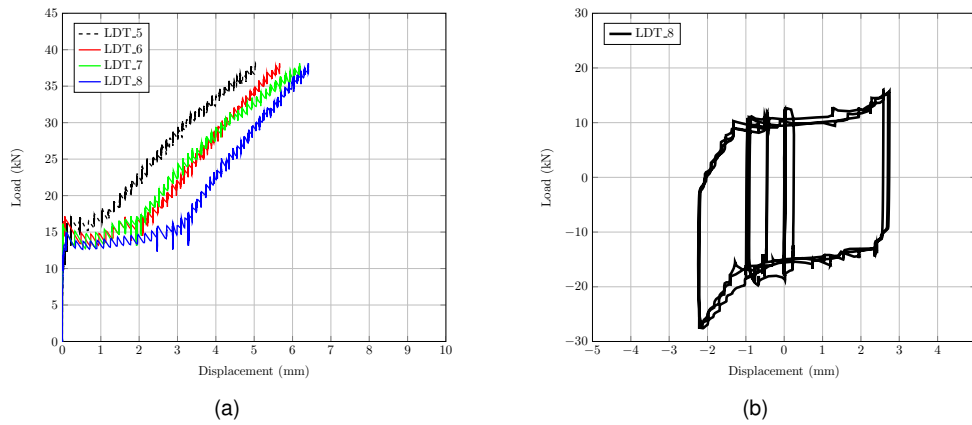


Figure 5.62: Load vs log slip: Monotonic test M_ST_90 (a) - cyclic test C_ST_90 (b).

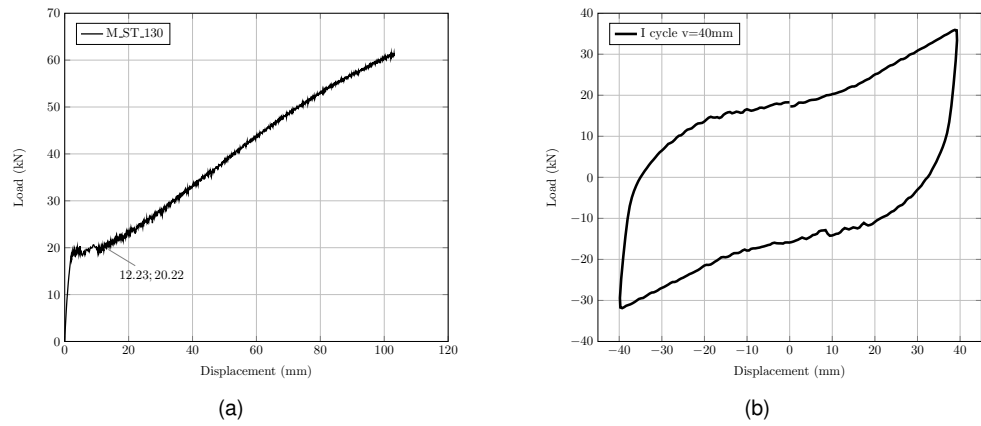


Figure 5.63: Load vs log slip: Monotonic test M_ST_90 (a) - cyclic test C_ST_90 (b).

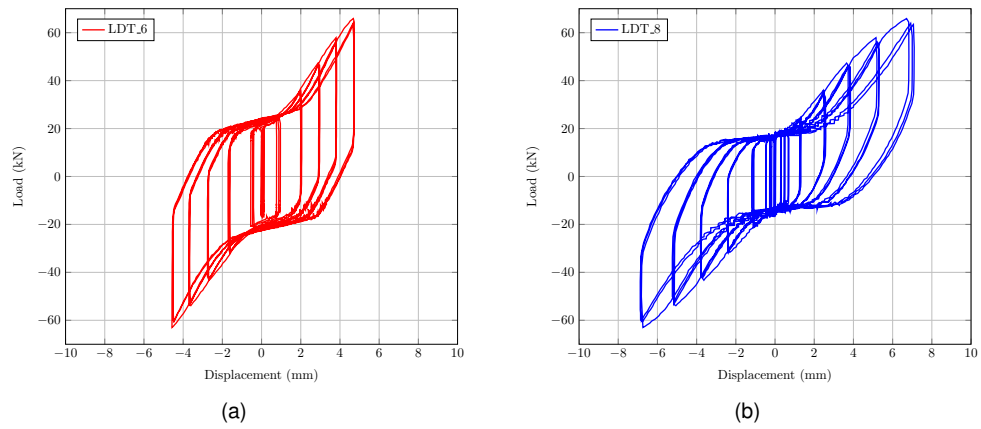


Figure 5.64: Load vs log slip for cyclic test C_ST_90 : transducer nr.6 (a) - transducer nr 8 (b).

Table 5.14. The value obtained during the tests on the corner joints are higher than the value obtained during the shear walls test.

Test	Friction force kN	Vertical load kN	Friction coefficient %
Monotonic test on shear wall			
M_ST_90	14.47	44	0.33
M_ST_130	17.78	44	0.4
M_ST_SH	7	16.7	0.42
M_TR_90	14.25	44	0.32
Cyclic test on shear wall			
C_ST_90	15	44	0.34
C_ST_130	17.75	44	0.4
C_ST_SH	5.65	16.7	0.34
C_TR_90	13.93	44	0.32
Monotonic test on corner joint			
M_ST_90_T_1	5	10	0.5
M_ST_90_T_2	4.83	10	0.48
M_ST_130_T_1	5.18	10	0.52
M_ST_130_T_2	4.72	10	0.47
Cyclic test on corner joint			
C_ST_90	6.65	10	0.66
C_ST_130	8	10	-
C_TR_90	5	10	0.5
C_TR_130	4.58	10	0.46

Table 5.14: Friction coefficient obtained from the experimental data.

The values obtained from the analysis of the acquired data are consistent with literature. Usually the frictional coefficient varies in a range between 0.2 and 0.6. About this phenomena a detailed review of the is reported in [65] and [66]. The value of the friction coefficient (static friction between non-moving surfaces, and kinetic friction between moving surfaces) are listed in Table 5.15. Another experimental campaign carried out by the Univesity of Minho ([65]) lead to higher values of the frictional coefficients. The wide range of variation depend from the different parameters is due to the nature of timber. The coefficients depend from the roughness between contact surfaces, from the moisture content and from the specific density of the material. Moreover also the angle between the direction of the force and the grain orientation influence the results. Moreover the results are probably influenced by the geometry of the logs (interlocks between the horizontal surfaces) and from the load condition.

Material	Density= $500\text{kg}/\text{m}^3$		Density = $440\text{kg}/\text{m}^3$		Density = $380\text{kg}/\text{m}^3$	
	μ_s	μ_d	μ_s	μ_d	μ_s	μ_d
Timber	0.24	0.20	0.25	0.21	0.27	0.22

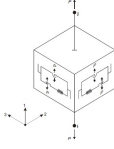
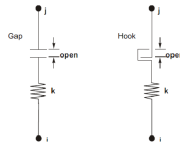

Table 5.15: Static and kinetic frictional coefficients according to [65],[66].

Test	Inter-log force [kN]	F_{max}^- [kN]	F_{max}^+ [kN]	μ
L1	10	-5.51	5.54	0.55
L2		-4.87	5.47	0.52
L3	30	-12.86	11.68	0.41
L4		-11.41	11.59	0.38
L5	50	-18.71	17.37	0.36
L6		-18.25	17.35	0.36
L7	70	-25.95	25.7	0.37
L8		-23.67	26.18	0.36

Table 5.16: *Test results from [?].*

5.4 Analytical simplified models

One of the goal of the research summarized in this document was the proposal and the assessment of the reliability of a rheological simplified model. For this purpose, the tests were organized in two steps. The first was the characterization of the mechanical behaviour of the single corner joint in order to obtain the input data of the model. In the second several full-scale test on walls (loaded both by vertical and horizontal forces) have been carried out to verify the difference between the experimental and analytical results. The model, designed as an assembly of spring elements - gap and friction pendulum was implemented in a FE software (SAP2000). The description of the links and the parameters are summarized in Table 5.17.

Friction pendulum	Gap elements	Elastic link
<p>Non-linear</p>  $f_s = \begin{cases} k_1 \cdot d_{u1} & d_{u1} \leq 0 \\ 0 & otherwise \end{cases}$ $f_{2uf} = -P \cdot \mu_2 \cdot z_2$ <p>Where: P is the total axial force exerted by the element on the connected joints, K_1 is the axial stiffness, d_{u1} is the axial deformation,</p> <p>μ_2 is the friction coefficient,</p> <p>z_2 is a internal hysteretic variables. In this case this parameter is set equal to one because the Wen plastic models was not taken into account, $slow_2$ is the friction coefficients at zero velocity, $fast_2$ is the friction coefficients at fast velocities, v is the resultant velocity of sliding.</p>	<p>Non-linear</p>  $f_{gap} = \begin{cases} k \cdot (du + open) & du + open \leq 0 \\ 0 & otherwise \end{cases}$ $f_{hook} = \begin{cases} k \cdot (du - open) & du - open > 0 \\ 0 & otherwise \end{cases}$ <p>Where: k is the spring constant,</p> <p>$open$ is the initial gap opening, d is the deformation.</p> <p>The Hook Link was implemented in the model to simulate cyclic loads in possible further studies.</p>	<p>Non-linear elastic</p>  $f = k_i \cdot d_i$ <p>Where: k is the spring constant</p> <p>d is the deformation. The subscript c/t corresponds to push-out/pull-out test on corner joints.</p>

As introduced in the previous sections three main parts (friction - gaps - interlocks) can be identified in the load-displacement curve of a LH wall. The friction pendulum link was used to model the friction behaviour between contacting surfaces of the logs. The post-slip stiffness in the shear directions due the pendulum radii of the slipping

surfaces was neglected by setting the radii to zero (indicating a flat surface). Only the slow friction coefficient (zero velocity) was taken into account (setting the rate value equal to zero). The full discussion can be found in [67] The gap links were used to simulate the influence of the mounting tolerance between the elements. Finally an equivalent spring was introduced to reproduce the effects of the two interlocks at the opposite side of the wall (as introduced in the previous section the mechanical behaviour of the joint depend from the load direction). This value was calculated, according to the "in parallel springs" scheme for the single overlapped logs ($k_{eq,i}$ for the k_t and k_c at the opposite corner) and as "in series springs" scheme for the whole wall (k_{eq} along the wall height).

$$K_{eq,i} = k_c + k_t$$

$$\frac{1}{K_{eq}} = \sum_{i=1}^n \frac{1}{K_{eq,i}}$$

The presence of the reinforcement system (i.e. self-tapping screws) was introduced as an equivalent additional equivalent spring.

$$K_{eq} = \frac{n_f \cdot k_f}{n}$$

Where n_f is the total number of fasteners in between two overlapped logs, k_f is the stiffness of the single fastener, n is the number of logs. In order to introduce the dovetail reinforce system described in section 5.2.1 a further step had to be introduced. These connections links four logs with a total number of 3 shear planes. Thus the total stiffness of the connection k_{dr} was converted in a single k_f stiffness by means of the "in series spring" scheme:

$$K_{dr} = \frac{1}{\frac{1}{k_f} + \frac{1}{k_f} + \frac{1}{k_f}}$$

So the stiffness adopted in the model was $k_f = 3 \cdot k_{dr}$

The analytical equation of the system in the most general form is:

$$F = \begin{cases} P \cdot \mu_s & d = 0 \\ P \cdot \mu_d + k_{eq,f} \cdot d & 0 < d \leq n \cdot gap \\ P \cdot \mu_d + k_{eq,f} + k_{eq} \cdot (d - n \cdot gap) \cdot d & d > n \cdot gap \end{cases}$$

Where:

- d is the total displacement at the top of the wall,
- n is the number of logs,
- gap is the mounting tolerance between the load bearing surfaces of the corner joint
- P is the vertical load,
- μ_s is the static friction
- μ_d is the dynamic friction
- $K_{eq, f}$ is the equivalent stiffness of the additional connectors
- K_{eq} is the equivalent stiffness of the corner joints.

The value of the parameters adopted in the analysis are summarized in Table 5.17. The gap and friction values are derived from the wall tests whereas the stiffnesses implemented are those acquired from the corner tests. It is important to underline the great variability of friction coefficient and gaps values between wall and corner joint tests.

	Gap [mm]	Friction [%]	Stiffness [N/mm]
Standard 90 mm	2	0.3	$k_{1c} = 4800 - k_{1t} = 3217$ for $0 < d < 3mm$ $k_{2c} = 2933 - k_{2t} = 2783$ for $3 < d < 6mm$ $k_{3c} = 1667 - k_{3t} = 1700$ for $6 < d < 9mm$
Standard 130 mm	0.8	0.4	$k_{1c} = 5467 - k_{1t} = 1730$ for $0 < d < 3mm$ $k_{2c} = 3267 - k_{2t} = 2970$ for $3 < d < 6mm$ $k_{3c} = 2100 - k_{3t} = 2700$ for $6 < d < 9mm$
Tirolerschloss	2	0.3	$k_{1c} = 1143 - k_{1t} = 923$ for $0 < d < 3mm$
	2	0.3	$k_{2c} = 1047 - k_{2t} = 800$ for $3 < d < 6mm$
	2	0.3	$k_{3c} = 315 - k_{3t} = 573$ for $6 < d < 9mm$
Dovetail reinforce	2	-	$k_1 = 3030$ for $0 < d < 3mm$
	2	-	$k_2 = 3650$ for $3 < d < 6mm$
	2	-	$k_3 = 3110$ for $6 < d < 9mm$

Table 5.17: Friction coefficient obtained from the experimental data.

In order to simplify the model and to remove the bending moment due to the length of the link an equivalent inclined spring was introduced, as shown in Figure 5.66. The non-linear behaviour enclose gaps, corner joints and reinforce system.

As pointed out in the previous paragraphs one of the interesting features of the analytical models is the possibility of taking into account the contribution of additional connectors. Using fasteners such as self-tapping screws or timber dowels the overall

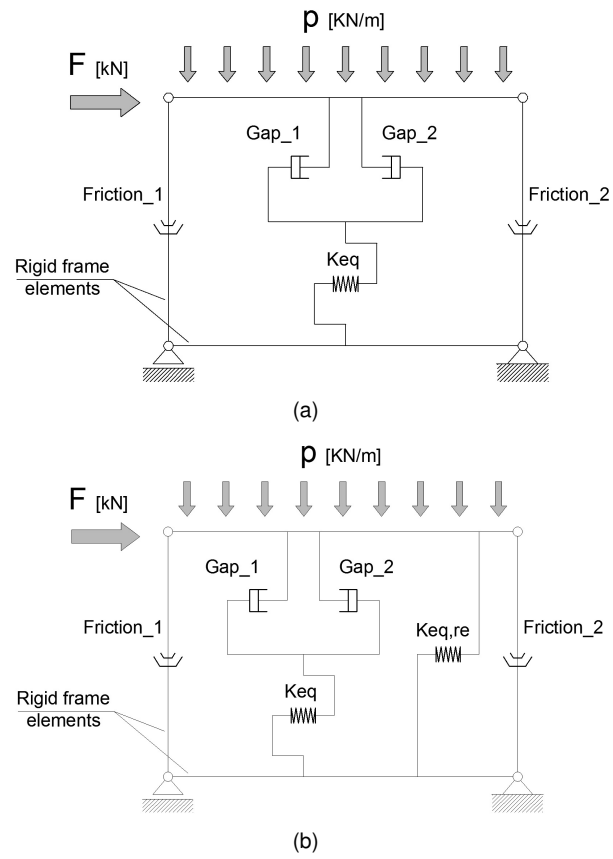


Figure 5.65: A simplified model without additional reinforce (a) - with additional reinforce (b).

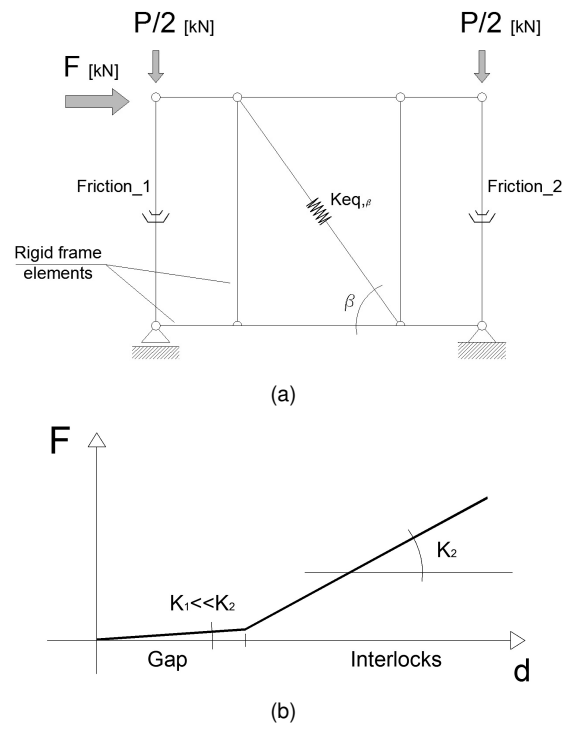
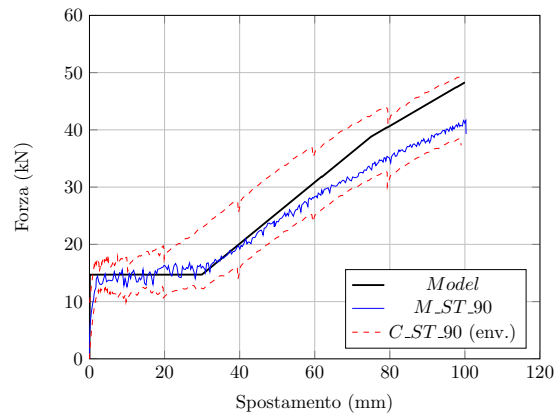
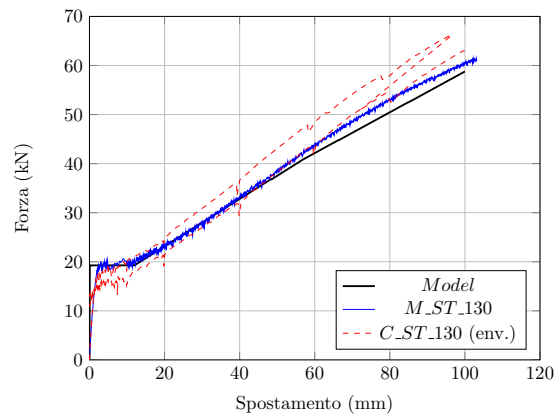


Figure 5.66: Model with single equivalent spring (a) - constitutive law of the equivalent spring (k_{eq}) (b).

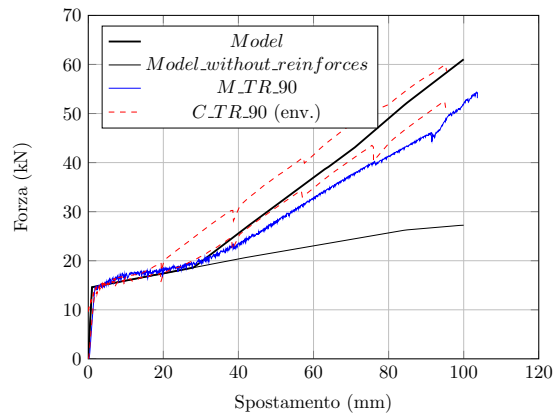


(a)

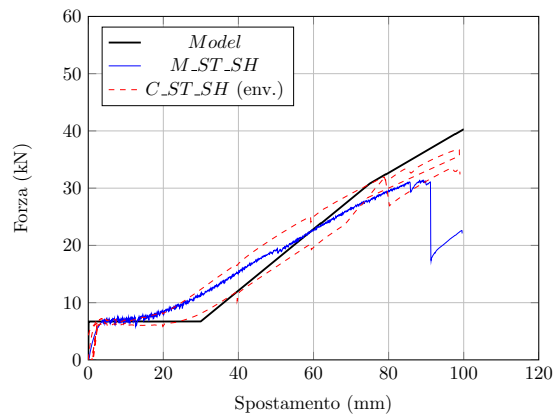


(b)

Figure 5.67: Comparison between model and test results (monotonic and envelope of the cyclic tests): force versus displacement of $M|C_{ST_90}$ (a) - $M|C_{ST_130}$ (b) .



(a)



(b)

Figure 5.68: Comparison between model and test results (monotonic and envelope of the cyclic tests): force versus displacement of $M|C_{TR_90}$ (a) - $M|C_{ST_SH}$ (b).

behaviour of the system is greatly improved. This solution is a suitable especially when a higher resistance of the wall is required or when the geometry of the building (few interlocks between walls).

The main technical advantages of this solution are attributable to the capacity of the fasteners to provides stiffness before that the contribution of the corner joints is active. This issue is crucial if the friction force between the log is neglected. Moreover if small diameters fasteners are adopted the failure mode is characterized by high ductility. On the other hand the disadvantages, besides the costs, are related to the compatibility with the shrinkage and the swelling of the logs.

Focusing on the use of self-tapping screws the reinforce system can be exploited both for the horizontal load carrying capacity and for the rocking mechanism. Thanks to the withdrawal capacity of these fasteners can balance the overturning moment introduced by the horizontal force (if the stabilizing moment due to the vertical load is overcome).

Shear reinforcement

If the reinforce system is designed to resist only to lateral loads the force on each fastener can be calculated as:

$$F_{v,Ed} = \frac{F}{n_{ef}}$$

Where F is the total force n_{ef} is the effective number of screws in the row. The load carrying capacity of the single fasteners, according to [46], can be calculated following the rules of the timber-to-timber connections. Assuming the geometry of a commercial product Table 5.18 the results are summarized in Table 5.19. The ultimate displacement of the screws were obtained from the research report [68].

Diameter	d	8 mm
Thread root diameter	d_n	5.4 mm
Effective diameter	d_{ef}	5.9 mm
Characteristic tensile strength	f_{uk}	1000 MPa
Yield moment	M_{yk}	31 Nm
Headside thickness	t_1	160 mm
Pointside penetration	t_2	80 mm
Characteristic timber density	ρ_{k1} e ρ_{k2}	$350 \frac{kg}{m^3}$

Table 5.18: *Geometry and materials adopted for the connection.*

If the equivalent spring that correspond to a total number of four screws between each log is implemented in the model the load versus displacement curves change as

Lateral load bearing capacity	$F_{v,Rk}$	4.2 kN
Slip modulus under service load	K_{SER}	2208 N/mm
Slip modulus for the ultimate limit state	K_u	1745 N/mm

Table 5.19: Mechanical parameters according to [46].

shown in Figure 5.69. The horizontal plateau is substituted by a inclined branch due to the stiffness of the screws. When the mounting tolerance is exceeded both screws and corner joint transfer the horizontal force to the other log.

Shear + tension reinforcement

If the withdrawal capacity of the reinforce system described in the previous paragraph is taken into account the axial force on each fasteners can be calculated as:

$$F_i = \frac{F \cdot h - P \frac{l}{2}}{k} \cdot (x_i - x)$$

$$k = \sum_{i=1}^n (x_i - x)^2 + \frac{x}{2} \cdot \sum_{i=1}^n (x_i - x)$$

Where F_i is the force on the i -th fasteners, F is the horizontal force, h and l are the heigh and the length of the wall, P is the vertical load, x_i is the distance between each connector and the center of rotation, x is the compression zone depth, b is the width of the logs.

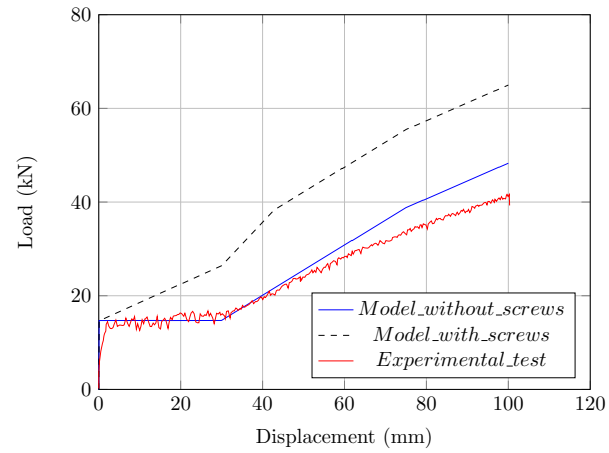
The load-carrying capacity of axially loaded screws is calculated as the minimum value between the withdrawal capacity of the threaded part, the pull-through strength of the screw head and the tension strength [46].

Outer diameter measured on the threaded part	d	8 mm
Thread root diameter	d_{no}	5.4 mm
Pointside penetration of the threaded part minus one screw diameter	l_{ef}	80 mm
Characteristic tensile strength	f_{uk}	1000 MPa
Characteristic withdrawal strength perpendicular to the grain;	$f_{ax,k}$	12.9 MPa
Characteristic timber density	ρ_k	350 $\frac{kg}{m^3}$

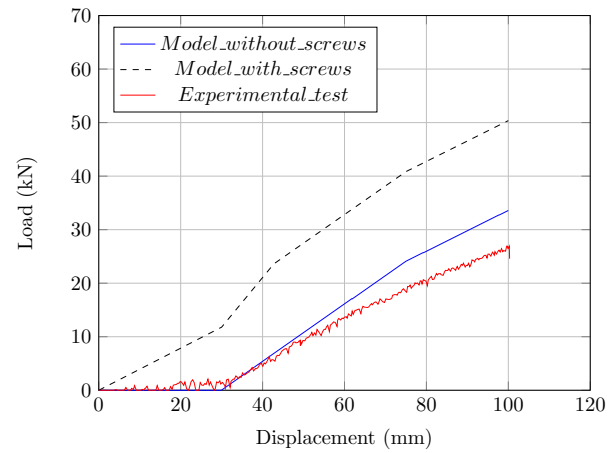
Table 5.20: Geometry and materials adopted for the connection.

Withdrawal capacity	$F_{ax,k,Rk}$	8.2 kN
Tension strength of the screw (thread root diameter)	$F_{u,k}$	22.1 kN
Pull-through strength of the screw head (washer 25mm/8.5mm)	F_{90}	3.2 kN

Table 5.21: Failure modes for axially loaded screws.



(a)



(b)

Figure 5.69: Influence of the reinforcement system: load vs displacement curves with friction contribution a) without friction contribution b).

According to table Table 5.21 the failure mode of the screw is related to the pull-through effect of the washer. However in order to compare the result with the experimental tests a mean value of 5 kN was adopted. In the presented load condition (shear $F_{v,Ed}$ + tension $F_{ax,Ed}$) according to [46] the ultimate condition is:

$$\left(\frac{F_{ax,Ed}}{F_{ax,Rd}}\right)^2 + \left(\frac{F_{v,Ed}}{F_{v,Rd}}\right)^2 \leq 1$$

where $F_{ax,Rd}$ and $F_{v,Rd}$ are the design load-carrying capacities of the connection.

The load vs displacement curve is obtained from the equilibrium equation considering the simultaneous presence of tensile force and shear on the connectors. The procedure can be summarized in the following steps:

- first has to be selected the position along the height of the wall h_k ;
- than the position across the wall z_i ;
- once fixed the level of horizontal force (an than the overturning moment M) the depth of the compressive zone x and the tensile forces on the screws in the different position k_i can be calculated;
- the displacement of the system taking into account the friction, gap, interlocks, screws components can be derived from:

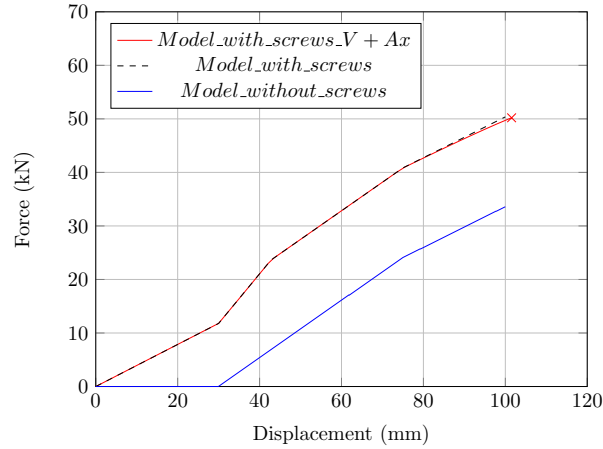
$$F_j = \begin{cases} P \cdot \mu_s + \sum_{i=1}^n F_{v,i} & \text{if } d \leq \text{gap} \\ P \cdot \mu_s + \sum_{i=1}^n F_{v,i} & d > \text{gap} \end{cases}$$

where $F_{v,i}$ is the is the lateral force on the i-th connector calculated as:

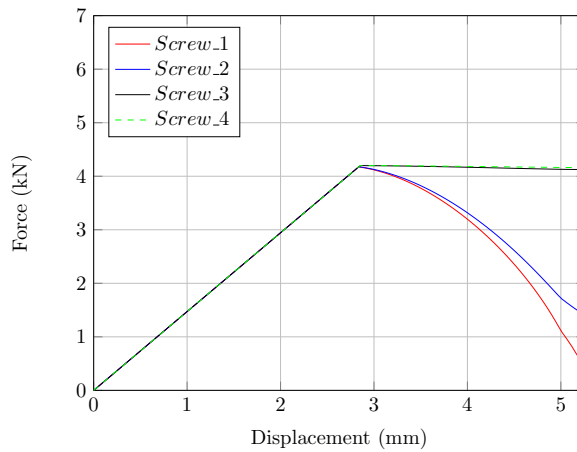
$$F_j = \begin{cases} k_s \cdot d & \text{if } d \leq d_y \text{ and } k_s \cdot d \leq F_{v,Max} \\ F_{v,Rd} & \text{if } d > d_y \text{ and } F_{v,Rd} \leq F_{v,Max} \\ F_{v,Max,i} & \text{if } F_{v,Rd} > F_{v,Max,i} \end{cases}$$

The aim of the previous formulae is the evaluation of the contribution of the connectors in the different range (elastic range, elasto-plastic range after d_y) considering the influence of the two limit resistance (lateral and lateral+axial resistance). The load displacement curve is obtained by the step summarized in the previous bullet-list by varying the F_j value from P_μ up to the failure of the most severely loaded screw in the group.

In order to highlight the influence of the tensile force on the fasteners the procedure was applied for three different cases. The first was the "standard case" considering both friction and vertical load contributions. In the second the friction force was neglected and so the vertical loads act only as stabilizing moment component. In the third the wall was not loaded by vertical forces.



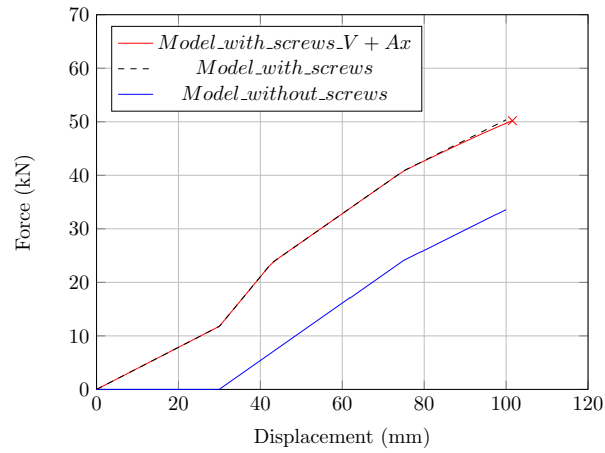
(a)



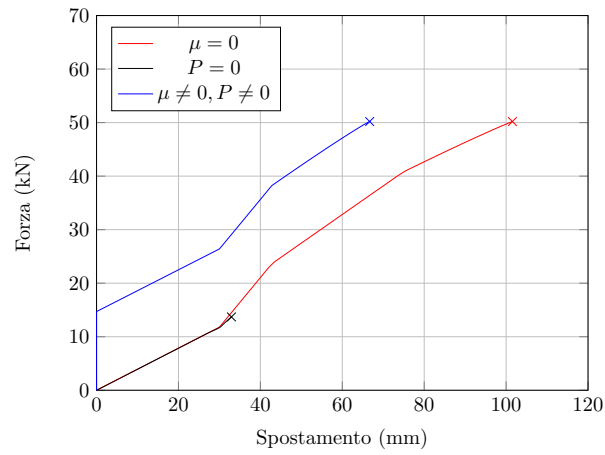
(b)

Figure 5.70: Results of the model for the 90 mm wall with Standard joints, with reinforce considering only the lateral behaviour or the combined action of axial and lateral forces ($V+Ax$) and without reinforce - load vs displacement curves a) - force vs displacement of the connectors b).

Figure 5.71 show the influence of the simultaneous axial and lateral loads on the reinforcement system. In other words if the connectors i.e. self-tapping screws supply



(a)



(b)

Figure 5.71: Results of the model for the 90 mm wall with Standard joint - without friction contribution a) - in the three different cases b).

both to the tension force (uplift due to the overturning moment) and horizontal load (seismic or wind force) the response of the reinforcement system is lower than the condition which only the lateral load bearing capacity is exploited. The gap between these two condition is emphasized in the unloaded wall ($P=0$ kN) where a maximum resistance of the reinforce system is about $13.7kN$ for a total displacement of $33mm$ instead of $50kN$ at $101mm$ ($P = 10.6kN$).

5.5 Discussion

The results summarized in the previous sections represent an initial step towards a deeper understanding of the horizontal in-plane load-bearing characteristics of log house constructions. The tests on the log house corner joints and on full-scale horizontal load bearing structures shows some relevant key features. In first, a mention have to be done on the reliability of the experimental data. The outcome of the tests on corner joints and the full-scale tests on walls shows the same resisting mechanisms and failure modes. Moreover the hysteresis loops were symmetric (symmetric distribution of the gaps) and the backbone curve of the cycles have been well approximated by the monotonic tests. These considerations are a good index of the efficiency of the test apparatus. The recorded data have been used to compare the efficiency of the different corner joint and to obtain some information about the behaviour of the short walls and the influence of the openings. Also the efficiency of a reinforce system was tested.

The friction between logs had a strongly influence on the load-displacement path. Therefore, the typical advantages and disadvantages of this resistant mechanism have to be considered. The system exhibit a good energy dissipation and a low impairment of strength. Nevertheless, the post-friction plateau characterized by a low-rise slope introduce an undesirable behaviour (governed only by the dynamic friction). Another issue was related to the permanent deformation after which the static friction was overcome (no restoring forces mechanisms provided). The most effective corner joint was the "standard" type (ST). The size of the cross section influenced the results. For the thinner logs a brittle shear failure had occurred while for the thicker one a ductile failure mechanisms related to the crushing of the fibres due to the compression orthogonal to the grain had occurred. The difference in terms of maximum load is about $20kN$ (32%). Moreover the mounting tolerance for the thicker logs (130mm) was lower.

Compared to the ST layout the Tiroler schloss corner joints (TR), during the test on corner joints, have shown lower stiffness and resistance. Therefore a reinforcement system could be a convenient solution when a high resistance is needed. The dovetail reinforcement system have shown good results during the full-scale tests on the walls and obtaining an overall behaviour similar to the standard configuration. However, as can be seen in Figure 5.25 the mounting tolerance affect also this connection therefore the low slope part of the curve was present in this configuration. The difference in terms of ultimate load, which correspond to a total displacement of

100mm, was about 12kN or 22 % (type ST sustained 41.4kN, whereas wall type TR sustained 53.2kN).

Two tests were performed on walls with openings in order to investigate the influence of the discontinuity on the mechanical behaviour. Some interesting conclusion were highlighted. The rocking effects on the two external parts of the walls near the openings lead to a lower stiffness and ultimate load bearing capacity and an to a increase of the forces on both anchoring systems. The effects of the permanent slip between the logs in the central parts were clearly visible during the tests Figure 5.50. The proposed simplified model was introduced to implement the behaviour of the single component suitable to predict the system response. The test results shows a good agreement with the analytical predictions. The main advantages of the "component method" is that the results can be easily interpreted and verified. A good agreement was found between the model outcome and the experimental data. Furthermore the models allowed interesting valuations on the behaviour in the presence of additional connectors (i.e. Self-tapping screws or dowels). The use of these connectors improves the capacity of the system and reduce the influence of the mounting tolerances. From this point of view the use of screws is more effective than the dovetails because the reinforcement is immediately activated (there are no additional gaps). Moreover if properly designed, taking into account the shrinkage and the swelling, the screws can also be used to reduce the effect of relative uplift between the logs.

The use of the reinforce system as self-tapping screws fills this lack and guarantee a most efficient and predictable behaviour. However deeper investigation must be carried out about the interaction of the walls in a real tri-dimensional building. These further studies on the LH constructive system will help to address the uncertainties related to the lateral loads design.

5.6 Conclusions

The horizontal and the vertical load bearing capacity of the LH as demonstrated by the tests summarized in this section are lower than the modern constructive system such as platform frame (light timber framing or CLT) or heavy timber frame buildings.

Moreover the ultimate resistance is strongly related to the timber connection properties and to its failure modes often due to shear failure of the interlocks (for the thinner logs) or to the crushing of the fibre in the transversal element (thicker logs). This

fact introduces the typical problems of the timber joints, as the presence of defects (knots, cracks) and the dependence of the resistance from the number of elements involved (weak link theory, Weibull). Moreover the limits introduced by the dimensional variation caused by the timber moisture changing require careful design of all the construction details and the constant monitoring of more complex structures. The choice of this type of structure must be carefully considered because a great attention must also be given to trivial aspects. As an example, according to the brief discussion reported in the other chapters, a rigid element cannot be fixed with rigid connections on the walls. The typical example is represented by the presence of fireplaces or other masonry structures, or more simply by furnishings that can not be fixed rigidly to the walls at different heights. Furthermore a periodical monitoring should be conducted on the main critical points of the structure (adjustable joints of the column, installations etc ..).

On the other hand the LH are widely and successfully used since the mediaeval age in all the central and Nordic regions of the globe. The seismic resistance in these, zone characterized by low seismicity, is a less stringent requirement compared to problems related to the movements due to the variation of moisture. Furthermore only one or two storey buildings are constructed with this system. The results illustrated in the previous chapters demonstrate that this system is capable to resist to seismic events. An interesting possibility to improve the characteristics of the system is given by the use of additional connectors between the logs. This solution must be taken into account especially for the Tirolerschloss, which during the tests shows a high deformability and a low load bearing capacity. Another topic discussed in this part of the thesis deals the possibility of using simple models. These analytical models have the advantage of representing all the stages without losing the accuracy of the most sophisticated modelling. The interpretation of the results of the analysis can be easily controlled and extension to buildings is not computationally demanding.

Appendix A

Common definition

The most common testing procedure in structural and earthquake engineering is the quasi-static testing, because of its relative simplicity and cost effectiveness. The term "quasi-static" testing indicates the the loads are applied at rates slow enough so that the material strain rate effects do not affect the results. Two different types of displacement-controlled, quasi-static tests have been carried out in line with the technical standard EN 12512 [64] and EN 26891 [69]: monotonic and cyclic. In particular, the displacement-controlled execution provides the application of a displacement with constant loading velocity in one or both directions. In accordance with Standard UNI EN 12512 [64], following values are used to analyse the results obtained from the monotonic and cyclic tests:

F_{max}	maximum load under monotonic loading;
F_y	yield load;
V_y	yield slip;
F_u	ultimate load;
V_u	ultimate slip;
D	ductility;
F_{max}^+	maximum load on the tensile side under cyclic loading;
F_{max}^-	maximum load on the compression side under cyclic loading;
E_d	energy dissipated per half cycle;
E_p	available potential energy;
ΔF	impairment of the strength.
ν_{eq}	equivalent viscous damping ratio which measures the dissipation of energy;

Yield load Depending on the respective curve shape, the yield load is determined as show below:

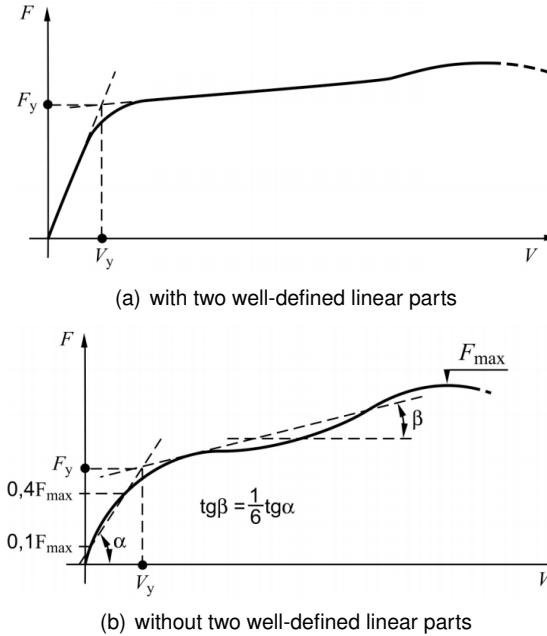


Figure A.1: Definition of yield values for load-sup curves [64].

Ultimate load The ultimate load value corresponds to (see Figure A.2):

- (a) failure; or
- (b) 80 % of the maximum load as a slip of less than 30mm; or
- (c) a joint slip of 30 mm whichever occurs first in the test.

According to the definition of the EN 26891 the maximum displacement during a monotonic test is 15 mm. This is fixed on the basic assumption that for this level of displacement the structure, of which the connection part, reaches the collapse due to excessive deformation. Nevertheless this limit for the analysis of connection under seismic load condition is not correct because the full load bearing capacity is not reached. Especially for dowel type fasteners the connection reach the ultimate value of strength for higher values. Thus the limits indicates in the first part of the UNI EN 12512 are adopted also in the monotonic tests.

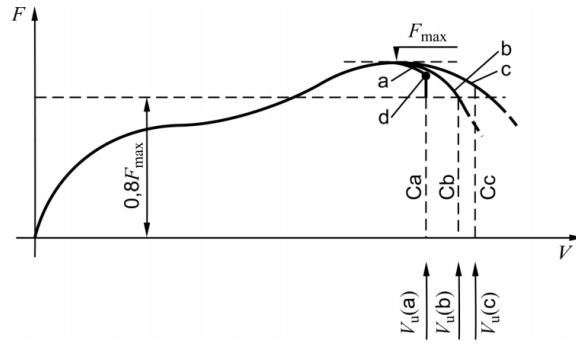


Figure A.2: Definition of ultimate values [64].

Ductility Representing the ability of a joint to undergo large amplitude slip in the plastic range without a substantial reduction of strength, ductility is one important indicator of how a structure will perform during an earthquake. It is measured by the ratio between ultimate slip and yield slip [64],

$$D = \frac{V_u}{V_y}. \quad (14)$$

Impairment of the strength Defined as the reduction in the load when attaining a given joint slip from the initial (1st) to the final (3rd) cycle of the same amplitude, this property indicates the ability of a connection or structure to sustain large deformation without significant strength deterioration.

Equivalent viscous damping ratio This measure provides a means with which to describe the energy dissipation characteristics, in other words, the ability to reduce the seismic input energy. It is measured as the ratio between the dissipated energy in one half cycle E_d , also known as hysteretic damping, and the available potential energy E_p , thus, determined by the equation:

$$\nu_{eq} = \frac{E_d}{2\pi \cdot E_p} \quad (15)$$

A.0.1 Test-protocol

The monotonic test protocol is implemented through an imposed displacement applied at a fixed velocity. This displacement vs time ratio is maintained constant dur-

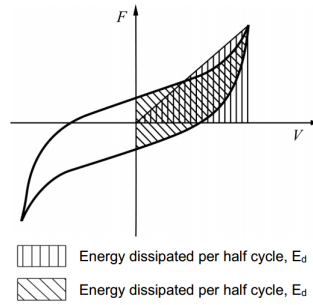


Figure A.3: Definition of equivalent viscous damping ratio for one cycle [64].

ing the test. For the cyclic test, on the other hand, different velocities were assumed according to the initial and final cycles. The amplitude for each set of cycles referred to the conventional slip was determined on the basis of results of static tests which have been carried out with samples of the same geometry and constraints.

Indispensable for a correct analysis according to the valid test protocols are:

- speed of progress of the jack,
- reference slip to evaluate the amplitude of the cycles,
- sequence of the various cycles, speed of progress, number of repetitions.

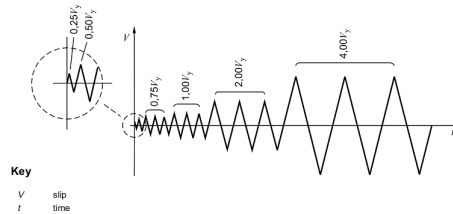


Figure A.4: Loading procedure adopted for the cyclic tests [64].

For the joint where the fully-cyclic behaviour is impossible because a fixed constraint prevent the reverse loading (i.e. the foundation for the hold-down device) a semi-cyclic protocol is defined. This time-displacement history is defined from zero up to the same stage of the fully cyclic procedure with the same number of repetitions.

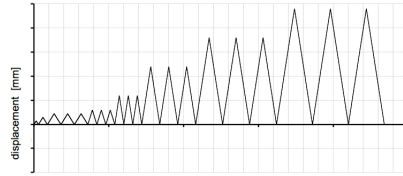


Figure A.5: Loading procedure adopted for the semi-cyclic tests.

Appendix B

Corner joint Tests

B.1 Timber Density/moisture

Test no.	Specimen ID code	W [mm]	L [mm]	H [mm]	V [cm ³]	Weight [g]	Density [kg/m ³]	Mean value [kg/m ³]
1	A1	117	89	68	708.1	284.80	402.2	407.7
	A	117	90	145	1526.9	630.89	413.2	
2	B1	117	129	68	1026.3	492.00	479.4	463.4
	B	117	129	143	2158.3	965.83	447.5	
3	C1	117	89	67	697.7	364.13	521.9	524.0
	C	117	89	143	1489.1	783.45	526.1	
4	D1	117	89	68	708.1	284.78	402.2	412.3
	D	117	89	144	1499.5	633.40	422.4	
5	E1	117	129	68	1026.3	437.45	426.2	437.2
	E	117	129	143	2158.3	967.32	448.2	
6	F1	117	129	68	1026.3	492.11	479.5	460.5
	F	117	129	143	2158.3	952.93	441.5	
7	E1	117	90	68	716.0	381.22	532.4	500.90
	E	117	90	144	1516.3	711.74	469.4	
8	G1	117	90	67	705.5	314.20	445.4	416.4
	G	117	89	144	1499.5	580.94	387.4	
9	H1	117	129	68	1026.3	500.10	487.3	464.4
	H	117	129	144	2173.4	959.55	441.5	
10	I1	117	129	68	1026.3	453.48	441.8	440.4
	I	117	129	143	2158.3	947.56	439.0	
13	D1	117	89	69	718.5	340.88	474.4	468.3
	D	117	89	137	1426.6	659.18	462.1	
14	A1	117	129	78	1177.3	532.43	452.3	454.4
	A	117	129	143	2158.3	985.46	456.6	
15	B1	117	88	69	710.4	302.19	425.4	437.1
	B	117	90	137	1442.6	647.37	448.7	
16	E1	117	88	69	710.4	342.78	482.5	475.8
	E	117	90	137	1442.6	676.70	469.1	
17	D1	117	129	79	1192.3	542.19	454.7	481.8
	D	117	129	101	1519.9	773.36	508.8	
18	E1	117	129	79	1192.3	531.32	445.6	461.9
	E	117	128	93	1392.8	666.04	478.2	
19	C1	117	88	69	710.4	336.40	473.5	453.0
	C	117	136	89	1416.2	612.37	432.4	
20	A1	117	89	69	718.5	317.66	442.1	438.3
	A	117	83	90	874.0	379.78	434.5	
21	F1	117	128	79	1183.1	543.12	459.1	467.6
	F	117	129	143	2158.3	1027.77	476.2	
22	B1	117	129	79	1192.3	535.68	449.3	461.6
	B	117	129	143	2158.3	1022.90	473.9	
24	C1	117	68	76	604.7	298.22	493.2	484.0
	C	117	129	143	2158.3	1024.62	474.7	

Table B.1: Specimens density.

B.2 Photo documentation

B.3 Corner joint *Standard*



Figure B.2: *Lateral crushing of the contact surface.*

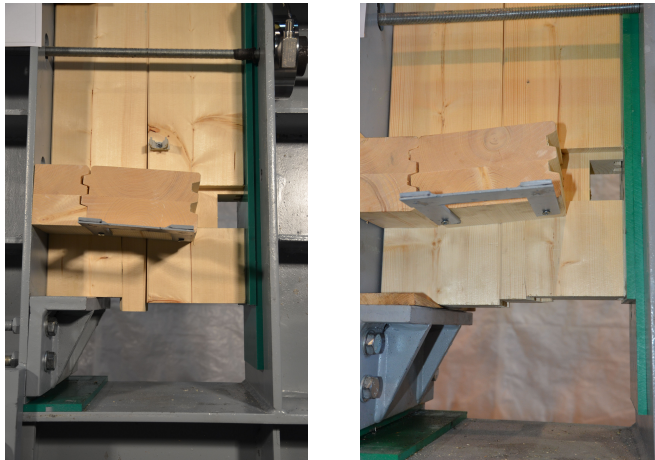


Figure B.3: *Shear failure along the grain.*



(a) Compression loading



(b) Tensile loading

Figure B.4: *Shear failure along the grain.*



Figure B.5: *Tensile failure along the grain due to longitudinal tensile stress.*

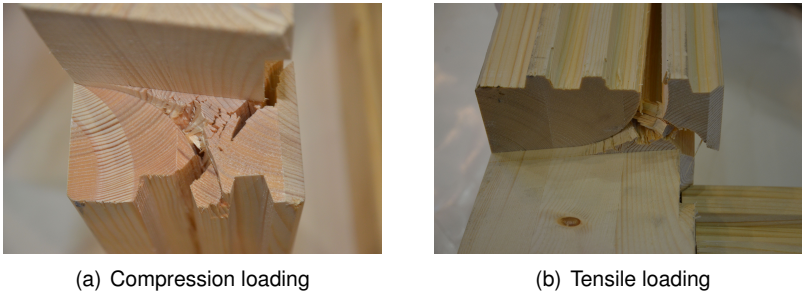
Test no.	Specimen ID code	Moisture Content														Mean value	
		[%]															
1	A	15.0	15.3	14.9	13.6	13.5	13.6	15.1	15.6	15.4	13.6	13.8	14.0	14.1	14.4	14.6	14.4
2	B	15.2	14.8	15.1	14.7	14.5	15.0	14.7	14.8	14.7	15.2	15.0	14.8				14.9
3	C	14.1	14.8	14.1	13.4	12.1	12.8	13.3	14.1	14.4	14.2	14.4	11.1	12.5	12.2	12.6	12.8
4	D	13.2	13.8	12.9	13.5	13.7	13.7	13.8	14.2	14.0	13.7	12.8	13.0	13.0	13.7	13.4	13.7
5	E	15.4	15.9	14.5	15.2	14.7	14.3	14.7	14.7	15.2	15.2	11.4	13.6	14.1	14.2	15.8	16.2
6	F	15.0	14.6	16.5	15.9	15.4	15.3	14.2	14.5	16.0	16.4	16.4	15.2	15.3	16.3	15.9	16.8
7	E	14.7	13.2	13.2	13.8	14.8	14.5	13.2	14.1	14.1	14.0	13.3	14.1	13.4	12.8	14.4	14.2
8	G	13.9	14.5	14.8	14.2	14.2	13.8	13.7	13.5	14.5	15.0	14.7	15.5	15.1	16.0	15.5	15.1
9	H	15.1	15.1	15.6	15.5	15.8	14.9	15.0	15.6	14.9	16.2	13.8	14.1	15.2	15.1	14.7	14.6
10	I	14.9	15.2	15.6	14.6	16.0	14.8	15.7	15.4	15.1	16.0	14.7	15.5	15.3	14.5	16.2	14.6
13	D	14.2	14.9	14.6	14.0	15.1	11.6	15.3	15.4	15.5	15.5	16.8	16.3	15.2	14.8	14.9	15.2
14	A	15.5	16.0	16.8	15.4	15.2	15.8	16.6	15.4	15.1	15.5	15.6	15.7	15.0	14.5	15.5	16.1
15	B	14.1	14.7	15.4	15.4	14.5	14.5	13.4	13.2	14.0	15.0	15.6	15.2	13.5	13.8	12.9	12.9
16	E	14.3	14.5	14.3	14.9	14.6	15.0	14.4	13.5	16.5	16.9	15.4	15.5	14.8	14.8	14.4	13.9
17	D	15.0	15.1	16.2	16.3	15.1	15.1	16.0	15.8	16.2	15.9	14.2	15.3	15.9	15.7	15.7	15.1
18	E	15.4	14.7	16.1	16.0	14.7	14.5	15.3	15.5	15.9	15.9	15.3	14.7	15.4	15.0	15.2	15.4
19	C	15.9	15.7	15.7	15.6	15.3	16.0	16.3	16.2	14.3	14.5	15.4	14.9	13.4	13.2	12.8	12.4
20	A	14.6	14.7	12.0	12.4	13.5	13.7	13.5	12.9	14.9	14.4	13.0	13.5	13.8	14.7	14.7	15.2
21	F	15.0	15.1	16.0	16.2	14.6	15.5	15.4	15.6	15.1	14.4	15.8	15.4	15.5	16.4	16.5	15.2
22	B	14.0	14.5	15.6	16.9	14.0	14.6	14.9	14.5	15.1	15.4	14.8	14.8	15.0	16.2	16.8	15.7
24	C	15.9	16.4	14.4	14.7	16.1	14.1	13.6	14.7	15.2	16.2	15.4	15.5	16.9	16.8	14.6	14.1

Table B.2: Specimens wood moisture.

B.4 Corner joint *Tiroler Schloss*



Figure B.6: Splitting caused by semi-circular leafs and protrusions provided for protection against wind and rain.



(a) Compression loading

(b) Tensile loading

Figure B.7: Splitting caused by semi-circular leafs and protrusions provided for protection against wind and rain.

B.5 Dovetail reinforcement system

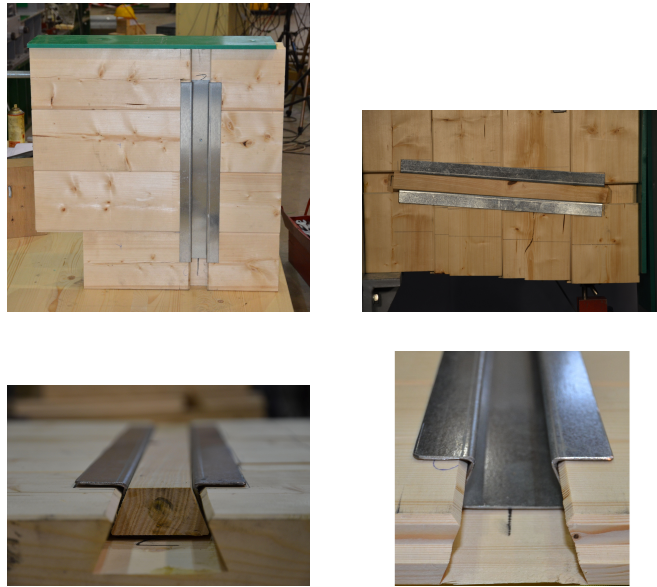


Figure B.8: *Reinforce system.*

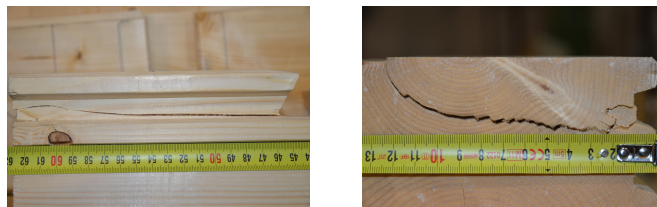


Figure B.9: *Shear failure along the grain².*

²This failure type occurred only at displacements larger than 30 mm.

Appendix C

Shear Walls

C.0.1 Monotonic test: M_ST_90

SPECIMEN CHARACTERISTICS	
Corner joint	STANDARD
Thickness	90 [mm]
Vertical Load	Uniformly distributed load 10.6 [kN/m]
Layout	-
Wall length	4.20 [m]
Load cell pre-load_Est	4.7 [kN]
Load cell pre-load_Ovest	2.0 [kN]
Laboratory notes	
The top log was connected only by means of screws; initial tightening of the LC nr.4 was 2 kN (no-effect on the test monotonic test because), All the curves were defined by the transducer 14 instead of transducer 2.	

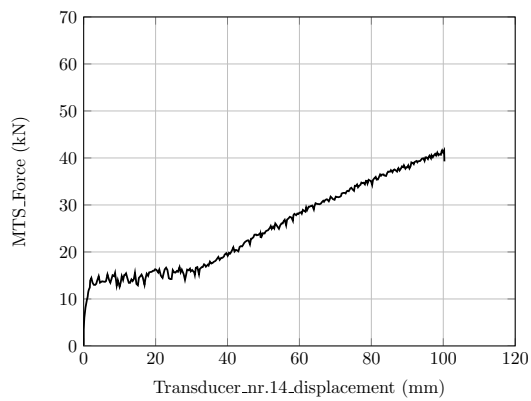


Figure C.1: Horizontal imposed displacement (tr. nr. 14) - Load (tr. nr. 1).

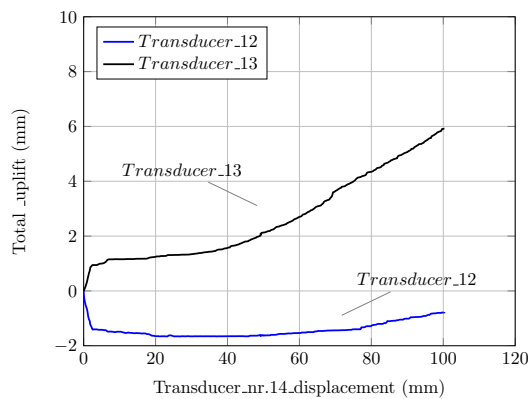


Figure C.2: Horizontal imposed displacement (tr. nr. 14) - Total displacement (tr. nr. 12/13).

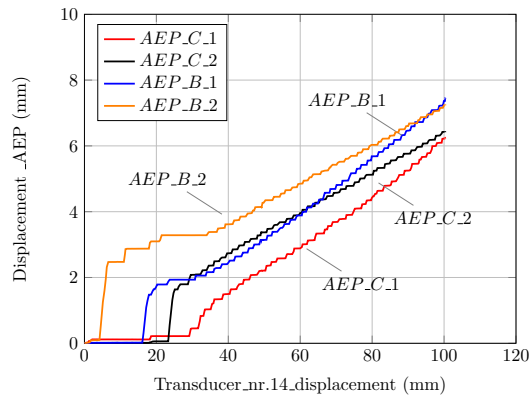


Figure C.3: Horizontal imposed displacement (tr. nr. 14) - Displacement AEP (tr. nr. 5/6/7/8).

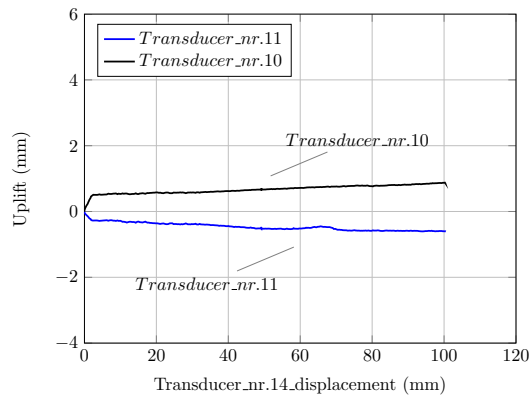


Figure C.4: Horizontal imposed displacement (tr. nr. 14) - Uplift (tr. nr. 10/11).

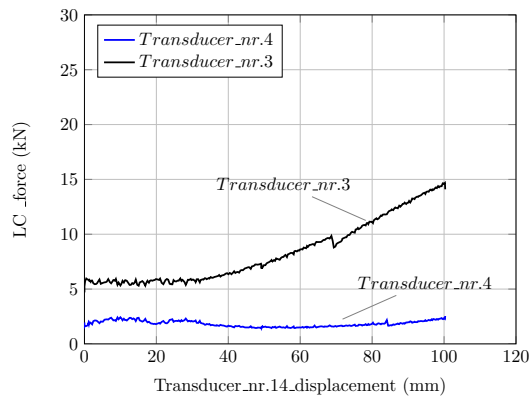


Figure C.5: Horizontal imposed displacement (tr. nr. 14) - Load cell force (tr. nr. 3/4).

C.0.2 Monotonic test: M_ST_OP

SPECIMEN CHARACTERISTICS	
Corner joint	STANDARD
Thickness	90 [mm]
Vertical Load	Uniformly distributed load 10.6 [kN/m]
Layout	parete con aperture
Wall length	4.20 [m]
Load cell pre-load_Est	5.35 [kN]
Load cell pre-load_Ovest	4.9 [kN]

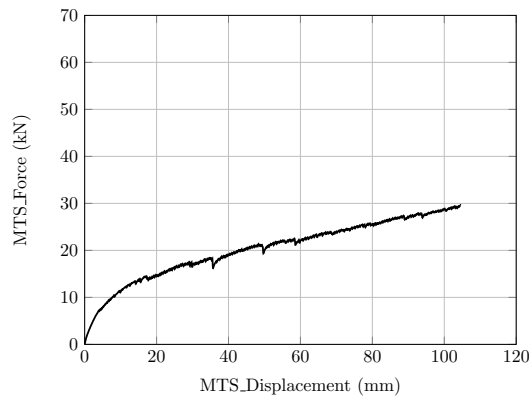


Figure C.6: Horizontal imposed displacement (tr. nr. 2) - Load (tr. nr. 1).

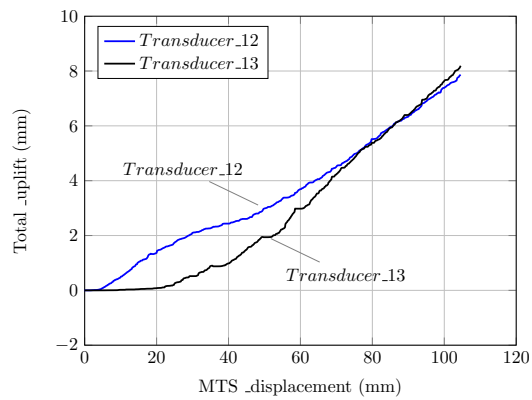


Figure C.7: Horizontal imposed displacement (tr. nr. 2) - Total displacement (tr. nr. 12/13).

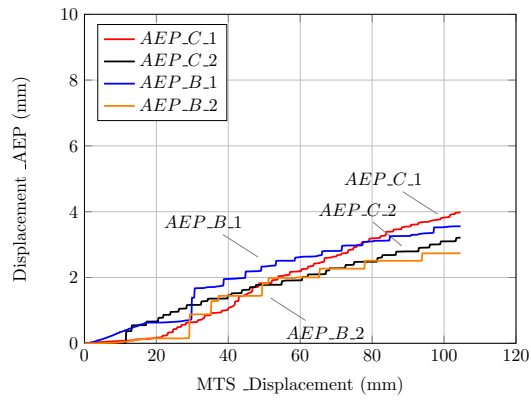


Figure C.8: Horizontal imposed displacement (tr. nr. 2) - Displacement AEP (tr. nr. 5/6/7/8).

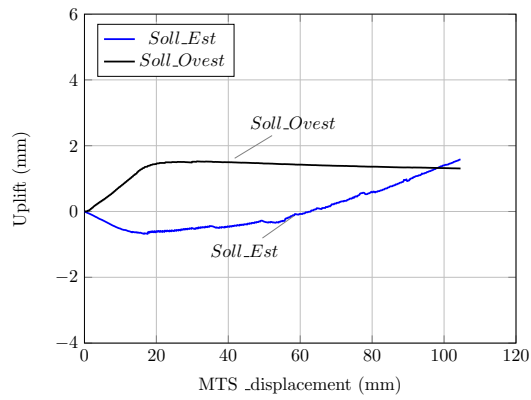


Figure C.9: Horizontal imposed displacement (tr. nr. 2) - Uplift (tr. nr. 10/11).

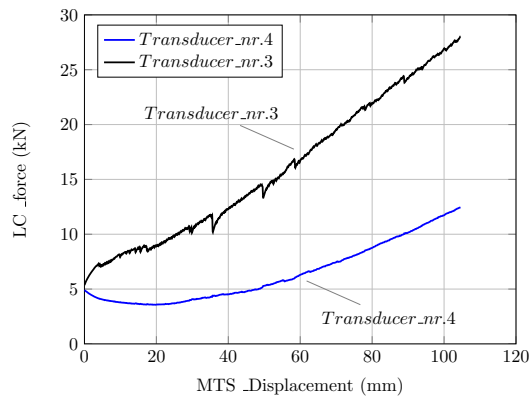


Figure C.10: Horizontal imposed displacement (tr. nr. 2) - Load cell force (tr. nr. 3/4).

C.0.3 Monotonic test: M_TR_90

SPECIMEN CHARACTERISTICS	
Corner joint	Tirolerschloss
Thickness	90 [mm]
Vertical Load	Uniformly distributed load 10.6 [kN/m]
Layout	rinforzi a coda di rondine
Wall length	4.02 [m]
Load cell pre-load_Est	4.77 [kN]
Load cell pre-load_Ovest	5.49 [kN]

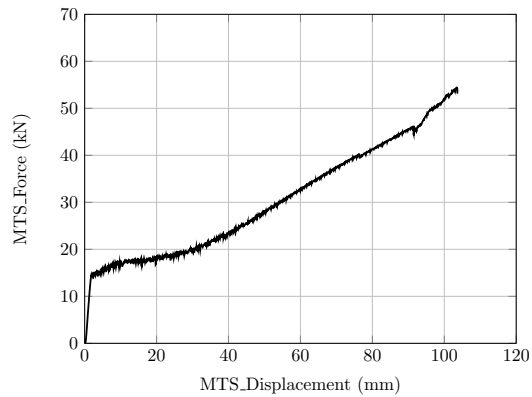


Figure C.11: Horizontal imposed displacement (tr. nr. 2) - Load (tr. nr. 1).

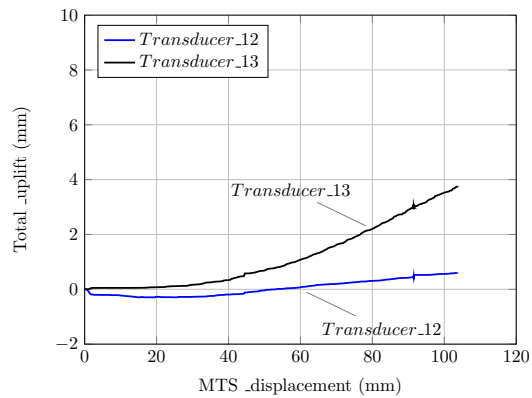


Figure C.12: Horizontal imposed displacement (tr. nr. 2) - Total displacement (tr. nr. 12/13).

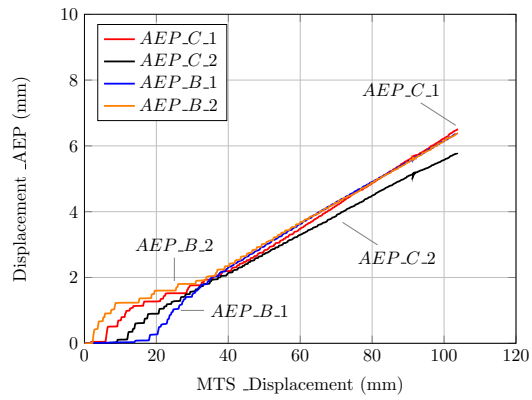


Figure C.13: Horizontal imposed displacement (tr. nr. 2) - Displacement AEP (tr. nr. 5/6/7/8).

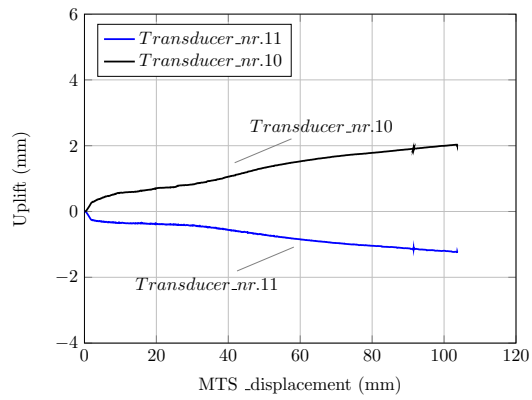


Figure C.14: Horizontal imposed displacement (tr. nr. 2) - Uplift (tr. nr. 10/11).

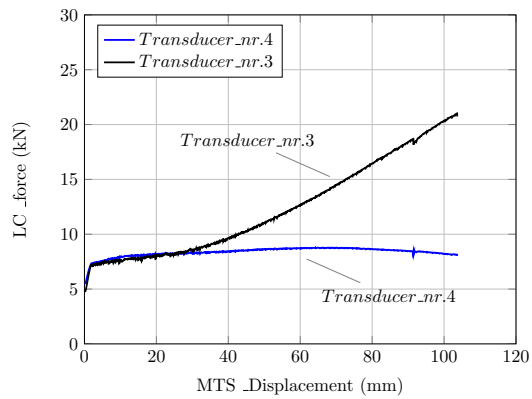


Figure C.15: Horizontal imposed displacement (tr. nr. 2) - Load cell force (tr. nr. 3/4).

C.0.4 Monotonic test: M_ST_130

SPECIMEN CHARACTERISTICS	
Corner joint	STANDARD
Thickness	130 [mm]
Vertical Load	Uniformly distributed load 10.6 [kN/m]
Layout	-
Wall length	4.31 [m]
Load cell pre-load_Est	5.12 [kN]
Load cell pre-load_Ovest	5.11 [kN]

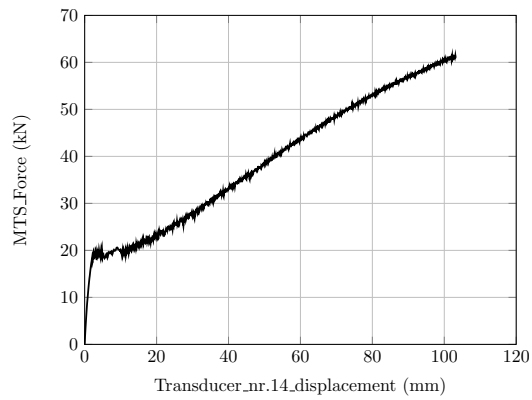


Figure C.16: Horizontal imposed displacement (tr. nr. 14) - Load (tr. nr. 1).

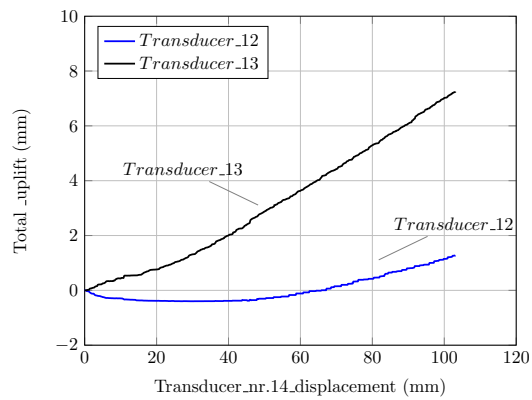


Figure C.17: Horizontal imposed displacement (tr. nr. 14) - Total displacement (tr. nr. 12/13).

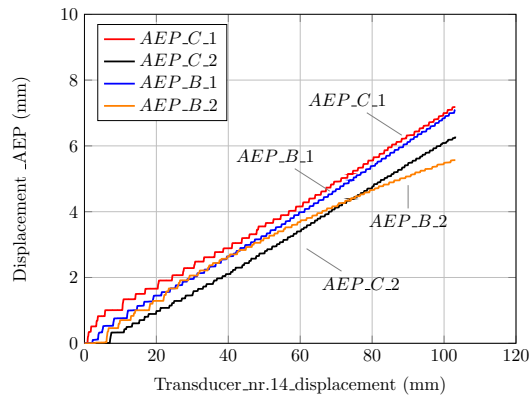


Figure C.18: Horizontal imposed displacement (tr. nr. 14) - Displacement AEP (tr. nr. 5/6/7/8).

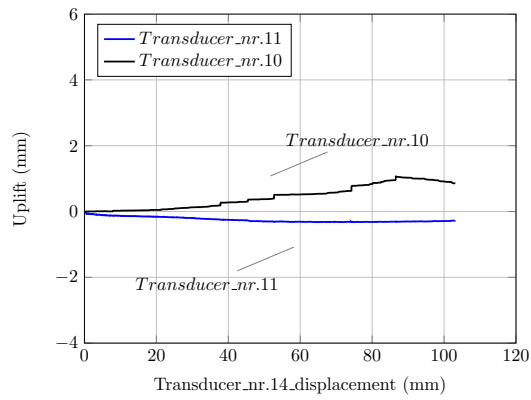


Figure C.19: Horizontal imposed displacement (tr. nr. 14) - Uplift (tr. nr. 10/11).

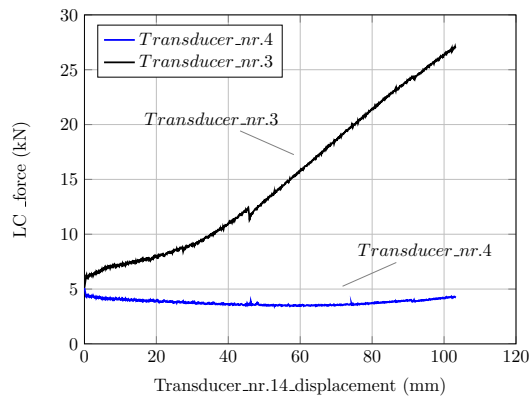


Figure C.20: Horizontal imposed displacement (tr. nr. 14) - Load cell force (tr. nr. 3/4).

C.0.5 Monotonic test: M_ST_SH

SPECIMEN CHARACTERISTICS	
Corner joint	STANDARD
Thickness	90 [mm]
Vertical Load	Uniformly distributed load 6.0 [kN/m]
Layout	-
Wall length	2.785 [m]
Load cell pre-load_Est	4.97 [kN]
Load cell pre-load_Ovest	5.14 [kN]

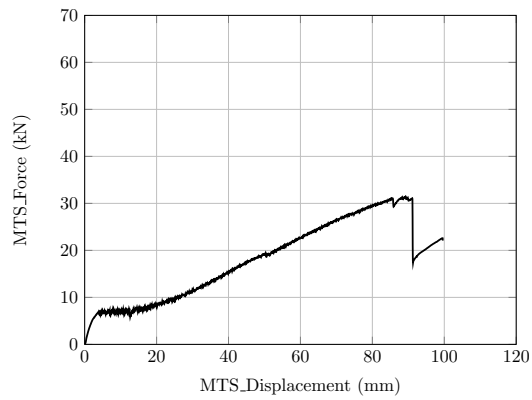


Figure C.21: Horizontal imposed displacement (tr. nr. 2) - Load (tr. nr. 1).

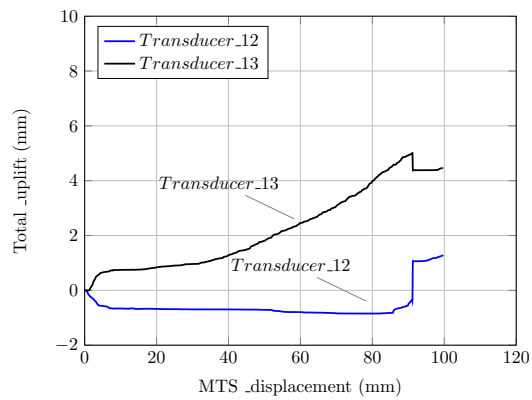


Figure C.22: Horizontal imposed displacement (tr. nr. 2) - Total displacement (tr. nr. 12/13).

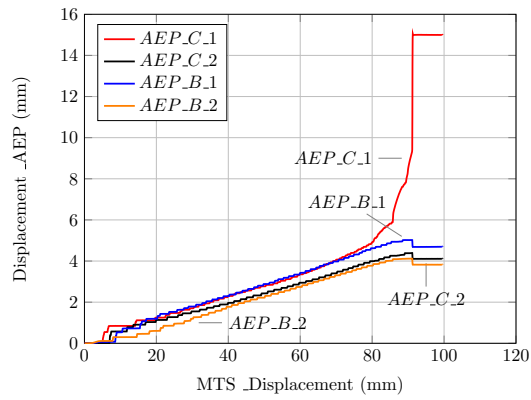


Figure C.23: Horizontal imposed displacement (tr. nr. 2) - Displacement AEP (tr. nr. 5/6/7/8).

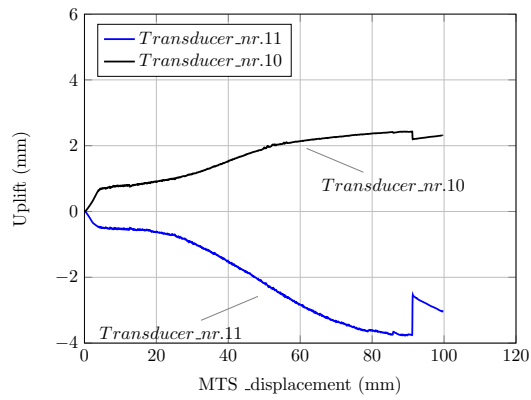


Figure C.24: Horizontal imposed displacement (tr. nr. 2) - Uplift (tr. nr. 10/11).

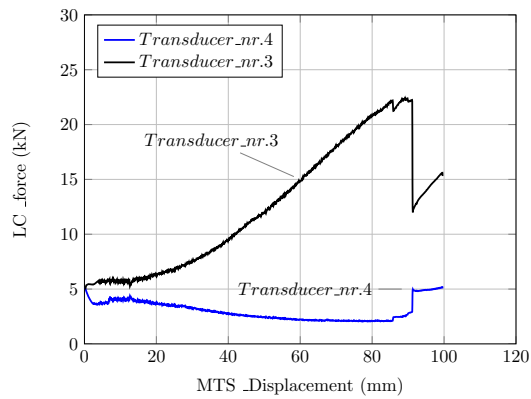


Figure C.25: Horizontal imposed displacement (tr. nr. 2) - Load cell force (tr. nr. 3/4).

C.0.6 Cyclic test: C_ST_90

SPECIMEN CHARACTERISTICS	
Corner joint	STANDARD
Thickness	90 [mm]
Vertical Load	Uniformly distributed load 10.6 [kN/m]
Layout	-
Wall length	4.20 [m]
Load cell pre-load_Est	4.8 [kN]
Load cell pre-load_Ovest	4.75 [kN]

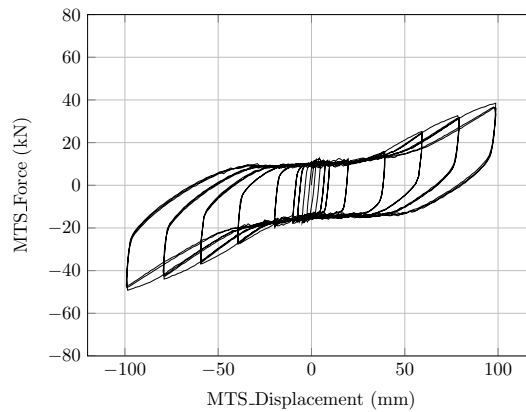


Figure C.26: Horizontal imposed displacement (tr. nr. 2) - Load (tr. nr. 1).

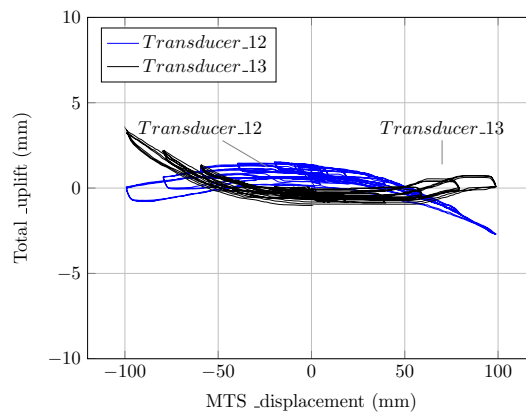


Figure C.27: Horizontal imposed displacement (tr. nr. 2) - Total displacement (tr. nr. 12/13).

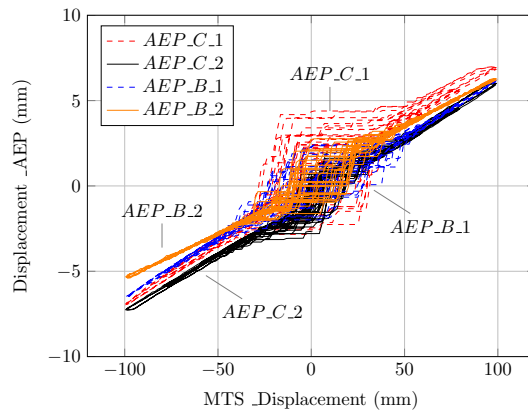


Figure C.28: Horizontal imposed displacement (tr. nr. 2) - Displacement AEP (tr. nr. 5/6/7/8).

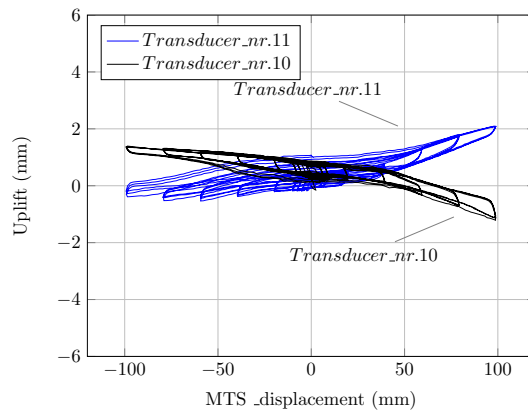


Figure C.29: Horizontal imposed displacement (tr. nr. 2) - Uplift (tr. nr. 10/11).

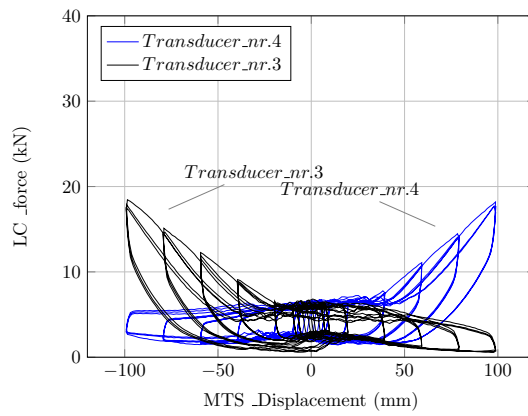


Figure C.30: Horizontal imposed displacement (tr. nr. 2) - Load cell force (tr. nr. 3/4).

C.0.7 Cyclic test: C_ST_OP

SPECIMEN CHARACTERISTICS	
Corner joint	STANDARD
Thickness	90 [mm]
Vertical Load	Uniformly distributed load 10.6 [kN/m]
Layout	parete con aperture
Wall length	4.20 [m]
Load cell pre-load_Est	4.95 [kN]
Load cell pre-load_Ovest	5.46 [kN]

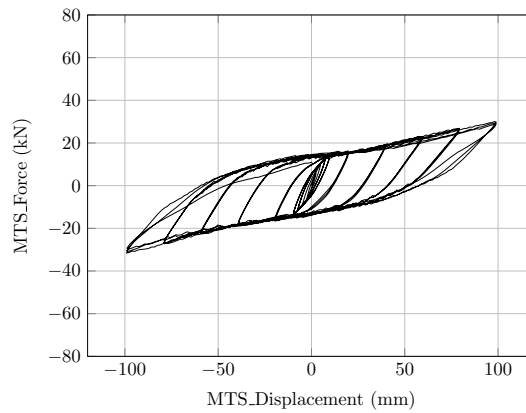


Figure C.31: Horizontal imposed displacement (tr. nr. 2) - Load (tr. nr. 1).

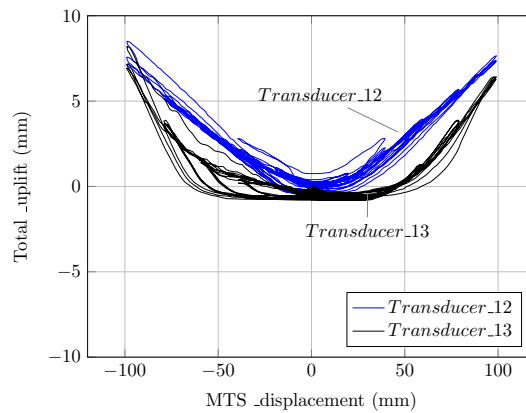


Figure C.32: Horizontal imposed displacement (tr. nr. 2) - Total displacement (tr. nr. 12/13).

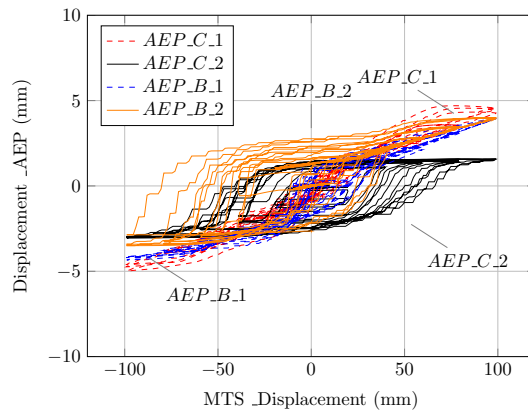


Figure C.33: Horizontal imposed displacement (tr. nr. 2) - Displacement AEP (tr. nr. 5/6/7/8).

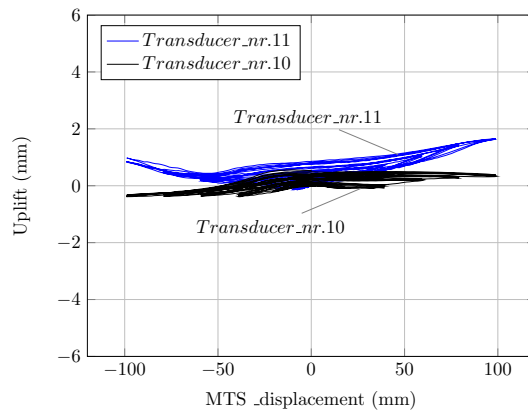


Figure C.34: Horizontal imposed displacement (tr. nr. 2) - Uplift (tr. nr. 10/11).

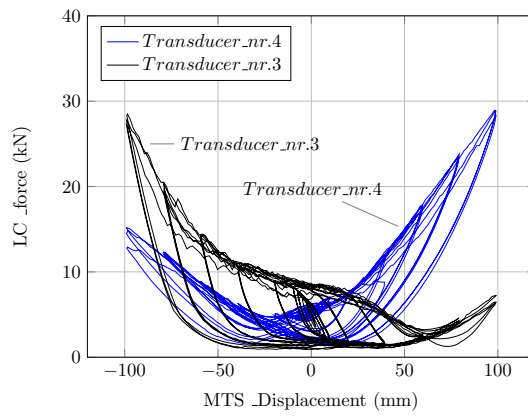


Figure C.35: Horizontal imposed displacement (tr. nr. 2) - Load cell force (tr. nr. 3/4).

C.0.8 Cyclic test: C_TR_90

SPECIMEN CHARACTERISTICS	
Corner joint	Tirolerschloss
Thickness	90 [mm]
Vertical Load	Uniformly distributed load 10.6 [kN/m]
Layout	rinforzi a coda di rondine
Wall length	4.02 [m]
Load cell pre-load_Est	5.1 [kN]
Load cell pre-load_Ovest	5.6 [kN]

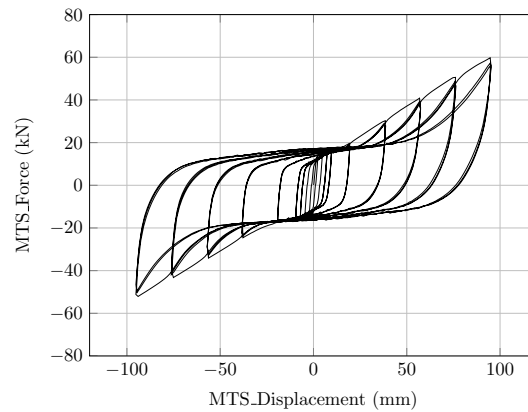


Figure C.36: Horizontal imposed displacement (tr. nr. 2) - Load (tr. nr. 1).

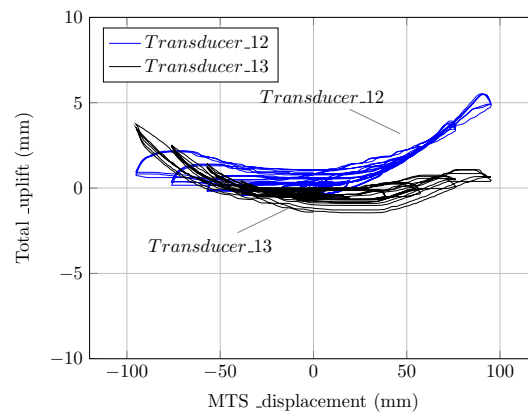


Figure C.37: Horizontal imposed displacement (tr. nr. 2) - Total displacement (tr. nr. 12/13).

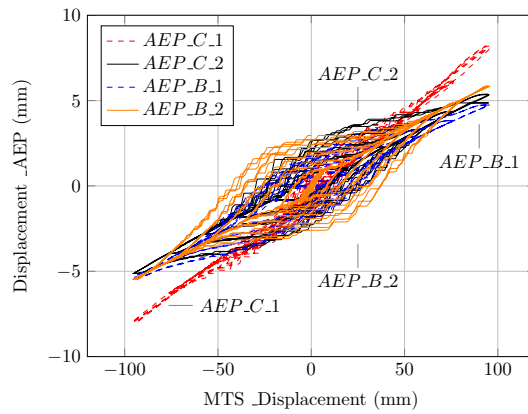


Figure C.38: Horizontal imposed displacement (tr. nr. 2) - Displacement AEP (tr. nr. 5/6/7/8).

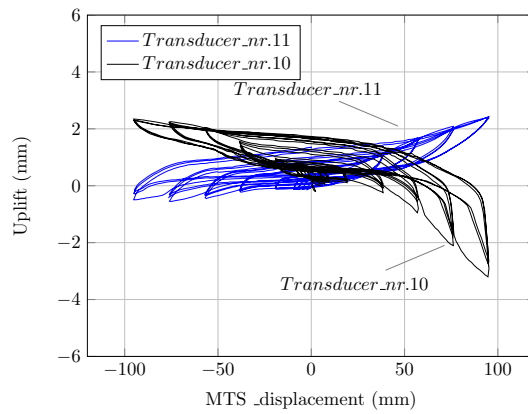


Figure C.39: Horizontal imposed displacement (tr. nr. 2) - Uplift (tr. nr. 10/11).

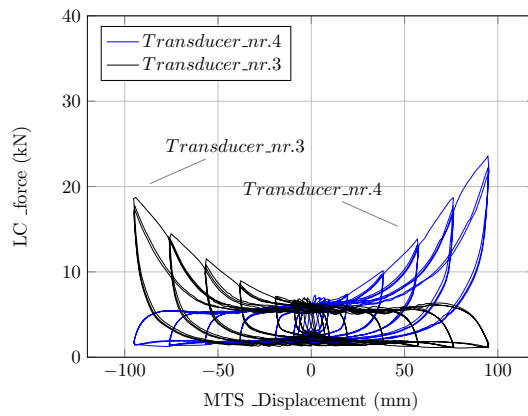


Figure C.40: Horizontal imposed displacement (tr. nr. 2) - Load cell force (tr. nr. 3/4).

C.0.9 Cyclic test: C_ST_130

SPECIMEN CHARACTERISTICS	
Corner joint	STANDARD
Thickness	130 [mm]
Vertical Load	Uniformly distributed load 10.6 [kN/m]
Layout	-
Wall length	4.31 [m]
Load cell pre-load_Est	4.87 [kN]
Load cell pre-load_Ovest	5.15 [kN]
Note di laboratorio	
Transducer nr. 12 was removed after the first hysteresis loop at v=100 [mm].	

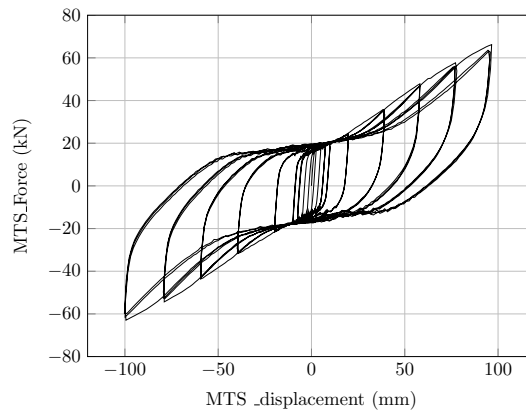


Figure C.41: Horizontal imposed displacement (tr. nr. 2) - Load (tr. nr. 1).

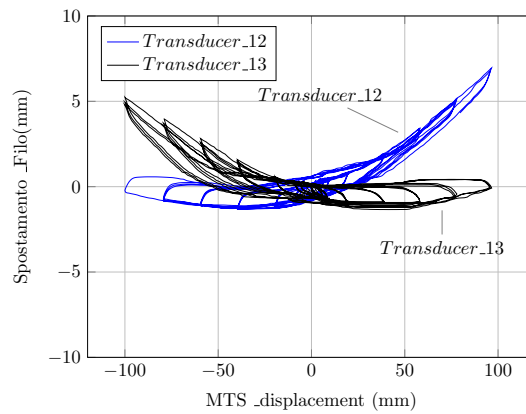


Figure C.42: Horizontal imposed displacement (tr. nr. 2) - Total displacement (tr. nr. 12/13).

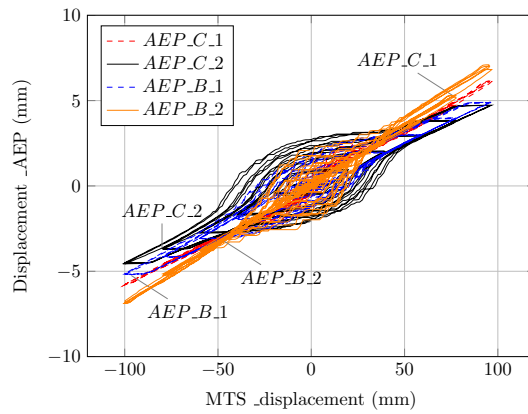


Figure C.43: Horizontal imposed displacement (tr. nr. 2) - Displacement AEP (tr. nr. 5/6/7/8).

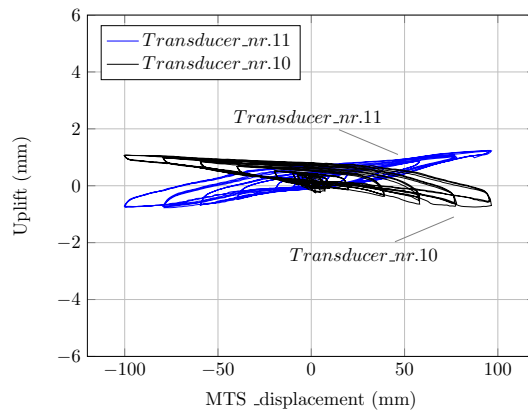


Figure C.44: Horizontal imposed displacement (tr. nr. 2) - Uplift (tr. nr. 10/11).

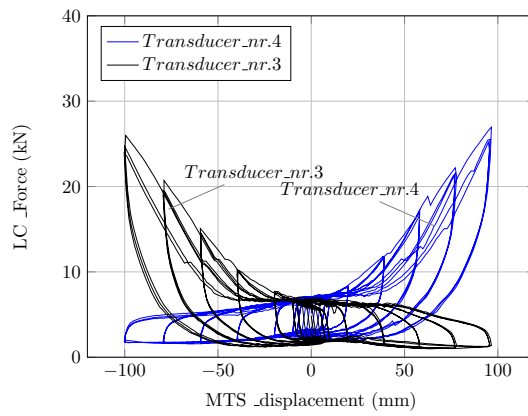


Figure C.45: Horizontal imposed displacement (tr. nr. 2) - Load cell force (tr. nr. 3/4).

C.0.10 Cyclic test: C_ST_SH

SPECIMEN CHARACTERISTICS	
Corner joint	STANDARD
Thickness	90 [mm]
Vertical Load	Uniformly distributed load 6.0 [kN/m]
Layout	-
Wall length	2.785 [m]
Load cell pre-load_Est	5.0 [kN]
Load cell pre-load_Ovest	5.42 [kN]

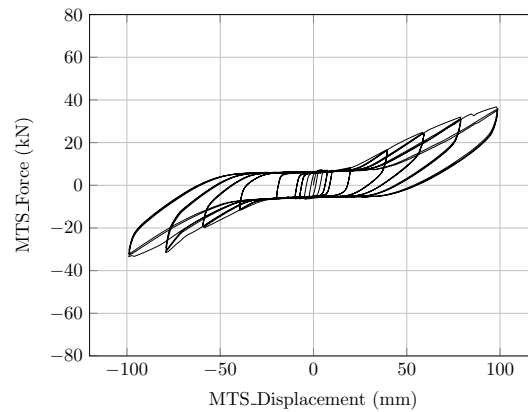


Figure C.46: Horizontal imposed displacement (tr. nr. 2) - Load (tr. nr. 1).

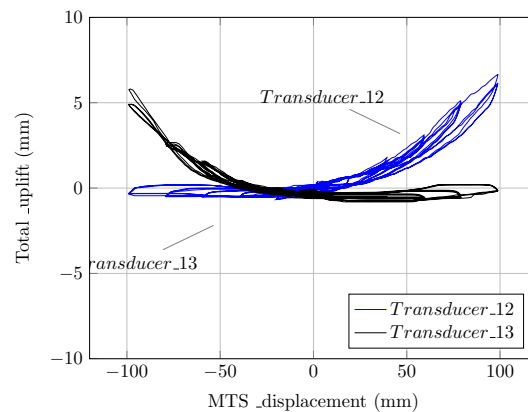


Figure C.47: Horizontal imposed displacement (tr. nr. 2) - Total displacement (tr. nr. 12/13).

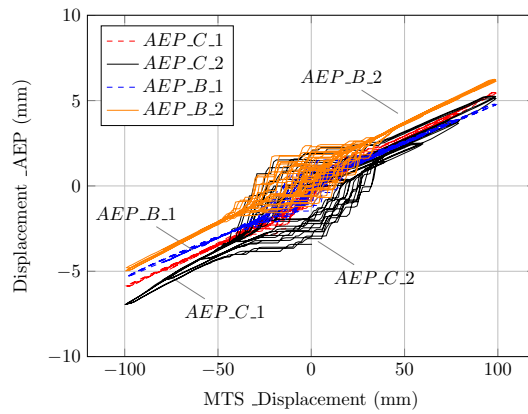


Figure C.48: Horizontal imposed displacement (tr. nr. 2) - Displacement AEP (tr. nr. 5/6/7/8).

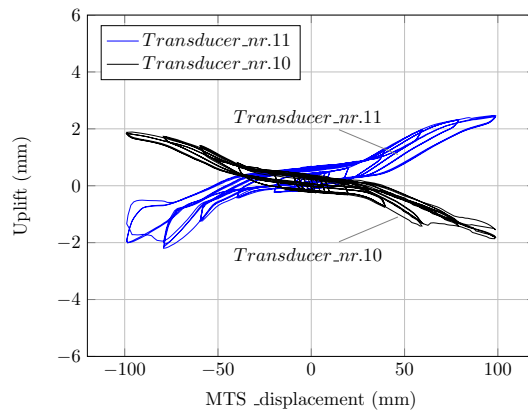


Figure C.49: Horizontal imposed displacement (tr. nr. 2) - Uplift (tr. nr. 10/11).

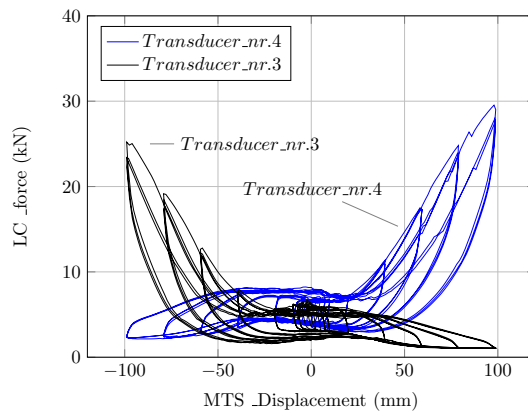


Figure C.50: Horizontal imposed displacement (tr. nr. 2) - Load cell force (tr. nr. 3/4).

C.0.11 Log-house shear-walls: Cyclic tests results

Table C.1: Test: C_ST_90

(a)

Displacement	0,25 Vy	0,5Vy	0,75 Vy			1,00 Vy			2,00 Vy		
Cycle	-	-	1st	2nd	3rd	1st	2nd	3rd	1st	2nd	3rd
F_{max}^+ [kN]	12,0	12,7	11,7	11,9	11,4	11,7	11,7	11,4	12,6	11,8	11,9
F_V^+ [kN]	11,5	11,3	10,6	10,6	9,8	10,0	11,0	10,7	10,7	9,6	10,7
V_{Fmax}^+ [mm]	2,4	4,3	5,5	6,3	3,0	8,5	8,9	9,5	19,4	17,9	19,1
V^+ [mm]	2,4	4,8	7,3	7,3	7,3	9,7	9,7	9,7	19,7	19,7	19,7
F_{max}^- [kN]	-17,3	-17,7	-17,9	-17,1	-16,5	-18,0	-17,5	-17,2	-19,7	-19,1	-18,5
F_V^- [kN]	-16,1	-17,6	-17,2	-16,4	-16,1	-17,2	-16,7	-16,4	-17,5	-16,9	-18,3
V_{Fmax}^- [mm]	-2,2	-5,0	-7,5	-7,5	-7,4	-9,3	-9,8	-9,7	-19,6	-19,6	-19,6
V^- [mm]	-2,5	-5,0	-7,5	-7,5	-7,5	-10,0	-10,0	-10,0	-19,9	-19,9	-19,8
E_d [J]	52,2	184,9	306,0	303,7	298,7	419,3	413,6	409,5	929,6	905,5	891,0
E_p [J]	20,4	44,2	64,7	61,8	60,7	85,8	83,6	81,9	174,1	167,8	181,5
ΔF^+ [kN]	-	-		0,8			-0,7			-0,1	
ΔF^- [kN]	-	-		1,1			0,7			-0,8	
ν_{eq} %	20,4	33,3	37,6	39,1	39,2	38,9	39,4	39,8	42,5	43,0	39,1

(b)

Displacement	4,00 Vy			6,00 Vy			8,00 Vy			10,00 Vy		
Cycle	1st	2nd	3rd	1st	2nd	3rd	1st	2nd	3rd	1st	2nd	3rd
F_{max}^+ [kN]	16,0	15,5	15,7	25,3	24,7	24,5	32,9	31,7	31,3	38,5	37,1	36,5
F_V^+ [kN]	13,9	13,7	14,1	23,9	23,8	24,0	30,0	29,7	29,7	37,3	36,1	36,0
V_{Fmax}^+ [mm]	39,4	39,4	39,3	58,7	59,2	59,1	78,9	78,8	79,2	98,7	98,6	98,5
V^+ [mm]	39,6	39,6	39,6	59,5	59,5	59,5	79,3	79,4	79,4	99,0	98,9	98,9
F_{max}^- [kN]	-27,6	-27,6	-27,3	-36,9	-36,3	-35,9	-43,9	-42,8	-42,4	-49,2	-48,0	-47,5
F_V^- [kN]	-25,5	-26,1	-25,6	-35,3	-34,9	-35,4	-41,0	-40,7	-40,6	-47,8	-47,3	-44,0
V_{Fmax}^- [mm]	-39,0	-39,5	-39,4	-58,8	-59,3	-59,2	-79,0	-78,9	-79,3	-98,5	-98,9	-98,9
V^- [mm]	-39,7	-39,7	-39,7	-59,6	-59,6	-59,6	-79,5	-79,5	-79,5	-99,3	-99,3	-99,3
E_d [J]	1940,9	1881,8	1892,3	3025,0	2906,9	2914,3	4246,1	4038,0	4019,7	5541,7	5236,3	5224,6
E_p [J]	506,1	518,7	507,9	1050,7	1041,0	1055,0	1627,7	1617,8	1616,8	2373,3	2349,4	2185,0
ΔF^+ [kN]		-0,2			-0,1			0,3			1,3	
ΔF^- [kN]		-0,1			-0,2			0,3			3,8	
ν_{eq} %	30,5	28,9	29,7	22,9	22,2	22,0	20,8	19,9	19,8	18,6	17,7	19,0

Table C.2: Test: C_ST_130

(a)

Displacement	0,25 Vy	0,5Vy	0,75 Vy			1,00 Vy			2,00 Vy		
Cycle	-	-	1st	2nd	3rd	1st	2nd	3rd	1st	2nd	3rd
F_{max}^+ [kN]	17,6	18,9	19,0	19,0	19,5	20,0	20,2	20,1	24,3	24,2	24,3
F_V^+ [kN]	16,7	17,4	18,3	18,3	19,1	18,1	19,8	18,8	23,9	22,0	22,7
V_{Fmax}^+ [mm]	2,3	4,9	7,2	7,3	7,4	9,2	9,8	9,7	19,6	19,6	19,6
V^+ [mm]	2,5	5,0	7,4	7,4	7,4	9,9	9,9	9,9	19,8	19,8	19,8
F_{max}^- [kN]	-15,5	-16,6	-16,2	-16,4	-16,2	-17,1	-17,5	-17,1	-21,3	-21,2	-21,5
F_V^- [kN]	-14,7	-16,4	-13,2	-15,4	-14,4	-15,2	-16,7	-16,2	-21,0	-19,8	-21,0
V_{Fmax}^- [mm]	-2,2	-4,6	-6,8	-7,2	-5,7	-8,5	-9,9	-9,2	-19,6	-19,6	-19,6
V^- [mm]	-2,4	-4,9	-7,4	-7,4	-7,4	-9,9	-9,9	-9,9	-19,8	-19,8	-19,8
E_d [J]	61,7	213,6	367,1	353,6	354,4	508,3	502,7	505,7	1157,9	1156,8	1155,4
E_p [J]	20,7	43,4	68,3	68,1	70,9	89,4	98,1	93,4	236,8	217,6	224,7
ΔF^+ [kN]	-	-	-	-0,7	-	-	-0,8	-	-	1,2	-
ΔF^- [kN]	-	-	-	-1,2	-	-	-0,9	-	-	0,0	-
ν_{eq} %	23,7	39,2	42,8	41,3	39,8	45,3	40,8	43,1	38,9	42,3	40,9

(b)

Displacement	4,00 Vy			6,00 Vy			8,00 Vy			10,00 Vy		
Cycle	1st	2nd	3rd	1st	2nd	3rd	1st	2nd	3rd	1st	2nd	3rd
F_{max}^+ [kN]	35,9	35,5	35,3	47,8	46,8	46,8	57,9	56,5	55,8	66,2	64,1	63,4
F_V^+ [kN]	33,4	33,2	33,1	46,4	45,4	45,7	57,2	56,0	53,3	64,4	62,7	62,6
V_{Fmax}^+ [mm]	38,8	38,7	39,1	58,1	58,0	58,1	77,7	76,8	76,6	96,6	95,6	95,4
V^+ [mm]	39,3	39,2	39,2	58,3	58,3	58,4	78,0	77,2	77,1	96,7	95,8	95,7
F_{max}^- [kN]	-31,9	-31,6	-31,5	-43,6	-43,2	-42,8	-54,4	-53,2	-52,6	-63,0	-61,4	-60,6
F_V^- [kN]	-29,4	-29,4	-29,6	-41,8	-41,6	-42,0	-53,5	-49,8	-50,1	-60,9	-59,7	-59,7
V_{Fmax}^- [mm]	-39,3	-39,7	-39,6	-59,5	-59,4	-59,2	-78,9	-79,0	-79,4	-99,9	-99,9	-99,9
V^- [mm]	-39,8	-39,8	-39,8	-59,7	-59,7	-59,5	-79,3	-79,4	-79,5	-100,1	-100,2	-100,3
E_d [J]	2575,8	2501,8	2515,6	4076,7	3917,3	3922,9	5778,2	5441,1	5412,8	7533,4	7024,1	6940,4
E_p [J]	656,0	650,9	649,1	1351,7	1322,2	1334,0	2228,9	2161,1	2054,9	3114,1	3003,1	2994,1
ΔF^+ [kN]	-	0,3	-	-	0,7	-	-	3,9	-	-	1,8	-
ΔF^- [kN]	-	-0,2	-	-	-0,2	-	-	3,4	-	-	1,2	-
ν_{eq} %	31,3	30,6	30,9	24,0	23,6	23,4	20,6	20,0	21,0	19,3	18,6	18,5

Table C.3: Test: C_ST_OP

(a)

Displacement	0,25 Vy	0,5Vy	0,75 Vy			1,00 Vy			2,00 Vy		
Cycle	-	-	1st	2nd	3rd	1st	2nd	3rd	1st	2nd	3rd
F_{max}^+ [kN]	5,8	10,1	12,7	12,7	12,6	14,0	14,1	14,1	16,4	15,8	15,8
F_V^+ [kN]	5,8	10,1	12,7	12,7	12,6	14,0	13,8	13,9	16,2	15,7	14,8
V_{Fmax}^+ [mm]	2,5	4,9	7,4	7,4	7,4	9,9	9,7	9,8	19,6	19,6	19,1
V_V^+ [mm]	2,5	4,9	7,4	7,4	7,4	9,9	9,9	9,8	19,8	19,7	19,7
F_{max}^- [kN]	-6,0	-9,3	-11,4	-11,2	-11,1	-13,5	-13,3	-13,3	-16,4	-16,3	-16,6
F_V^- [kN]	-6,0	-9,2	-11,4	-11,2	-11,1	-13,1	-13,3	-13,2	-16,1	-15,8	-16,5
V_{Fmax}^- [mm]	-2,4	-4,8	-7,3	-7,3	-7,2	-9,6	-9,7	-9,7	-19,2	-18,5	-19,4
V_V^- [mm]	-2,4	-4,9	-7,3	-7,3	-7,3	-9,7	-9,7	-9,7	-19,6	-19,6	-19,6
E_d [J]	7,0	32,0	79,2	80,9	80,4	136,6	135,7	132,8	519,1	548,7	551,4
E_p [J]	7,2	25,0	47,0	46,9	46,8	69,3	68,2	68,6	159,6	155,3	161,0
ΔF^+ [kN]	-	-	0,1			0,1			1,4		
ΔF^- [kN]	-	-	0,3			0,0			-0,4		
ν_{eq} %	7,7	10,2	13,4	13,7	13,7	15,7	15,8	15,4	25,9	28,1	27,3

(b)

Displacement	4,00 Vy			6,00 Vy			8,00 Vy			10,00 Vy		
Cycle	1st	2nd	3rd	1st	2nd	3rd	1st	2nd	3rd	1st	2nd	3rd
F_{max}^+ [kN]	18,7	19,3	18,8	23,2	23,0	23,1	26,8	26,8	26,8	30,2	29,5	28,9
F_V^+ [kN]	18,7	19,3	18,8	22,7	22,7	22,3	26,7	26,5	26,7	30,2	29,2	28,7
V_{Fmax}^+ [mm]	39,2	39,2	39,6	59,4	59,4	58,9	79,1	79,0	78,9	99,0	99,0	98,9
V_V^+ [mm]	39,6	39,6	39,6	59,4	59,4	59,5	79,3	79,3	79,2	99,0	99,0	99,1
F_{max}^- [kN]	-18,5	-18,6	-18,5	-22,5	-22,7	-22,7	-27,3	-27,2	-27,1	-31,6	-30,9	-30,0
F_V^- [kN]	-18,3	-17,8	-18,4	-22,1	-22,0	-22,4	-27,0	-27,2	-27,1	-31,1	-30,6	-29,8
V_{Fmax}^- [mm]	-38,5	-38,0	-35,4	-59,2	-58,7	-59,1	-78,4	-78,8	-79,1	-98,6	-98,5	-98,9
V_V^- [mm]	-39,3	-39,3	-39,3	-59,2	-59,2	-59,2	-79,2	-79,1	-79,1	-99,0	-99,1	-99,1
E_d [J]	1521,3	1523,4	1528,2	2478,9	2456,8	2452,4	3375,7	3357,8	3315,8	4072,7	3780,9	3268,4
E_p [J]	369,5	381,2	372,9	675,9	674,3	663,9	1068,7	1075,9	1071,6	1541,5	1514,2	1475,2
ΔF^+ [kN]	-0,2			0,4			-0,1			1,5		
ΔF^- [kN]	-0,2			-0,3			-0,1			1,4		
ν_{eq} %	32,8	31,8	32,6	29,2	29,0	29,4	25,1	24,8	24,6	21,0	19,9	17,6

Table C.4: Test: C_TR_90

(a)

Displacement	0,25 Vy	0,5Vy	0,75 Vy			1,00 Vy			2,00 Vy		
Cycle	-	-	1st	2nd	3rd	1st	2nd	3rd	1st	2nd	3rd
F_{max}^+ [kN]	13,6	15,7	16,4	15,8	15,6	16,9	16,4	16,2	19,6	19,1	19,1
F_V^+ [kN]	13,4	15,2	15,7	15,2	15,0	15,8	16,0	15,8	17,9	17,6	17,7
V_{Fmax}^+ [mm]	2,3	4,5	7,1	7,2	7,2	9,4	9,6	9,6	19,2	19,2	19,2
V_V^+ [mm]	2,4	4,8	7,2	7,2	7,3	9,7	9,7	9,7	19,5	19,5	19,5
F_{max}^- [kN]	-14,6	-15,4	-15,8	-15,2	-15,1	-16,1	-15,8	-15,3	-17,4	-17,3	-17,2
F_V^- [kN]	-14,1	-15,2	-14,6	-14,5	-14,4	-15,3	-14,4	-15,0	-15,6	-15,5	-16,9
V_{Fmax}^- [mm]	-2,2	-3,7	-6,5	-7,0	-7,0	-8,9	-9,2	-9,4	-19,1	-19,0	-19,0
V_V^- [mm]	-2,2	-4,6	-7,1	-7,1	-7,0	-9,5	-9,5	-9,5	-19,3	-19,3	-19,2
E_d [J]	42,0	163,2	280,5	272,1	267,3	394,2	394,6	390,1	959,9	951,1	947,6
E_p [J]	15,8	36,5	56,8	55,1	54,3	76,6	77,4	76,6	173,8	171,0	172,0
ΔF^+ [kN]	-	-		0,7			0,0			0,2	
ΔF^- [kN]	-	-		0,2			0,3			-1,3	
ν_{eq} %	21,1	35,6	39,3	39,3	39,2	41,0	40,6	40,6	44,0	44,3	43,9

(b)

Displacement	4,00 Vy			6,00 Vy			8,00 Vy			10,00 Vy		
Cycle	1st	2nd	3rd	1st	2nd	3rd	1st	2nd	3rd	1st	2nd	3rd
F_{max}^+ [kN]	30,3	29,6	29,3	41,0	39,6	38,9	50,9	48,7	48,0	59,9	57,4	56,3
F_V^+ [kN]	28,1	27,8	27,9	39,9	39,0	38,6	50,6	46,8	46,6	58,6	56,6	56,1
V_{Fmax}^+ [mm]	38,5	38,5	38,5	57,3	57,2	57,1	75,8	76,3	76,2	95,2	94,8	94,8
V_V^+ [mm]	38,7	38,7	38,7	57,6	57,5	57,4	76,1	76,3	76,4	95,4	95,1	95,1
F_{max}^- [kN]	-24,6	-24,1	-23,9	-34,3	-33,3	-32,8	-43,5	-41,9	-41,1	-52,5	-50,7	-49,8
F_V^- [kN]	-22,3	-22,3	-22,4	-33,0	-32,5	-32,5	-40,3	-39,7	-39,5	-51,2	-50,1	-49,6
V_{Fmax}^- [mm]	-37,8	-38,3	-38,2	-56,7	-56,7	-56,7	-75,6	-76,2	-76,1	-94,9	-95,0	-94,8
V_V^- [mm]	-38,4	-38,4	-38,5	-57,0	-57,0	-57,0	-76,0	-76,3	-76,3	-95,2	-95,3	-95,1
E_d [J]	2170,7	2090,0	2106,6	3548,4	3317,2	3339,3	5086,4	4693,8	4691,0	6698,8	6193,3	6167,8
E_p [J]	543,8	538,4	539,7	1147,9	1120,6	1109,6	1925,2	1787,4	1779,6	2797,0	2693,6	2666,3
ΔF^+ [kN]		0,2			1,2			4,0			2,5	
ΔF^- [kN]		-0,1			0,5			0,8			1,5	
ν_{eq} %	31,8	30,9	31,1	24,6	23,6	24,0	21,0	20,9	21,0	19,1	18,3	18,4

Table C.5: Test: C_ST_SH

(a)

Displacement	0,25 Vy	0,5Vy	0,75 Vy			1,00 Vy			2,00 Vy		
Cycle	-	-	1st	2nd	3rd	1st	2nd	3rd	1st	2nd	3rd
F_{max}^+ [kN]	6,9	7,4	7,1	6,7	6,6	7,0	6,7	6,7	8,3	8,0	8,0
F_V^+ [kN]	6,7	7,0	7,0	6,6	6,1	6,7	6,4	6,2	8,1	7,8	7,8
V_{Fmax}^+ [mm]	2,2	4,3	7,3	6,9	7,3	9,6	9,4	9,7	19,7	19,6	19,6
V_V^+ [mm]	2,5	5,0	7,4	7,4	7,4	9,9	9,9	9,9	19,8	19,8	19,8
F_{max}^- [kN]	-6,4	-6,5	-6,3	-6,2	-6,1	-6,4	-6,3	-6,1	-6,2	-6,1	-6,0
F_V^- [kN]	-6,3	-6,2	-6,3	-5,7	-6,1	-5,9	-6,2	-5,6	-5,8	-5,9	-5,6
V_{Fmax}^- [mm]	-2,5	-4,4	-7,4	-7,2	-7,4	-9,8	-9,4	-9,7	-19,5	-19,7	-16,7
V_V^- [mm]	-2,5	-5,0	-7,5	-7,5	-7,5	-9,9	-9,9	-9,9	-19,9	-19,9	-19,8
E_d [J]	24,6	85,5	143,7	139,2	137,0	193,4	191,4	190,9	432,6	423,1	416,8
E_p [J]	8,2	17,3	25,8	24,5	22,6	33,0	31,7	30,8	79,8	77,3	77,3
ΔF^+ [kN]	-	-		0,9			0,5			0,2	
ΔF^- [kN]	-	-		0,2			0,3			0,2	
ν_{eq} %	23,8	39,3	44,4	45,2	48,3	46,7	48,0	49,4	43,2	43,6	42,9

(b)

Displacement	4,00 Vy			6,00 Vy			8,00 Vy			10,00 Vy		
Cycle	1st	2nd	3rd	1st	2nd	3rd	1st	2nd	3rd	1st	2nd	3rd
F_{max}^+ [kN]	16,6	16,5	16,4	25,0	24,7	24,5	32,0	31,2	30,8	36,8	35,7	35,1
F_V^+ [kN]	16,5	15,2	15,3	24,1	23,9	23,9	31,4	30,9	30,7	35,6	34,8	34,6
V_{Fmax}^+ [mm]	39,2	39,2	39,6	59,2	59,2	59,1	78,9	78,8	78,7	98,4	98,8	98,7
V_V^+ [mm]	39,6	39,6	39,6	59,3	59,3	59,3	79,1	79,1	79,1	98,9	98,9	98,9
F_{max}^- [kN]	-11,8	-11,6	-11,5	-20,2	-19,8	-19,6	-31,9	-30,8	-30,5	-33,5	-32,8	-32,2
F_V^- [kN]	-11,6	-10,3	-10,3	-19,3	-19,1	-19,1	-31,5	-30,8	-30,5	-32,4	-32,0	-31,8
V_{Fmax}^- [mm]	-39,3	-39,3	-39,7	-59,3	-59,3	-59,3	-78,9	-78,8	-79,2	-96,5	-98,9	-98,8
V_V^- [mm]	-39,7	-39,7	-39,7	-59,4	-59,5	-59,5	-79,2	-79,2	-79,2	-99,0	-99,0	-99,1
E_d [J]	894,8	866,9	865,0	1435,5	1335,7	1327,5	2073,3	1882,0	1859,8	2806,5	2479,5	2428,7
E_p [J]	326,5	301,7	303,3	713,7	707,9	708,7	1245,9	1223,1	1213,0	1761,7	1722,3	1708,6
ΔF^+ [kN]		1,2			0,2			0,8			1,1	
ΔF^- [kN]		1,3			0,2			1,0			0,6	
ν_{eq} %	21,8	22,9	22,7	16,0	15,0	14,9	13,2	12,3	12,2	12,7	11,5	11,3

C.1 Photo documentation

This section report the failure observed during the tests on different layout described in the previous sections.

C.2 Tests on 90 mm and 130 mm wall thickness



Figure C.51: *Wall deformed shape.*



Figure C.52: *Detail of the corner joint*

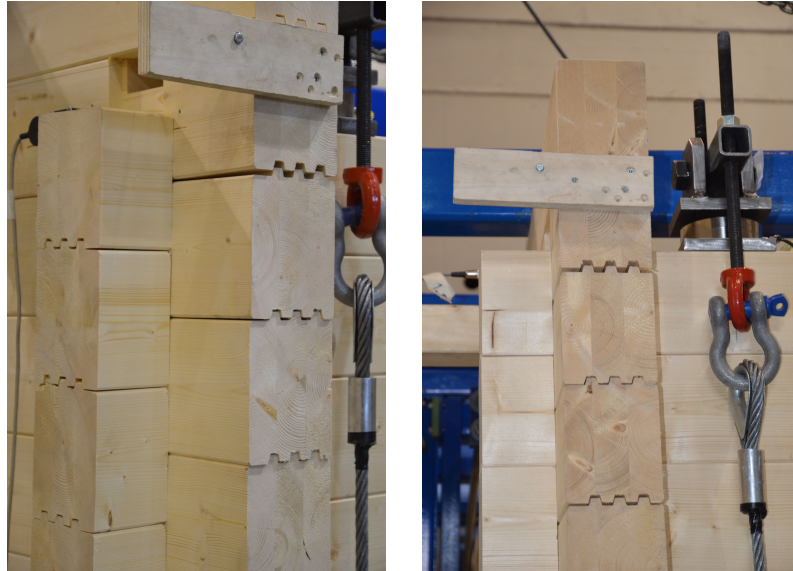


Figure C.53: *Uplift of the top logs.*



Figure C.54: *Effect of the compression perpendicular to the grain.*

C.3 Tests on wall with openings



Figure C.55: *Wall deflection.*



Figure C.56: *Sliding and overturning of the external and internal parts of the wall.*



Figure C.57: (a) Separation of the steel profile on the side of the opening (out of plane reinforce)- (b) permanent slip of the part between two openings.



Figure C.58: Shear failure - cyclic test.



Figure C.59: *Shear failure - monotonic test.*



Figure C.60: *Shear failure - monotonic test.*

C.4 Tests on Tirolerschloss corner joint style walls



Figure C.61: *Wall deformed shape.*

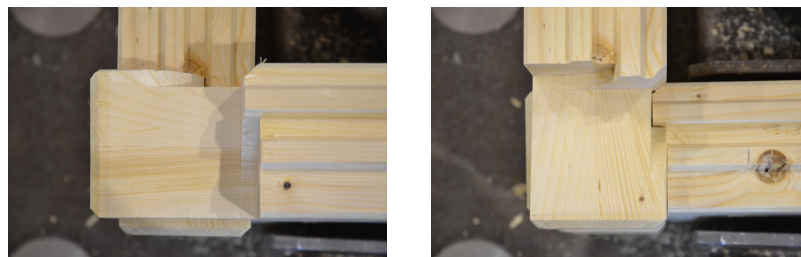


Figure C.62: *Detail of the Tirolerschloss corner joint.*



Figure C.63: *Relative displacement of the corner joint parts.*



Figure C.64: *Crushing of the fibres due to the compression orthogonal to the grain.*

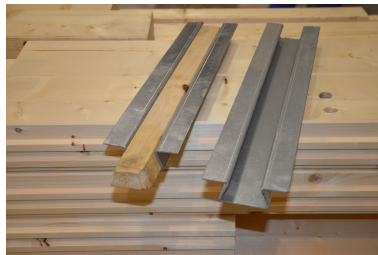


Figure C.65: *Dovetail reinforce system.*

C.5 Tests on shorter walls

C.5.1 Monotonic test



Figure C.66: *Frontal view of the specimen.*



Figure C.67: *Failure of the corner joint - "T" load condition according to section 5.2.1.*

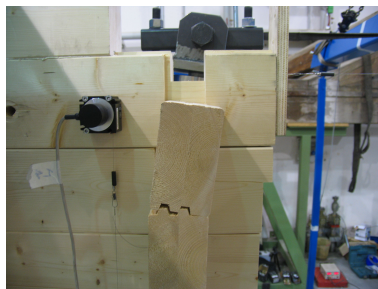


Figure C.68: *Failure of the corner joint - "C" load condition according to section 5.2.1.*

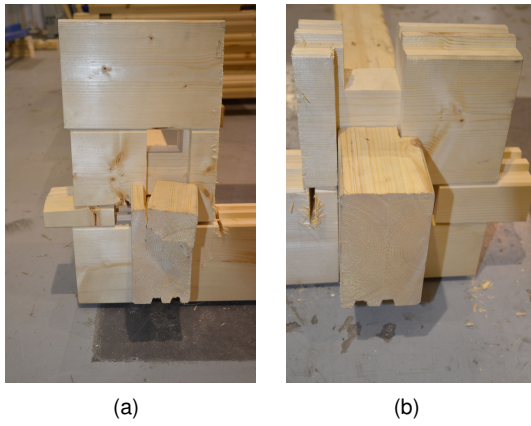


Figure C.69: (a) corner joint - "T" - (b) corner joint - "C" .

C.5.2 Cyclic test

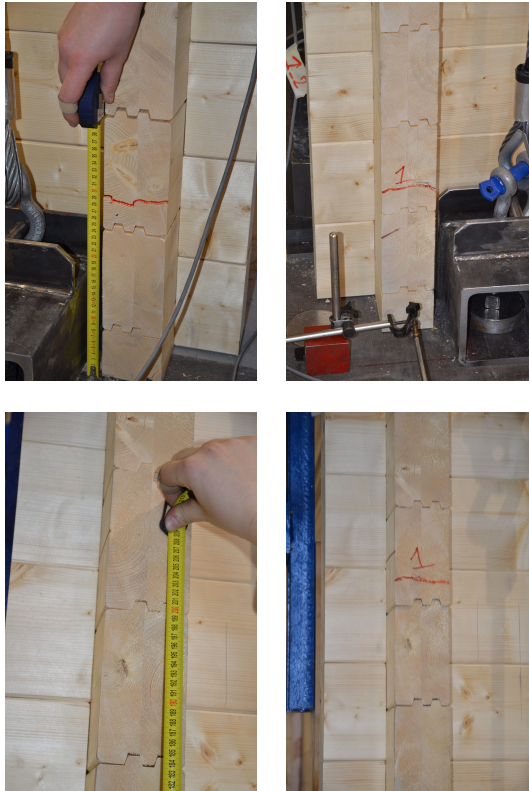


Figure C.70: Shear failure on the first hysteresis loop at $v_y = 100$ mm.

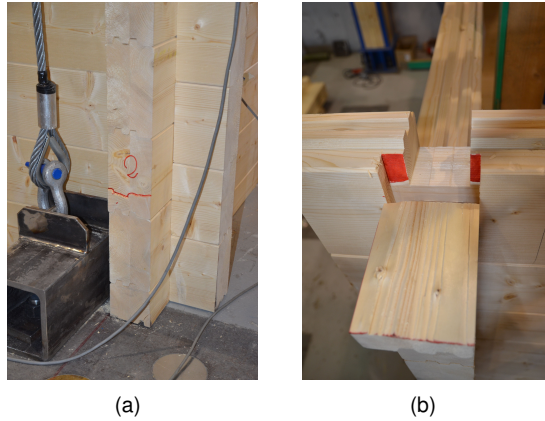


Figure C.71: (a) Shear failure on the second hysteresis loop at $v_y = 100$ mm.- (b) failure of the corner joint - "C".



Figure C.72: Shear failure on the bottom logs :(a) failure of the corner joint - "C" - (b) failure of the corner joint - "T".

Bibliography

- [1] EN1995-1-1:2004/A1:2008:E. Design of timber structures Part 1-1: General-common rules and rules for building, 2004. CEN, European Committee for Standardization, Brussels, Belgium.
- [2] CEN. En1998-1 eurocode 8: Design of structures for earthquake resistance - part 1: General rules, seismic actions and rules for buildings, 2005.
- [3] American forest and paper association. *Details for conventional wood frame construction*. American forest and paper association, 2001.
- [4] W Graf. The shakeout scenario: Woodframe buildings. Technical report, United States Geological Survey (Pasadena CA) and California Geological Survey (Sacramento CA), 2007.
- [5] R. Tomasi and T. Sartori. Mechanical behaviour of connections between wood framed shear walls and foundations under monotonic and cyclic load. *Construction and Building Materials*, 44:682–690, 2013.
- [6] T. Sartori and R. Tomasi. Experimental investigation on sheathing-to-framing connections in wood shear walls. *Engineering Structures*, xx:xx, (in press).
- [7] P. Grossi, T. Sartori, and R. Tomasi. Tests on timber frame walls under in-plane forces: Part 1. *Proceedings of the Institution of Civil Engineers-Structures and Buildings*, vol. Special Issue on Seismic:in press, 2015.
- [8] J. Porteous and A. Kermani. *Structural Timber Design to Eurocode 5*. Wiley-Blackwell 2nd Edition edition, 2013.
- [9] E. Acler, M. Piazza, R. Tomasi, and M Webber. Experimental investigation of the behaviour of different types of connections between the xlam panels and the

concrete slab. In *Proceedings of the Structural Engineering World Conference, Como Cernobbio, Italy 2011*, 2011.

- [10] EN 594:2011. EN 594:2011: Timber structures - Test methods - Racking strength and stiffness of timber frame wall panels, 2011. CEN, European Committee for Standardization, Brussels, Belgium.
- [11] B. Dujic, S. Aicher, and R. Zarnic. Testing of wooden wall panels applying realistic boundary conditions. In *World Conference on Timber Engineering 2006, WCTE 2006*, 2006.
- [12] R. Finn. Scientific report on dynamic tests of timber frame structure. Technical report, COST Action E29 Innovative Timber & Composite Elements / Components for Buildings – Short Term Scientific Mission, 2006.
- [13] J. D. Dolan and A. Toothman. Monotonic and cyclic tests of shear walls with gypsum wallboard, fibreboard, and hardboards sheathing, report no. wmel-2002-03. Technical report, Washington State University - Wood Materials and Engineering Laboratory, 2003.
- [14] T. Sartori, M. Piazza, and P. Tomasi, R. and Grossi. Characterization of the mechanical behaviour of light-frame timber shear walls through full-scale tests. In *World Conference on Timber Engineering 2012, WCTE 2012*, volume 3, pages 180–188, 2012.
- [15] Ministero delle infrastrutture e dei trasporti. Decreto ministeriale 14 gennaio 2008 "nuove norme tecniche per le costruzioni e circolare 2 febbraio 2009 istruzioni per l'applicazione delle nuove norme tecniche per le costruzioni di cui al d.m. 14 gennaio 2008, 2008.
- [16] CEN. Uni en 338:2009 - structural timber - strength classes, 2009.
- [17] CEN. En 1993-1-8:2005 eurocode 3: Design of steel structures, part 1-8: Design of joints.
- [18] CEN. Uni en 14358 timber structures- calculation of characteristic 5-percentile values and acceptance criteria for a sample, March 2007.
- [19] A. Polastri. *Caratterizzazione del comportamento di giunti semirigidi per strutture lignee in zona sismica*. PhD thesis, Università di Trento - Ingegneria delle Strutture: modellazione, conservazione e controllo dei materiali e delle strutture, 2010.

-
- [20] D Casagrande, S. Rossi, T. Sartori, and R. Tomasi. Analytical and backup numerical modelling for seismic response of timber shear walls in multi-storey buildings: a unified approach. *Proceedings of the Institution of Civil Engineers-Structures and Buildings*, special issue on seismic test on timber buildings:xx, 2014.
- [21] DIN 1052: 2008. Design of timber structures. General rules and rules for buildings, 2008. DIN Deutsches Institut für Normung, Berlin, Germany.
- [22] Jürgen Ehlbeck, Heinrich Kreuzinger, Günter Steck, and Hans Joachim Blaß. *DIN 1052 Erläuterungen*. Bruderverlag, 4 2005.
- [23] NZS. Nzs 3603: 1996 timber structures standard.
- [24] CSA 086-09:2009-Engineering design in wood. Csa 086-09:2009-engineering design in wood, May, 2008.
- [25] INTERNATIONAL CODE COUNCIL. 2009 international building code, 2009.
- [26] Bo Källsner and UlfArne Girhammar. Analysis of fully anchored light-frame timber shear walls-elastic model. *Materials and Structures*, 42:301–320, 2009.
- [27] D. Casagrande, S. Rossi, T Sartori, and R. Tomasi. Analytical and numerical analysis of timber framed shear walls. In *World Conference on Timber Engineering 2012, WCTE 2012*, volume 5, pages 497–503, 2012.
- [28] A. Conte, M. Piazza, R. Tomasi, and T. Sartori. Experimental investigation on connections between wood framed shear walls and foundations,. In *Structural Engineering World Congress, Villa Erba, Como, Italy, 2011*, Cernobbio, Como, Italy, 2011.
- [29] D. Casagrande, S. Rossi, and G. Tomasi, R.and Mischi. Timber-frame wall, elasto-plastic behaviour, analytical model, ductility, seismic capacity. *Construction & Building Materials*, pages in–press, 2015.
- [30] D. Casagrande, T. Sartori, and R. Tomasi. Capacity design approach for multi-storey timber-frame buildings. In *INTER-2014, Bath*, 2014.
- [31] D Fischer, A. Filiatrault, B. Folz, C-M. Uang, and F. Seible. Shake table tests of a two-story woodframe house. Technical report, CUREE-Caltech Woodframe Project, 2001.

- [32] I.P. Christovasilis, A. Filiatrault, and A. Wanitkorkul. Report nw-01: Seismic testing of a full-scale two-story light-frame wood building : Neeswood benchmark test. Technical report, University at Buffalo, November 2007.
- [33] A. Ceccotti, C. Sandhaas, M. Okabe, M. Yasumura, C. Minowa, and N. Kawai. Sofie project - 3d shaking table test on a seven-storey full-scale cross-laminated timber building. *Earthquake Engng Struct. Dyn.*, 42:2003-2021, 2013.
- [34] R. Tomasi, T. Sartori, D. Casagrande, and M. Piazza. Shake table testing of a full scale prefabricated three-storey timber framed building. *Journal of Earthquake Engineering, Taylor and Francis*, 2014.
- [35] T. Sartori, D. Casagrande, R. Tomasi, and M. Piazza. Shake table test on 3-storey light-frame timber building. In *World Conference on Timber Engineering 2012, WCTE 2012*, volume 2, pages 262-268, 2012.
- [36] J. Van de Lindt. Evolution of wood shear wall testing, modeling, and reliability analysis: Bibliography. *Practice Periodical on Structural Design and Construction*, 9(1):44-53, 2004.
- [37] T. Vogt, J. Hummel, M. Schick, and W. Seim. Experimental tests for innovative and earthquake-resistant timber-constructions. *Bautechnik*, 91 (1):pp. 1-14, 2014.
- [38] Deutsches Institut für Bautechnik (DIBT). Eta-03/0050 - fermacell fibre gypsum boards-fibre gypsum boards used for planking and lining of building components, 14 nov 2006, 2006.
- [39] Deutsches Institut für Bautechnik (DIBT). extension to the design for use in seismic zones z-9.1-434 - national extended application (d) for eta-03/0050- fermacell fibre gypsum boards-fibre gypsum boards used for planking and lining of building, 2006.
- [40] O. S. Bursi and D. Wagg. *Modern Testing Techniques for Structural Systems: Dynamics and Control*. Springer Science & Business Media, 22 giu 2009 - 349 pagine.
- [41] M. Piazza, R. Tomasi, P. Grossi, A.C. Costa, and P.X. Candeias. Seismic performance of multi storey timber - rubner house building -final report. Technical report, SERIES report n. 227887, 2013.

-
- [42] P. Candeias. Physical modelling, instrumentation and testing, series Inec training course. In (<http://www.series.upatras.gr>), September 23, 2012, Lisbon, Portugal.
- [43] J.W. Van de Lindt, D.V Rosowsky, A. Filiatrault, and M.D. and Davidson R.A. Symans. Development of a performance-based seismic design philosophy for mid-rise woodframe construction. progress on the neeswood project. In *Proceedings of WCTE 2006 - World Conference on Timber Engineering - Portland, OR, USA*, August 6-10, 2006.
- [44] Normenausschuss Holzwirtschaft und Möbel and Normenausschuss Bauwesen. Din 4074-1 strength grading of wood - part 1: Coniferous sawn timber, june 2012.
- [45] EOTA. European technical approval maanhonka log house eta-05/0190 (30 november 2005), 09 2005.
- [46] CEN. En1995-1-1:2009 design of timber structures part 1-1: General-common rules and rules for building, 2009.
- [47] B. Heimeshoff and R. Kneidl. Zur abtragung vertikaler lasten in blockwänden. *Holz als Roh - und Werkstoff*, 50:173–180, 1992.
- [48] M. Popovski. Testing of lateral resistance of handcrafted log walls phase i and ii. Technical report, Prepared for International Log Builders' Association, 2002.
- [49] R. Leichti, R. Scott, T. Miller, and J. Sharpe. Lateral resistance of walls and anchorage in log structures. *Structural Practices*, pages 40–44, 2006.
- [50] J. M. Branco and J. P. Araújo. Structural behaviour of log timber walls under lateral in-plane loads. *Engineering Structures*, 40:371–382, 2012.
- [51] J. M. Branco, P. B. Lourenço, and C. A. Aranha. Shaking table tests of a two-storey log house. *Proceedings of the ICE - Structures and Buildings*, in press, 2014.
- [52] M Andreolli, P. Grossi, T. Sartori, and R. Tomasi. Design and production of an heavy timber reaction frame for a laboratory setup. in *Second International Conference on Structure and Architecture, Guimaraes, Portugal: [University of Minho], 2013. Proceedings of: ICSA 2013, Guimaraes, Portugal, 24-26 july, 2013*, 2013.

- [53] A. J. M. Leijten, S. Franke, P. Quenneville, and R. Gupta. Bearing strength capacity of continuous supported timber beams: Unified approach for test methods and structural design codes. *JOURNAL OF STRUCTURAL ENGINEERING*, 2012.
- [54] L. Bleron, L. Denaud, R. Collet, and R. Marchal. Experimental study of locally loaded timber in compression perpendicular to the grain. *European Journal of Environmental and Civil Engineering*, 15 (3):pp.357–366, 2011.
- [55] H. Blass and R. Görlacher. Compression perpendicular to the grain. *Proceedings of the 8th World Conference on Timber Engineering, Vol. II, Lahti, Finland, 2004*, 2004.
- [56] Brussels Belgium CEN, European Committee for Standardization. En 408:2010: Timber structures. structural timber and glued laminated timber. determination of some physical and mechanical properties.
- [57] M. Andreolli, R. Tomasi, and A. Polastri. Experimental investigation on in-plane behaviour of cross-laminated timber elements. Technical report, Department of Structural and Mechanical Engineering, University of Trento, Italy, 2011.
- [58] CEN. En 384:2010 - determination of characteristic values of mechanical properties and density, 2010.
- [59] F Al-Bender and K. De Moerlooze. Characterization and modeling of friction and wear: an overview. *Sustainable Construction and Design*, 2:19–28, 2011.
- [60] U. Parlitz, A. Hornstein, D. Engster, F. Al-Bender, V. Lampaert, T. Tjahjowidodo, S. D. Fassois, D. Rizos, C. X. Wong, K. Worden, and G. Manson. Identification of pre-sliding friction dynamics. *Chaos*, 14, March 2004.
- [61] Bo N.J. Persson. *Sliding Friction: Physical Principles and Applications*. Springer, June 2000.
- [62] Ario Ceccotti, Maurizio Follesa, and Marco Pio Lauriola. *Le strutture di legno in zona sismica*. C.L.U.T., Torino, Italy, January 2007.
- [63] Societa svizzera degli ingegneri e degli architetti. Sia 265:2003. Timber Structures, 2003.
- [64] Technical Committee CEN/TC. En 12512. Timber structures - Test methods - Cyclic testing of joints made with mechanical fasteners, June 2006.

- [65] A. Koizumi Q. Meng, T. Hirai. Frictional coefficient between timber and structural sheet materials. *IUFRO*, Proc. IUFRO All Div.5 Conference, 2007, 2007.
- [66] T Hirai, Q. Meng, K. Sawata, A. Koizumi, Sasaki, and Y. A. Uematsu. Some aspects of frictional resistance in timber construction. In *Proceedings of the 10th world conference on timber engineering, WCTE., July 2008.*, 2008.
- [67] M. Brunetta, L. Bandini, and M. De Lorenzi. *CSI Analysis Reference Manual*, 2011.
- [68] M. Piazza, R. Tomasi, and A. Crosatti. Indagine sperimentale su sistemi di connessione legno-legno con elementi a gambo cilindrico ed elementi di superficie. Technical report, Facoltà di Ingegneria - Dipartimento di Ingegneria Meccanica e Strutturale, 2008.
- [69] EN 2689:1991. EN 2689: Timber structures. Joints made with mechanical fasteners. General principles for the determination of strength and deformation characteristics, 1991. CEN, European Committee for Standardization, Brussels, Belgium.